SPECTROSCOPIC PROPERTIES OF SOME LANTHANIDE B-DIKETOENOLATES

Thomas Douglas Brown

A Thesis Submitted for the Degree of PhD
at the
University of St Andrews

1973

SPECTROSCOPIC PROPERTIES OF SOME LANTHANIDE β-DIKETOENOLATES

A Thesis

presented for the degree of

DOCTOR OF PHILOSOPHY

in the Faculty of Science of the

University of St. Andrews

by

Thomas Douglas Brown, B.Sc.

September 1973

United College of
St. Salvator and St. Leonard,
St. Andrews.

A Man would do nothing,

if he waited until he could do it so well

that no one would find fault

with what he has done.

CARDINAL NEWMAN

DECLARATION

I declare that this thesis is my own composition, that the work of which it is a record has been carried out by me, and that it has not been submitted in any previous application for a Higher Degree.

This thesis describes results of research carried out at the Department of Chemistry, United College of St. Salvator and St. Leonard, University of St. Andrews, under the supervision of Dr. T.M. Shepherd since the 1st of October 1970.

T.D. BROWN

CERTIFICATE

I hereby certify that T. Douglas Brown has spent eleven terms of research work under my supervision, has fulfilled the conditions of Ordinance No. 12 (St. Andrews), and is qualified to submit the accompanying thesis in application for the Degree of Doctor of Philosophy.

T.M. Shepherd
Director of Research

ACKNOWLEDGEMENTS

I would like to thank Dr. T.M. Shepherd for his continued interest, help and encouragement during the course of this work. My thanks are also due to Dr. C.R.S. Dean for help with computational problems, to the technical staff of the Chemistry Department for all their assistance and to all my past and present friends and colleagues too numerous to mention.

I am indebted to the Science Research Council for a grant to finance this work and to Professor Lord Tedder and Professor P.A.H. Wyatt for providing research facilities.

Finally, I wish to thank Mrs. W. Pogorzelec for patiently typing this thesis.

CONTENTS

Page

Page

Summary

The temperature dependence of the $^5D_4$ Tb^{3+} level in crystalline $Tb(dpm)_3$ has been determined and its anomalous behaviour has been interpreted in terms of thermal depopulation to a low lying triplet level in the solid complex . Comparisons are made with the behaviour shown by the adducts of this compound in the solid state and in solution. In solution molecular weight and conductance measurements indicate some dissociation of the monomeric units.

Large variations in the quantum efficiency of Tb^{3+} tetrakis compounds differing only in the nature of the cation, have been observed. Thermal depopulation of the $^5D_4$ Tb^{3+} level to the ligand triplet level has been established in two series of terbium β-diketoenolates (hfaa and tfaa). This is insufficient to completely explain the quantum efficiency differences. Relative quantum yields of these compounds and related europium compounds in solution and in the solid state have been measured and these results are discussed.

Spectroscopic and analytical evidence of 9-coordination in adducts of tetrakis β-diketoenolate compounds is presented and the isolation of some such compounds is reported. The ability of tetrakis compounds to increase their coordination sphere to nine in solution is demonstrated using an nmr technique.

The occurrence of intermolecular energy transfer in solution containing lanthanide chelates has been observed. The possibility of triplet-triplet transfer has been investigated and the data indicate that this is possible over relatively short distances. Lanthanide-lanthanide transfer has been established and the results are consistent with a diffusion controlled process. The efficiency of this process

is relatively low. Intermolecular energy transfer in some crystalline chelates has been observed and is interpreted in terms of triplet-triplet and lanthanide-lanthanide transfer processes.

CHAPTER 1

INTRODUCTION

1. LANTHANIDE CHEMISTRY

(a) Introduction

The rapid growth in the literature of lanthanide chemistry over the last two decades can be largely attributed to the development of satisfactory separation techniques making the elements and their compounds commercially available in a high degree of purity. The history of the discovery of the lanthanides, summarised by Trifonov[1] indicates the difficulties that chemists in the 18th and 19th centuries encountered in their attempts to isolate these elements. Large scale ion-exchange techniques have been developed to replace the tedious methods of fractional crystallisation, precipitation and decomposition for the separation of the lanthanides[2].

The lanthanides are characterised by the progressive filling of the 4f shell of their electronic configurations. They occur as a group of fourteen elements commencing with the element cerium with an atomic number (z = 58) and ending with the element lutecium (z = 71). The neutral lanthanides possess the common feature of a xenon electronic configuration plus two or three outer electrons ($6s^2$ or $5d6s^2$)[3]. They are highly electropositive elements[4] and most but not all lanthanide chemistry is concerned with the tripositive state. Ln^{3+} ions exhibit numerous coordination numbers with organic ligands and inorganic species, a topic which is discussed in more detail in section (1c). Since it is only the antepenultimate 4f electronic shell that differs in the electronic configuration of these ions their chemistries are very similar however, because of the lanthanide contraction[2,3] slight variations in chemical properties occur within the same oxidation state.

The practical applications of the lanthanides and their compounds are increasing and books by Topp[2] and Trifonov[1] and papers by Blasse[5], Mathers[6] and Yocom[7] illustrate their versatility in modern technology.

(b) Coordination Chemistry

General Introduction

The lanthanide ions have predominantly 'class a' character and show a reluctance to coordinate to donor atoms other than oxygen and nitrogen. The behaviour of the Ln^{3+} ions towards coordinating agents which are capable of forming chelate rings show some regular trends due to the decrease in ionic radius in passing from Ce^{3+} to Lu^{3+}. This results in a fairly regular trend towards increased stability with increasing atomic number, although there are some notable exceptions[8]. The types of ligands with which the lanthanide ions form stable complexes and the effect of complexation on the absorption spectra of lanthanide ions in solution are discussed below in the following sections.

Type of bonding

The spectra of simple lanthanide salt solutions consist of very sharp, almost line-like peaks arising from the electronic transitions involving the 4f electrons. When these ions are coordinated very little change is usually found in the absorption spectra[9], indicating the unavailability of the 4f electrons to participate in the bonding. This contrasts with the variation found in the absorption spectra of the transition metal ions where the absorption spectra arise from transitions involving the d electrons which are usually intimately involved in the bonding. There has as yet been no conclusive evidence presented to show that f orbitals play a major role in the bonding of lanthanide compounds. A number of these absorption spectra together with much of the earlier literature may be found in an article by Vickery[10].

Appreciably stable complex species, relative to the hydrated cations, are obtained only when chelating ligands are employed, particularly when these ligands contain highly electronegative donor atoms (e.g. oxygen). The inability of changes in environment to affect the absorption spectra of Ln^{3+} ions and the preferential affinity for electronegative coordinating atoms is understood from a knowledge of the radius and electron configuration of these lanthanide ions. The significance of the electronic configuration is appreciated from the following considerations. The stabilities of coordination compounds of the d-type transition metal ions are related to the participation of the d electrons and the involvement of the filled or unfilled s and p orbitals in the metal-ligand bond. The lanthanide ions differ from each other in the number of electrons in the 4f orbital, which is effectively shielded from interaction with ligand orbitals by electrons in the 5s and 5p orbitals. If participation of other ion orbitals in lanthanide-ligand bonding is to occur, it must of necessity involve normally unoccupied higher energy metal orbitals (e.g.5d,6s,5p) and bonding of this type would be expected only with the most strongly coordinating ligands. Significantly lanthanide-ligand attractions are thus largely electrostatic in character and the complexes formed by these cations compare more closely with those derived from alkaline earth ions (e.g.

Ca^{2+}, Ba^{2+}). The stabilities of lanthanide complexes are about as much greater than those of the alkaline earths as would be predicted on the basis of simple electrostatic considerations i.e. greater stability because of greater ionic charge with a variation due to the changes in the ionic radius superposed on this. Examples of this may be seen in the $\log_{10}K$ values for the stability constants with EDTA: Ca^{2+}, 11.0; Ba^{2+}, 7.76; La^{3+}, 15.13; Lu^{3+}, 20.00[11].

Nitrogen donors

In the past decade, numerous lanthanide complexes of the nitrogen donor ligands 1,10-phenanthroline(I) and 2,2'-dipyridyl(II) have been isolated using non-aqueous solvents and anhydrous starting materials[9,12-18]. Chelates have also been isolated with ligands such as phthalocyanine(III)[19,20],

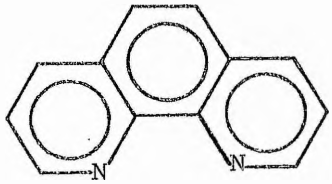

I

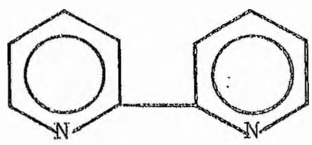

II

pyridine(IV)[21], urotropine(V)[22,23], and 2,2',6',2"-terpyridyl(VI)[24] while a recent review by Forsberg[25] and papers by Foster *et al*[26-28], respectively describe the isolation of lanthanide complexes containing 2,4,6-tri-α-pyridyl-1,3,5-triazine(VII) and

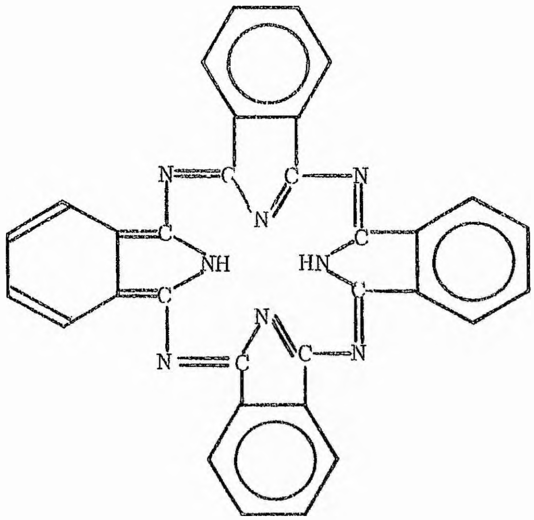

III

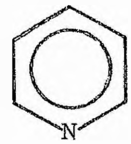

IV

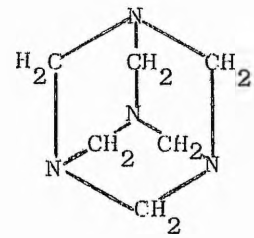

V

1,8-naphthyridine(VIII) as ligands. Sinha[9], has demonstrated the necessity of thermodynamic stability for the formation of amine complexes in aqueous solution to prevent hydroxide formation. Strongly basic donors which might otherwise be expected to form strong metal-nitrogen bonds, generate a sufficient concentration of hydroxide ion in aqueous solution to precipitate the highly insoluble lanthanide hydroxide[29]. It is therefore apparent that the ability of the lanthanide ions to coordinate with neutral nitrogen donors can best be evaluated in non-aqueous media of moderate polarity.

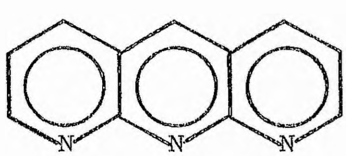

VI

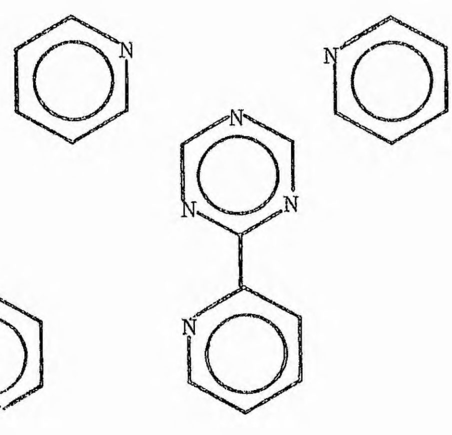

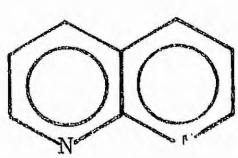

VIII

VII

The nitrogen ligands mentioned above have all relatively weak basic strengths. However, adducts derived from the more basic nitrogen donors (e.g. NH_3) have also been prepared[30-33]. These species are generally obtained by reacting the gaseous amine directly with the anhydrous salt, the compounds are obtained as crystalline powders and possess considerable thermal stability, but limited hydrolytic stability; they are rapidly hydrolysed upon exposure to the atmosphere.

In contrast to the behaviour observed with weakly basic nitrogen donors, high coordination number complexes containing only nitrogen atoms in the coordination sphere may be obtained with strongly basic donors, even in the presence of coordinating anions such as nitrate and chloride.

Oxygen donors

The coordination chemistry of the lanthanide ions with molecules containing oxygen donors has been extensively reviewed by Moeller *et al*[34]. The oxygen donor atoms are usually contained in the functional groups such as carboxylate(IX), hydroxyl(X), aldehydic(XI) and carbonyl(XI) of an aromatic or aliphatic molecule.

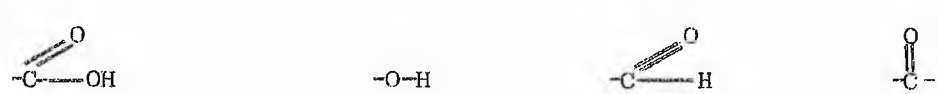

IX X XI XII

Aliphatic acid complexes of the lanthanide ions have been investigated, especially those of acetic[35-37], formic[38], isbutyric[39] and propionic acids[40], but invariably chelation with bidentate oxygen donors leads to greater stability with respect to dissociation into the component species than does complex formation with monodentate ligands. Consequently molecules such as 2,2'-biphenyldicarboxylic acid(XIII)[41], 1,8-naphthalic acid(XIV)[42,43], phthalic acid(XV)[42,43], aliphatic and aromatic alcohols[44-47], β-diketones[48-53] and molecules containing two types of oxygen functional group [37,54-59] [e.g. salicylic acid(XVI)] form relatively stable lanthanide complexes.

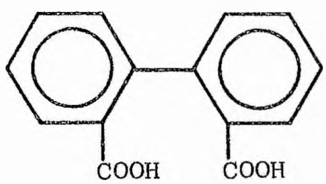

XIII

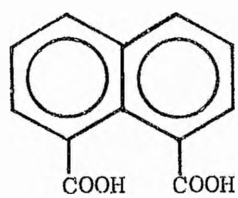

XIV

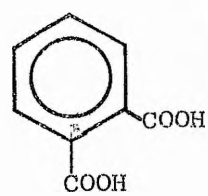

XV

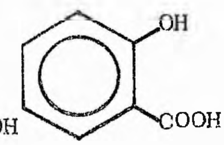

XVI

Donors other than oxygen and nitrogen

Molecules capable of behaving as bidentate ligands and containing donors other than oxygen and nitrogen have received little attention. A few ligands containing both oxygen and sulphur donor atoms, such as mercaptoacetic acid(XVII), S-ethylthioglycolic acid(XVIII), α-mercaptopropionic acid(XIX) and β-mercaptopropionic acid(XX) have been investigated[60,61]. However stability constant data for lanthanide complexes with these ligands indicate that they are acting as monodentate ligands, reflecting the reluctance of the sulphur donor atom to coordinate; possibly because of steric hinderance due to the size and/or the affinity for coordination towards class b metals of the sulphur atom.

$HS-CH_2-COOH$

XVII

$CH_3-CH_2-S-CH_2-COOH$

XVIII

$CH_3-CH(SH)-COOH$ [SH drawn below CH]

XIX

$HS-CH_2-CH_2-COOH$

XX

Jørgensen[62] mentions some unstable complexes of the lanthanides with dialkyldithiocarbamate ($RNCS_2^-$, where R = ethyl or butyl), while investigations by Surls *et al*[63], have indicated comparatively stable lanthanide complexes with the thiocyanate ion (NCS^-). Complex formation with halides has been reported, the fluoride ion having the greatest tendency for complexation with Ln^{3+} ions yielding complex ions such as LnF^{2+} [9]. Cyclopentadiene, a molecule which forms covalent sandwich compounds with transition metals (e.g. ferrocene) also gives rise to lanthanide compounds of the general formula $Ln(Cp)_3$, where (Cp) is the cyclopentadienyl anion[64,65]. Magnetic and spectral data however indicate that the bonding in these compounds is ionic rather than covalent.

β-diketoenolate complexes

The investigations reported in this thesis are largely involved with lanthanide β-diketoenolates and consequently the coordination chemistry of these chelates is discussed in this separate section. β-diketone complexes are known for almost every metal and many non-metals in the periodic table[66]. Lanthanide ions form well characterised compounds with β-diketones which have the general formula:

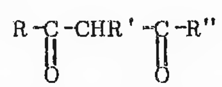

where R, R' and R" can be any alkyl or aryl substituent. These compounds always contain the β-diketoenolate anion bonded as a bidentate chelating agent via two oxygen atoms forming a six-membered ring (see XXI). Although carbon-bonded β-diketone complexes have been reported for some class b transition metals[67-70] none has yet been isolated containing the class a lanthanide ions.

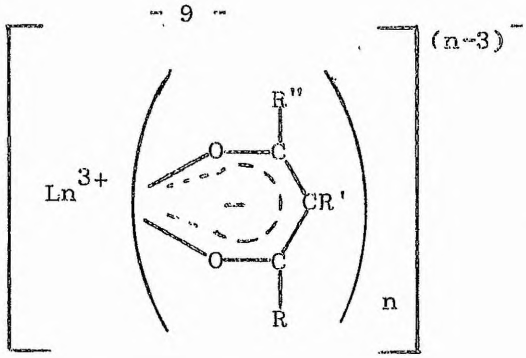

n = 3 or 4

XXI

The β-diketoenolate ligand which is derived by removal of a hydrogen ion from the parent molecule can give rise to two main classes of compound, which can be distinguished by their ratio of ligand to metal ion. Neutral tris complexes are obtained when the ratio of ligand to metal in the preparation is 3 to 1, while anionic tetrakis chelates are obtained when the ligand to metal ratio is 4 to 1 or greater. In most cases because of the lanthanide ions' affinity for higher coordination (see section 1c) the tris compounds are usually isolated as solvates. The degree of solvation appears to be dependent on the reaction conditions while attempted removal of the coordinated solvent in many cases leads to decomposition of the complex. The tetrakis compounds because of their anionic nature are isolated with cations, such as protonated amines of quaternary salts. A large number of β-diketone complexes can be synthesised both as tris and tetrakis complexes employing different ligands, while in addition tetrakis complexes can form a homologous series of compounds having the same ligand but differing in the accompanying cation. The isolation of mixed β-diketoenolate ligand lanthanide complexes has recently been reported by Dutt et al[71]. Examples of the ligands which have been employed to isolate lanthanide β-diketoenolate complexes are summarised in Table 1.1[72-75].

Table 1.1

Systematic name	Trivial name	Abbreviation used
1,3-diphenyl-1,3-propanedione	dibenzoylmethane	Hdbm
2,4-pentanedione	acetylacetone	Haa
1,1,1-trifluoro-4-(2-thienyl)2,4-butanedione	thienoyltrifluoro-acetylacetone	Httfaa
1-phenyl-1,3-butanedione	benzoylacetone	Hba
1,1,1-trifluoro-4-phenyl-2,4-butanedione	benzoyltrifluoro-acetone	Hbtfa
1,1,1-trifluoro-2,4-pentanedione	trifluoroacetyl-acetone	Htfaa
1,1,1,5,5,5-hexafluoro-2,4-pentanedione	hexafluoroacetyl-acetone	Hhfaa
2,2,6,6-tetramethyl-3,5-heptanedione	dipivaloylmethane	Hdpm
1,1,1,2,2,3,3-heptafluoro-7,7-dimethyl-4,6-octanedione		Hfod

(c) Coordination Number

Lanthanide ions because of their large size (ionic radius Ce^{3+}, 0.1034 nm, cf Cr^{3+}, 0.063 nm) form compounds having high coordination numbers. Compounds with coordination numbers of 6, 7, 8, 9, 10 and 12 have been established[76]. A recent paper by Bradley et al[77], reports the synthesis and characterisation of three coordinate lanthanide complexes which are hydrolytically unstable and must be handled in strictly anaerobic conditions. The most common coordination number exhibited by these ions is 8, 9 and 10 which is in marked contrast to the transition metals where coordination numbers of 4 and 6 are common although some class a transition metal ions do form octacoordinate compounds[78,79].

Most of the lanthanide compounds which have been characterised or postulated as having coordination numbers of 10 and 12 contain the nitrate group as a bidentate ligand[26,28,80-82], although Foster et al[27], have synthesised compounds containing only the didentate 1,8-naphthyridine in the lanthanide coordination sphere which they have characterised by molar conductance, ir and nmr studies as having coordination numbers of 10 and 12. The ability of the nitrate group[83,84] as well as naphthyridines[79,85-88] attain high coordination numbers has also been reported for the first row transition metals even with those having class b character[83-88].

Numerous tris and tetrakis β-diketoenolate lanthanide complexes have been isolated where octacoordination is assumed[73,74]. It appears that this is the most common coordination number for this type of chelate although, the varying degree of solvation in the case of the tris chelates provides complexes having coordination numbers of 6, 7, 8 and 9[89]. Bidentate[73] and monodentate[90,91] ligands have been employed as adducts to obtain octacoordinate compounds (e.g. see XXII and XXIII) with tris β-diketoenolates. Workman et al[92], have synthesised and characterised nine-coordinate tetrakis β-diketoenolates containing dimethylformamide and water as an adduct. Early workers[73] had assumed the parent compound and the similar compound containing the water to be geometrical isomers.

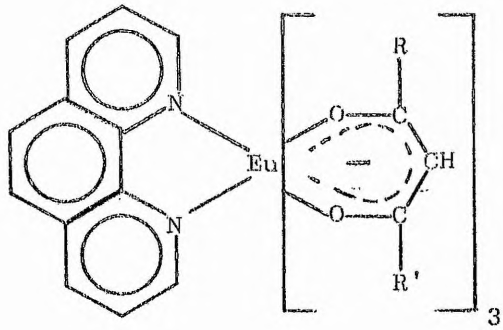

XXII

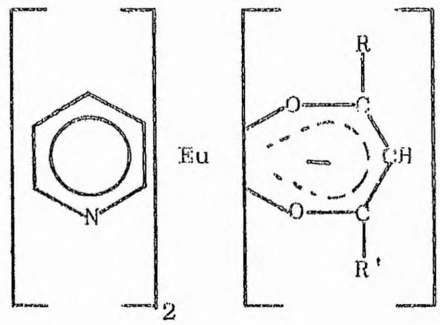

XXIII

(d) Spectroscopic Properties of Lanthanide Ions and Chelates

Spectral and magnetic properties of Ln^{3+} ions

The perturbation by the chemical environment on the 4f electrons is usually extremely small because they lie so deep inside the lanthanide ions. This means that the spectroscopic and magnetic properties of these ions, which are largely properties of the uncompletely filled 4f shell, are closely related to those of the simple gaseous ions[93]. Despite the complexities of the lanthanide spectra there is therefore an essential simplicity in the correlation of gas-ion and ionic-compound spectra in the lanthanides which is absent elsewhere in the periodic table (cf transition metal ions). Moreover, because the 4f electrons do not penetrate close to the atomic nucleus, their spin and orbital angular momenta may be treated by the simple Russell-Sanders (RS) coupling approximation, which is not normally useful for electrons in heavy atoms. In addition the spin-orbit coupling constants are quite large (several thousand cm^{-1}). With the exception of Eu^{3+} and Sm^{3+} the lanthanides have ground states with a single well defined value of the total angular momentum, J, with the next lowest, J, state at energies many times kT at ambient temperature ($\sim$200 cm^{-1}) above, and hence virtually unpopulated. Thus the magnetic susceptibilities, χ , and moments, μ, may be calculated by considering only this well defined J state. Indeed such calculations using the Langevin equation i.e.

$$\chi = N\mu^2/3kT \qquad 1.1$$

where $\mu = g\sqrt{[J(J+1)]}$ in Bohr magnetons 1.2

and g, the Landé factor, is given by

$$g = \frac{1 + (J+1) + S(S+1) - L(L+1)}{2J(J+1)} \qquad 1.3$$

give results which are in excellent agreement with experiment values. Table 1.2 below summarises the RS ground state terms for the Ln^{3+} ions and shows the agreement of the observed and calculated magnetic moments.

Table 1.2

Ln^{3+}	4f configuration	RS ground state	Landé factor	μ calc.	μ obs.
Ce	$(4f^1)$	$^2F_{5/2}$	6/7	2.54	2.5
Pr	$(4f^2)$	$^3H_4$	4/5	3.58	3.5
Nd	$(4f^3)$	$^4I_{9/2}$	8/11	3.62	3.6
Pm	$(4f^4)$	$^5I_4$	3/5	2.68	
Sm	$(4f^5)$	$^6H_{5/2}$	2/7	0.84	1.5
Eu	$(4f^6)$	$^7F_0$	1	0	3.4
Gd	$(4f^7)$	$^8S_{7/2}$	2	7.94	8.0
Tb	$(4f^8)$	$^7F_6$	3/2	9.72	9.3
Dy	$(4f^9)$	$^6H_{15/2}$	4/3	10.63	10.6
Ho	$(4f^{10})$	$^5I_8$	5/4	10.60	10.4
Er	$(4f^{11})$	$^4I_{15/2}$	6/5	9.59	9.5
Tm	$(4f^{12})$	$^3H_6$	7/6	7.57	7.4
Yd	$(4f^{13})$	$^2F_{7/2}$	8/7	4.54	4.5
Lu	$(4f^{14})$	$^1S_0$	1	0	0

It should be emphasised that magnetic behaviour depending on J values is quantitatively different from that depending on S values, that is "spin only" behaviour, which gives a fair approximation for many of the regular transition elements. Only for the $4f^7$ and $4f^{14}$ cases, where there is no orbital angular momentum (L = 0) do the two treatments give the same results.

The most common type of transition giving rise to lanthanide absorption and emission spectra is that associated with a re-arrangement of electrons inside the 4f shell and a corresponding change in the interelectronic repulsion. Such transitions are Laporte forbidden so that the intensity of absorption is weak. The bands are narrow and relatively little shifted or split (ligand field) by changes in chemical environment. This is in marked contrast with the spectra of the d-transition metals where the spectral profile is markedly dependent on chemical environment. The order of perturbation for the lanthanide ions are crystal field < spin orbital coupling < interelectronic repulsion whereas, the order of perturbation for the 3d-transitions are spin orbit coupling < crystal field < interelectronic repulsion[94].

Luminescence of lanthanide ions

Absorption spectra have been obtained for all lanthanide ions[95,96]. Just as it is possible to observe radiative transitions from excited states of organic molecules (see section 1.2), emission from excited levels of the lanthanide manifolds can also be observed. These radiative transitions are usually incorrectly referred to as ion-fluorescence as they involve a change in multiplicity. However the term fluorescence prevents confusion when these ions are coordinated to organic molecules where excitation can lead to ligand phosphorescence as well as radiative transitions from the lanthanide manifolds.

As a consequence of the shielding of the 4f electrons the profile of the ion-fluorescence from the lanthanide manifolds are little affected by the change in chemical environment although the quantum efficiencies can vary quite considerably. Fluorescent quenching of various lanthanide salts in numerous hydrolytic solvents have been investigated by Kropp et al[97], who conclude that the relatively high energy stretching modes of the hydroxyl bonds are responsible for quenching, although the degree of quenching is dependent both on the associated anion and hydrolytic solvent. As an example the anhydrous chlorides of the lanthanides all exhibit line fluorescence by direct excitation of the ions[98]. When coordinated with water only Gd^{3+}, Tb^{3+}, and Eu^{3+} emit strongly, Sm^{3+} and Dy^{3+} weakly, the other showing only very weak or no fluorescence[99]. If D_2O is used instead of H_2O , dramatic enhancement in the fluorescent intensity of certain ions occur[97,100-104] this also being the case when other deuterated solvents are substituted for the parent solvent[97]. Luminescence from all the lanthanide ions has been observed by Heller[95] when studying these ions in aprotic selenium oxychloride ($SeOCl_2$) solutions.

Luminescence of lanthanide chelates

Weissman[105] first observed that direct excitation of the organic moiety in certain lanthanide chelates results in fluorescence characteristic of intra-4f transitions of the metal ions. This indirect population of the emitting levels of the lanthanide ions is analogous to the indirect population of the T_1 state in organic molecules where the initial absorption process is $S_i \leftarrow S_o$. The population of the T_1 state results in non-radiative transitions between various energy levels of the organic molecule, transitions which are discussed in section 1.2.

The mechanism for this intramolecular energy transfer in numerous lanthanide chelates has been extensively investigated. Several mechanisms have been reported[106-111], but investigations with various ligands[96,103,107], lanthanide ions[107] and triplet quenchers[104] suggest that the mechanism proposed by Whan et al[112], is the most reasonable. A diagramatic representation of the energy transfer processes is illustrated in Fig. 1.1. The mechanism involves direct excitation of the ligand ($S_i \leftarrow S_o$),

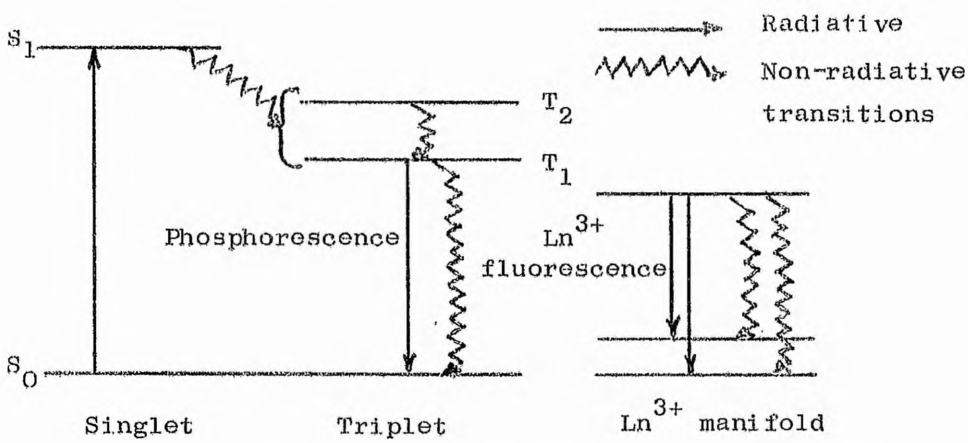

Fig. 1.1 Mechanism for intramolecular energy transfer

followed by non-radiative energy transfer processes forming a ligand triplet. The ligand triplet may then lose its energy by a combination (although one process may predominate) of phosphorescence ($T_1 \rightarrow S_o$) and non-radiative transfer to the lanthanide excited levels. When transfer to the excited lanthanide levels occurs the molecule may return to the ground state via the competitive radiative lanthanide fluorescence and non-radiative processes (see Fig. 1.1).

Consistent with this mechanism Whan et al[110], classified complexes of the lanthanide ions into three categories based upon their fluorescent properties. The first category includes complexes of Gd^{3+} and Lu^{3+} which do not exhibit metal ion fluorescence. In the case of Lu^{3+} there are no infra-4f transitions possible due to the completely filled 4f shell, while the lowest lying level of Gd^{3+} ($\sim$32,000 cm^{-1}) lies above the triplet levels of most organic molecules, precluding energy transfer from the ligand to the metal ion and subsequently ion-fluorescence. The second category includes Sm^{3+}, Eu^{3+}, Tb^{3+} and Dy^{3+}, which exhibit strong metal-ion fluorescence since these ions have energy acceptor levels close to the donating triplet level of the organic molecule. The third category includes complexes of Pr^{3+}, Nd^{3+}, Ho^{3+}, Tm^{3+} and Yb^{3+} which exhibit weak metal-ion fluorescence. Each of these metal ions possesses several closely spaced energy levels, thus increasing the probability of non-radiative transitions via cascade mechanisms.

Energy diagrams of the pertinent levels of Tb^{3+}, Eu^{3+}, Sm^{3+}, Gd^{3+} and Nd^{3+} along with their Russell-Saunders terms are given in Fig. 1.2 as investigations reported in this thesis are mainly concerned with these ions.

(e) Lanthanide Ions as Nmr Shift Reagents

Introduction

Nmr spectroscopy is a valuable technique for structural investigations of complex organic molecules. However, owing to the relatively low sensitivity of proton chemical shifts to changes in chemical and stereochemical environment, the application of nmr spectroscopy has been somewhat restricted.

Shift reagents are used in nmr spectroscopy to reduce the equivalence of nuclei by altering their magnetic environment, and are of two types: aromatic solvents such as benzene or pyridine, and paramagnetic metal complexes. The

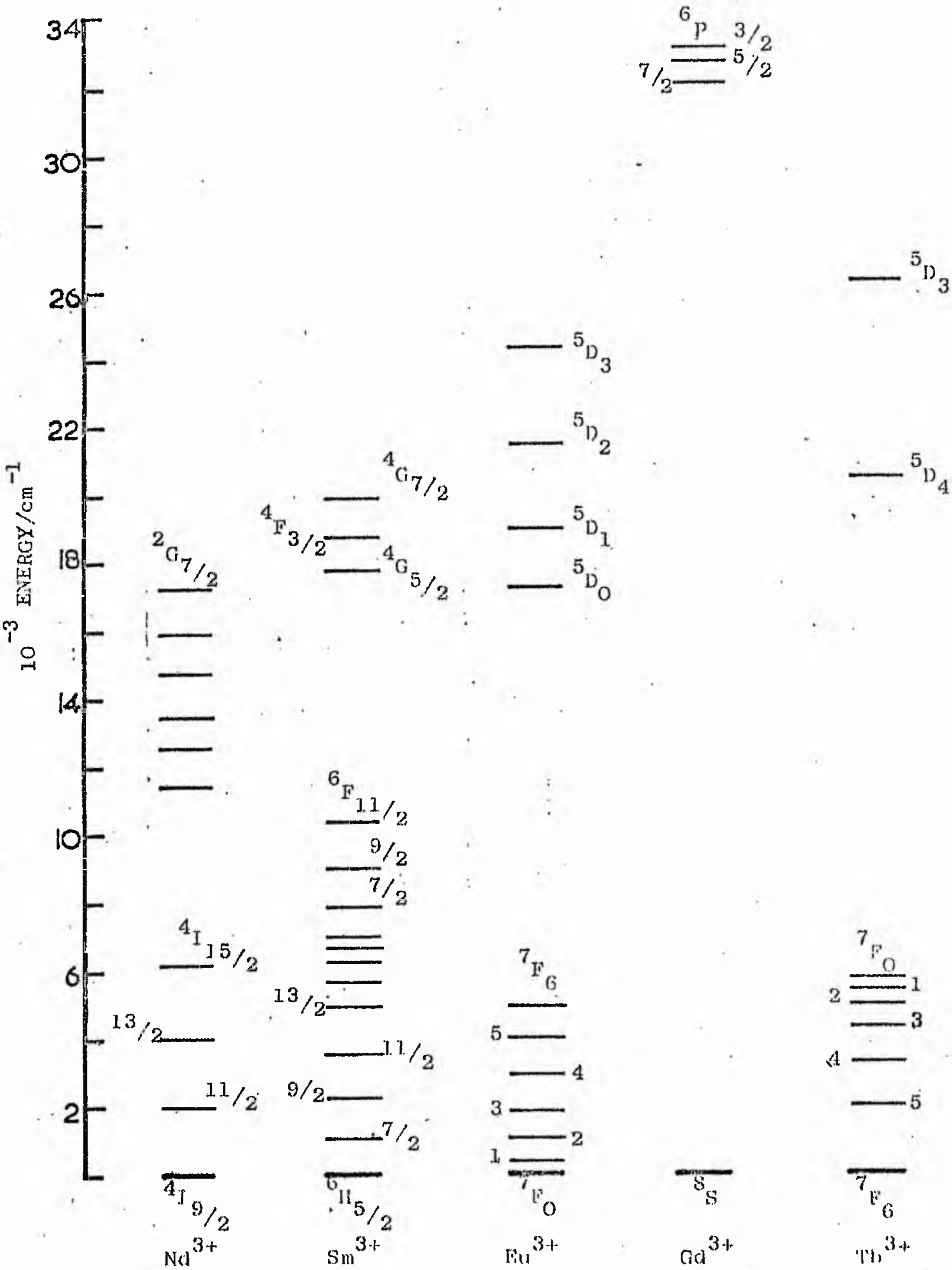

Fig. 1.2 Pertinent energy levels for some Ln^{3+} ions

latter function by coordinating to suitable donor atoms in the molecule under study, thereby expanding their coordination shell and forming a new complex in solution. Apart from effects due to shielding by bonding electrons, the chemical shifts are altered by the paramagnetic metal by transfer of electron spin density, via covalent bond formation, from the metal ion to the associated nuclei (contact shift), or by magnetic effects of the unpaired electron magnetic moments (pseudocontact shift). First row transition-metal complexes can be used as shift reagents and operate by both contact and pseudocontact mechanisms, although the former predominates owing to the covalent character of these compounds. Unfortunately, these shift reagents exhibit an abverse effect on the resolution of the nmr spectra by causing severe line broadening. In 1969 Hinckley[113] initiated a major advance in this field by introducing the use of a lanthanide-metal complex as a shift reagent and since then it has become established that lanthanide complexes produce far less linewidth broadening and give shifts which are caused largely by the pseudocontact mechanism.

Substrate-lanthanide shift reagent interactions

The lanthanide shift reagent (LSR) usually consists of a six-coordinate metal complex which readily increases its coordination number in solution by accepting one or more further ligands[113]. The substrate coordinates to the LSR by virtue of the requirement that it contains heteroatoms which exhibit some degree of Lewis basicity. Addition of the LSR to a solution of substrate in a normal nmr solvent leads to the formation of an equilibrium mixture as shown in equations 1.4 and 1.5

$$L + S \underset{}{\overset{K_1}{\rightleftharpoons}} (LS) \qquad 1.4$$

$$(LS) + S \underset{}{\overset{K_2}{\rightleftharpoons}} (LS_2) \qquad 1.5$$

where L and S are the concentrations of the LSR and substrate respectively and (LS) the concentration of the complex formed in solution: the ratio of these species depends on K_1 and K_2 the association constants. The association constant, K_2, is usually assumed negligible, i.e. predominantly 1:1 complex formation occurs although there is recent evidence for 2:1 complex formation[90,91]. Owing to the magnetic interactions with the metal ion in the complex substrate (LS) the nmr position of associated nuclei in the substrate differ from those in the uncomplexed state. The equilibrium in solution between these species is rapid on the nmr timescale[114], so that only a single average signal is recorded for each nucleus in different environments. This does not mean that the whole spectrum is merely displaced since factors such as the distance of the nuclei from the metal ion cause a differential expansion of the spectrum. Consequently, the foremost use of a LSR is in effectively increasing the resolution in many cases producing first order spectra.

Shift mechanism

In the lanthanide-substrate complex interactions between the paramagnetic metal ion and the nuclei of the substrate causes changes in the chemical shift of the nuclei. Two types of interaction between the metal ion and ligand have been proposed, contact and pseudocontact interactions and the resulting shifts referred to as contact and pseudocontact shifts.

Pseudocontact[115] shift is caused by dipolar interaction between the nucleus and the electron spin magnetisation of the paramagnetic metal ion. Two theories, that of McConnell _et al_[116], and Bleany[117] have been developed giving an expression for the magnitude of the pseudocontact shift, both of which can be expressed by equation 1.6

$$\delta = \frac{X(3\cos^2\theta_i - 1)}{r_i^3} \qquad 1.6$$

where θ_i is the angle between (a) the distance vector, r_i, joining the metal cation to the particular nuceus, i, in the complexed substrate, and (b) the crystal field axis of the complexed substrate often assumed as the line joining the metal atom to the lone-pair-bearing atom; X, being a constant the value of which depends on the particular theory used[116,117].

Contact shifts[115] occur by direct electron-nucleus magnetic interaction as distinct from the classical dipolar interactions. Consequently shifts occur by movement of unpaired electron spin density from the metal cation to the ligand by covalent bond formation. Hence, this mechanism operates through the metal cation coordinating bond and so depends on the degree of covalency in this bond. The interaction is independent of the $3\cos^2\theta - 1$ term and falls off rapidly with increasing distance except in conjugated systems, which facilitate delocalisation of unpaired electrons. The distinction between contact and pseudocontact shift is important for a better understanding of the factors affecting the lanthanide induced shift (LIS). The assumption that lanthanides interact by a pseudocontact mechanism is based on their high electropositive character and the shielding of the f orbitals[3]. As the lanthanides form complexes by electrostatic interactions, this precludes the operation of a contact mechanism of the same order of magnitude as those found with the first row transition-block metal complexes[118], but even with as little as 1% covalency contact shift should be observed[119]. Therefore, even with LSRs a small degree of contact shift is possible[119] and is seen in deviations from equation 1.6, particularly for protons attached to the carbon atoms nearest the lone-pair donor atoms.

Lanthanide ions and chelates as LSRs

Choice of lanthanide ions used as LSRs are dependent on two factors;(a) their relative inability to line broaden nmr spectra, a factor which precludes the transition metals as good shift reagents; (b) the magnitude of the shifts produced. Ideally the LSR should provide a large shift, with minimal line broadening. Values of these two factors are quoted by Mayo[120] for the lanthanide ions. It is concluded that a compromise must be made as the largest shifts are obtained by using the lanthanides that give the greatest line broadening e.g. Tb^{3+} and Tm^{3+}. Consequently Eu^{3+} and Pr^{3+} are used most extensively as these metal ions produce large enough shifts with a sufficiently small broadening effect to allow gross multiplet absorption bands to be resolved at relatively large shifts.

As a result of the solvents used in nmr investigations the LSR is usually in the form of a soluble chelate which is preferably free from solvated water molecules as this leads to weak competition with further ligands. The most widely employed ligands contain the bulky tertiary-butyl group incorporated in highly fluorinated molecules. This overcomes solubility problems and produces larger shifts than unfluorinated chelates. Comparison of numerous LSRs indicate the following order of shifting power;

$$Eu(fod)_3 > Eu(pfd)_3 > Eu(fhd)_3 > Eu(dpm)_3$$

where fod = 1,1,1,2,2,3,3-heptafluoro-7,7-dimethyloctane-4,6-dione anion, pfd = 1,1,1,2,2-pentafluoro-6,6-dimethylheptane-3,5-dione anion, fhd = 1,1,1-trifluoro-5,5-dimethylhexane-2,4-dione anion and dpm = dipivaloylmethane anion.

Ernst et al[121] have found an almost linear correlation of pKa with LIS for a series of substituted anilines. The basicity factor of the substrate appears to be an important criterion on which to judge the effectiveness with which a group will give a LIS, although factors such as steric hindrance cannot be ignored[122].

2. GENERAL PHOTOCHEMISTRY

A useful definition of photochemistry has been given by Wayne[123] which states, "Photochemistry is the study of interactions between light and matter and is concerned both with chemical changes brought about by the absorption of light and with the emission of radiation from energy rich species."

(a) Light Absorption and its Physical Consequences

The essential feature of photochemistry is the participation of excited atoms or molecules in chemical and/or physical processes. It is therefore necessary to understand photochemical and photophysical processes that atoms and molecules can undergo, processes which have been defined by Leermakers[124] and Noyes et al[125], respectively. Basic to any photo process is the absorption of a quantum of light, a photon. When a photon of energy is absorbed by a molecule this may give rise to an electronic transition, usually involving the promotion of an electron in a bonding or non-bonding molecular orbital to an antibonding orbital (see Fig. 1.3). The molecule is thus

Fig. 1.3 Molecular Orbital Picture of Excited States

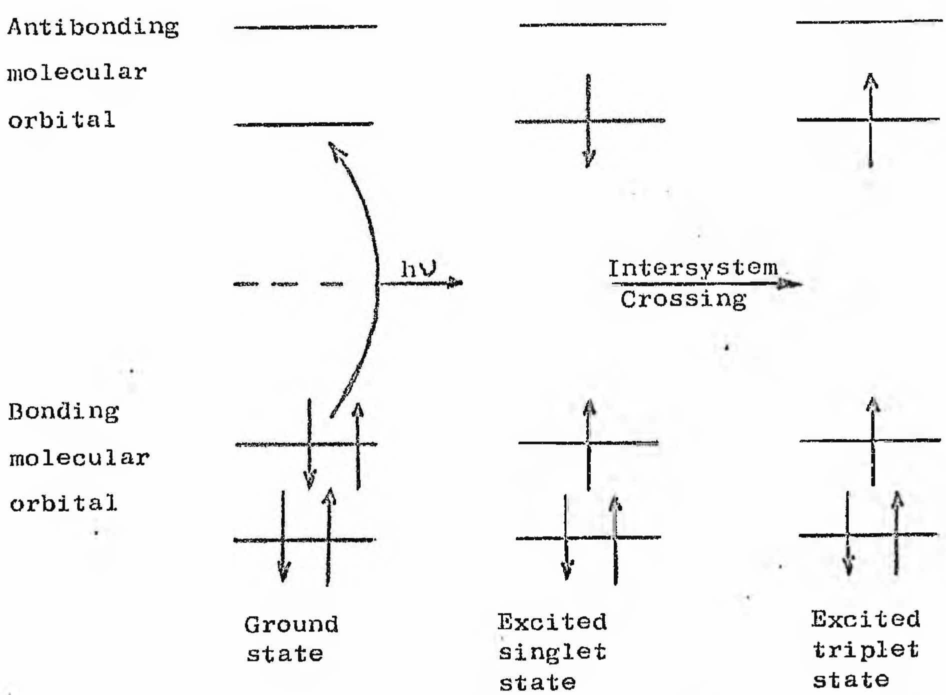

Figure 1.4 Jablonski Diagram

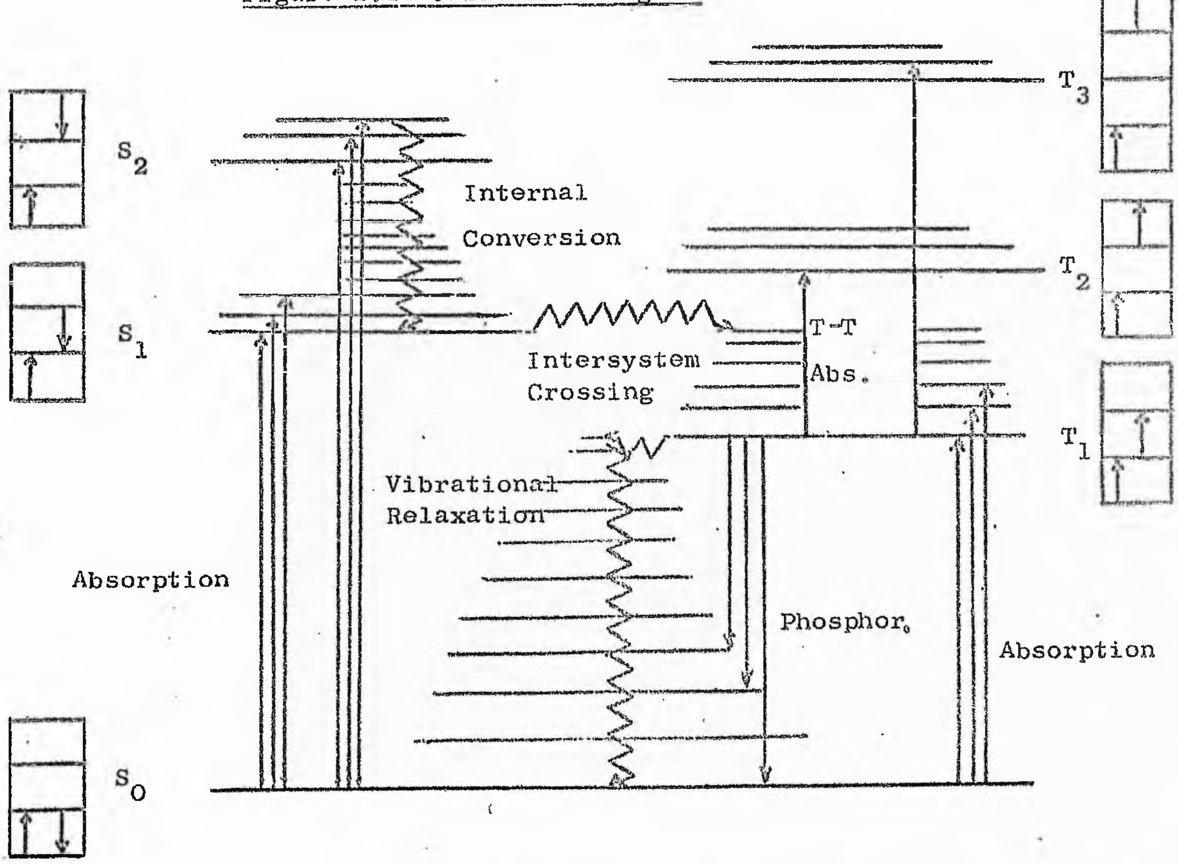

raised to an electronically and usually vibrationally excited state from which a photochemical or any one of a number of photophysical processes may occur. In general, there will be a number of such possible excited states for any molecule. For example, naphthalene[136] possesses two distinct absorption bands in the near ultraviolet corresponding to two different electronic transitions from the ground state. The ground states of most organic molecules have all electrons paired. The resultant spin, S, therefore equals zero and the multiplicity, M, (defined as 2S + 1) is unity. By using the convention introduced by Terenin[127] and Lewis et al[128,129], a ground state with multiplicity equal to one is designated a singlet state, symbolised S_0. Since spin is usually conserved in an electronic transition the resulting excited states will also be singlets with no net spin and may be designated S_1, S_2, S_3 etc. For every excited singlet state there will be a corresponding state where the excited electron has its spin parallel with the electron in the highest ground state orbital. The total spin, S, in this case is therefore one, the spin multiplicity three and the state referred to as a triplet state[127-129]. These triplet states according to Hunds first rule[130] will be lower in energy than the corresponding excited singlets.

As indicated above a molecule in an excited state can subsequently undergo photochemical and/or photophysical processes. Since we are mainly interested in the latter, photophysical processes will be discussed in more detail. Recent reviews by Day[131], Noyes et al[125], and Lower et al[132], and papers by Suppan[133], Turro[134] and Swenton[135] deal with the more photochemically orientated processes. The primary photophysical processes may be illustrated by means of a Jablonski diagram[136,137] (Fig. 1.4), which indicates the various intramolecular processes initiated by photon absorption. The box beside each electronic energy level indicates the molecular orbital electron configuration which best describes that level; the spin components of the two highest energy electrons are shown. The sub-boxes within each large box are molecular orbitals of the excited states of that particular molecule, the lowest sub-box being the highest filled molecular orbital of the ground state singlet, S_0. Only the two highest energy electrons are considered in Fig. 1.4, the others are paired in such a way that their total spin angular momentum is zero.

After absorption of a photon by a molecule, an electron is raised from the zero ground state vibrational level to a vibrational level of one of the molecules, electronic excited states. This process occurs in ca 10^{-15} seconds and is short relative to all other radiative and non-radiative processes, a fact made use of in the Frank-Condon principle[138,139]. Absorption can occur to any of the excited S_1, S_2, S_3 etc. states. However in almost every case an electron in an excited electronic vibrational level will rapidly lose its excess vibrational energy (10^{-11} - 10^{-14} seconds)[140] and return to the zero vibrational level of the corresponding electronic state, a process referred to as vibrational relaxation (see Fig. 1.4). With the exception of the S_0 and S_1 states, the energy separation between S_i and $S_{i\pm1}$ states are usually small, resulting in considerable overlap of their vibrational levels. Consequently any electron raised to an excited state of higher energy than S_1 will rapidly lose its excess energy and return to the S_1 state, a process referred to as internal conversion (see Fig. 1.4). This situation leads to the formulation of a general rule by Kasha which states, "In organic molecules in condensed media, the emitting level of a given multiplicity is the lowest excited level of that multiplicity." There are few exceptions to this rule, the only well substantiated one being the azulene molecule[142-144] where observed emission corresponds to the $S_2 \rightarrow S_0$ transition, although recent papers by Easterly et al[145,146], Dawson et al[147] and Kobyshev et al[148] present evidence for $S_2 \rightarrow S_0$ transitions in other molecules.

A molecule in the S_1 state can be deactivated by a radiative process, $S_1 \rightarrow S_0$, known as fluorescence (see Fig. 1.4). Interesting comparisons can be made between first excited state absorption spectra where the band shape is indicative of the vibrational spacings in the first excited state, S_1, and the fluorescent band shape which is indicative of the vibrational spacings of the ground state, S_0. Non-radiative deactivation of the S_1 state can occur via quenching processes where the excited S_1 state loses its energy to the immediate environment by kinetic interaction. Many authors are of the opinion[149-152] while others disagree[153-159] that the excited S_1 state may also be deactivated via the competitive non-radiative internal conversion process to the ground state ($S_1 \rightsquigarrow S_0$).

Radiative transitions between states of different multiplicities [e.g. between singlets and triplets ($S \leftrightarrow T$)] are theoretically forbidden. In practice because of spin-orbit coupling these transitions do take place although with extremely low probability compared to singlet-singlet ($S \leftrightarrow S$) or triplet-triplet ($T \leftrightarrow T$) spin-allowed transitions (see Fig. 1.4). The first spectroscopically observed singlet-triplet transition was reported by Sklar[160]. Population of a triplet level by direct absorption from the ground state is clearly a difficult process experimentally because the absorption is so weak. However intersystem crossing (see Fig. 1.4) can in many cases compete favourably with the previously mentioned deactivation routes of the first excited singlet state, S_1, and with subsequent internal conversion produce a molecule in the zero vibrational level of the first excited triplet state, T_1 (see Fig. 1.4). Since the radiative or non-radiative transition from the first excited triplet to the ground state is "forbidden" the lifetime of the T_1 state is relatively long (cf fluorescence). As a result of this long lifetime the T_1 state is usually very prone to environmental quenching. Care has to be exercised when studying processes from this level to ensure that the deactivation rate of the T_1 state is not influenced by quenching impurities e.g. molecular oxygen. The deactivation processes available to the T_1 state are analogous to those of the S_1 state, the radiative process $T_1 \longrightarrow S_0$ being referred to as phosphorescence (see Fig. 1.4). If the T_1 state can obtain sufficient thermal energy from the environment to promote itself to a higher vibrational level intersystem crossing of the type $T_1 \rightsquigarrow S_1$ may occur. Once the S_1 state is produced all the deactivation routes described above become available. The emission $S_1 \longrightarrow S_0$ after the subsequent $T_1 \rightsquigarrow S_1$ intersystem crossing is known to occur, a process called delayed fluorescence[123,161] (see Fig. 1.5).

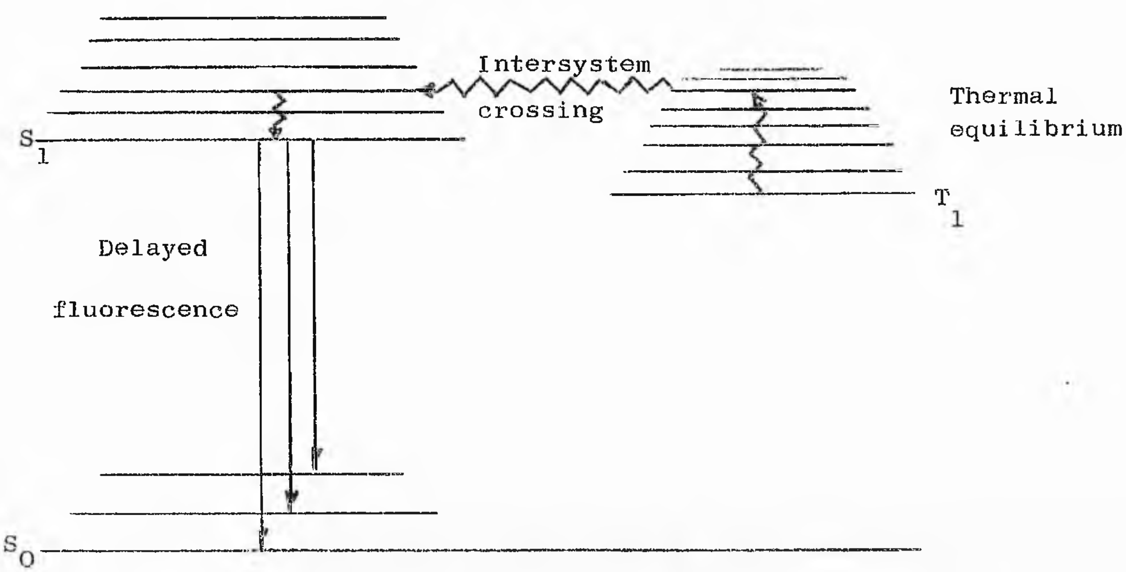

Fig. 1.5 Illustration of delayed fluorescence

The various primary photophysical processes which have been discussed above are summarised below.

Terminology	Definition	Rate(s^{-1})	Typical process
Absorption	Promotion of an electron to an energetically higher level.	10^{15}	$S_i \leftarrow S_0$
Internal Conversion	A non-radiative transition between two different electronic states of the same multiplicity.	10^{11}-10^{15}	$S_i \rightsquigarrow S_1$
Vibrational Relaxation	Transition from a non-equilibrium vibrational energy distribution in a given electronic state to the thermally equilibriated vibrational energy distribution relative to the zero-point energy of that same state.	$\geqslant 10^{12}$	$S_i^{V_i} \rightsquigarrow S_i^{V_0}$
Fluorescence	A radiative transition between two levels of the same multiplicity.	10^7-10^9	$S_1 \rightarrow S_0 + h\nu$
Intersystem Crossing	A non-radiative transition from an electronic state of a given spin multiplicity to an electronic state of a different spin multiplicity.	10^8	$S_1 \rightsquigarrow T_i$
Quenching and/ or Internal Conversion (see text)	Kinetic interaction with the adjacent environment.	10^5-10^7	$S_1 \rightsquigarrow S_0$
Phosphorescence	A radiative transition between two states of the same molecule which are of different multiplicity.	10-10^3	$T_1 \rightarrow S_0$
Quenching and/ or Intersystem Crossing		10-10^3	$T_1 \rightsquigarrow S_0$

(b) Nature of Electronic Transitions and States

The language of absorption spectroscopy is a mixture of quantum mechanical terms and words which describe empirically the appearance of spectra. Many types of notations have been developed to describe the differences between ground and electronically excited states of a molecule. A number of useful notations have been developed based upon the bonding properties of electrons before and after excitation. Only the classification of transitions first used by Kasha[141] will be considered here, although others are discussed in the reviews of Mulliken[162,163] and Platt[164,165].

In a typical organic molecule there can in general be three "types" of electrons, namely those residing in sigma bonding orbitals (σ), those residing in pi bonding orbitals (π), and if a heteroatom is present, those residing in the non-bonding orbitals (n). Excitation of one of these electrons will place it in a higher energy orbital; in the case of polyatomic molecules this will usually be a σ^* or π^* antibonding molecular orbital. Quite clearly a difference in the "type" of electron promoted and the higher energy orbital involved will have a profound effect on the electronic distribution of the excited state as well as the energy of the excited state. As reference will be made in subsequent chapters to π,π^* and n,π^* transitions they will be discussed in more detail below.

π,π^* transitions

A $\pi^* \leftarrow \pi$ transition may be pictorally represented as in Fig. 1.6, using the carbonyl chromophore as the example.

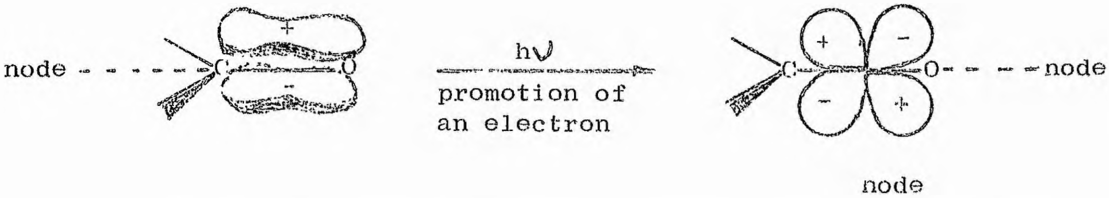

Fig. 1.6 Molecular orbital illustration of a $\pi^* \leftarrow \pi$

The π^* state orbital differs from the ground state π orbital in that it has an additional nodal plane perpendicular to the bond axis giving it antibonding character. There is considerable orbital overlap of the π^* and π states, giving rise to a low energy, high intensity ($\varepsilon_{max} \sim 10^4$-$10^5$) transition providing spin and symmetry rules are not forbidden. Both $S_1 \rightarrow S_0$ and $T_1 \rightarrow S_0$ π^*, π transitions are well documented for aromatic hydrocarbons, however the singlet-triplet splitting of the π, π^* states are generally large and the emission process from S_1 usually competes favourably with intersystem crossing generally resulting in relatively high fluorescent yields (Φf) compared to phosphorescent yields (Φp).

n,π^* transitions

Consideration of the non-bonding (n) orbital of a carbonyl oxygen and the antibonding π^* orbital of the chromophore (see Fig. 1.7) indicates there is very little overlap between such orbitals. Therefore, when an electron is promoted from the n to the π^* orbital, a $\pi^* \leftarrow n$ transition, the transition probability will in general be low (ε_{max} < 2000). Due to this small overlap the deactivation transition, $\pi^* \rightarrow n$, will have a relatively long lifetime and will be much more subject to non-radiative transitions than the $\pi^* \rightarrow \pi$ transition. Intersystem crossing will become an important deactivation path because of the

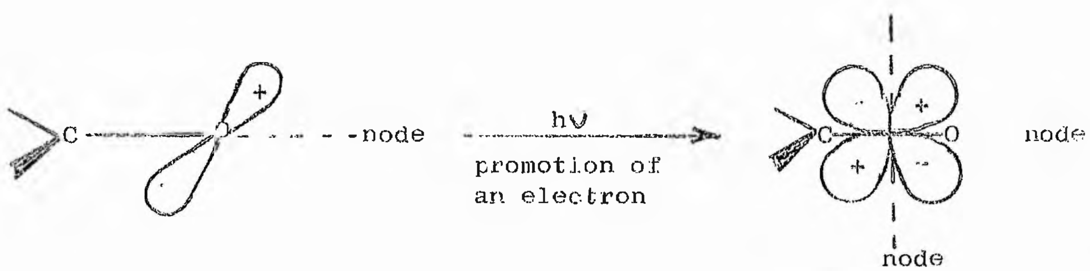

Fig. 1.7 Molecular orbital illustration of a $\pi^* \leftarrow n$ transition

long lifetime of the singlet n,π^* state and the small singlet n,π^*-triplet splitting. Phosphorescence is the radiative process usually associated with n, π states[140]. In molecules where both π,π^* and n,π^* transitions are possible, e.g. benzophenone, it is usually the n,π^* state which corresponds to the first excited singlet state, S_1 [140].

(c) Quantum Yield

A concept of major importance in photochemistry, which was first emphasised by Einstein, is that of quantum yield (or quantum efficiency), Φ. Since photochemistry has become so diverse the term quantum yield has obtained many definitions. However, as we are mainly interested in photophysical processes only the pertinent definitions will be given, although more extensive discussions can be found in books by Parker[139], Wayne[123] and Leermakers[124].

It has been shown in the preceding sections that the ground state and the lowest excited singlet and triplet states are the three most important states for the luminescence of most molecules. If only two of these states are involved in the processes of excitation and emission a suitable definition of Φ is "Quantum yield is the number of photons emitted by a particular excited state divided by the number of photons absorbed in going from the ground state to the same excited state." On the other hand, emission can occur from excited states which are difficult to populate directly. The direct absorption $T_1 \leftarrow S_0$ is weak, consequently, it is usual to excite the S_1 state by the $S_1 \leftarrow S_0$ absorption process and rely on the degradation of the S_1 state via intersystem crossing to populate the T_1 state; after which the emission $T_1 \rightarrow S_0$ can occur. The quantum yield for this process may be defined as, "The number of photons emitted by a particular excited state divided by the number of photons absorbed in going from the ground state to some other higher excited state."

3. INTERMOLECULAR ENERGY TRANSFER

(a) Introduction

Intermolecular transfer of electronic excitation energy is well known to occur in the vapour, liquid and solid phases, although the mechanisms by which the process occurs are clearly dependent upon the conditions. In solution and in the gas phase, the mechanism may be collisional in nature, i.e. diffusion controlled. The rapid deactivation of triplet states by molecular oxygen has been known for a considerable time, and the quenching of reaction paths by oxygen is often used as a diagnostic method to detect triplet state intermediates. Intermolecular energy transfer in solution is an important technique widely used to excite acceptor molecules specifically to an excited state of a particular multiplicity, therby distinctions can be made between the physical and the chemical properties of excited states of different multiplicities.

Intermolecular energy transfer may occur by radiative processes involving the emission of a photon by the donor molecule and its subsequent absorption by the acceptor molecule. It may also occur by a non-radiative process due to the interaction between donor and acceptor molecules during the lifetime of the donor, prior to its emission of a photon. Non-radiative transfer due to Coulombic (e.g. dipole-dipole) interactions may take place over distances of approximately 2-6 nm, which are large compared to molecular diameters and those due to electron-exchange interactions over distances of approximately 0.6-1.5 nm somewhat larger than the molecular diameter (ca 0.6 nm). In solutions collisional interaction due to Coulombic, electron exchange, exciton resonance and charge-transfer interactions, may yield excimers or exciplexes, the dissociation of which provide a further mechanism of non-radiative energy transfer. The principle mechanisms of energy transfer from an excited donor molecule ($^1M^*$ and $^3M^*$) to an acceptor molecule in a singlet ground state (^1Y) may be classified as follows.

Radiative transfer

singlet-singlet:

$$^1M^* \longrightarrow {}^1M + h\nu_f; \qquad {}^1Y + h\nu_f \longrightarrow {}^1Y^* \qquad 1.7$$

triplet-singlet:

$$^3M^* \longrightarrow {}^1M + h\nu_p; \qquad {}^1Y + h\nu_p \longrightarrow {}^1Y^* \qquad 1.8$$

Singlet-triplet and triplet-triplet radiative transfer processes are normally negligible because of the low $T_1 \longleftarrow S_0$ absorption intensity of the acceptor, ^1Y.

Collisional transfer due to exciplex formation

singlet-singlet:

$$^1M^* + {}^1Y \longrightarrow {}^1(M \cdot Y)^* \longrightarrow {}^1M + {}^1Y^* \qquad 1.9$$

triplet-triplet:

$$^3M^* + {}^1Y \longrightarrow {}^3(M \cdot Y)^* \longrightarrow {}^1M + {}^3Y^* \qquad 1.10$$

Non-radiative transfer due to electron exchange interaction

singlet-singlet:

$$^1M^* + {}^1Y \longrightarrow {}^1M + {}^1Y^* \qquad 1.11$$

triplet-triplet:

$$^3M^* + {}^1Y \longrightarrow {}^1M + {}^3Y^* \qquad 1.12$$

Non-radiative transfer due to Coulombic interaction

singlet-singlet:

$$^1M^* + {}^1Y \longrightarrow {}^1M + {}^1Y^* \qquad 1.13$$

triplet-singlet:

$$^3M^* + {}^1Y \longrightarrow {}^1M + {}^1Y^* \qquad 1.14$$

Singlet-triplet and triplet-triplet Coulombic transfer is normally negligible because of the low T_1-S_0 transition moment.

The conditions for Coulombic transfer (1.13 and 1.14) are similar to those for radiative transfer (1.7 and 1.8) namely an overlap of the donor emission spectrum and the acceptor absorption spectrum, and an allowed transition in the acceptor. The conditions for electron-exchange transfer (1.11 and 1.12) are similar to those for collisional transfer (1.9 and 1.10), namely short-range interaction between the donor and acceptor molecules and spin conservation in the transition. Summarising, singlet-singlet transfers can occur radiatively, collisionally, by electron-exchange and by Coulombic interactions; triplet-triplet transfer can occur collisionally or by electron-exchange interaction; triplet-singlet transfer can occur radiatively or by Coulombic interactions.

(b) Intermolecular Energy Transfer between Organic Molecules

Triplet-triplet energy transfer is the most commonly observed transfer process in solution. It was first clearly demonstrated by Terenin _et al_[166], who studied the quenching of donor phosphorescence by different triplet acceptors in rigid media at 77 K. Ermolaev[167], by studying other rigid solution systems demonstrated that the triplet-triplet transfer process was consistent with electron-exchange interaction. Triplet-triplet energy transfer in fluid solution was first investigated by Bäckström _et al_[168], who used biacetyl as the donor in benzene solution at room temperature. Porter _et al_[169], investigated triplet-triplet energy transfer by the method of flash photolysis whereby they studied the decay time of the donor. They were able to exclude the singlet-triplet process as a possible energy transfer mechanism route by the fact that the donor fluorescence yield was unchanged by the presence of acceptor. Smaller *et al*[170], studied triplet-triplet transfer from phenanthrene·d_{10} to naphthalene·d_8 in viscous solution at 87°K. They observed by esr the decay of the donor triplet concentration and the rise and decay of the acceptor triplet concentration following flash excitation. Evidence for triplet-singlet energy transfer was first obtained by Ermolaev *et al*[171], from observations of donor phosphorescence quenching and sensitised acceptor fluorescence in rigid solutions at 77 K. Their results confirmed that the transfer occurs by long-range dipole-dipole interactions. Bennett *et al*[172], have made a detailed kinetic study of triplet-singlet transfer from phenanthrene·d_{10} to rhodamine B in cellulose acetate. High molecular weight polymer matrices have been used to study singlet-singlet energy transfer between pyrene donor and perylene acceptor[173].

In molecular aggregates or crystals, coupling between molecules may occur as a result of increased interaction energies. Exciton theory using either the 'bound' or 'free' exciton concepts successfully explains many features of absorption and emission spectra in crystals. Long range transfer from a 'host' to a 'guest' molecule can occur by migration of the 'host' exciton until it meets a 'guest' molecule which acts as an energy 'trap'. Both singlet and triplet exciton transfer mechanisms have been shown to operate in organic crystals[174]. Singlet exciton transfer generally operate through Coulombic interaction while triplet exciton transfer is more likely to occur via exchange interactions[174]. Many of the organic crystals studied are doped polybenzenoid systems e.g. naphthalene, anthracene, phenanthrene and biacetyl[174]. An exciton mechanism for energy transfer of many organic aggregates may be confirmed by the absence of sensitised luminescence in solution.

(c) Intermolecular Energy Transfer Involving Lanthanide Ions

Intermolecular energy transfer may take place from a triplet excited organic molecule to a lanthanide compound by a diffusion-controlled process, in a manner analogous to the triplet-singlet and triplet-triplet energy transfer processes described above. Both chelated and unchelated lanthanide ions have been investigated using various ketones as sensitisers[175-183]. El-Sayed et al[175,176], found evidence that the benzophenone triplet can transfer its energy to europium chelates by a diffusion-controlled process and Matovich et al[177], have reported that, in acetophenone and other aromatic ketones, lanthanide salts can be excited via the solvent. Ballard et al[178], studied the concentration dependence of the emission spectra of solutions of the nitrates of Sm^{3+}, Dy^{3+}, Tb^{3+} and Eu^{3+}. They interpreted their results in terms of diffusion-controlled transfer from the acetophenone triplet to the lanthanide ions. Heller et al[179], found that the luminescent levels of Tb^{3+} and/or Eu^{3+} could be sensitised by diffusion-controlled transfer of energy from the triplet state of numerous aromatic aldehydes and ketones in acetic acid. Filipescu et al[180-183], have studied the photokinetics of energy transfer to Tb^{3+} and Eu^{3+} ions in aromatic ketones.

Lanthanide-lanthanide energy transfer processes have recently been investigated in inorganic glasses[184-189]. Antipenko et al[184], have demonstrated the increase in the effectiveness of non-radiative energy transfer between lanthanide ions in aqueous solution by the addition of LiCl which lead to the formation of complex aggregates. Sommerdijk et al[185,186], have observed infrared excited visible luminescence in lattices doped with Yb^{3+} and Er^{4+}. They conclude that lanthanide-lanthanide energy transfer is in part responsible for the ion-fluorescence. Van Vitert *et al*[187-188], have studied lanthanide-lanthanide transfer processes in tungstates and conclude that they are due to multipole-multipole interactions. Effects of temperature and concentration on the energy transfer process between Er^{3+} and Ho^{3+} in yttrium alluminium garnet have been discussed by Karpick *et al*[189].

4. INTRODUCTION TO THE EXPERIMENTAL INVESTIGATIONS

The attainment of laser action in solution with several fluorescent lanthanide chelates[112,190-198] served as a stimulus for renewed interest in their coordination chemistry. In order to produce laser action, the lanthanide ion must be capable of excitation with the available light sources at a rate sufficient to achieve the necessary degree of population inversion[199]. In lanthanide chelates the population inversion is attained by pumping the absorption band of the organic moiety, from which energy is transferred intramolecularly to the lanthanide ion. Only the Eu^{3+} and Tb^{3+} ions when chelated have sufficiently high quantum yields to be considered as potentially useful lasing materials in solution[194]. However, Eu^{3+} chelates have received most of the attention in this field because of their higher quantum yields and better monochromatic emission characteristics. In fact, the first laser activity from a Tb^{3+} chelate was reported by Bjorklund *et al*[195], as late as 1967. They observed laser action from terbium *tris* trifluoroacetylacetonate in p-dioxane and acetonitrile at room temperature.

The potential laser action from these chelates encouraged investigations into the path, mechanism, and overall quantum efficiency of the energy transfer process. Unfortunately, investigations were in general limited to Eu^{3+} chelates which were known to produce laser action, e.g. piperidium europium <u>tetrakis</u> benzoyltrifluoroacetonate (XXIV) and related salts[200]. However, direct investigations of these luminescent processes has been hampered by the fact that spectroscopic properties observed in solution do not always arise from a single species

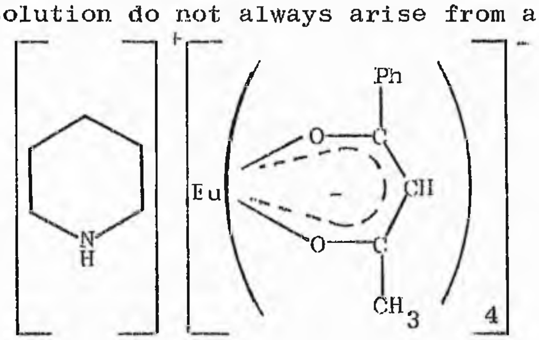

(XXIV)

but in many cases from a mixture produced by dissociation[201]. Samelson <u>et al</u>[201], dealing with Eu^{3+} lasing materials have attempted to characterise the numerous species present in various solvents and conclude that for both <u>tris</u> and <u>tetrakis</u> chelates at concentrations as high as 10^{-2} M that there is appreciable dissociation in all the solvents studied. Many of these chelates are unstable to the high energy flashes required to produce laser action[191]. This factor and that of absorption coefficients lead to the investigations employing ketone sensitisers in solutions containing chelated[175,176,202] and unchelated[177-183,203] lanthanide ions. The energy initially absorbed by the sensitiser is transferred intermolecularly to the lanthanide species with subsequent fluorescence from the ion emitting levels. The fact that the sensitiser absorbed the spectral flash overcame the problem of decomposition of the lanthanide chelates in solution. Little attention has been given to energy transfer processes and quantum yields of lanthanide chelates other than those pertinent to laser applications, although investigations reported in recent papers have determined quantum yields and elucidated energy transfer mechanisms of unchelated ions in inorganic glasses and other media[184-189,204-219].

In this thesis the elucidation of energy transfer processes in lanthanide chelates in solution and the solid state has been attempted in the case of several fluorescent Tb^{3+} and Eu^{3+} β-diketoenolates. Particular attention has been given to mixed chelate systems where the possibility of chelate triplet-triplet and/or lanthanide-lanthanide energy transfer has been investigated. Relative quantum efficiencies have been determined for homologous series of *tetrakis* Tb^{3+} and Eu^{3+} chelates in solution and the solid state to determine the cation dependence on their fluorescent properties. Lifetime measurements of numerous lanthanide chelate systems have been determined to aid the elucidation of transfer mechanisms. The importance of studying the solid chelates where the chemical species have been characterised by elemental analysis is demonstrated by molecular weight and conductance measurements on these or similar chelates in solution. Both types of measurement indicate varying degrees of dissociation depending on the particular chelate, making positive identification of the species under investigation difficult or impossible.

CHAPTER 2

EXPERIMENTAL TECHNIQUES

1. SYNTHESIS OF LANTHANIDE β-DIKETOENOLATE COMPLEXES

(a) INTRODUCTION

Numerous methods for the synthesis of β-diketoenolate lanthanide complexes have appeared in the literature[50,72-75,89,109,112,194,220-232], many of which have been critically examined by Lyle *et al*[72]. However much of the earlier work[109,194,224,225] is of dubious value. Information regarding the methods of preparation were often vague and analytical and melting point figures were not always reported. Many of these earlier papers referred to the work of Crosby *et al*[109], who stated only that chelates were precipitated from solutions of the lanthanide chloride and diketone in ethanol, water or methanol by addition of piperidine. In a later paper, Whan *et al*[112], reported the preparation of lanthanide tris(1,3-diphenyl-1,3-propanedionato) chelates. In this procedure an alcoholic solution of the lanthanide chloride and a 25% excess of ligand was treated with piperidine and concentrated to precipitate the product. It was observed that it was necessary to submit the product to prolonged vacuum drying at 125-150^{o}C to drive off an "extra mole of chelating ligand", before obtaining the desired *tris* product. Many workers adopted this "piperidine method" of Crosby *et al*, without subsequent analysis and characterisation and therefore the purity of the compounds prepared is doubtful.

Another inconsistancy in the literature is the reported degree of hydration of particular *tris* chelates[50,89]. Pope et al[50], have also noted inconsistancies in melting points appearing in the literature, supposedly of the same compound. Investigations by Pope et al[50], concluded that only mono- and trihydrates are formed. More recent work by Richardson et al[89] has included the isolation of anhydrous, mono-, di- and trihydrates which were the results of particular crystallisation and drying procedures. Synthesis of tris chelates reported in this thesis indicate, that the degree of hydration is dependent on ion size and the steric hindrance of the coordinating ligands. Specific synthetic procedures have been used to obtain chelates required for subsequent investigations and these are described below. The preparative procedures, microanalysis and melting points for particular chelates are summarised in Table 2.1. Microanalysis were obtained using a Perkin Elmer Model 240 elemental analyser.

(b) Preparative Methods

Lanthanide salts

99.9% Eu_2O_3, Gd_2O_3, Nd_2O_3, Tb_2O_3, Er_2O_3 (Koch-Light) and Sm_2O_3 (Rare Earth Products) were converted to the chloride by refluxing in concentrated hydrochloric acid ($\sim$11M) until dissolution was complete. The lanthanide chloride was obtained by removal of excess HCl and water employing a rotary evaporator.

Ligands

Acetylacetone (Fisons), benzoylacetone (BDH), benzoyltrifluoroacetylacetone (Fluka), dipivaloylmethane (Ralph N. Emanuel), hexafluoroacetylacetone, trifluoroacetylacetone (Koch-Light) and 1,1,1,2,2,3,3-heptafluoro-7,7-dimethyloctane-4,6-dione (Fluorochem) were used without further purification. 3-Cyanoacetylacetone and ethyl diacetylacetate were prepared by the following methods.

TABLE 2.1

Analytical data for lanthanide chelates

Compound	M.p.[a]/°C	ANALYSIS Found % C	H	N	Calc % C	H	N	Preparative Method [b]
$Tb(aa)_3 3H_2O$	140-141	35.3	5.3	-	35.3	5.4	-	(a)
$Tb(aa)_4K$	> 250[c]	40.5	5.1	-	40.4	4.7	-	(d)
$Tb(ba)_4$pipH	133-134	60.9	5.5	1.5	60.7	5.4	1.6	(e)
$Tb(btfa)_3 2H_2O$	135-137	42.5	2.7	-	42.8	2.6	-	(a)
$Tb(btfa)_4$pipH	166-167	49.1	3.2	1.1	48.9	3.3	1.3	(e)
$Tb(3CNaa)_3 2H_2O$	263[d]	38.3	3.8	7.4	38.1	3.9	7.4	(a)
$Tb(dpm)_3$	176-177	55.8	8.3	-	55.9	8.1	-	(g)
$Tb(dpm)_3$pyr	132-133	58.2	7.8	1.9	57.9	7.9	1.8	(h)
$Tb(edaa)_3 \cdot H_2O$	63[d]	42.0	4.9	-	41.7	5.1	-	(a)
$Tb(fod)_3 H_2O$	47[d]	33.6	2.8	-	33.9	3.0	-	(a)
$Tb(hfaa)_3 \cdot 2H_2O$	120-121	21.9	0.8	-	22.1	0.9	-	(b)
$Tb(hfaa)_4$pipH	110-111	28.2	1.6	1.1	28.0	1.5	1.3	(f)
$Tb(hfaa)_4 NH_4$	207-208	23.9	0.7	1.4	23.9	0.8	1.4	(f)
$Tb(hfaa)_4 Ph_4As$	136-137	38.4	1.7	-	38.5	1.8	-	(c)
$Tb(hfaa)_4 Me_4N$	244-245	27.0	1.5	1.4	27.1	1.5	1.3	(c)
$Tb(hfaa)_4 Et_3NH$	136-137	28.4	1.9	1.2	28.7	1.8	1.3	(f)
$Tb(hfaa)_4 Bu^tNH_3$	93-94	26.7	1.6	1.3	27.1	1.5	1.3	(f)
$Tb(hfaa)_4$picH·pic	97-98	32.2	1.6	2.2	32.7	1.6	2.4	(f)
$Tb(hfaa)_4$pyrH·pyr	76-77	31.1	1.2	2.4	31.4	1.3	2.4	(f)
$Tb(hfaa)_4$pyrH	145-146	27.8	0.9	1.3	28.1	0.9	1.3	(f)
$Tb(tfaa)_3 \cdot 2H_2O$	139-140	27.4	2.5	-	27.5	2.5	-	(a)
$Tb(tfaa)_4$pipH	100-101	34.9	3.3	1.7	35.0	3.3	1.6	(e)
$Tb(tfaa)_4 NH_4$	174-175	30.2	2.7	2.1	30.4	2.5	1.8	(e)
$Tb(tfaa)_4 Ph_4As$	162-163	45.7	3.2	-	45.8	3.1	-	(c)
$Tb(tfaa)_4 Na$	> 250[c]	30.4	2.0	-	30.2	2.0	-	(d)
$Tb(tfaa)_4 K$	> 250[c]	29.6	2.0	-	29.6	2.0	-	(d)
$Tb(tfaa)_4 Cs$	214-215	26.6	1.8	-	26.6	1.8	-	(d)
$Gd(aa)_3 \cdot 3H_2O$	141-142	35.1	5.2	-	35.4	5.3	-	(a)
$Gd(aa)_4 K$	> 250[c]	40.3	4.9	-	40.5	5.3	-	(d)
$Gd(ba)_4$pipH	133-134	60.9	5.7	1.8	60.9	5.4	1.6	(e)
$Gd(btfa)_3 \cdot 2H_2O$	141-143	43.1	2.8	-	43.0	2.6	-	(a)
$Gd(btfa)_4$pipH	161-162	49.2	3.3	1.5	49.0	3.3	1.3	(e)
$Gd(3CNaa)_3 H_2O$	265[d]	39.6	3.4	7.8	39.5	3.7	7.7	(a)
$Gd(dpm)_3$	177-178	56.2	8.3	-	56.1	8.1	-	(g)
$Gd(dpm)_3$pyr	133-134	57.8	8.2	1.6	58.1	7.9	1.8	(h)

Compound	M.p.[a]/°C	ANALYSIS						Preparative Method [b]
		Found %			Calc %			
		C	H	N	C	H	N	
$Gd(cdaa)_3H_2O$	96[d]	42.2	5.0	-	41.9	5.1	-	(a)
$Gd(fod)_3H_2O$	54[d]	33.6	3.1	-	33.9	3.0	-	(a)
$Gd(hfaa)_3 \cdot 2H_2O$	124-125	22.3	0.8	-	22.1	0.9	-	(b)
$Gd(hfaa)_4pipH$	128-129	28.2	2.0	1.6	28.0	1.5	1.3	(f)
$Gd(hfaa)_4NH_4$	205-206	24.0	0.8	1.4	24.0	0.8	1.4	(f)
$Gd(hfaa)_4Ph_4As$	136-137	38.3	1.7	-	38.6	1.8	-	(c)
$Gd(hfaa)_4Me_4N$	235-236	27.1	1.5	1.5	27.2	1.5	1.3	(c)
$Gd(hfaa)_4Et_3NH$	134-135	28.7	2.0	1.2	28.7	1.8	1.3	(f)
$Gd(hfaa)_4Bu^tNH_3$	95-96	27.5	1.9	1.6	27.2	1.5	1.3	(f)
$Gd(hfaa)_4picH \cdot pic$	97-98	32.6	1.6	2.5	32.8	1.6	2.4	(f)
$Gd(hfaa)_4pyrHpyr$	78-79	31.4	1.3	2.4	31.5	1.3	2.5	(f)
$Gd(tfaa)_3 \cdot 2H_2O$	142-143	28.7	2.4	-	28.4	2.2	-	(a)
$Gd(tfaa)_4pipH$	90-92	35.2	3.5	1.6	35.1	3.3	1.6	(e)
$Gd(tfaa)_4NH_4$	170-171	30.6	2.6	1.9	30.5	2.5	1.8	(e)
$Gd(tfaa)_4Ph_4As$	158-159	45.8	3.1	-	45.8	3.1	-	(c)
$Gd(tfaa)_4Na$	> 250[c]	30.3	2.1	-	30.3	2.0	-	(d)
$Gd(tfaa)_4K$	> 250[c]	30.0	2.0	-	29.7	2.0	-	(d)
$Gd(tfaa)_4Cs$	214-215	26.9	2.1	-	26.6	1.8	-	(d)
$Eu(aa)_3 \cdot 3H_2O$	141-142	35.6	5.4	-	35.8	5.4	-	(a)
$Eu(dpm)_3$	181-182	56.3	8.1	-	56.5	8.2	-	(g)
$Eu(fod)_3H_2O$	56[d]	33.9	3.1		34.1	3.0		(a)
$Eu(hfaa)_4Ph_4As$	135-136	38.7	1.8	-	38.8	1.8	-	(c)
$Eu(hfaa)_4Me_4N$	231-232	27.4	1.6	1.4	27.3	1.5	1.3	(c)
$Eu(hfaa)Et_3NH$	131-132	28.6	2.0	1.3	28.9	1.9	1.3	(f)
$Eu(hfaa)Bu^tNH_3$	95-96	27.0	1.7	1.5	27.3	1.5	1.3	(f)
$Eu(hfaa)_4picH \cdot pic$	97-98	32.7	1.6	2.4	32.9	1.6	2.4	(f)
$Eu(hfaa)_4pyrH$	147-148	28.2	0.9	1.3	28.3	0.9	1.3	(f)
$Eu(hfaa)_42NH_2pyrH$	113-114	27.8	1.2	2.8	27.9	1.0	2.6	(f)
$Eu(hfaa)_4quinH \cdot$	124-125	31.3	1.0	1.3	31.4	1.1	1.3	(f)
$Eu(tfaa)_4Ph_4As$	140-141	45.7	3.1	-	46.0	3.1	-	(c)
$Sm(aa)_3 \cdot 3H_2O$	140-141	35.9	5.2	-	35.9	5.4	-	(a)
$Nd(aa)_3 \cdot 2H_2O$	160-161	38.5	5.1	-	37.7	5.2	-	(a)

a Uncorrected thermometer

b See Text

c Compounds char before melting

d completely melts at that temperature, appears to lose water earlier

pipH = piperidinium cation; picH = 4-methyl pyridinium cation;
pic = 4-methylpyridine; pyrH = pyridinium cation; pyr = pyridine;
$2NH_2pyrH$ = 2-amino-pyridine; quinH = quinolinium cation

3-cyanoacetylacetone (3CNHaa)

The method used was a modification of that reported by Fackler[233]. Sodium acetylacetonate[234] was dissolved in absolute ethanol and cooled to $0^{o}C$. Cyanogen (Matheson Co. Inc.) was passed through the solution until the uptake of gas was complete, the exit gases being passed through sodium hydroxide solution. The intermediate imido compound was filtered by suction and immediately treated with 3M sodium hydroxide solution. After dissolution was complete, ice was added and the solution neutralised with 6M hydrochloric acid. The β-diketone which crystallised from the solution was filtered off and purified by precipitation as the copper(II) complex with aqueous copper(II)acetate and subsequent decomposition of the complex with dilute sulphuric acid. The β-diketone was finally recrystallised from 1:6:30 acetone-ethanol-water and was used without subsequent analysis.

Ethyl diacetylacetate (Hedaa)

This ligand was synthesised by the method of Spassow[235]. A mixture of magnesium turnings (0.5 mole), ethyl acetoacetate (1 mole), and acetyl chloride (1.5 mole) in dry benzene was heated under reflux for two hours, care being taken to exclude moisture. The yellow reaction mixture was cooled in an ice bath and the liquid portion decanted into a separating funnel. The residue was washed with portions of ether and the ethereal solution poured onto ice. The ether-water mixture was then added to the benzene solution in the separating funnel, and the mixture shaken thoroughly; the aqueous layer was drawn off and discarded. The benzene-ether solution was washed once with 5% sodium bicarbonate solution followed by washing with water and finally dried over calcium chloride. The ether and most of the benzene was removed by distillation from a water bath. The remainder of the benzene was removed at 50°C at 50 mm pressure. The ethyl diacetylacetate was precipitated as the copper(II) complex using aqueous copper(II)acetate. Subsequent decomposition of the complex with dilute sulphuric acid and ether extraction of the ligand followed by vacuum distillation afforded the ligand which distilled between 95-97°C at 12 mm. The ligand was used without subsequent analysis.

Lanthanide chelates

Method (a) *tris* hydrates

The ligand (3 mole) and the lanthanide chloride (1 mole) were added to a 50% ethanol solution. The pH of the solution was slowly raised to pH 6.3 by dropwise addition of 0.5M ammonium hydroxide solution. Precipitation in many cases occurred around pH 6.0.

Method (b) Hhfaa *tris* hydrates

The ligand (3 mole) and the lanthanide chloride (1 mole) were dissolved in a 50% ethanol solution. 0.5M sodium hydroxide was added to the boiling solution until the pH reached 6.3. In many cases the product was an oil which was extracted with ether and recrystallised from n-hexane.

Method (c) quaternary salts of *tetrakis* chelates

Aqueous solutions of lanthanide salt (1 mole) and the quaternary salt (2.5 mole) were added to a 95% ethanol solution of the ligand (4 mole) and sodium hydroxide (4 mole). The volume was reduced by boiling until crystallisation began. Sufficient ethanol to redissolve the product was added and the solution cooled to afford the product.

Method (d) alkali metal salts of tetrakis chelates

An aqueous solution of lanthanide salt was added dropwise to a rapidly stirred 95% ethanol solution of the ligand (4.5 mole) and the alkali metal hydroxide at room temperature. Precipitation took place almost instantaneously. In the case of acetylacetone a boiling ethanol solution was necessary to give the desired product.

Method (e) amine salts of tetrakis chelates

An aqueous solution of the lanthanide salt (1 mole) was added dropwise to a 95% ethanol solution of the ligand (4.5 mole) and the amine base (4.5 mole). In many cases the product crystallised from solution on standing. The addition of small amounts of water gave more rapid precipitation from the solution.

Method (f) amine salts of tetrakis Hhfaa chelates

A 95% ethanol solution of the ligand (4 mole), amine base (8 mole) and lanthanide salt was boiled to remove most of the ethanol before drowning the solution in water to give the crude product.

Method (g) Hdpm tris chelates

A 50% ethanol solution of the lanthanide salt (1 mole) was added to a 75% ethanol solution containing the ligand (3 mole) and sodium hydroxide (3 mole). The solution was reduced in volume by means of a rotary evaporator before the addition of water to precipitate the product.

Method (h) adducts of tris (dpm) chelates

Adducts of tris (dpm) chelates were prepared by recrystallising the anhydrous chelate from the complexing solvent.

All compounds were dried under vacuum using calcium chloride as desiccant. The *tris* compounds with the exception of the dpm complexes which were purified by vacuum sublimation were submitted for analysis without further purification. The *tetrakis* hfaa chelates were purified from chloroform,the others from ethanol-water mixtures.

2. GROUND STATE ABSORPTION SPECTROSCOPY

Two spectrophotometers, a Unicam SP500 and a Unicam SP800 were used to record absorption spectra. The SP800, a continuous scanning spectrophotometer, was used to obtain absorption curves as a function of wavelength between 200 nm and 850 nm. The SP500 with its temperature control facilities was used for more accurate measurements of optical density at specific wavelengths between 185 nm and 1000 nm. All measurements were carried out in optically balanced fluorescence quartz cells with PTFE stoppers, using as reference the pure solvent. All optical densities, unless otherwise stated, have been recorded on the SP500 at ambient temperature. Extinction coefficients are quoted in units of $cm^{-1} mol^{-1} l$. The units of extinction coefficient may be converted to SI units, $m^2 mol^{-1}$, by multiplying by 10.

3. EMISSION SPECTROSCOPY

Two spectrofluorimeters were used to obtain emission and excitation spectra both in the solid and liquid state. General descriptions of these are given below.

(a) Perkin Elmer Hitachi MPF-2A

The MPF-2A, in conjunction with its phosphorescence, solid sampler and constant temperature cell holder accessories allowed measurement of emission and excitation spectra of solids and solutions over the temperature range 77K to ambient.

The MPF-2A uses a standard R106 photomultiplier and two grating monochromators (600 lines mm^{-1}). The excitation monochromator permits irradiation of a sample with monochromatic light between the range 200-700 nm while the emission monochromator selectively measures the intensity of the light emitted from the sample between 200-800 nm. Both monochromators are continuous scanning within their respective ranges. Emission and excitation spectra were initially obtained as a function of photomultiplier current against wavelength. Excitation spectra were obtained by setting the emission monochromator at a wavelength at or near the emission maximum and scanning with the excitation monochromator, while the emission spectra were obtained by exciting the sample at or near the absorption maximum and scanning with the emission monochromator. Resolution of the various spectra depended on the emission and excitation slit widths. These slits could be set to give a band pass of approximately 1 to 40 nm.

The light source was a 150 watt Xenon lamp giving a near continuum from ca 270-800 nm. Changes in light fluctuations during scanning procedures could be directly compensated for by using the instrument's 'reference' mode. Before dispersion at the excitation monochromator the light beam is split, one portion being focused onto a reference photomultiplier where a reference signal, which is used in the ratio recording mode to allow for changes in intensity, is produced. The other portion is dispersed by the excitation monochromator and focused onto the sample. Light emitted by the sample, after dispersion by the emission monochromator is focused onto the R106 photomultiplier producing a signal related to the emission intensity which was subsequently amplified and relayed to a pen recorder.

Although all spectra represented in this thesis and produced by the MPF-2A have been obtained using the reference mode, numerous experimental investigations using the direct mode (i.e. there is no compensation for intensity fluctuations) indicate that only minor fluctuations in the lamp intensity occur over short periods of time.

(b) High Resolution Spectrofluorimeter

A locally designed spectrofluorimeter was used to measure high resolution spectra of solid materials and solutions over a temperature range of 77K to ca 360K. It consisted of an emission 1200 lines mm^{-1} monochromator incorporated in a Hilger Watts Monospek 1000. The light source used was a water cooled medium-pressure mercury lamp filtered to pass only the 365.5 nm radiation. The exciting light was focused onto the sample which could be set at any angle to the incident radiation by means of a rotatable cell which was located in a four windowed dewar with cell housing (see Fig. 2.1). Light emitted from the sample was focused by means of a lens onto the monochromator incident slits and the dispersed light from the monochromator excident slits was focused onto the EMI 9526 photomultiplier. The signal to noise ratio was enhanced by using a phase sensitive detector (Brookdeal Electronics) before subsequent amplification and relay of the signal to a pen recorder (Leeds and Northrup Speedomax). The solution and solid sample cells used in conjunction with the Monospek are illustrated in Figs. 2.2 and 2.3 respectively.

Comparison of the emission spectra of identical samples obtained from the MPF-2A and the Monospek (see Fig. 2.4) indicated

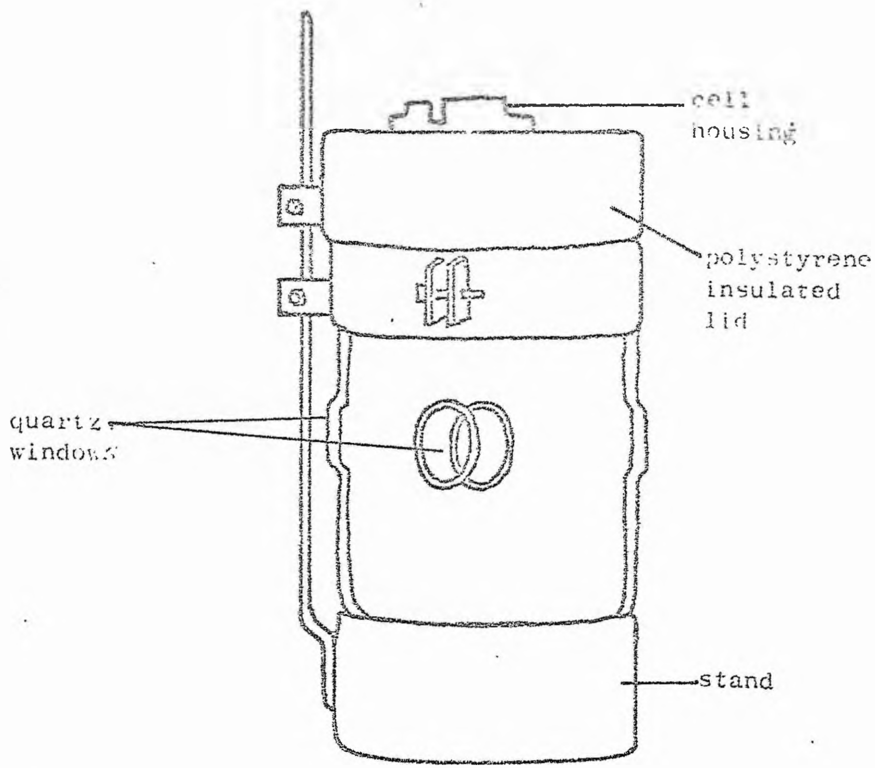

Fig. 2.1 Sample dewar

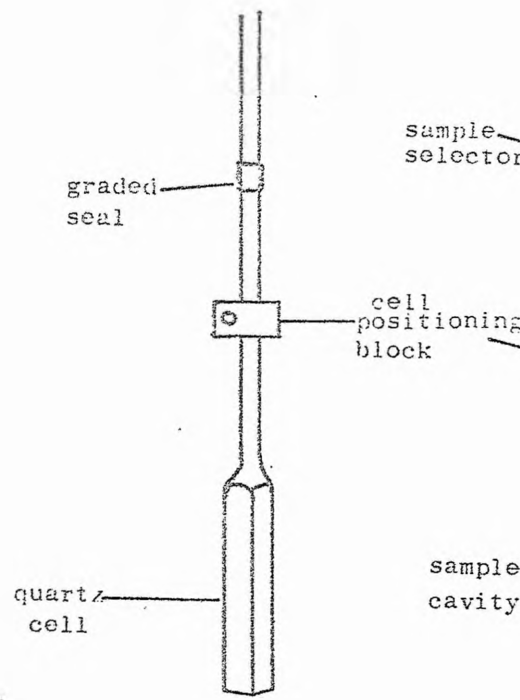

Fig. 2.2 Solution cell

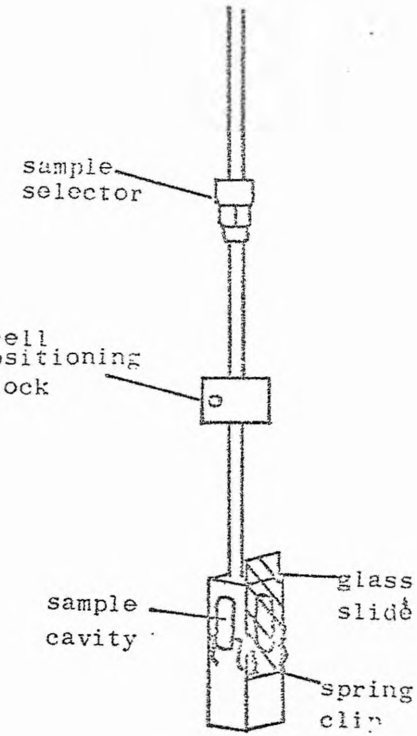

Fig. 2.3 Solid sampler

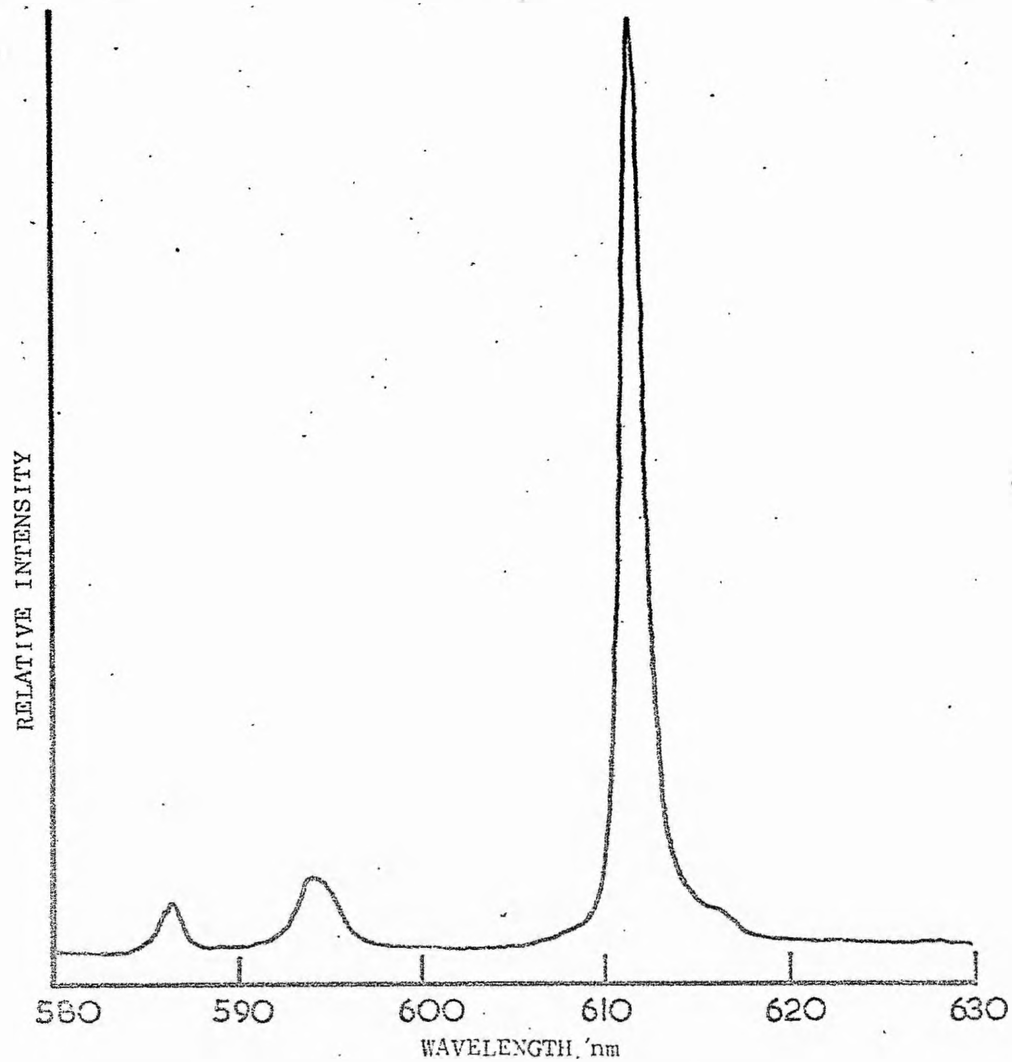

Fig. 2.4a Corrected emission spectrum obtained using the high resolution spectrofluorimeter for solid $Eu(hfaa)_4$·[illegible]$_4$ at 293K

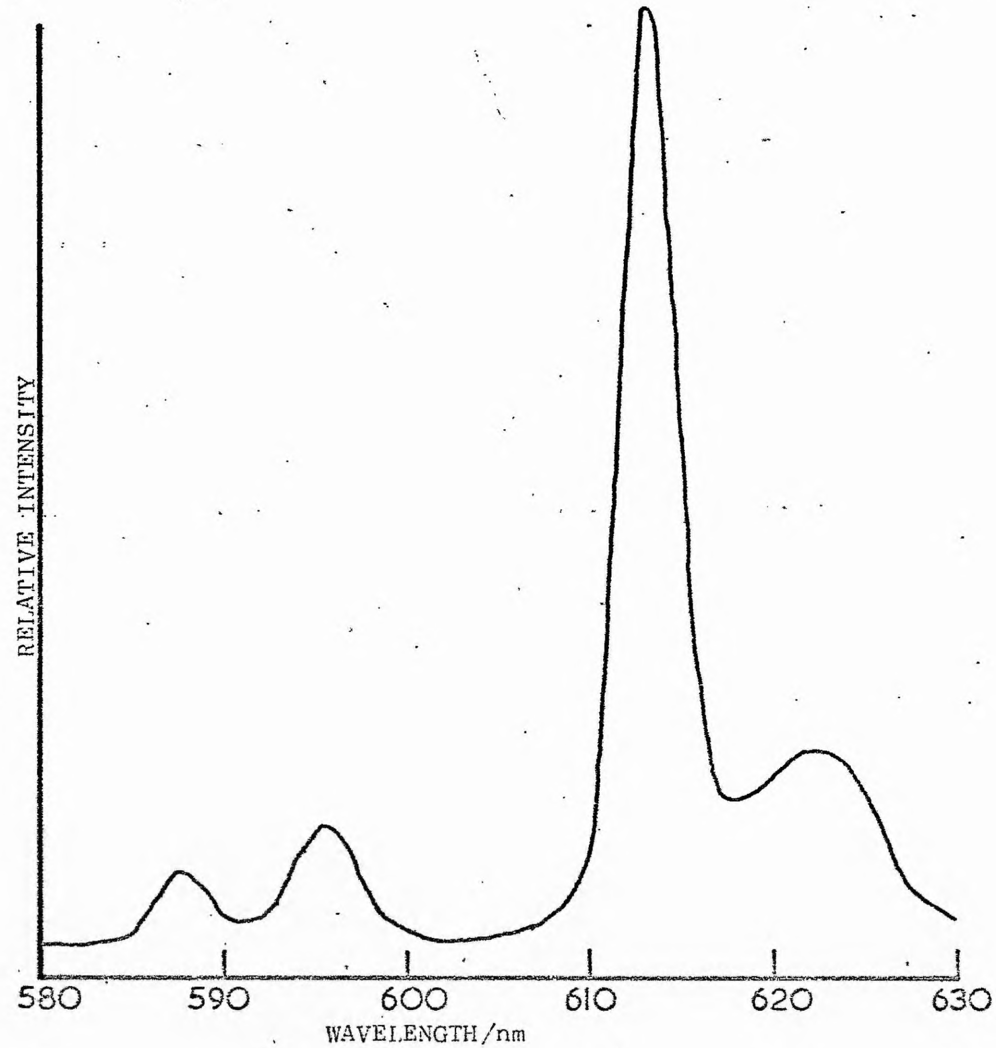

Fig. 2.4b Corrected emission spectrum obtained using the Hitachi for solid $Eu(hfaa)_4 \cdot Me_4N$ at 293K

the necessity of the high resolution spectrofluorimeter where exact profile was required,e.g. for quantum efficiency measurements. Also in the red region of the spectrum there is a greater fall in photomultiplier response in the R106 than in the EMI 9526 photomultiplier. As an example, the MPF-2A has been used to give satisfactory quantum efficiency results when there is little fine structure in the emission bands[238] although it gave erroneous results when the sharp structured fluorescence bands of the lanthanides were examined. An illustration of the high resolution instrument is given in Fig. 2.5

Fig. 2.5 Illustration of high resolution instrument

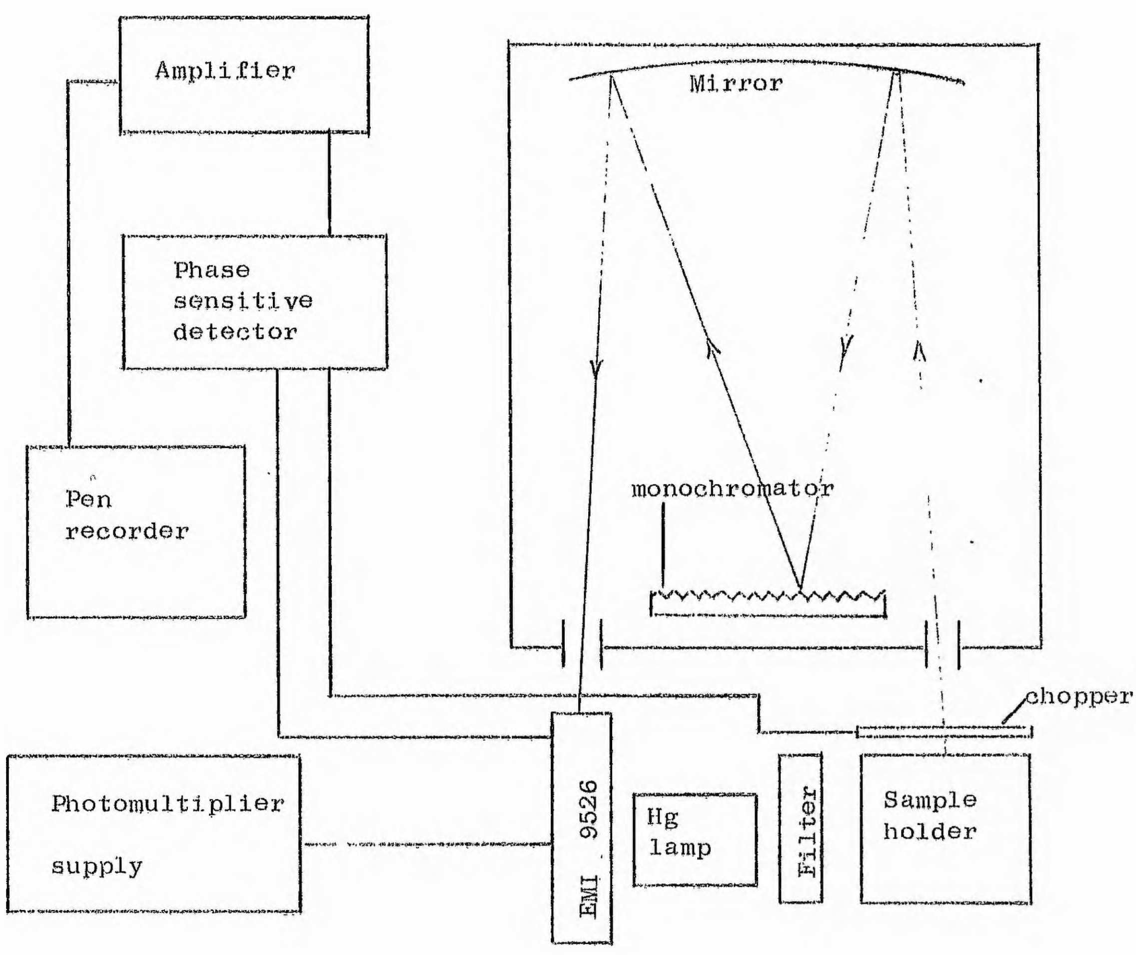

(c) Sampling Techniques

Parker[139] has emphasised the paramount importance of clean apparatus, pure samples and solvents when measuring both qualitative and quantitative photophysical processes. Consequently all glassware was immersed in chromic acid, copiously washed with distilled water and dried before use. Solvents and organic reagents were fractionally distilled or recrystallised from an appropriate solvent before use. All lanthanide chelates were submitted for carbon, hydrogen and, where appropriate, nitrogen analyses.

Solutions

Emission spectral profiles were recorded using the right angled viewing technique[139]. Organic molecules having overlaps between their emission and absorption bands inevitably suffer from self absorption. This self absorption is referred to as the inner filler effect and is usually avoided by employing very dilute solutions (optical density < 0.02), otherwise corrections have to be made[139]. Emission from lanthanide chelates are shifted well to the red, relative to their absorption bands, therefore no inner filler restrictions are imposed on concentration.

Numerous organic molecules are quenched by dissolved oxygen in fluid and solid solutions and precautions usually have to be taken when measuring quantitative luminescence to prevent such quenching. Two methods were employed to remove dissolved oxygen from the solutions studied

(a) bubbling dry nitrogen gas into the solution to displace the dissolved oxygen, and

(b) degassing by a freeze/pump/thaw process and keeping the solution under vacuum during measurement.

Method (a) was used when the sample cell was the standard PTFE stoppered fluorescence cell, while method (b) was used when low temperature fluorescence and phosphorescence measurements were made. The apparatus employed in the vacuum degassing is shown in Fig. 2.6. The solution is degassed in the pyrex flash by repetitive employment of method (b) until all the dissolved air is removed. The solution is then transferred to the evacuated quartz tube which has been designed to fit the phosphorescence accessory of the MPF-2A, and the emission intensity measured.

Comparison of quantitative measurements e.g. intensities, lifetimes and quantum efficiencies of the lanthanide chelates using both degassed and undegassed solution have indicated that oxygen quenching is not an important deactivation process. Most investigations involving lanthanide chelates in solution therefore preclude the initial degassing procedure.

Front face illumination was employed in the investigations of energy transfer between different lanthanide chelates in solution as this is the best method for measuring quantitative emission from concentrated solutions[139]. This was achieved on the MPF-2A using the solid sampler which was adapted to hold a 1 mm pathlength quartz cell. The cell was held at an angle of 30^{o} to the incident beam and the emission from the front surface of the cell detected. Reproducibility was improved by placing a defocusing lens in front of the incident beam causing most of the sample to be illuminated. This minimised the errors which could arise from slight positional changes of the cell after removal and subsequent replacement. It would found necessary to illuminate at or near the absorption maximum of the ligand chelate, otherwise erroneous results were obtained because of slight differences in the optical densities near the tail of the respective chelate absorption

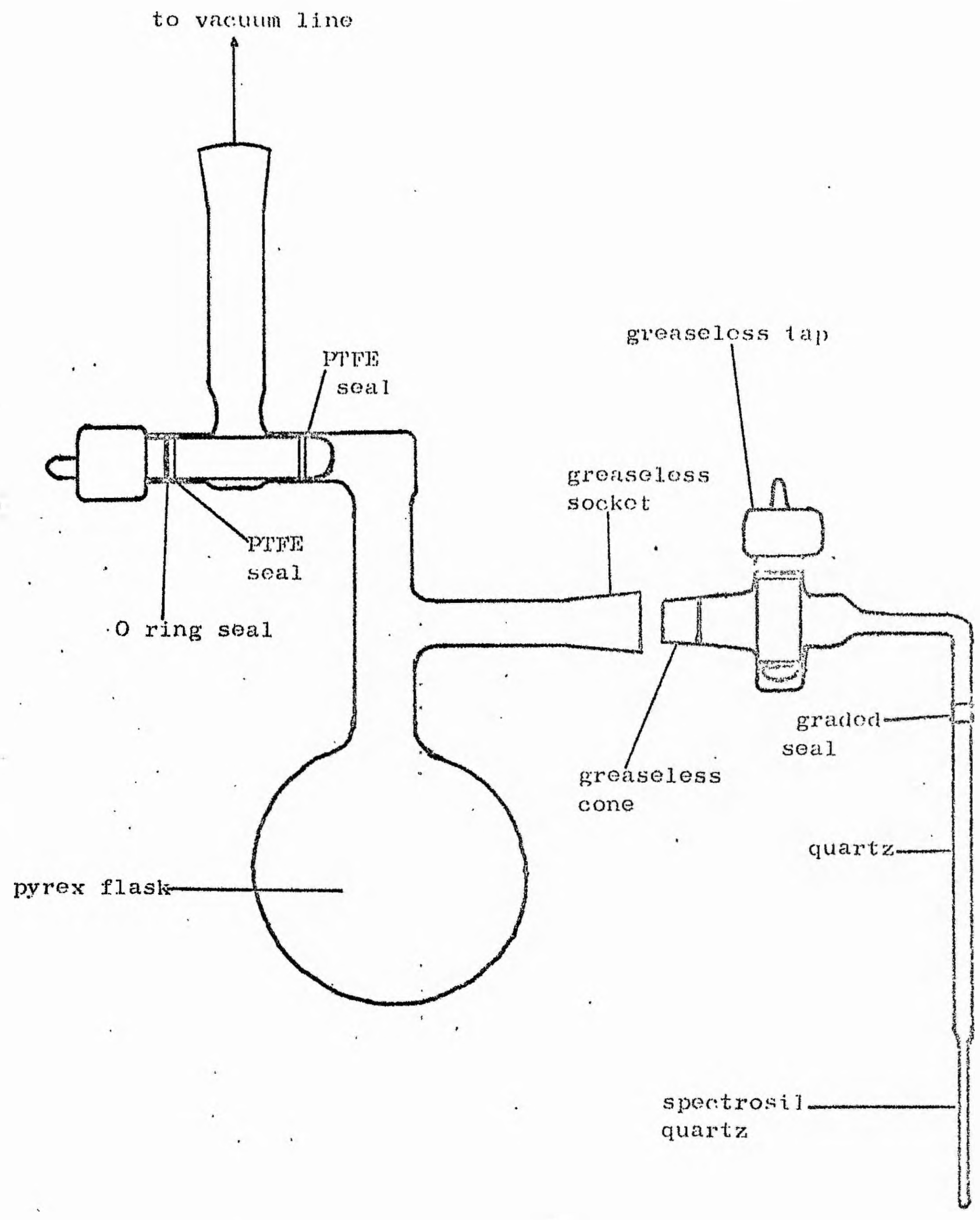

Fig. 2.6 Illustration of apparatus used for vacuum degassing

bands at specific concentrations.

Solids and solid solutions

Phosphorescence and total emission spectra of solid solutions at 77K were obtained using the phosphorescence accessory of the MPF-2A. In the case of the solids both the MPF-2A with the solid sampler accessory and the Monospek were employed although low temperature quantitative investigations were exclusive to the Monospek. Measurements involving the MPF-2A in conjunction with the phosphorescence accessory, which had the chopper removed, were obtained using right-angled optics[139]. The sample was placed in a quartz tube which fitted into a dewar containing liquid nitrogen. Front face viewing was employed in measurements using the Monospek, the sample being placed in the apparatus illustrated in Fig. 2.1, 2.2 and 2.3. The temperature of the sample was controlled by boiling liquid nitrogen and continually passing the cold vapour round the dewar. The rate of boiling and an external heater determined the temperature which was measured using a Chrom-Alumel thermocouple. Frosting of the dewar windows was preventing by blowing warm dry nitrogen gas around the outside of the dewar.

Many solvents and mixed solvents form cracked or opaque glasses when cooled to 77K[236] thus making quantitative measurements of solid solutions impossible. Stray light can be scattered from cracks on the sample surface and interfere with the measurements of total luminescence. When employing the MPF-2A this can be overcome by using the chopper which cuts off the scattered light and short lifetime fluorescence allowing longer lifed phosphorescence to be measured. However quantitative phosphorescence measurements are still not possible because the sample geometry is extremely difficult to reproduce.

The mixed hfaa and tfaa chelates, employed in the energy transfer work, were prepared by allowing the chloroform solution containing the appropriate amounts of mixed chelates to slowly evaporate to dryness. Methanol was used as the solvent in the case of the acetylacetone chelates. The recrystallised mixed chelates were all ground to similar particle size before subsequent investigations.

(d) Correction of Excitation Spectra

To obtain an excitation spectrum the intensity of the luminescence band is recorded as a function of wavelength or frequency of the monochromator used to provide the monochromatic exciting light. The apparent excitation spectrum so obtained is a plot of the product $I\phi\varepsilon$ against wavelength or frequency[139] i.e.

$$P_{(\lambda)} = I_{(\lambda)}\varepsilon_{(\lambda)}\phi \qquad 2.1$$

where $P_{(\lambda)}$ is the photomultiplier output at wavelength λ, $I_{(\lambda)}$ the radiative output of the source at wavelength λ, $\varepsilon_{(\lambda)}$ the molar extinction coefficient of the sample at wavelength λ and ϕ the quantum yield of the sample. The quantity $\varepsilon_{(\lambda)}\phi$ is a fundamental characteristic of the solution and a plot of $\varepsilon_{(\lambda)}\phi$ against wavelength gives the absolute excitation spectrum. $I_{(\lambda)}$ is dependent on the nature of the source and the characteristics of the monochromator. To obtain the true excitation spectrum the intensity of exciting light reaching the sample, I, must be determined as a function of wavelength. This may be done by means of (a) sensitive thermopiles,

(b) calibrated phototubes,

(c) the ferrioxalate actinometer,

(d) fluorescent screen quantum counters and

(e) photographic methods.

The method used to calibrate the MPF-2A was a modification of method (d) described by Argauer _et al_[237], and involved the comparison of the absorption and excitation bands of a dilute fluorescent solution.

If a fluorescent solution of a pure compound is illuminated with light of wavelength λ and intensity $I_{(\lambda)}$ and the intensity of fluorescence reaching the detector is $P_{(\lambda)}$ in arbitrary units, then

$$P_{(\lambda)} = k\, \phi_{(\lambda)} I_{(\lambda)} A_{(\lambda)} \qquad 2.2$$

where $A_{(\lambda)}$ is the fraction of exciting light absorbed by the solution, $\phi_{(\lambda)}$ the quantum yield for the same wavelength and k a constant depending on the units and geometry of the system. If the maximum absorption of the band of least frequency occurs at wavelength λ_1, then

$$\frac{P_{(\lambda)}/I_{(\lambda)}}{P_{(\lambda_1)}/I_{(\lambda_1)}} \; \frac{\phi_{(\lambda_1)}}{\phi_{(\lambda)}} \; A_{(\lambda_1)} = A_{(\lambda)} \qquad 2.3$$

If the quantity, $Q \equiv \frac{P_{(\lambda)}/I_{(\lambda)}}{P_{(\lambda_1)}/I_{(\lambda_1)}} A_{(\lambda_1)}$ is plotted against wavelength a fluorescence excitation spectrum of the solution is obtained, that is a plot of $A_{(\lambda)}$ against wavelength, only if $\phi_{(\lambda_1)}/\phi_{(\lambda)}$ is unity, i.e. ϕ is independent of wavelength. Measurement of absolute quantum yields of organic compounds in solution have been shown in the main to be independent of the exciting wavelength. This means the absorption and excitation spectra are identical for compounds having a constant quantum yield over the wavelength scanned. Therefore comparison of the apparent excitation and absorption spectra will allow the spectral distribution of the source to be calculated. The compound employed, the experimental technique and the results obtained in the calibration of the MPF-2A are discussed by J.F. Ireland[238].

(e) Correction of Emission Spectra

An absolute fluorescence spectrum is a plot of fluorescence intensity, measured in relative quanta per unit wavenumber interval against wavenumer. When a spectrofluorimeter is used at constant slit width and constant detector sensitivity the curve obtained is the apparent emission spectrum[139]. To determine the absolute spectrum the apparent curve has to be corrected for changes in sensitivity of the photomultiplier, the band width of the monochromator and the transmission of the monochromator with wavenumber. Thus, if $dQ/d\bar{\nu}$ represents the fluorescence intensity at any wavenumber $\bar{\nu}$, the observed photomultiplier output, $A\bar{\nu}$, which corresponds to the apparent emission spectrum is given by equation 2.4

$$A\bar{\nu} = \frac{dQ}{d\bar{\nu}} \quad P\bar{\nu}B\bar{\nu}L\bar{\nu} = \left(\frac{dQ}{d\bar{\nu}}\right) \quad S\bar{\nu} \qquad 2.4$$

where $P\bar{\nu}$ = output per quantum from the photomultiplier at wavenumber $\bar{\nu}$,

$\bar{B}$ = band width in wavenumber units at wavenumber $\bar{\nu}$,

$L\bar{\nu}$ = fraction of light transmitted by the spectrofluorimeter at wavelength $\bar{\nu}$.

The quantity $S\bar{\nu}$ is the spectral sensitivity factor of the monochromator - photomultiplier combination; the absolute emission spectrum is calculated from the apparent emission spectrum by dividing it point by point by $S\bar{\nu}$. This spectral sensitivity curve may be obtained in various ways[237,238-241] by taking measurements using:

(a) a calibrated tungsten lamp (for the visible region),

(b) a fluorescence screen monitor for the ultraviolet region,

(c) a thermopile,

(d) fluorescent solutions which function as quantum counters,

(e) reference solutions, the absolute fluorescence spectra of which have been previously determined.

Both spectrofluorimeters were calibrated using method (e). If the absolute luminescence spectrum has been determined precisely for a serious of compounds that emit over the range for which a spectral sensitivity factor is required, then measurement of the uncorrected spectra of the compounds with the instrument to be calibrated permits direct calculation of $S\bar{\nu}$ by direct application of equation 2.4.

The compounds and the experimental technique employed to obtain the sensitivity factors are discussed by J.F. Ireland[238]. Calibration of the MPF-2A was carried out by Ireland[238] and that of the Monospek by Dean[242]. Comparison of the two sets of values indicates the better response characteristics of the EMI 9526 photomultiplier compared to the R106 photomultiplier especially in the red region of the spectrum.

(f) Automatic Digitalisation and Correction of Excitation and Emission Spectra

Manual correction of excitation and emission spectra can be extremely tedious, particularly with complicated spectra. It is therefore advantageous to have some form of automation in spectral corrections. Several directly correcting spectrofluorimeters have been described where the correction function is stored internally e.g. on a mechanical can or its electrical analogue[243-246]. Indirect correction of spectra using computers has also been used[247,248] but the full potential of these computer-based methods can only be realised if the spectral data can be conveniently and rapidly transferred to a computer-readable form. The apparatus described below achieves this requirement using automatically punched paper tape. A schematic diagram of the apparatus is shown in Fig. 2.7.

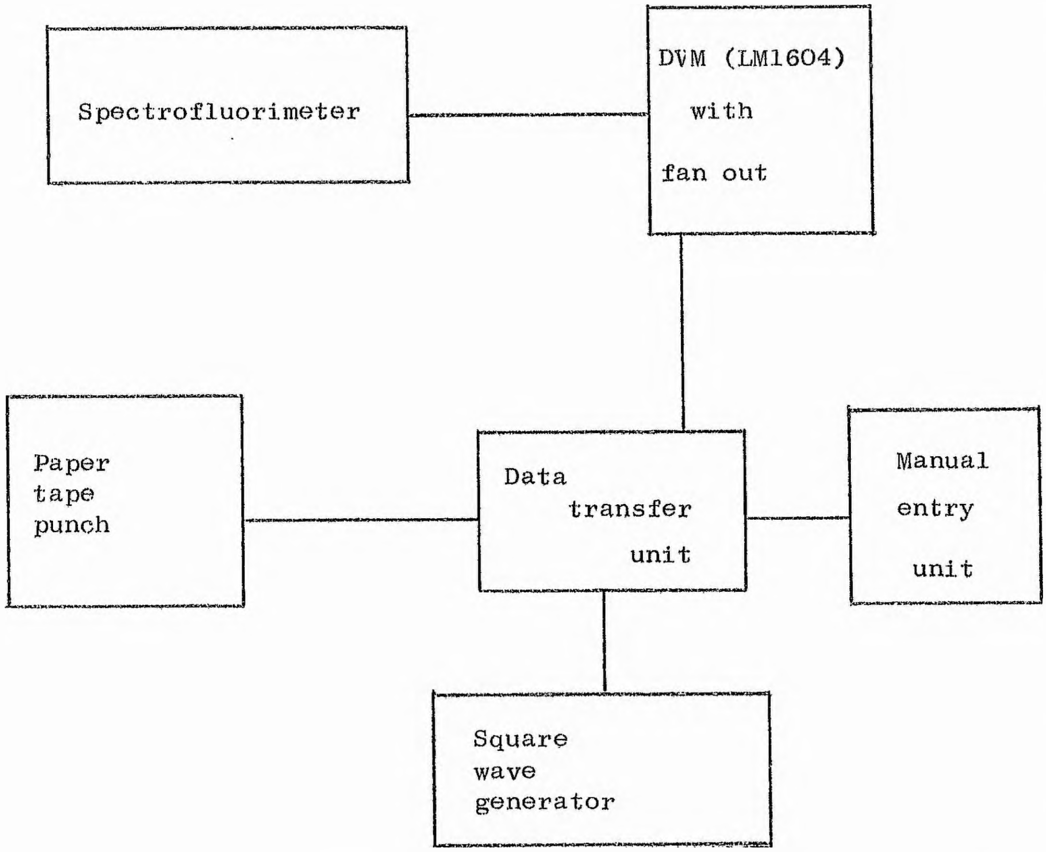

Fig. 2.7 Diagram of automatic digitalisation apparatus

The output signal from the particular spectrofluorimeter is connected to a Solartron LM 1604 digital voltmeter (DVM) with an EX 3054 positive logic fan-out unit. The voltmeter is interlinked with a Solartron 3230 data transfer unit, with a Facit 4070 paper tape punch acting as an output device. This arrangement allows for the uncorrected detector voltage of the spectrofluorimeter to be sampled and recorded at rates up to a maximum of about four samples per second. Slower sampling rates are obtained by initiating the sample cycle from a variable square wave generator.

Operation

To record a spectrum over the wavelength region, λ_1 to λ_2, the tape punch is only operated between these limits. A symbol indicating the end of the data set is punched on the tape via a Solartron 3209 manual entry unit. Since the wavelength scan is linear with time the wavelength corresponding to the nth record on the tape may be computed from equation 2.5,

$$\lambda_n = \lambda_1 + (n-1)(\lambda_2 - \lambda_1)/(N-1) \qquad 2.5$$

where N is the total number of records. N is counted during the subsequent processing of the tape. This method has been found to be more convenient and accurate than attempting to obtain readings at predetermined intervals. λ_1, λ_2 and a spectrum identification number are manually punched before each spectrum is recorded. The tape is now a digital record of the uncorrected spectrum and can be processed in conjunction with a predetermined response function to give a corrected spectrum.

Computer processing

The computer used was an IBM 360/44 with a Honeywell 3691 paper tape reader. The program is written in Fortran IV with the exception of a short translation program in PL360. The tape is read, and the data transferred directly into the computer core storage. The program SPECTRUM was used which supercedes the SPERA and SPEKB programs[238]. A brief description of SPECTRUM is given below.

Program SPECTRUM: This program incorporates the Spectral correction factors for both the MPF-2A (emission and excitation) and the Monospek and will therefore correct spectra for changes in photomultiplier sensitivity at source fluctuations with change in wavelength. It will allow corrected spectra, which have been normalised to a 100 units maximum intensity, to be plotted as a function of wavelength and/or wavenumber. Spectrum also allows;

(a) averaging of several spectra to reduce noise,

(b) integration of area under the corrected spectrum,

(c) subtraction of blanks to allow for changing baseline,

(d) plotting of inserts to show magnified sections of the spectrum,

(e) storing of spectra on magnetic tape whereby a particular spectrum may be replotted on a different format.

It provides a line printer output of wavelength with corresponding normalised corrected intensities, the increment between each wavelength reading and the normalisation factor, which is the figure the largest corrected intensity value is multiplied by to normalise it to a 100 units. The various options required when using SPECTRUM are requested by means of information punched on control cards which are submitted with the tape before subsequent processing. The program SPECTRUM was written by Dr. C.R.S. Dean, a listing being given in the appendix.

4. EXCITED STATE LIFETIME MEASUREMENTS

(a) Introduction

Two basic techniques have been generally used for direct measurement of excited state lifetimes[170,249]. The first method, introduced by Gaviola[250,251], is that of phase and/or modulation fluorometry. The phase and/or modulation of the fluorescent or phosphorescent emission is compared with the phase and/or modulation of the exciting light. In the second method, commonly referred to as pulse fluorometry, the sample is excited by intermittent light pulses of short duration and the fluorescence decay observed directly during the intervals between the excitation pulses. This method requires a light pulse source which cuts off in a time shorter than or comparable with the fluorescence lifetime and a detector system with a fast response time. The first accurate method of this type in the nanosecond region was made by Brody[252].

Several methods, modifications of the two basic techniques, have been described for lifetime measurements. Ware[249] and Birks[170] give extensive reviews on both techniques and their numerous modifications. Huntley _et al_[253], have described a nanosecond fluorimeter combined with an on-line computer, while Witt[254] has described several set-ups using time averaging computers for improvement of sensitivity. Sampling oscilloscopes have been used by Schöfer _et al_[255], and time averaging techniques employed by Studer _et al_[256]. In this work an apparatus capable of measuring lifetimes above 60 μs has been constructed and is described below.

(b) Description of Apparatus

A schematic representation of the apparatus used to obtain lifetimes of fluorescent solids and solution over the temperature range 77K to _ca_ 330K is given in Fig. 2.8. Fluorescence from the particular emission band of interest was detected normal to the exciting light by adapting the Monospek 1000 for lifetime measurements. The duration (1 μs - 70 μs) and intensity of the flash were determined by the capacitance (0.01 μF, 0.1 μF, 33 μF and 220 μF were available). Discharge across the tube was initiated by a trigger pulse from the signal averager (Data Laboratories 200, DL102, point averager). After a predetermined delay, depending on the duration of the flash, the photomultiplier

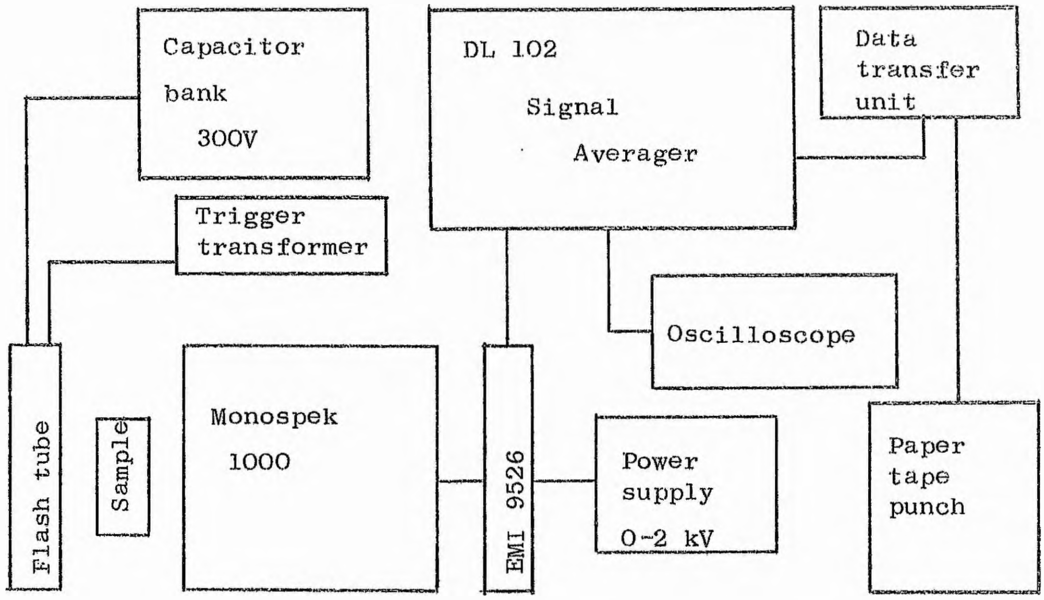

Fig. 2.8 Schematic representation of lifetime apparatus

output was sampled for a period of time and the curve stored. The sample cycle may be repeated for 2^n sweeps where n = 0 to 8 and the curves averaged to give an adequate signal to noise ratio. The averaging procedure and the final decay curve were monitored on the oscilloscope. The intensity of the curve was transferred at predetermined time intervals onto paper tape by means of the data transfer unit previously described in section 2.3f. Subsequent computer processing of the tape was carried out using the program LIFETIME.

Operation

The delay before, sweep time, delay after and the sampling cycle controls of the signal averager were preset depending on the intensity and lifetime of the sample. Information about averages, temperature, sweep time and delay were manually punched onto the paper tape before the data stored in the averager was transferred. The rate of output from the averager and the sampling rate of the paper tape unit were synchronised such that fifty values were transferred during the output procedure. The paper tape was then processed using program LIFETIME. A brief description of LIFETIME is given below, while a listing is given in the apprendix.

Program LIFETIME: This program ignores the first six and last thirteen intensity values and performs a least-squares regression obtaining a best straight-line relationship between the natural logarithm of the fluorescent intensity and time. On the basis of the slope of this line the program calculates half and exponential lifetimes, the difference and percentage difference between calculated and experimental intensities from which the percentage standard deviation from true exponentiality is determined. All this data was recorded on a line printer output along with the number of averages performed, sample temperature, sweep time and delay before. LIFETIME was written by Dr. C.R.S. Dean in conjunction with Dr. T.M. Shepherd. The lifetimes obtained by this method were reproducible to better than $\pm$ 25 μs.

In earlier investigations of lanthanide chelate lifetimes a simplified version of the apparatus described was used[257,258]. The decay curve, obtained without monochromation, was transferred to an X-Y recorder. Intensity values were manually obtained from the X-Y plot before subsequent computer processing. However, comparison of results obtained by both apparatus agreed within experimental error.

5. DETERMINATION OF QUANTUM YIELDS

(a) Introduction

Absolute quantum yields have important practical value. They allow one to assess the sensitivity of a proposed fluorimetric determination and the extent of interferences[139]. They are necessary for calculated thresholds for laser action[259] and for judging the suitability of materials as wavelength shifters in optically pumping experiments or for use as energy donors[139,260]. Yields coupled with luminescence data, also allows the evaluation of the purity of materials[139]. Theoretically, absolute yields are of central importance for the study of non-radiative processes in molecules[139,161,260,261], for correlation of predicted luminescence lifetimes with observed lifetimes[262] and for making assignments of electronic transitions[263].

To determine quantum yield directly it is necessary to compare the rate of absorption of exciting light with the total rate of emission of fluorescence of all wavelengths and in all directions. In principle this is simple but in practice numerous difficulties arise. A recent review by Demas et al[264], brings together information on various techniques for measuring quantum yields and points out the advantages and disadvantages of each experimental method. Absolute quantum yields can be determined by comparing fluorescence intensities with light scattered from a particle which acts as a pure dipolar scatterer (no absorption, uniform size and dimensions considerably less than those of the wavelength of light). Vavilov[265] has used magnesium oxide as a solid reflector while Weber et al[266], employed optically dilute colloidal solutions which behave as almost ideal dipole scatterers, in quantum yield determinations of luminescent solutions. As an example both oyster glycogen and colloidal silica[267] have been found to act as dipole scatterers over a wide range of wavelengths, their scattering being fully consistent with Rayleigh's scattering equations, with no optical absorption at wavelengths greater than

270 nm. The inherent difficulties experienced in the measurement of absolute quantum yields of solid substances are indicated in papers by Lipsett[268], Nygaard[269], Kristianpoller[270] and Allison *et al*[271]. The most widely employed technique in the determination of quantum yields, because of experimental simplicity[139], is that in which the quantum yield of a compound is determined relative to a compound of known absolute quantum yield. This is the technique employed in this work and will therefore be discussed in greater detail.

In the absence of self absorption the total rate of luminescence is proportional to $I_o \mathcal{E} c l \phi$, where I_o is the incident light intensity, $\mathcal{E}$ the molar extinction coefficient, c the sample concentration, l the cell path lenght and ϕ the quantum yield of the sample. The integrated area under the corrected luminescence spectrum is also proportional to the rate of luminescence emission. Therefore, if luminescence emission spectra of two solutions are measured with the same instrument geometry and the same intensity of exciting light, the ratio of the two observed luminescence intensities is given by equation 2.6.

$$\frac{\text{area}_2}{\text{area}_1} = \frac{I_o \mathcal{E}_2 c_2 l_2 \phi_2 (\eta_2)^2}{I_o \mathcal{E}_1 c_1 l_1 \phi_1 (\eta_1)^2} = \frac{\phi_2}{\phi_1} \frac{\text{optical density of } 2 (\eta_2)^2}{\text{optical density of } 1 (\eta_1)^2} \qquad 2.6$$

where η = the refractive index of the solution. A change in refractive index of the solution results in a variation in the angle of emerging rays from a plane cuvelle-air interface[272], causing a change in the sample geometry. The inclusion of the terms in equation 2.6 allows for the change in sample geometry caused by differences in η when comparing quantum yields of samples in different solvents.

(b) Experimental

Relative quantum yields in solution

Many lanthanide β-diketoenolate complexes tend to dissociate in organic solvents, especially at low concentrations i.e. $< 10^{-5}$M. The exact nature of the species present at low concentrations are not known. Consequently, quantum yields were determined at concentrations where dissociation was known to be relatively small i.e. 10^{-2}M. All measurements were carried out at 20°C ± 1°C.

Front face illumination using the MPF-2A was employed to obtain accurate values of peak heights under identical conditions. The peak heights were measured from uncorrected emission spectra, obtained by illuminating the samples at or near their absorption maxima. The solid sampler accessory was adapted to hold a 1 mm pathlength cell (see Fig. 2.9). The precautions, which were

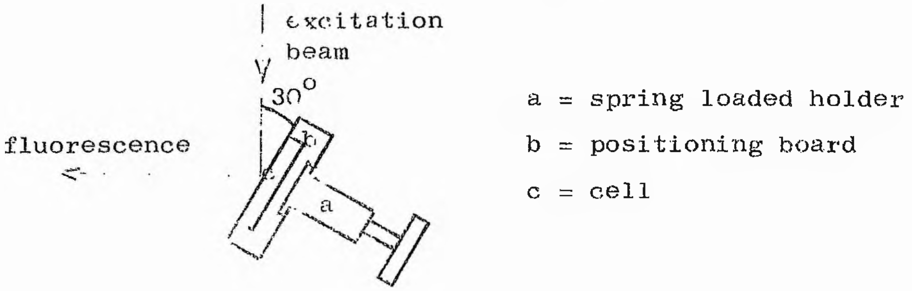

Fig. 2.9 Solid sampler accessory adapted for 1 mm cell

discussed earlier in section 2.3 were adopted to ensure minimal geometry differences incurred by removal and subsequent replacement of the sample cell. Under these conditions more than 99% of the incident radiation was absorbed in less than 100 μm of solution.

Since the resolution of the MPF-2A is insufficient to completely resolve the fine structure of the lanthanide ion emissions, even in solution, the emission spectra were also measured, using right angled viewing on the Monospek. Correct emission profiles were obtained using SPECTRUM as previously described, thus giving a relationship between the area, A_i, and the emission profile. In the same solvent the quantum yields of different complexes, ϕ_i, will be proportional to $A_i I_i^H(\lambda) / I_i^M(\lambda)$ where $I_i^H(\lambda)$ and $I_i^M(\lambda)$ are the emission intensities of the emission spectra obtained from the MPF-2A and the Monospek respectively at wavelength λ, the relative yields may be obtained from expression 2.7.

$$\frac{\phi_2}{\phi_1} = \frac{A_2 I_2^H(\lambda) I_1^M(\lambda)}{A_1 I_1^H(\lambda) I_2^M(\lambda)} \qquad 2.7$$

This ratio was independent of the value of λ where λ falls within the emission bands of the complexes under consideration. The measurements were carried out in duplicate using ethanol and acetonitrile as solvent, the results being reproducible to better than $\pm$ 3%.

Relative solid quantum yields

Due to the very sharp emission profiles of the solids precluding the use of the MPF-2A in spectral measurements, a slightly modified technique to the one described above for solution quantum yield determinations was adopted. The correction spectra were obtained using front face illumination using the Monospek in conjunction with the solid sampler holder shown in figure 2.3. Conditions were, as near as possible, identical during each measurement. Slit widths and photomultiplier voltage were fixed while investigations indicated the lamp intensity was stable over the period of measurement. The main source of error arose from the slight difficulty in reproducing the exact sample geometry between subsequent measurements.

Correction factors for the differences in sample absorption, between samples, were obtained by comparing the incident radiation reflected by a particular sample, (R_S), to that reflected from pure magnesium oxide (R_{MgO}) at the illuminating wavelength i.e. 365.5 nm. The fraction of the light absorbed, Ia, by the sample was obtained from expression 2.8.

$$Ia = \frac{R_{MgO} - R_S}{R_{MgO}} \qquad 2.8$$

The relative quantum yields of the solids may be obtained from expression 2.9.

$$\frac{\phi_2}{\phi_1} = \frac{(area)_2 (Ia)_1}{(area)_1 (Ia)_2} \qquad 2.9$$

In the case of the europium chelates all measurements were duplicated and shown to be reproducible to better than $\pm$ 10%. In the case of the terbium chelates only single determinations were performed.

6. NMR SPECTRA

Nmr spectra were measured on a Varian HA-100 MHz Spectrometer at a probe temperature of 40°C using freshly prepared solutions. The nmr solvents $CDCl_3$, CD_3CN (Fluorochem) and the organic substrate γ-picoline (Koch-Light) were fractionally distilled and stored over molecular sieves. The organic substrate was added by means of a Hamilton syringe to the nmr tube containing a known concentration of LSR dissolved in the nmr solvent. Particular care was taken at all stages to ensure anhydrous conditions since observed shifts were very sensitive to traces of moisture.

7. MOLECULAR WEIGHT DETERMINATIONS

(a) Introduction

Molecular weight determinations were obtained using a thermometric method employing a Mechrolab Vapour Pressure Osmometer Model 301A. Thermometric determinations of molecular weight under quasi-isopiestic conditions have been carried out by several workers with systems of non-volatile solutes in various volatile solvents[273-277]. In the various methods used, a steady state temperature above the ambient temperature is obtained in a partially isolated solution phase exposed to the solvent vapour. The temperature rise of the solution caused by the vapour condensing on its surface is the basis of the determination.

(b) Description and Operation of the 301A Osmometer

The 301A osmometer consists of two principle units, the sample chamber assembly containing the various elements of the osmometer and the control unit containing a Wheatstone bridge, a null indicator and a heater input control circuit. A drop of pure solvent and solution are suspended on the thermistors, side by side in a closed chamber saturated with solvent vapour. As a consequence of the difference in vapour pressure between the two drops, a differential mass transfer occurs between the two drops and the solvent vapour resulting in greater condensation on the solution drop than evaporation from the solvent drop. This transfer causes a temperature difference between the two drops because of the heat of vaporisation which is proportional to the vapour pressure lowering and hence proportional to the solute concentration. Since this temperature shift is a colligative effect, the instrument may be calibrated with a concentration series of known solute. Unknowns in the same solvent may then be read directly from the calibration curve. The instrument was calibrated using benzil in CCl_4 at a temperature of 37^{o}C and the accuracy determined using 1,3,5-trinitrobenzene. The accuracy was found to be better than $\pm$ 10%.

8. CONDUCTANCE MEASUREMENTS

Conductance measurements were obtained using a Wayne Kerr Universal Bridge B221 in conjunction with the cell illustrated in

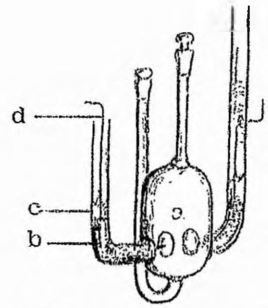

a = platinum electrodes
b = mercury
c = wax cover
d = conducting wire

Fig. 2.10 Conductance cell

Fig. 2.10. The cell constant which was found to be reproducible to better than $\pm$ 0.5% was obtained using KCl solutions of known concentrations. All measurements were obtained at a temperature of 25^{o}C $\pm$ 1^{o}C using a thermostatted water bath.

Acetonitrile (Hopkin and Williams) was purified by stirring over KOH pellets for 24 hours, filtering onto $CaCl_2$ and stirring over the $CaCl_2$ for 24 hours. The acetonitrile was then filtered onto P_2O_5 refluxed for 4 hours before being distilled onto fresh P_2O_5 and refluxed for a further 2 hours. Afterwhich, it was distilled onto and stored under molecular sieves. Methanol (Fisons) quoted to have less than 0.1% water was stored under molecular sieves after fractional distillation and used directly.

CHAPTER 3

LANTHANIDE TRIS DIPIVALOYLMETHANATO COMPLEXES

1. INTRODUCTION

Lanthanide tris dipivaloylmethanato complexes, $Ln(dpm)_3$ have been the subject of recent investigations because of (a) their relatively high volatilities[278] and (b) their potential applications as lanthanide shift reagents[279,280]. Tetrakis complexes of dipivaloylmethane (1) have not been isolated presumably due to the

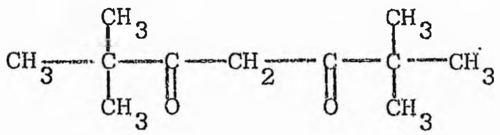

1

bulky tertiary substituents. This steric factor may also explain the relative ease with which anhydrous tris chelates can be prepared.

Sicre et al[278], have obtained vapour pressure and thermodynamic data for several $Ln(dpm)_3$ chelates. Their results indicate that the volatility of these chelates increases as the atomic number of the lanthanide ion increases (e.g. the vapour pressure of $Lu(dpm)_3$ and $Nd(dpm)_3$ are ca 1.0 and 0.08 mm respectively at 170°C), a factor which has allowed the separation of a mixture of lanthanide chelates by fractional distillation[281] and gas chromatography[75]. These chelates, especially those of Eu^{3+} and Pr^{3+} (see chapter 1.1e), have been widely used as lanthanide shift reagents since they can be isolated in an anhydrous state. X-ray crystal structures have been determined for a few solid Ln^{3+} tris dipivaloylmethanato complexes[90,282-285]. The anhydrous Pr^{3+} [283] and hydrated Dy^{3+} [284] dipivaloylmethanato complexes have been shown to consist of dimeric units, the former chelate being seven-coordinate with two β-diketo-enolate oxygen atoms shared by both the Pr^{3+} ions (see figure 3.1).

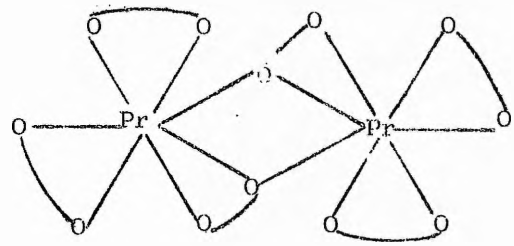

Fig. 3.1 Illustration of seven-coordination in $Pr_2(dpm)_6$

Crystal structures of Ho^{3+} [285] and Eu^{3+} [90] tris dipivaloylmethanato adducts show that they are monomeric having C_2 symmetry with the two-fold axis passing through the lanthanide ions.

There is uncertainty regarding the nature of the species present in solution. Two interpretations have been made of nmr data in carbon tetrachloride solution, one suggesting the presence of a majority[279] and the other a minority[280] of the dimeric species $Ln_2(dpm)_6$ (Ln = Eu, Pr) in addition to the monomer. Reported molecular weights in solution indicate the presence of monomeric species[278,286,287]. Mode et al[286], determined the molecular weights for four $Ln(dpm)_3$ chelates in n-hexane and found them to be within ± 1% of the monomeric molecular weight. Ghorta et al[287] obtained values for $Ln(dpm)_3$ chelates in carbon tetrachloride solution and found them to be 12-17% lower than the theoretical molecular weights for the monomer, which they attributed to the difficulties of excluding moisture from the experimental system.

2. ANOMALOUS TRIPLET STATE BEHAVIOUR IN SOLID TRIS (DIPIVALOYLMETHANATO)-TERBIUM(III)

(a) Emission Spectra

The uncorrected emission spectra of solid $Tb(dpm)_3$ obtained at $20^{o}C \pm 1^{o}C$ with an excitation wavelength of 320 nm is shown in figure 3.2. The spectrum is characteristic of all terbium β-diketoenolate chelates in that it consists of three main peaks corresponding to Tb^{3+} transitions, $^5D_4 \longrightarrow {}^7F_6$ (ca 490 nm), $^5D_4 \longrightarrow {}^7F_5$ (ca 550 nm) and $^5D_4 \longrightarrow {}^7F_4$ (ca 590 nm). The transitions $^5D_4 \longrightarrow {}^7F_3$, $^7F_2$, $^7F_1$ and $^7F_0$ which lie further to the red are not shown due to their relatively weak intensity and the poor photomultiplier sensitivity in the region above 600 nm.

Since the lowest Gd^{3+} excited level, the $^6P_{7/2}$ state, lies ca 33,000 cm^{-1} above the ^8S ground state, deactivation of the lowest triplet level of the chelated ligand cannot occur via the lanthanide ion as most ligand triplets lie well below the $^6P_{7/2}$ level. The enforced phosphorescence of the Gd^{3+} chelates at low temperature therefore allows the triplet energy to be determined. The triplet levels of various lanthanide chelates are relatively independent of the central ion[140] therefore the ligand triplet values obtained from the emission spectra of the Gd^{3+} chelates are assumed to be a good approximation to those of the Tb^{3+} chelates. Emission spectra measured at 77K with an excitation wavelength of 320 nm of the analogous crystalline, $Gd(dpm)_3$, and its mono-pyridine adduct, $Gd(dpm)_3py$, are shown in figures 3.3 and 3.4 respectively. The spectrum of the $Gd(dpm)_3py$ chelate is identical in profile to the mono-ethanol adduct, $Gd(dpm)_3EtOH$ and the mono-d_1-ethanol adduct $Gd(dpm)_3EtOD$ emission spectra. The spectrum of solid $Gd(dpm)_3$ differs in profile from that of the adducts in having, in addition to a peak at 400 nm, a stronger peak at 424 nm. This difference could be attributed either to an enhanced radiative transition from the triplet level to a vibrationally excited level of the ground state or possibly as the 0-0 band of a second triplet level which is present in the anhydrous complex but not in the adducts.

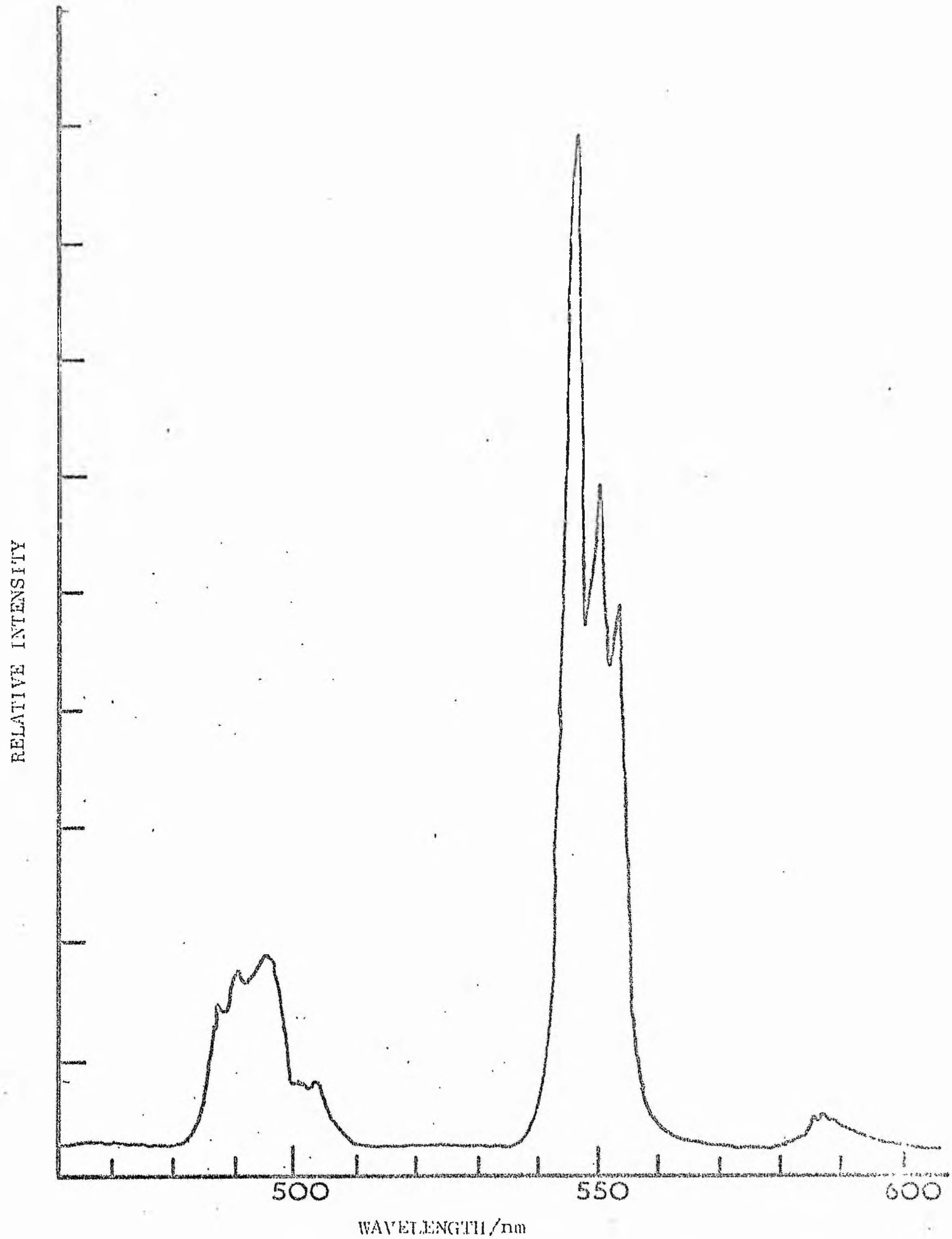

Fig. 3.2 Emission spectrum of solid $Tb(dpm)_3$

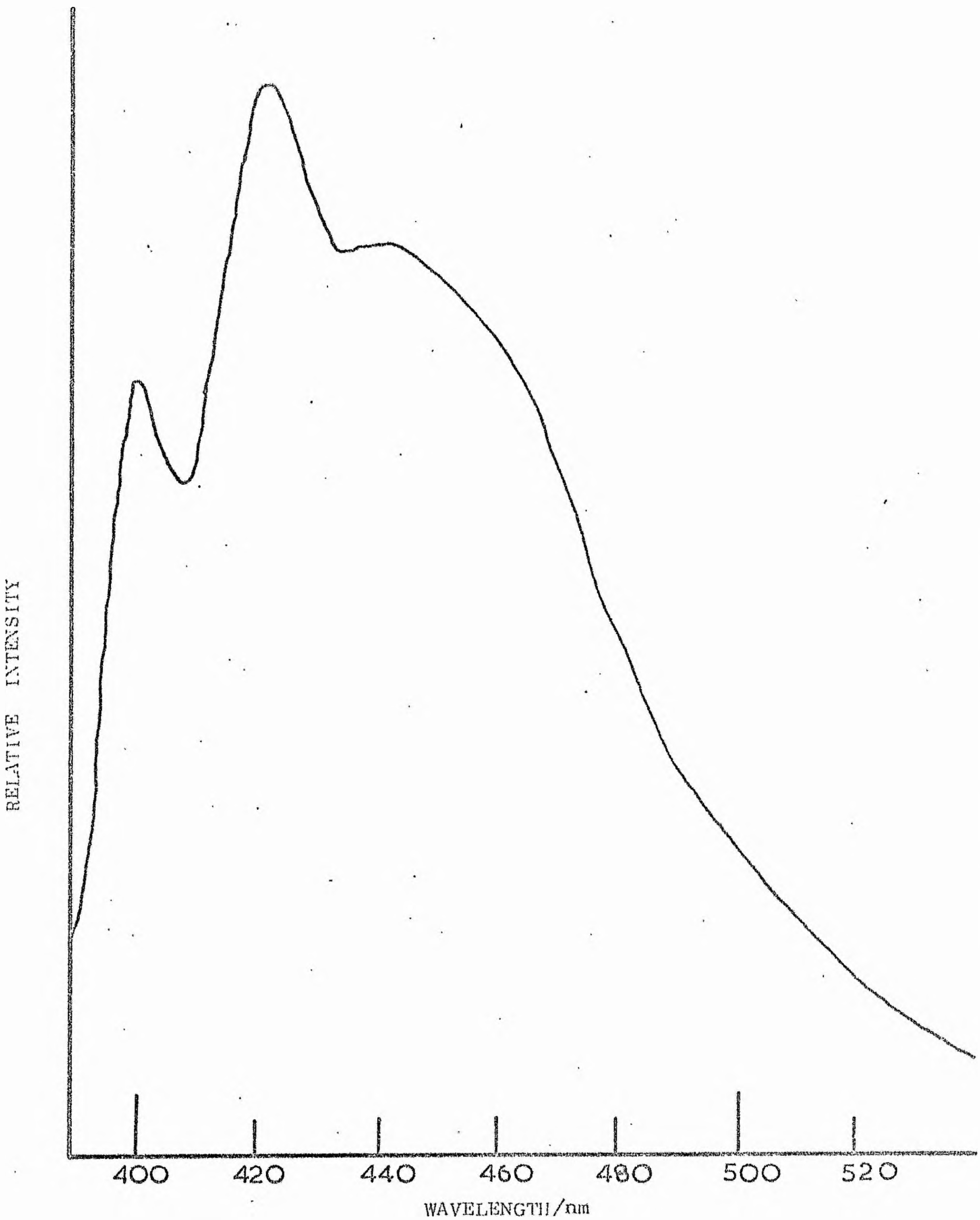

Fig. 3.3 Emission spectrum of $Gd(dpm)_3$

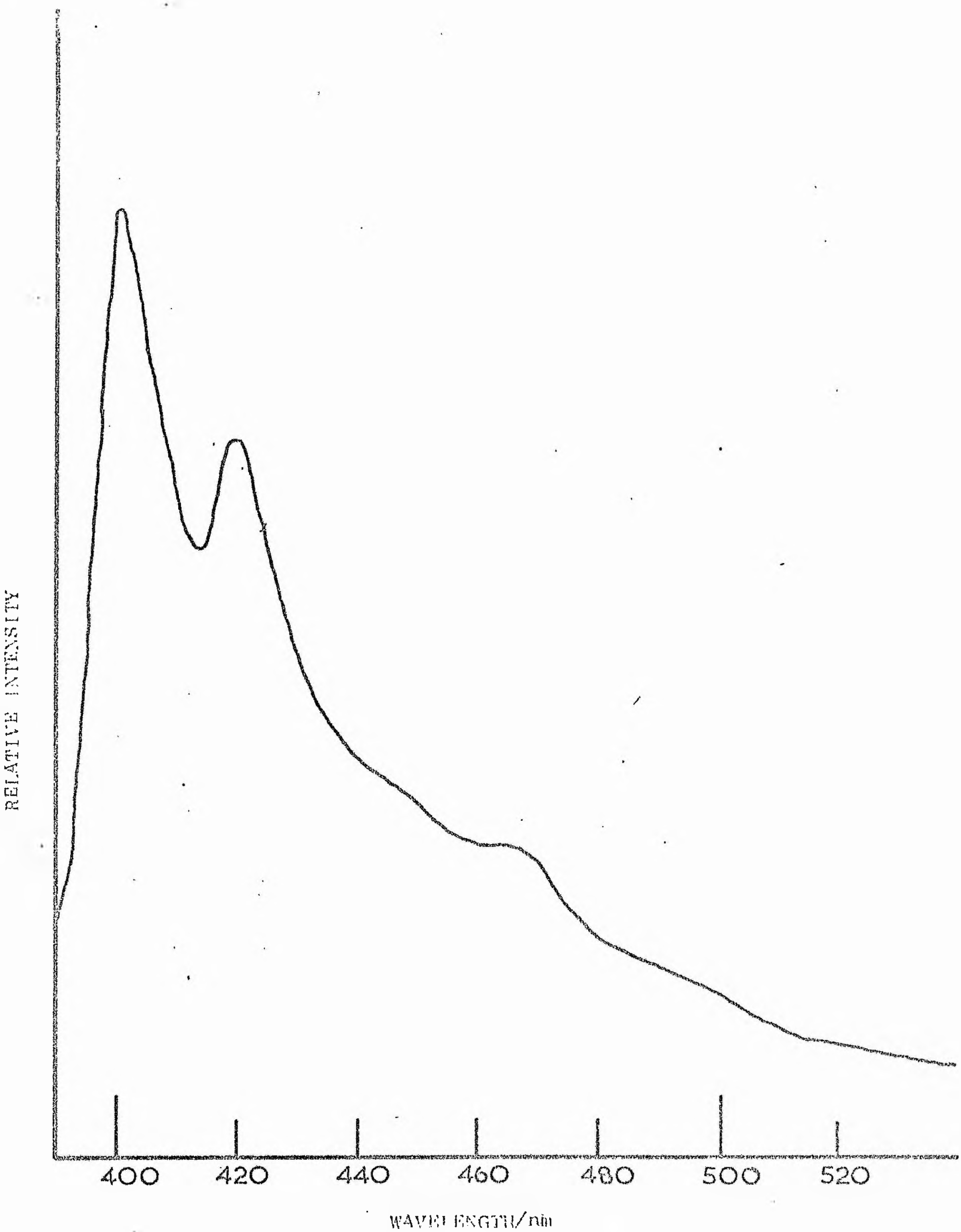

Fig. 3.4 Emission spectrum of $Gd(dpm)_3py$

(b) Fluorescent Decay Times of $Tb(dpm)_3$ and its Pyridine, Ethanol and d_1-Ethanol Adducts

The relationship between the exponential decay times of the Tb^{3+} $^5D_4$ level, τ, and the sample temperature for solid $Tb(dpm)_3$ and its adducts over the temperature range 77-323K are shown in figure 3.5. τ for $Tb(dpm)_3$ remains constant between 77K and ca 250K and thereafter decreases rapidly with increase in temperature. This is in marked contrast to the behaviour shown by the monoadducts where τ for the pyridine adduct remains constant, within experimental error over the temperature range studied and the ethanol adducts show only a relatively small decrease in τ at higher temperatures. It was found that the relative quantum efficiency of $Tb(dpm)_3$ decreased at higher temperatures as τ decreased; the efficiencies of the ethanol adduct remained almost constant over the temperature range. The deuteriated adduct, $Tb(dpm)_3EtOD$, has τ values some 5% higher than those of the corresponding EtOH adduct indicating that the deactivation of the $^5D_4$ level involving OH vibrational modes only occurs to a very limited extent.

(c) Discussion

Dawson et al[288], have attributed the weak fluorescence of some terbium chelates in methanol and toluene solutions to a thermal depopulation mechanism of the $^5D_4$ terbium emitting level. They observed that when the $^5D_4$ emitting level of $[Tb(tfaa)_4]^-NH_4^+$ and $[Tb(ba)_4]^-pipH^+$ (pipH = piperidinium cation) was pumped directly at ca 270K more than 99.5% of the energy reaching the $^5D_4$ level was dissipated non-radiatively. This was in marked contrast to the europium chelates studied where more than 80% of the energy reaching the $^5D_0$ emitting level, by direct excitation,was emitted as ion

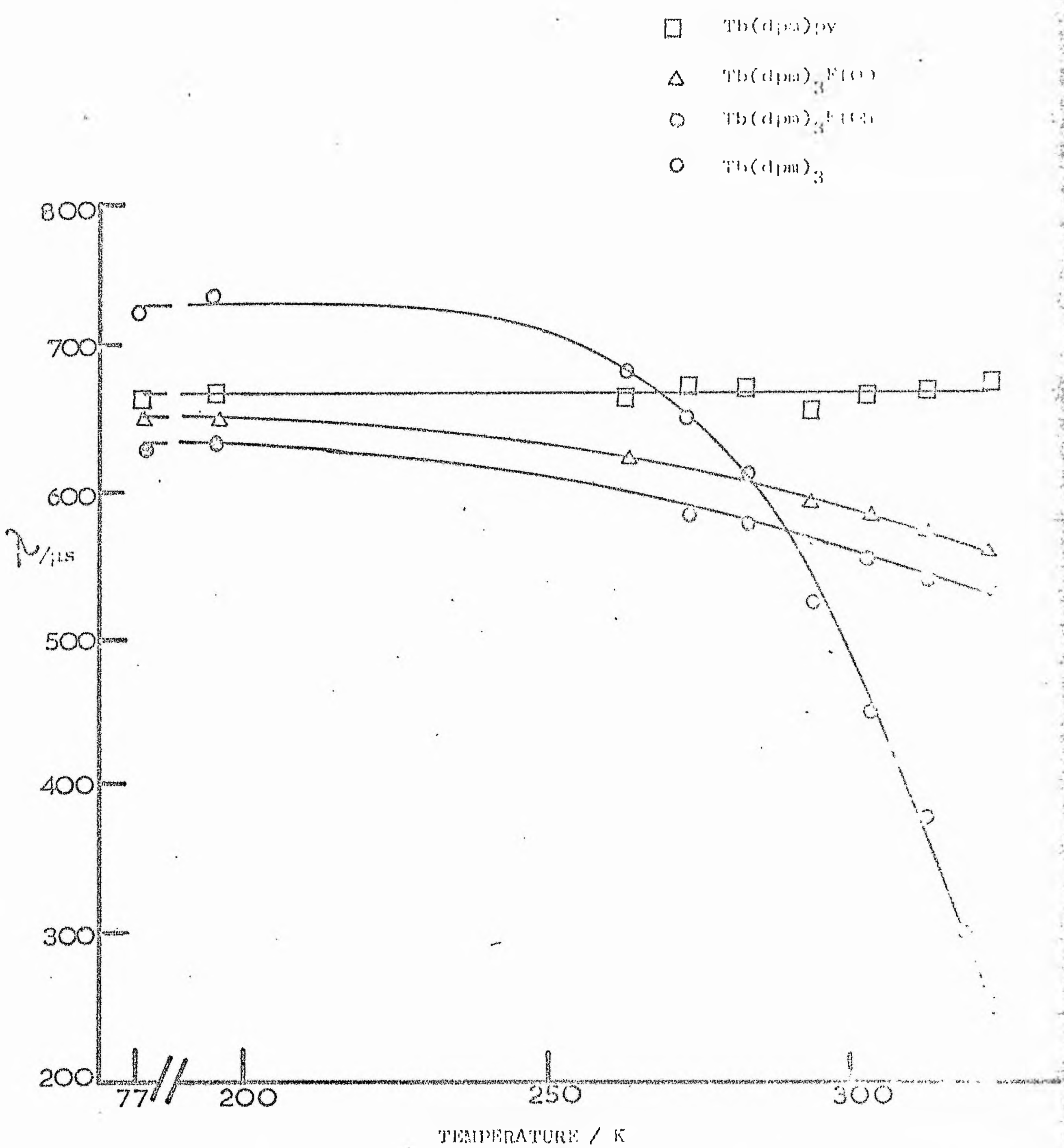

Fig. 3.5 Lifetime temperature dependence of $Tb(dpm)_3$ ... its ...

fluorescence. They concluded that the loss of energy from the terbium $^5D_4$ level was due to a thermal depopulation mechanism involving the low lying ligand triplet. In the case of the europium chelates significant thermal depopulation to the ligand triplet was precluded because of the larger energy separation between the $^5D_0$ emitting level which lies ca 17,000 cm^{-1} above the ground state and the ligand triplet level, although back-donation from the $^5D_0$ to the $^5D_1$ ion level of Eu^{3+} has been observed as a deactivation process for the $^5D_0$ level[204].

A possible explanation of the anomalous behaviour shown by crystalline $Tb(dpm)_3$ is the occurrence of one or more temperature-dependent deactivation processes which operate much less strongly, if at all, in the solid adducts. Such a process or processes, which may be represented by an overall deactivation rate constant, k(T), would be accompanied by temperature-independent deactivation with the rate constant k'. The observed lifetime, τ is then given by equation 3.1, or if τ' is the decay time in the absence of any

$$\frac{1}{\tau} = k(T) + k' \qquad 3.1$$

temperature-dependent deactivation then k(T) may be expressed by equation 3.2. If a single process occurs in the solid $Tb(dpm)_3$

$$k(T) = \frac{1}{\tau} - \frac{1}{\tau'} \qquad 3.2$$

whereby the $^5D_4$ level is thermally depopulated to a ligand level at energy E above the lanthanide level then k(T) may be expressed in the form of an Arrhenius equation, 3.3, where the exponential term

$$k(T) = \frac{1}{\tau} - \frac{1}{\tau'} = A\exp(-E/RT) \qquad 3.3$$

may be regarded as the fraction of the chelate molecules excited to the ion emission level which are thermally activated to the triplet level at temperature, T. Figure 3.6 shows an energy level diagram representing the possible energy transfer processes from the ligand triplet, T_1, in the terbium chelates. Intersystem crossing within the ligand and the multiplet structure of the ^7F terbium level are omitted. k_4, the temperature-dependent back-

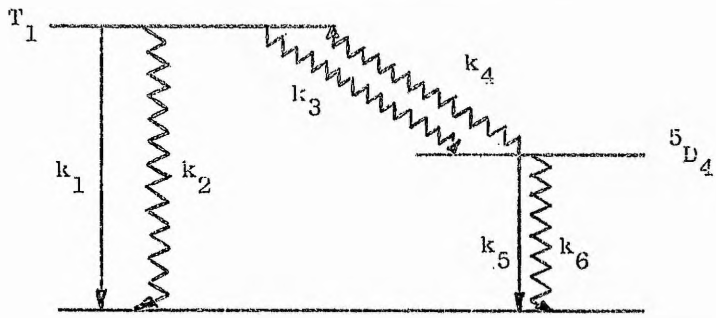

Fig. 3.6 Energy level diagram showing possible transfer processes from the ligand triplet, T_1, in Tb^{3+} chelates

donation rate constant and k(T) the rate of depopulation of the $^5D_4$ level can be related by the equation 3.4 (see appendix for

$$k(T) = k_4(k_1+k_2)/(k_1+k_2+k_3) \qquad 3.4$$

derivation). The observed lifetime at temperature T, τ_T, can be expressed in the form of the rate constants shown in equation 3.5. It is therefore possible if back-donation occurs to determine

$$\tau_T = \frac{1}{[k_5+k_6+k(T)]} \qquad 3.5$$

the energy E and obtain a value of the pre-exponential term A. The value of τ for $Tb(dpm)_3$ at 77K (i.e. 730 μs) may be reasonably taken as τ' since no significant decrease in τ occurs between 77 and 250K. Equation 3.3 may be rewritten as equation 3.6 and a plot

$$\log_{10}(^1/\tau_T - {}^1/\tau_{77}) = \frac{-E}{2.303\ RT} + \log_{10}A \qquad 3.6$$

of $\log_{10}(^1/\tau_T - {}^1/\tau_{77})$ i.e. $\log_{10}k(T)$ against 1/T should be linear with a slope equal to -E/2.303R and intercept $\log_{10}A$. Table 3.1

contains the various τ values at their respective temperatures for solid $Tb(dpm)_3$ from which log $(^1/\tau_T - ^1/\tau_{77})$ and 1/T are calculated.

Table 3.1

Lifetime data for solid $Tb(dpm)_3$

Lifetime $\tau/\mu s$	Temperature T/K	$\frac{10^{-2}}{\tau_T}$ $/s^{-1}$	$(^1/\tau_T - ^1/\tau_{77})$ $/s^{-1}$	$\log_{10}(^1/\tau_T - ^1/\tau_{77})$ $/s^{-1}$	10^4 $\frac{K}{T}$
712	250	14.04	34.63	1.5934	40.00
688	260	14.53	83.62	1.9223	38.46
676	265	14.79	109.4	2.0391	37.73
660	270	15.15	145.3	2.1623	37.03
648	275	15.43	173.3	2.2387	36.36
628	280	15.92	222.4	2.3472	35.71
600	285	16.67	296.8	2.4725	35.09
572	290	17.48	378.4	2.5780	34.48
540	295	18.52	482.0	2.6830	33.90
500	300	20.00	630.1	2.7994	33.33
450	305	22.22	852.4	2.9306	32.79
400	310	25.00	1130	3.0531	32.26
348	315	28.73	1504	3.1772	31.75

The resulting straight line plot in figure 3.7 supports the presence of a single temperature-controlled mechanism for the deactivation of the $^5D_4$ emitting level over the temperature range used in the plot. Determinations of E and R from the plot give values of E = 3050 cm^{-1} and A = 1.6×10^9 s^{-1}. Treatment of the slight temperature dependence shown by the ethanol adducts were attempted but did not give straight line plots. The value of E obtained above suggests that $Tb(dpm)_3$ has a ligand triplet some 3050 cm^{-1} above the Tb^{3+} $^5D_4$ level ($\sim$ 20,500 cm^{-1} above ground state) and that this level is absent in the adducts.

The emission peak at <u>ca</u> 23,600 cm^{-1} in crystalline $Gd(dpm)_3$

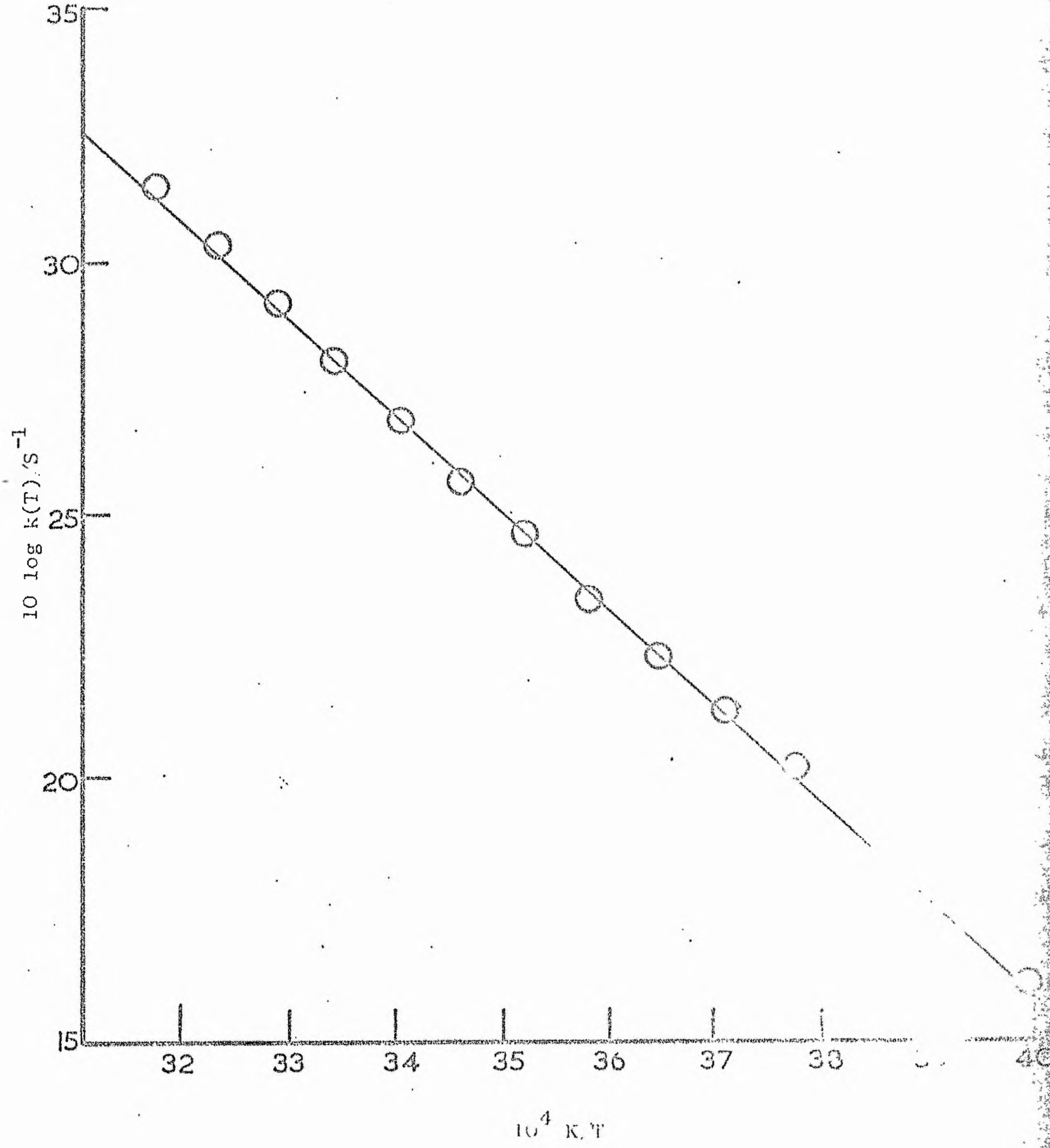

Figure 3.7 Plot of log K(T) against 1/T

which is absent in the adducts (see figures 3.3 and 3.4) is in good agreement with the predicted value of 23,550 cm^{-1} obtained from the temperature dependence of τ in $Tb(dpm)_3$. It is therefore suggested that this peak is the 0-0 peak of a second triplet level in solid $Gd(dpm)_3$. $Tb(dpm)_3$ is isomorphous with $Pr(dpm)_3$ and a similar dimeric molecular unit with seven-coordinate Tb^{3+} ions is indicated[283]. It was also noted by Bennet et al[289], that sublimed crystals of $Tb(dpm)_3$ contained some orthorhombic crystals in addition to the predominant monoclinic form. All spectroscopic measurements were therefore carried out on both sublimed samples of $Tb(dpm)_3$ and with samples recrystallised from n-hexane. The results obtained were identical within experimental error. The presence of two triplet levels in the 25,000-23,000 cm^{-1} region may be correlated with the known dimeric structures of $Tb(dpm)_3$ and $Gd(dpm)_3$. It is suggested that the higher triplet state at 25,000 cm^{-1} is characteristic of the dipivaloylmethanato ligand with both oxygen atoms bonded to a single lanthanide ion, i.e. the situation in the solid monomeric adducts and in the four ligands of the dimeric unit $Ln_2(dpm)_6$ whereas the lower triplet is characteristic of the bridging dipivaloylmethanato ligands in the dimer. The increased electron withdrawing effect caused by the proximity of the bridging oxygen atoms of the two lanthanide ions is quantitatively consistent with the triplet state occurring at lower energy. For example, solid lanthanide hexafluoroacetylacetonates have an average triplet value of 21,900 cm^{-1} [258]. The structure of the dimer[283] indicates that relatively large deviations from planarity occur in the chelate rings involved in bridging and this is likely to affect the ligand electronic levels. Similar deviations from planarity have been reported for polymeric acetylacetonato complexes[289-291].

3. NATURE OF THE SPECIES PRESENT IN SOLUTION

(a) Absorption Spectra

Absorption spectra of $Tb(dpm)_3$ and $Tb(aa)_3 \cdot 3H_2O$ at concentrations of ca 10^{-5}M in ethanol and carbon tetrachloride are shown in figures 3.8 and 3.9 respectively. It was observed that the profile and peak maxima of these spectra altered with time, eventually in ca 24 hours reaching the limiting spectra which are also illustrated in figures 3.8 and 3.9. Figure 3.10 shows the absorption spectra of acetylacetone in ethanol and carbon tetrachloride while figure 3.11 shows the initial and limiting absorption spectra of sodium acetylacetonate in ethanol. The insolubility of sodium acetylacetonate in carbon tetrachloride precluded the measurement of its absorption spectrum in that solvent. Table 3.2 summarises the initial and final absorption maxima for the appropriate samples and solvents. The initial absorption maximum for $Tb(dpm)_3$ in ethanol is in good

Table 3.2

Data on absorption maxima

Sample	Solvent	Initial λ_{max} (nm)	Final λ_{max} (nm)
$Tb(aa)_3 \cdot 3H_2O$	EtOH	288	282
$Tb(aa)_3 \cdot 3H_2O$	CCl_4	290	273
$Tb(dpm)_3$	EtOH	287	276
$Tb(dpm)_3$	CCl_4	283	275
acetylacetone	EtOH	272	272
acetylacetone	CCl_4	273	273
$Na^+(aa)^-$	EtOH	288	275

agreement with the value obtained by Archer et al[280], i.e. 287 nm. Their value of 278 nm for the chelate in carbon tetrachloride

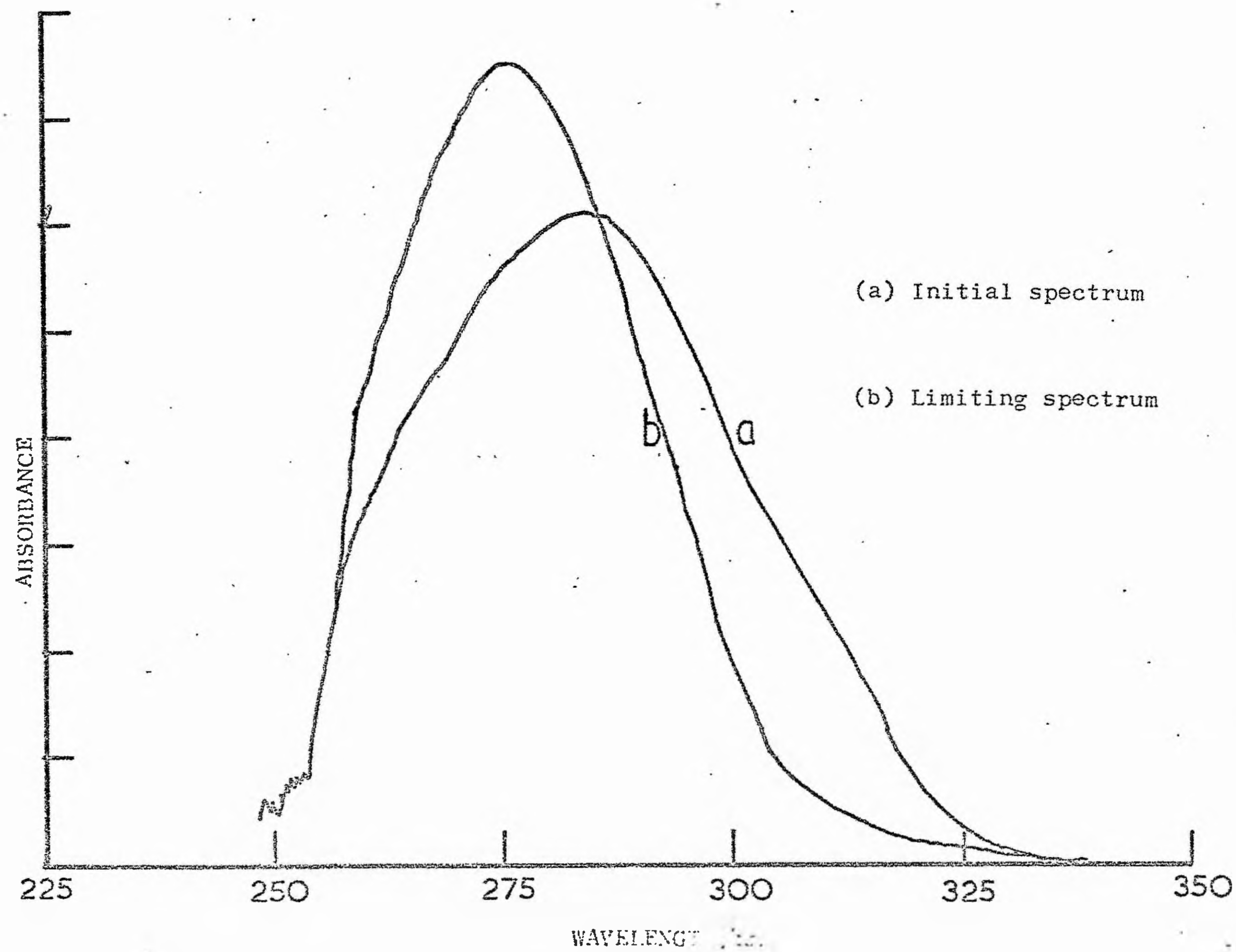

Fig. 3.8a Absorption spectra of $Tb(dpm)_3$ in CCl_4

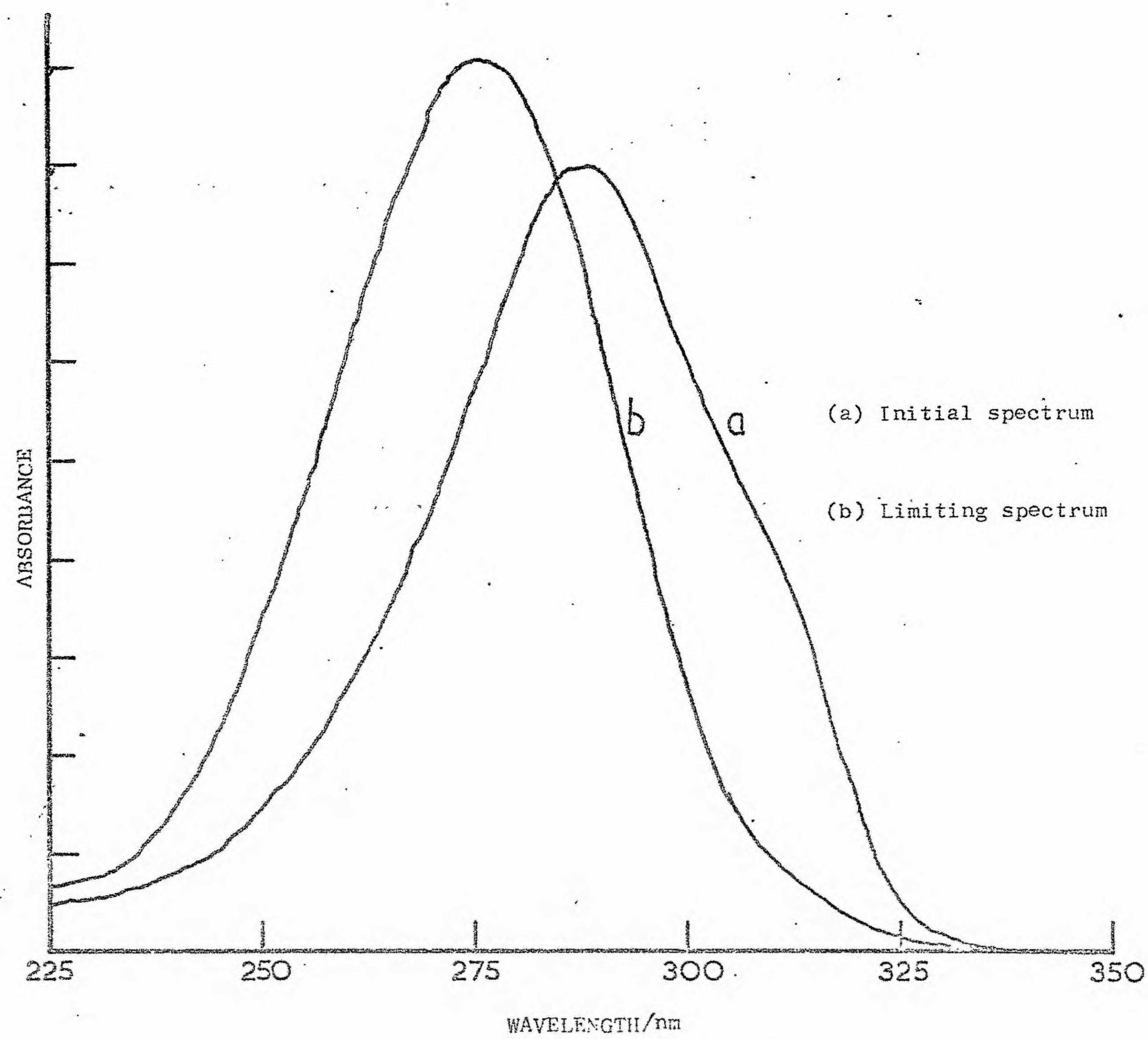

Fig. 3.8b Absorption spectra of $Tb(dpm)_3$ in EtOH

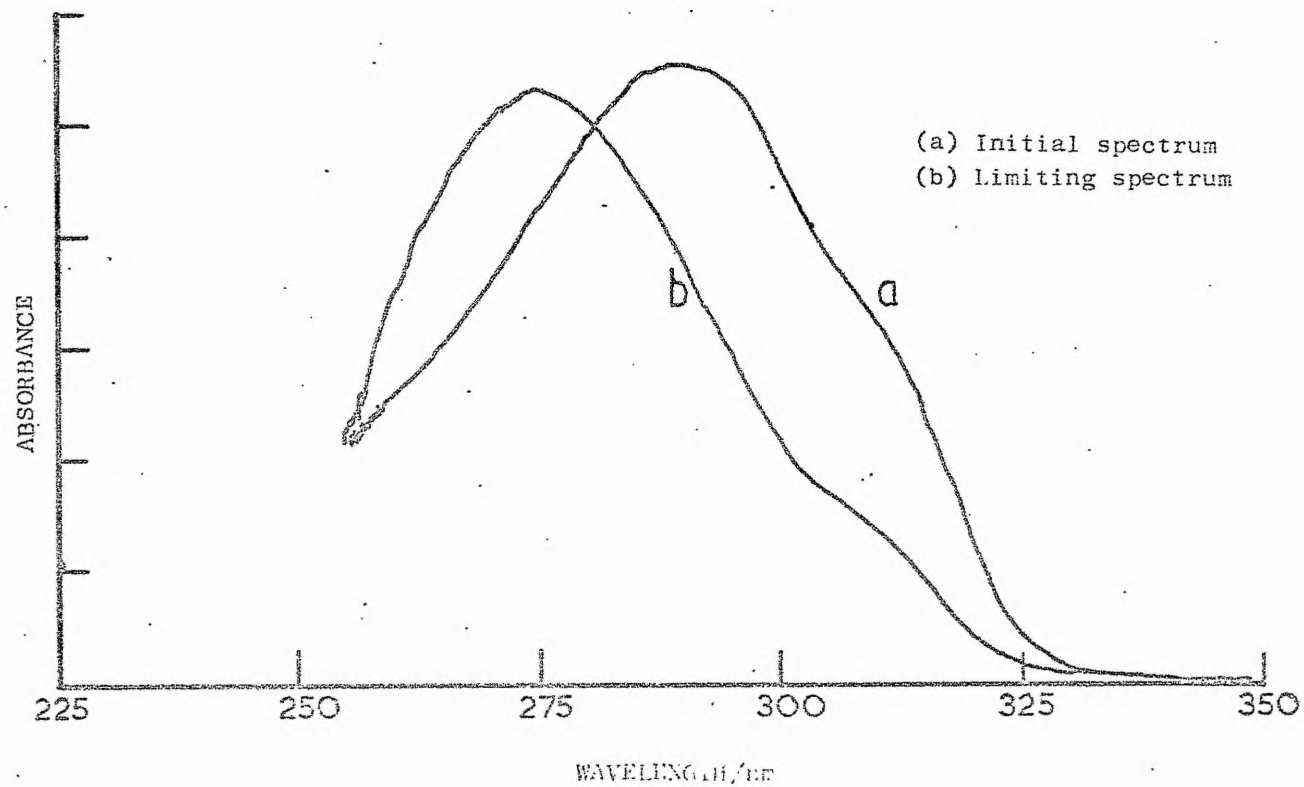

Fig. 3.9a Absorption spectra of $Tb(aa)_3 \cdot 3H_2O$ in CCl_4

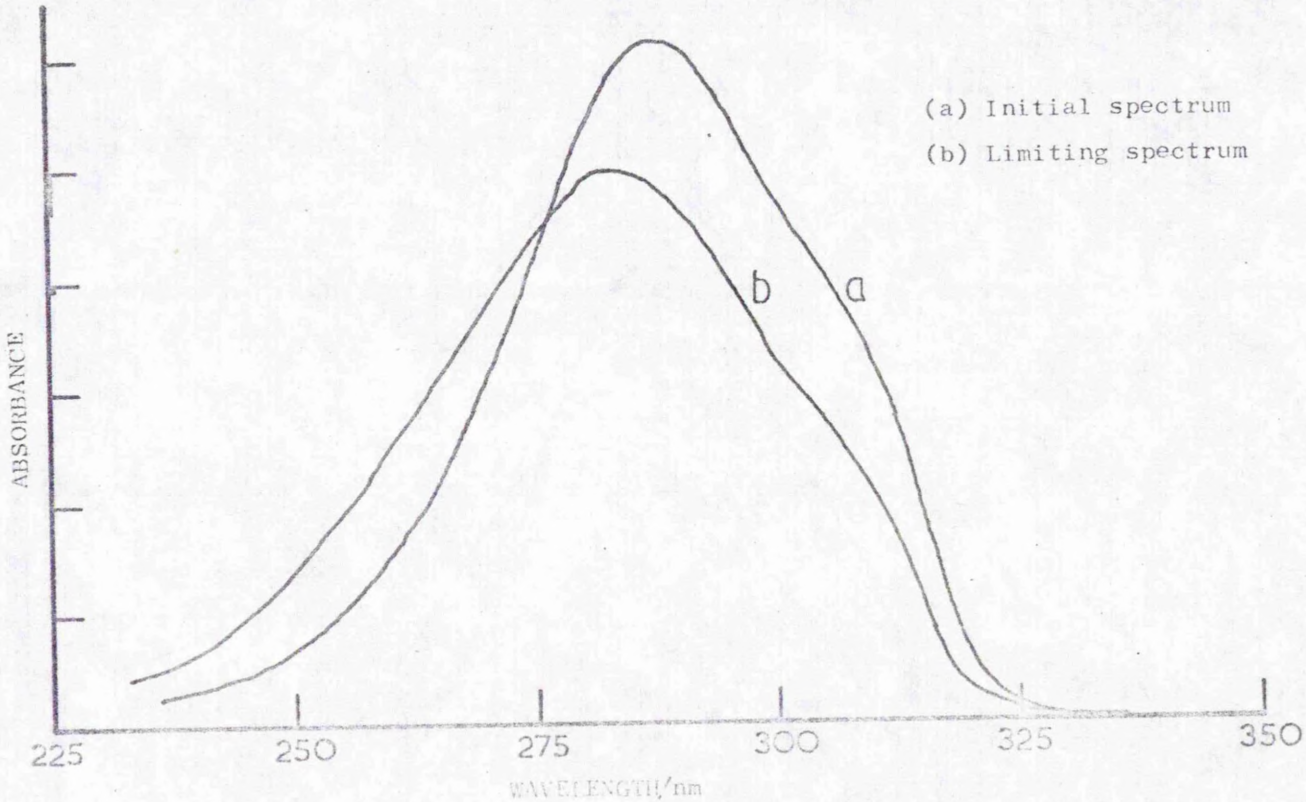

Fig. 3.9b Absorption spectra of [illegible]b(aa)$_3$·3H$_2$O in EtOH

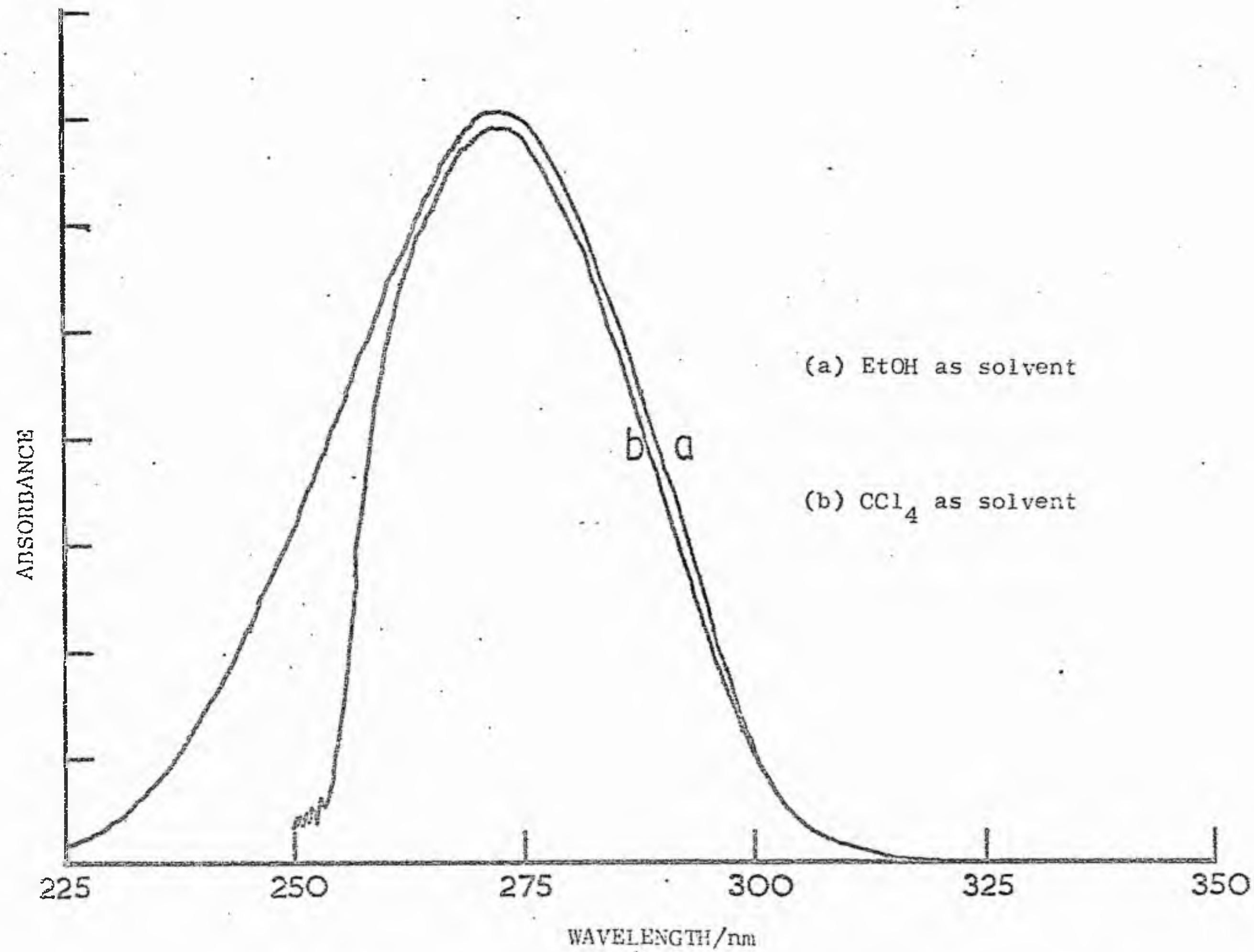

Fig. 3.10 Absorption spectra of acetylacetone in EtOH and CCl_4

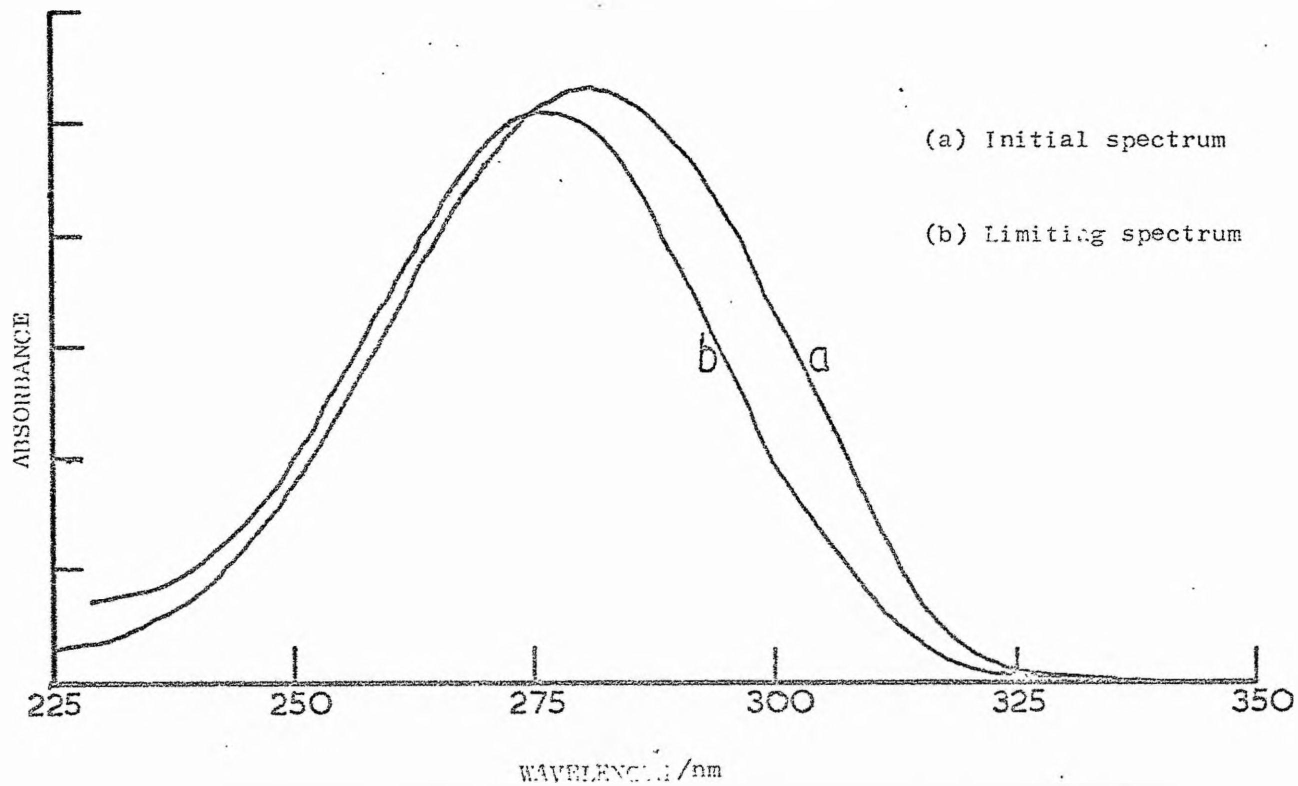

Fig. 3.11 Absorption spectra of sodium acetylacetonate in EtOH

solution is intermediate between the initial and final absorption maxima in figure 3.8. Thompson et al[292], obtained a value of 271 nm for the absorption maximum of acetylacetone which they attributed to the enol tautomer. Unfortunately, they did not state the solvent in which the measurement was carried out, however, their value appears to be in good agreement with the values obtained in ethanol and carbon tetrachloride (see table 3.2).

The spectra of the fresh solutions are consistent with the presence of a strong $\pi-\pi^*$ transition at ca 285 nm and a weaker $n-\pi^*$ transition being responsible for the shoulder at ca 310 nm.

(b) Excitation Spectra

Corrected excitation spectra of $Tb(dpm)_3$ and $Tb(aa)_3 \cdot 3H_2O$ in ethanol and carbon tetrachloride solutions, obtained using front face illumination by detecting the fluorescence at 550 nm as a function of the excitation wavelength are illustrated in figures 3.12 and 3.13 respectively. Freshly prepared solutions were employed to obtain the excitation spectra. Determinations of the excitation spectra using solutions that were prepared 24 hours prior to the measurements were only successful in the case of $Tb(aa)_3 \cdot 3H_2O$ in ethanol, the excitation spectrum being identical to that obtained for the freshly prepared solution. Table 3.3 summarises the excitation maxima for the appropriate chelates and solvents. It is apparent that the excitation maxima do coincide with the absorption maxima reported in table 3.2.

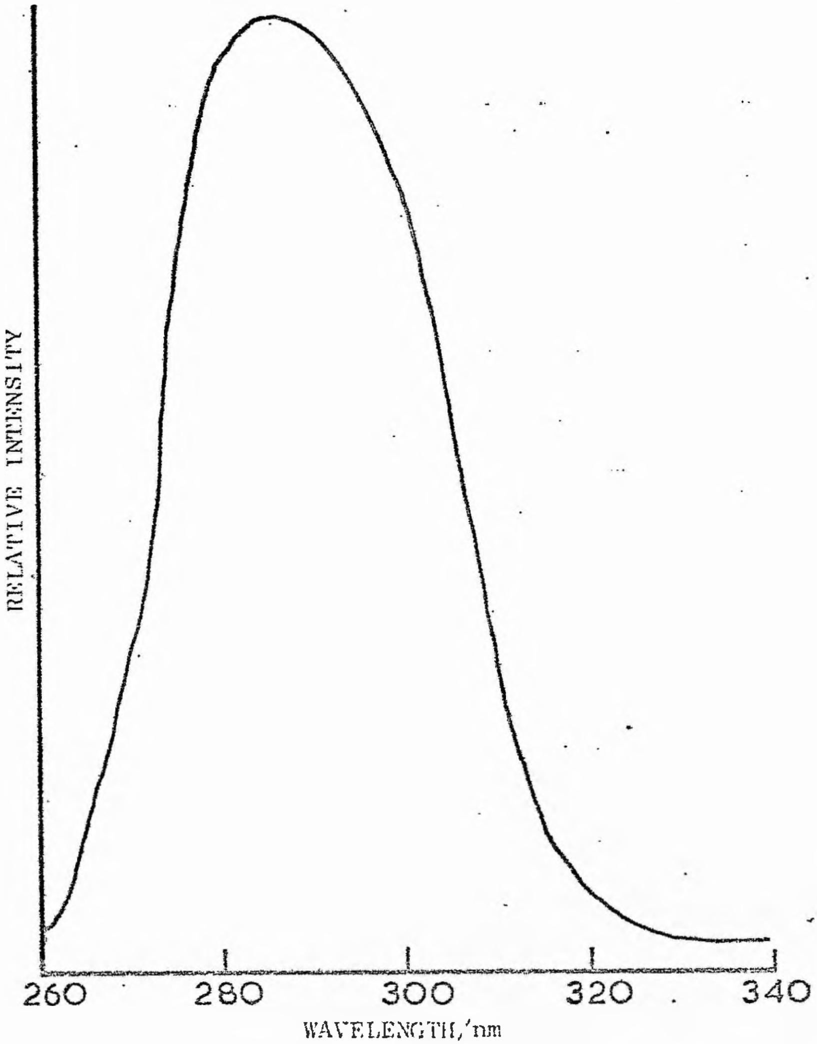

Fig. 3.12a Excitation spectrum of $Tb(dpm)_3$ in CCl_4

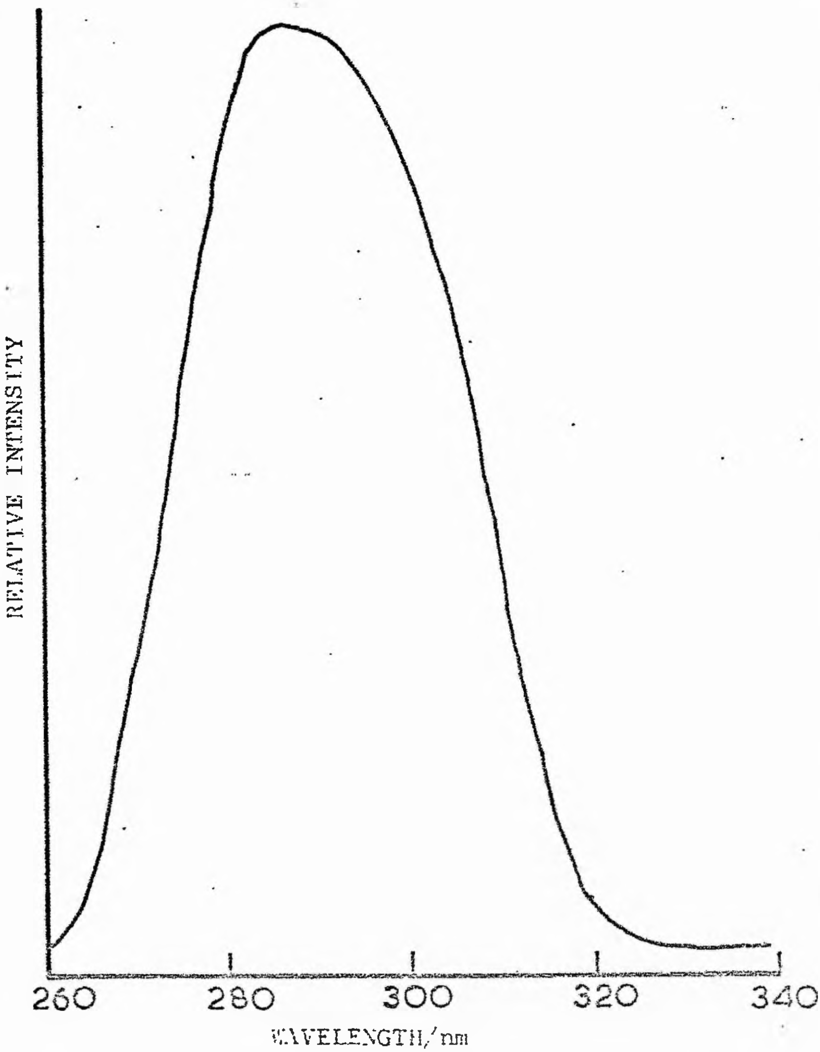

Fig. 3.12b Excitation spectrum of $Tb(dpm)_3$ in EtOH

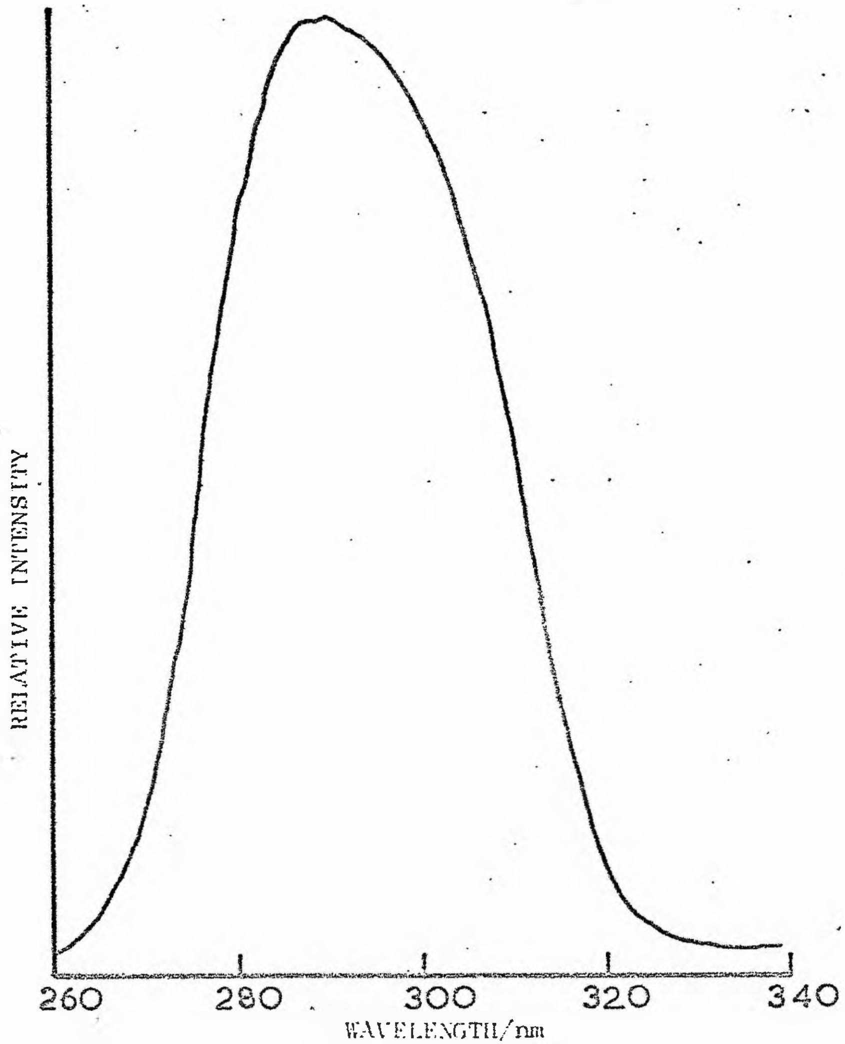

Fig. 3.13a Excitation spectrum of $Tb(aa)_3 \cdot 3H_2O$ in CCl_4

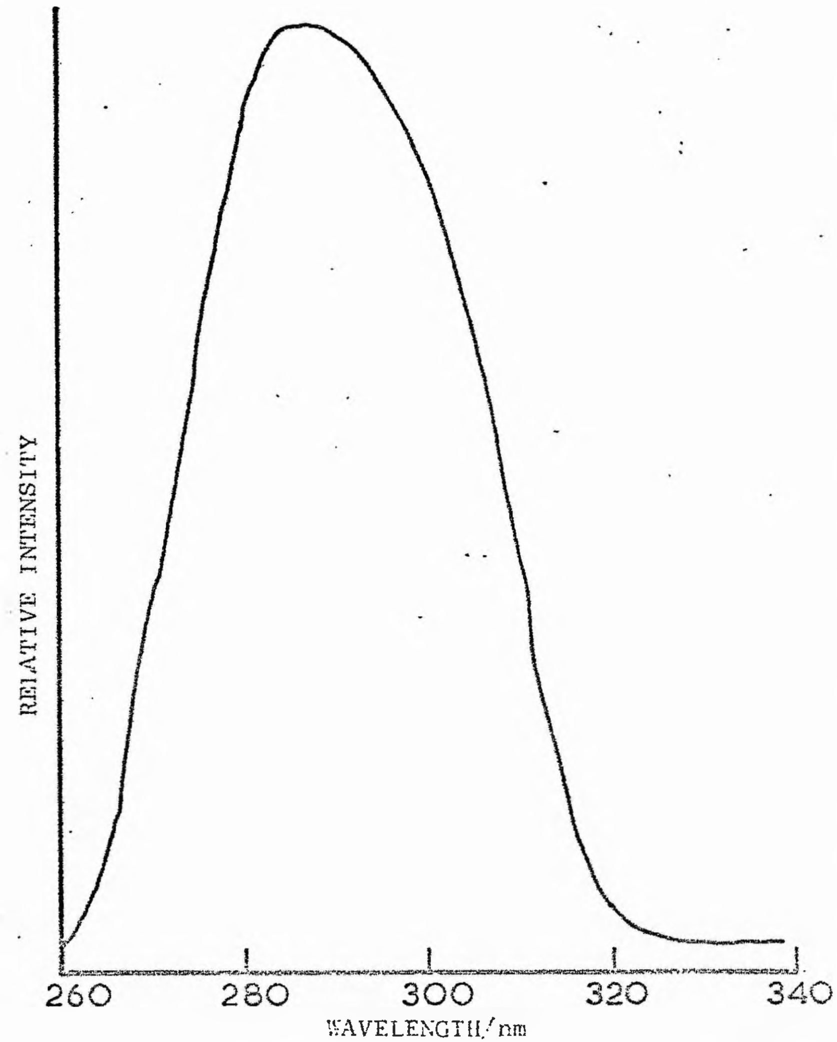

Fig. 3.13b Excitation spectrum of $Tb(aa)_3 \cdot 3H_2O$ in EtOH

Table 3.3

Data on excitation maxima

Sample	Solvent	λ_{max} nm
$Tb(dpm)_3$	EtOH	287 ± 1
$Tb(aa)_3 \cdot 3H_2O$	EtOH	288 ± 1
$Tb(dpm)_3$	CCl_4	283 ± 1
$Tb(aa)_3 \cdot 3H_2O$	CCl_4	290 ± 1

(c) Molecular Weight Determinations

Molecular weight determinations have been made for $Tb(dpm)_3$ and its mono-pyridine and ethanol adducts at concentrations between 10^{-1} and 8×10^{-3}M in ethanol and carbon tetrachloride solution (Table 3.4). The restricted concentration range was due to instrumental limitations. The apparent molecular weights for the

Table 3.4

Molecular weight data

Sample	concentration /m l^{-1}	Solvent	apparent M. Wt.	monomer M. Wt.
$Tb(dpm)_3$	5×10^{-2}	CCl_4	472 ± 40	708
$Tb(dpm)_3$	10^{-2}	CCl_4	435 ± 40	708
$Tb(dpm)_3$	8×10^{-3}	CCl_4	446 ± 40	708
$Tb(dpm)_3$	10^{-1}	EtOH	659 ± 60	708
$Tb(dpm)_3$	5×10^{-2}	EtOH	631 ± 60	708
$Tb(dpm)_3$	2×10^{-2}	EtOH	631 ± 60	708
$Tb(dpm)_3py$	10^{-2}	CCl_4	651 ± 60	787
$Tb(dpm)_3EtOH$	10^{-2}	CCl_4	524 ± 50	754

$Tb(dpm)_3$ chelate and its adducts in the solvents employed are all lower than the calculated molecular weight of the respective monomeric chelates, a slight decrease being observed with decrease in concentration. The values of $Tb(dpm)_3$ in carbon tetrachloride are ca 33-35% lower than that expected for monomeric $Tb(dpm)_3$. A similar observation was reported by Ghotra et al[287], although their values for a similar concentration range were only 12-17% lower.

(d) Conductance Measurements

Table 3.5 summarises the equivalent conductance measurements obtained for some tris and tetrakis chelates in acetonitrile and methanol at 25 ± 1°C. The measurements using acetonitrile as solvent were obtained with concentrations between 10^{-2} - 10^{-6}M, while the concentration limits using methanol as solvent were 10^{-2} - 10^{-4}. Equivalent conductance measurements for the chelates in methanol could not be accurately calculated for concentrations lower than 10^{-4}M because of the relatively high conductance of the methanol.

Table 3.5

Equivalent conductance values for some terbium chelates

Compound	Solvent	Equivalent Conductance					Molarity
		10^{-2}	10^{-3}	10^{-4}	10^{-5}	10^{-6}	
$Tb(tfaa)_3 \cdot 2H_2O$	MeCN		7.56	39.75	78.13	94.44	
$Tb(edaa)_3 \cdot 3H_2O$	MeCN		3.99	12.36	21.46	68.69	
$Tb(tfaa)_4 \cdot pipH$	MeCN	109.24	111.95	120.55			
$Tb(aa)_3 \cdot 3H_2O$	MeCN		1.89	6.22	46.36	253.28	
$Tb(btfa)_4 pipH$	MeCN		105.99	114.62	148.54	266.16	
$Tb(3CNaa)_3 \cdot 2H_2O$	MeCN		9.23	38.68	62.68	68.69	
$Tb(btfa)_3 \cdot 2H_2O$	MeCN		6.36	28.85	113.64	283.33	
$Tb(tfaa)_4 \cdot pipH$	MeOH	51.99	76.41	81.57			
$Tb(aa)_3 \cdot 3H_2O$	MeOH		15.03	55.81			
$Tb(3CNaa)_3 \cdot 3H_2O$	MeOH	4.08	9.87	38.64			
$Tb(btfa)_4 pipH$	MeOH		29.19	98.74			

(e) Discussion

In very dilute solutions, ca 10^{-6}M of mixed alcohols, mixed nitriles, EPA and mixed substituted benzene solvents, Samelson et al[201], have obtained evidence for the existence of free solvated Ln^{3+} ions and chelated ligands which were formed by the extensive dissociation of the lanthanide chelates. Hurt et al[293], on the basis of molecular weight determinations and conductance measurements concluded that the species formed by the dissociation of the lanthanide chelates investigated were dependent on the particular solvent employed. The results obtained by Hurt et al[293], and Samelson et al[201], for $Eu(btfa)_4 \cdot pipH$ agree qualitatively with the conductance measurement reported in table 3.5 for $Tb(btfa)_4 \cdot pipH$ in methanol and acetonitrile.

The absorption spectra of both $Tb(dpm)_3$ and $Tb(aa)_3 \cdot 3H_2O$ in ethanol and carbon tetrachloride were observed to undergo a blue shift and change in profile with time. The shoulder in the initial spectra at ca 310 nm was not observable, except for $Tb(aa)_3 \cdot 3H_2O$ in ethanol, in the limiting spectra. The limiting spectra were very similar in profile to that of acetylacetone in both ethanol and carbon tetrachloride. A similar spectral shift with time was observed for sodium acetylacetonate in ethanol. An absorption spectrum of a freshly prepared solution of $Tb(dpm)_3$ in a 60:40 ethanol:water mixture had similar spectral and profile characteristics to that of the limiting $Tb(dpm)_3$ spectra (see figure 3.14). This suggests that the water present in the initial solvents may be responsible for the observed spectra shifts and may explain the differences of the absorption maximum reported in table 3.2 and the value obtained by Archer et al[280], for $Tb(dpm)_3$ in carbon tetrachloride solution. The fact that no excitation spectra could be obtained, employing solutions which had been prepared 24 hours prior to

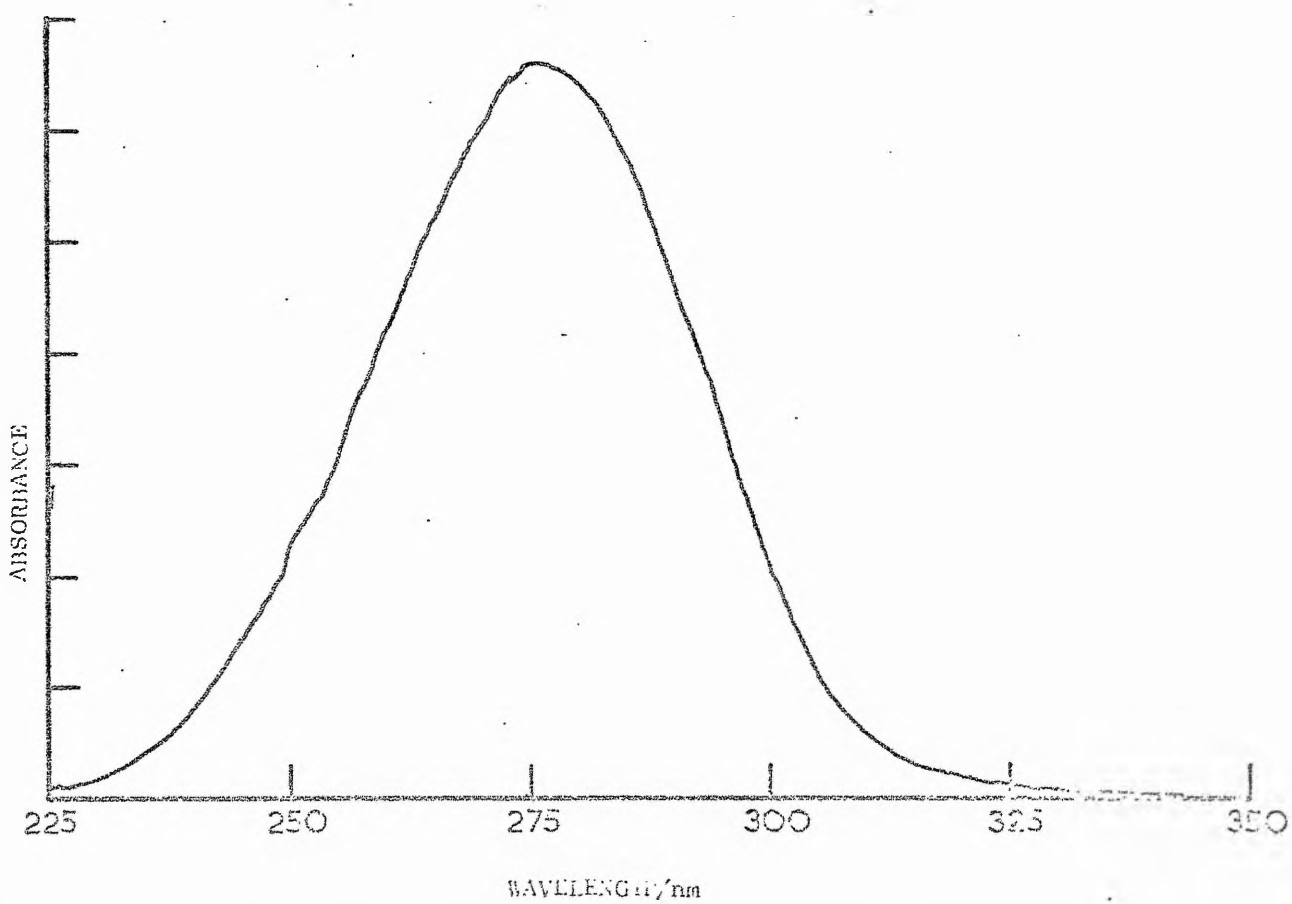

Fig. 3.14 Absorption spectrum of $Tb(dpm)_3$ in 60:40 $EtOH:H_2O$

measurement suggests that the terbium chelates are undergoing an irreversible dissociation, forming species which have at most extremely low quantum yields. Consideration of the absorption and excitation spectra therefore suggests a dissociation scheme of the type indicated below where L is the β-diketoenolate anion. The

$$Tb(L)_3 + H_2O \rightleftharpoons Tb(L)_2OH + LH \qquad 3.7$$

$$Tb(L)_2OH + H_2O \rightleftharpoons Tb(L)(OH)_2 + LH \qquad 3.8$$

$$Tb(L)(OH)_2 + H_2O \rightleftharpoons Tb(OH)_3 + LH \qquad 3.9$$

rate and extent of the irreversible dissociation would thus be dependent on the amount of water present in the initial solvent. The amount of water required for the reaction schemes of 3.7, 3.8 and 3.9 with an initial chelate concentration of 10^{-5}M is ca 6×10^{-5} % which will be present even in the most carefully dried solvents. (Preliminary investigations of the photodecomposition of $Tb(dpm)_3$ in carbon tetrachloride where ultraviolet irradiation over a period of time produced a white precipitate consistent with that expected for $Tb(OH)_3$ supports the reaction scheme proposed above.) The excitation spectra of $Tb(dpm)_3$ and $Tb(aa)_3 \cdot 3H_2O$ in both ethanol and carbon tetrachloride solutions indicate that both the π-π^* and n-π^* absorption transitions contribute to the Tb^{3+} fluorescence. Rapid internal conversion from the π,π^* singlet to the n,π^* singlet probably occurs. These results are consistent with the observations of Dawson et al[238].

As a general rule, in organic molecules the singlet-triplet splitting of π,π^* energy levels is relatively large compared to the corresponding splitting for n,π^* energy levels (see chapter 1.2). This suggests that when the energy difference between $S_1(n,\pi^*)$ and $S_2(\pi,\pi^*)$ states is small the lowest triplet level may be $T_1(\pi,\pi^*)$. The probability of intersystem crossing is enhanced when the two states involved are of different electronic type[140]. Figure 3.15 therefore illustrates the possible energy transfer mechanism in lanthanide β-diketoenolate complexes.

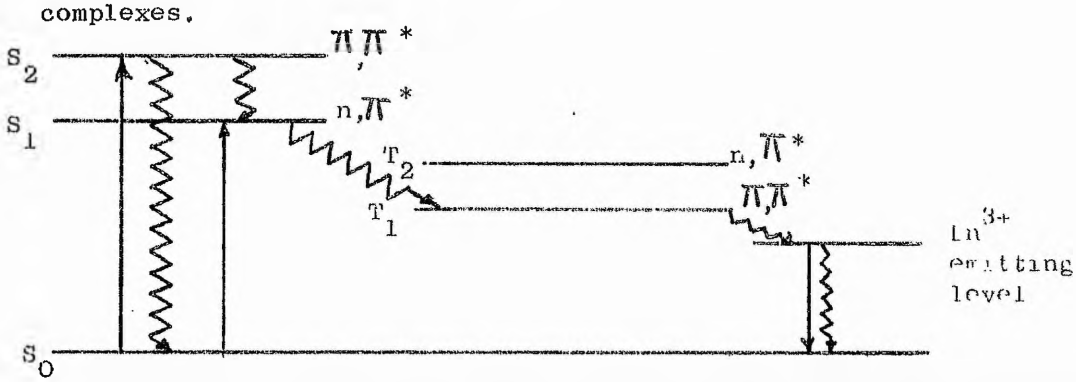

Fig. 3.15 Illustration of the possible energy transfer mechanism in Ln^{3+} chelates

Molecular weight measurements on $Tb(dpm)_3$ in ethanol and carbon tetrachloride solution indicate that the species present are essentially monomeric but dissociate slightly in solution. Ethanol appears to be a better solvent than carbon tetrachloride for preventing dissociation possibly because of its greater coordinating ability towards the Ln^{3+} ions which would lead to a more solvent stable chelate. Mackie et al[122], using nmr spectroscopy have determined association constants, Ka, of various organic substrates with $Eu(dpm)_3$ in d-chloroform solution for the reaction illustrated in equation 3.10, S being the organic substrate.

$$Eu(dpm)_3 + S \underset{}{\overset{Ka}{\rightleftharpoons}} Eu(dpm)_3 \cdot S \qquad 3.10$$

It can be shown that Ka is related to the degree of dissociaton, α, of the complex-substrate molecule by equation 3.11 and α related to

$$Ka = \frac{(1-\alpha)}{c\alpha^2} \qquad 3.11$$

the apparent molecular weight, $M. Wt._{app.}$, by the equation 3.12 where M. Wt. is the true molecular weight of the complex-substrate molecule.

$$\alpha = \frac{M.\ Wt. - M.\ Wt._{app.}}{M.\ Wt._{app.}} \qquad 3.12$$

Equations 3.11 and 3.12 are only valid when the simple association reaction of equation 3.10 is considered. Using the Ka values obtained by Mackie et al[122], for 2-phenylethanol and 4-methylpyridine i.e. 100 and 140 l mol^{-1} respectively, and assuming similar values for ethanol and pyridine in carbon tetrachloride solution, utilisation of equations 3.11 and 3.12 allows the apparent molecular weights predicted by nmr spectroscopy for $Tb(dpm)_3EtOH$ and $Tb(dpm)_3py$ to be calculated. Assuming in the case of $Tb(dpm)_3$ that there is an equilibrium between the water present in carbon tetrachloride, similar treatment would allow the calculation of the apparent molecular weight for that species in solution. Table 3.6 summarises the molecular weights predicted by nmr and the values obtain by osmometry for $Tb(dpm)_3$ and its adducts. The results for the adduct

Table 3.6

Molecular weight values from nmr and osmometry data

Sample	nmr $M.\ Wt._{app.}$	osmometry $M.\ Wt._{app.}$
$Tb(dpm)_3EtOH$	465	524 ± 50
$Tb(dpm)_3py$	504	651 ± 60
$Tb(dpm)_3 \cdot H_2O$	448	435 ± 40

molecular weights predicted by nmr are low compared to the values obtained by osmometry suggesting that complete dissociation to chelate and organic substrate is not fulfilled in carbon tetrachloride. The value obtained assuming Ka for water to be 100 l mol^{-1} i.e. similar to 2-phenylethanol is in good agreement with the value obtained by osmometry presenting evidence for the existence of $Tb(dpm)_3 \cdot H_2O$ in solution.

Precise interpretation of conductance measurements are extremely difficult because of the complex dissociation that may occur at low concentrations. Tetrakis chelates appear to undergo greater ionic dissociation of the type shown in equation 3.13 in acetonitrile than in methanol, possibly because of the higher dielectric constant of acetonitrile leading to enhanced stability

$$Tb(L)_4^-(cation)^+ \rightleftharpoons Tb(L)_4^- + (cation)^+ \qquad 3.13$$

of the ions. The better coordinating ability of methanol may be the reason for the greater ionic dissociation of the tris chelates in methanol compared to that in acetonitrile. Dissociation of one or more β-diketoenolate anions from the tris chelate may lead to the formation of a higher coordinated lanthanide species as illustrated by equation 3.14. The probability of dissociation

$$Ln(L)_3 + xMeOH \rightleftharpoons [Ln(L)_n(MeOH)_x]^{(3-n)^+}[(L)_{3-n}]^{(3-n)^-} \qquad 3.14$$

occurring via equation 3.14 is greatly reduced when acetonitrile is the solvent because of its poor coordinating ability.

(f) Conclusion

It is apparent that the species present in organic solutions of lanthanide chelates is dependent on the particular chelate, chelate concentration and solvent. At very low concentration ca 10^{-6}M and often quite high concentration ca 10^{-2}M there is appreciable dissociation making characterisation of the species being investigated difficult if not impossible. It would therefore be advantageous to employ concentrations where dissociation is kept to a minimum. Extremely small percentages of water present in the solvent appear to have an adverse effect on the stability of some tris lanthanide chelates especially when working at low concentrations. This may be attributed to an irreversible process involving the solvent and caused by the lanthanide ions affinity for higher coordination. The solvents with higher dielectric constants encourage ionic dissociation of tetrakis lanthanide chelates while a better coordinating solvent such as methanol appears to increase the dissociation of tris chelates. Although $Tb(dpm)_3$ exists as a dimeric unit in the crystalline state investigations on its mono-adducts and molecular weight determination in ethanol and carbon tetrachloride are indicative of monomeric rather than dimeric species which are to a slight extent dissociated in solution.

CHAPTER 4

THE INFLUENCE OF CATIONS ON THE FLUORESCENCE PROPERTIES OF SOME SOLID TETRAKIS TERBIUM(III) COMPLEXES

1. INTRODUCTION

Little attention has been given to investigations on the effects of differing environment on the fluorescent properties of solid terbium chelates. Investigations of environmental effects have generally been restricted to various europium salts and complexes both in the solid state and in various solvents.

Charles *et al*[294], have studied the properties of some europium *tetrakis* chelates derived from benzoyltrifluoroacetone with different cations in the crystalline state and in acetonitrile solution. They observed that the fluorescence properties of the chelates in the solid state are dependent, to a significant extent on the nature of the cation. In acetonitrile solution the *tetrakis* complexes are largely dissociated to the cation and $[Eu(btfa)_4]^-$, the observed solution fluorescence being in most instances independent of the cation. They concluded that when the intensity of solution fluorescence was dependent on the cation that it was due to interaction between anion and cation to give equilibrium concentrations of the corresponding *tris* chelate having a lower quantum yield than the *tetrakis* complexes. Equations 4.1 and 4.2 illustrate the proposed interactions where QH^+ is the cation.

$$QH^+ + [Eu(btfa)_4]^- \rightleftharpoons Q + Hbtfa + Eu(btfa)_3 \qquad 4.1$$

or

$$QH^+ + [Eu(btfa)_4]^- \rightleftharpoons (QH)^+(btfa)^- + Eu(btfa)_3 \qquad 4.2$$

Emission spectra of ten europium *tetrakis* chelates derived from fluorinated β-diketones of type (I) were shown to have a marked profile and intensity differences in both the solid state and in acetonitrile solution[226]. The fluorescence intensity in the solid

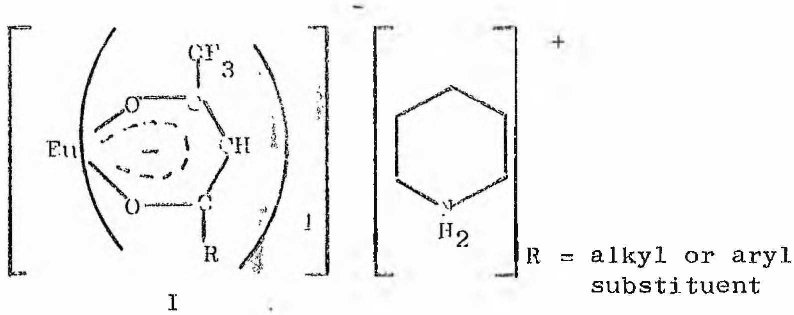

I

state was found to be principally dependent on the local symmetry conditions about the coordinated europium atom rather than upon electronic effects associated with resonance and inductive interactions of the group R with the chelate ring. Other examples of changes in crystalline europium emission spectra from a chelate anion upon changing the nature of the cation have been given by Melby *et al*[73] and Bauer *et al*[74].

Substituent effects on the emission spectra of some poorly characterised europium and terbium chelates in EPA solution (5 parts diethyl ether, 5 parts 3-methylpentane and 2 parts absolute ethanol by volume) at concentrations of $\sim 10^{-5}$M at 77K have indicated that local symmetry conditions can affect the various energy transfer processes leading to lanthanide fluorescence[224]. Appreciable variations in the relative intensity and number of individual lines in the fluorescence spectra of the different substituted lanthanide chelates was observed. It was concluded that the various substituents change both the symmetry and the effective perturbation of the molecular field surrounding the ion and modify the interaction of the 4f-shell of the ion with its environment.

Hass *et al*[204,205,295] have investigated the change in radiative and nonradiative energy transfer processes caused by environmental changes by employing simple europium salts e.g. $Eu(ClO_4)_3$ dissolved in various protonated and deuterated solvents. The line shape and intensity of their absorption and emission spectra where shown to depend strongly on the solvent and anion. Radiative and nonradiative rate constants were determined from absolute quantum yield and lifetime data and were found to have similar environmental dependence . Quenching of Eu^{3+} fluorescence by various anions was demonstrated, the order of quenching ability for the anions investigated being $CNS^- > Cl^- > NO_3^- > ClO_4^-$. The fluorescence quenching of the $^5D_0$ Eu^{3+} level in $Eu(ClO_4)_3$ in mixtures of water and acetonitrile was shown to be proportional to the number of water molecules entering the first solvation layer[295]. The quenching reaches its value in pure water when there are nine water molecules per Eu^{3+} ion, suggesting that each water molecule may act independently in the quenching process. The rate of quenching by one water molecule was found to be 1100 s^{-1}.

Radiative quantum efficiencies of various terbium chelates dissolved in acrylic and bettle resin have been shown to be enhanced by adduct formation using tripyrazoylborate. The enhancement was explained by further shielding of the Tb^{3+} ion from low frequency vibrations of the solid state resin environment[296]. The probability of relaxation between two excited levels, $^5D_3$ and $^5D_4$ of Tb^{3+} ions have been shown to be dependent on the host lattice when embedded in various inorganic glasses[297]. Absolute values of the relaxation probabilities from $^5D_3$ to $^5D_4$ levels of Tb^{3+} ions have been obtained experimentally and further the dependence of the probability on the concentration of Tb^{3+} as well as on the type of other lanthanide ions present was studied[219]. It was concluded that the increase of the

Tb^{3+} concentration as well as coexistence of other lanthanide ions cause strong effects on the relaxation process from $^5D_3$ to $^5D_4$ levels of the Tb^{3+} ions, and that the effects are attributed to the resonance energy transfer between the ions caused by electrical multipole interactions. Nonradiative relaxation rates $^5D_3 \rightsquigarrow {}^5D_4$ and fluorescence lifetimes, $^5D_3 \longrightarrow {}^7F_j$ and $^5D_4 \longrightarrow {}^7F_j$ were all found to be markedly dependent on the inorganic glass host[297].

2. THERMAL DEPOPULATION OF THE $^5D_4$ LEVEL IN SOLID TETRAKIS TERBIUM(III) CHELATES

(a) Lifetimes

Lifetimes of the Tb^{3+} $^5D_4 \longrightarrow {}^7F_j$ transitions in solid hydrated tris hexafluoroacetylacetone (hfaa), trifluoroacetylacetone (tfaa) and several corresponding anionic tetrakis complexes having different concomitant cations have been determined at 77K and where possible at various temperatures up to 323K. All the complexes investigated showed decreases in lifetime at higher temperatures but the profiles of temperature-dependence differed considerably from chelate to chelate. The temperature-dependence of the Tb^{3+} lifetime for the various chelates are summarised in table 4.1 while figure 4.1 illustrates the diversity of the behaviour shown by some of the chelates. Most of the solid chelates have detectable lifetimes at room temperature which is in marked contrast to the behaviour of the chelates in solution where low quantum yields have precluded measurement.

(b) Triplet Energies

The triplet energies for the various terbium chelates were

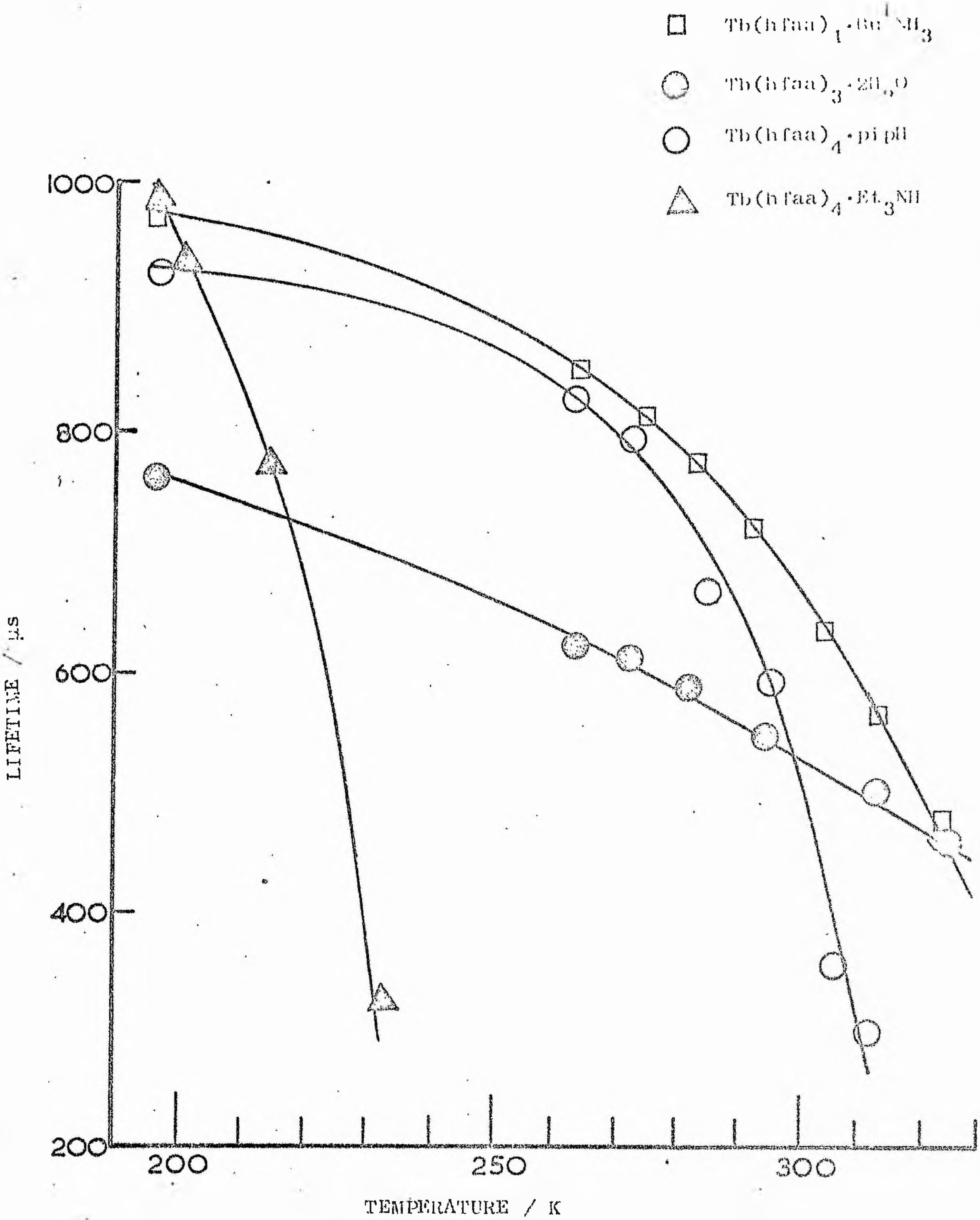

Fig. 4.1 Lifetime v temperature plots for some solid Tb^{3+} chelates

Table 4.1

Lifetime v temperature for solid terbium chelates

Compound	Lifetime / μs								
	77K	195K	263K	273K	283K	293K	303K	313K	323K
$Tb(hfaa)_3 \cdot 2H_2O$	849	768	620	618	585	553	540	500	468
$Tb(hfaa)_4 \cdot pipH$	991	932	829	793	655	589	349	302	
$Tb(hfaa)_4 \cdot NH_4$	1166	1087	369						
$Tb(hfaa)_4 \cdot Ph_4As$	626	607	426[a]	385[b]	249[c]				
$Tb(hfaa)_4 \cdot Me_4N$	1347	559	263[d]						
$Tb(hfaa)_4 \cdot Et_3NH$	1305	1004	338[b]						
$Tb(hfaa)_4 \cdot Bu^tNH_3$	1066	988	862	815	785	730	635	569	487
$Tb(hfaa)_4 \cdot picH \cdot pic$	843	732	415	377	316				
$Tb(tfaa)_3 \cdot 2H_2O$	891	844	702	628	519	473			
$Tb(tfaa)_4 \cdot pipH$	1407	1206	770						
$Tb(tfaa)_4 \cdot NH_4$	1110	1034	754	722	539	481			
$Tb(tfaa)_4 \cdot Ph_4As$	1250	1250	1100	968	881	659	485	405	
$Tb(tfaa)_4Na$	1081	1080	884	733	704	610	530		
$Tb(tfaa)_4K$	1276	1213	780	521					
$Tb(tfaa)_4Cs$	1080	1078	842	662	630	503			

Lifetime measured at a 218K; b 233K; c 248K; d 226K

determined by measuring the ligand phosphorescence of the analogous gadolinium chelates at 77K with an excitation wavelength of 340 nm. The emission profiles for the chelates within the two homologous series were very similar and are illustrated in the case of the hfaa chelated by $Gd(hfaa)_4 \cdot Bu^tNH_3$ (figure 4.2) and in the case of the tfaa chelates by $Gd(tfaa)_4 \cdot Na$ (figure 4.3). A notable feature of most of

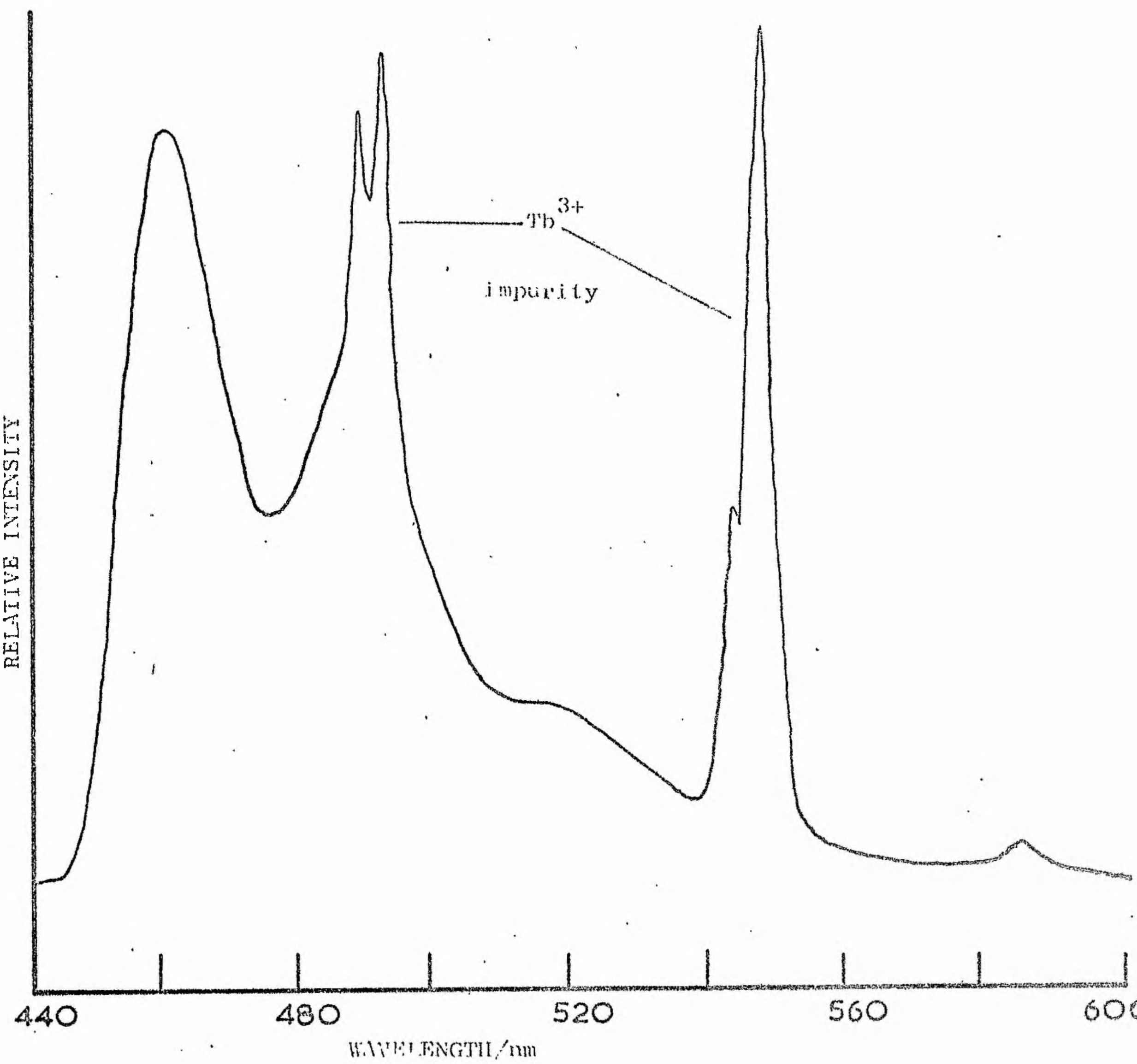

Fig. 4.2 Uncorrected emission spectrum of solid $Gd(hfaa)_4 \cdot Bu^tNH_3$

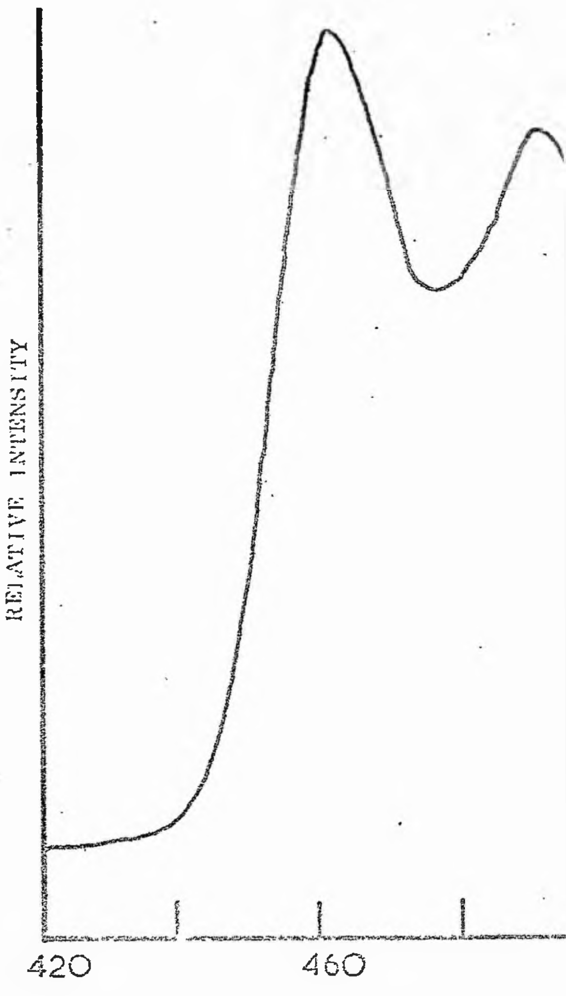

Fig. 4.3 Uncorrected emissi

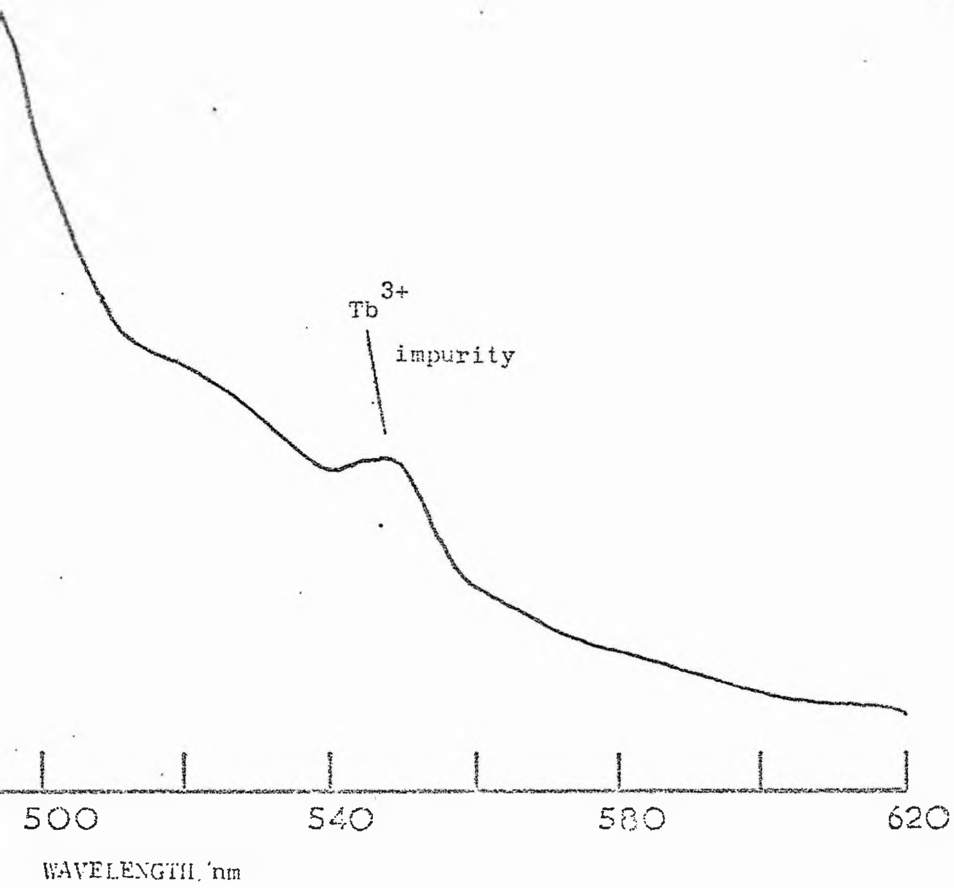

...n spectrum of solid Gd(tfaa)$_3$ ...

these spectra are the lanthanide emissions due to impurities (see discussion). The triplet maxima, ν_T, for the various chelates are summarised in table 4.2. The triplet levels in the hfaa complexes vary over ca 800 cm^{-1} with a mean value of 21,900 cm^{-1} which is

Table 4.2

Ligand triplet energies, ν_T, of solid gadolinium complexes

Compound	Triplet value ν_T/cm^{-1}	Compound	Triplet value ν_T/cm^{-1}
$Gd(hfaa)_3 2H_2O$	21,280	$Gd(tfaa)_3 \cdot 2H_2O$	22,080
$Gd(hfaa)_4 pipH$	21,410	$Gd(tfaa)_4 pipH$	21,280
$Gd(hfaa)_4 NH_4$	21,740	$Gd(tfaa)_4 NH_4$	21,830
$Gd(hfaa)_4 Ph_4As$	22,080	$Gd(tfaa)_4 Ph_4As$	22,220
$Gd(hfaa)_4 Me_4N$	21,280	$Gd(tfaa)_4 Na$	21,790
$Gd(hfaa)_4 Me_3NH$	21,280	$Gd(tfaa)_4 K$	21,790
$Gd(hfaa)_4 Bu^tNH_3$	21,790	$Gd(tfaa)_4 Cs$	21,790
$Gd(hfaa)_4 picH.pic$	21,280		

similar to the value reported for hfaa chelates in solid solution[288]. The range of the tfaa complexes is slightly larger but all are considerably lower than 23,000 cm^{-1}, the value obtained in solid solution[288]. It is evident that the triplet-level energy can be critically dependent on the environment of the ligand.

(c) Emission Spectra

The emission spectra of the crystalline terbium chelates when excited at 340 nm at 77K all exhibit sharp line fluorescence characteristic of the Tb^{3+} ion. Spectral profiles and intensities of the fluorescence bands are markedly dependent on the cation, this dependence being illustrated for the hfaa complexes by figures 4.4 and 4.5 and for the tfaa chelates by figures 4.6 and 4.7. The profile of the emission spectra are determined by the local environment of the bonded Tb^{3+} ion which influence the $^5D_4 \longrightarrow {}^7F_j$ transition probabilities within the Tb^{3+} manifold. These spectral differences therefore imply a cation dependence on the local symmetry conditions around the Tb^{3+} ions.

A dependence of local symmetry on the structure in the solid state is not unexpected since, in the solid, the arrangement of the oxygen atoms bonded to the terbium may be distorted from otherwise favoured configurations to accommodate crystal packing requirements. The degree of distortion will, in turn, be influenced by the size and shape of the cation. Similar profile differences have been reported by Charles et al[226] for a series of solid europium btfa chelates.

(d) Discussion

The emitting $^5D_4$ level of Tb^{3+} lies ca 20,000 cm^{-1} above the $^7F_6$ ground state and it has been established that thermal depopulation of this level may occur in terbium chelates in solution[288] and in the solid state (see chapter 3). Back donation of energy occurs to a triplet state of the ligand and the rate of this temperature-dependent depopulation, k(T), may be expressed in terms of τ_T, the observed lifetime at temperature T and τ' the lifetime in the absence of any back-donation by equation 3.2. If the energy is back-donated to a single acceptor level of the ligand at energy E above the $^5D_4$ terbium level then k(T) may be expressed in the form of the Arrhenius equation 3.3. Figure 3.6 shows an energy level diagram representing this situation.

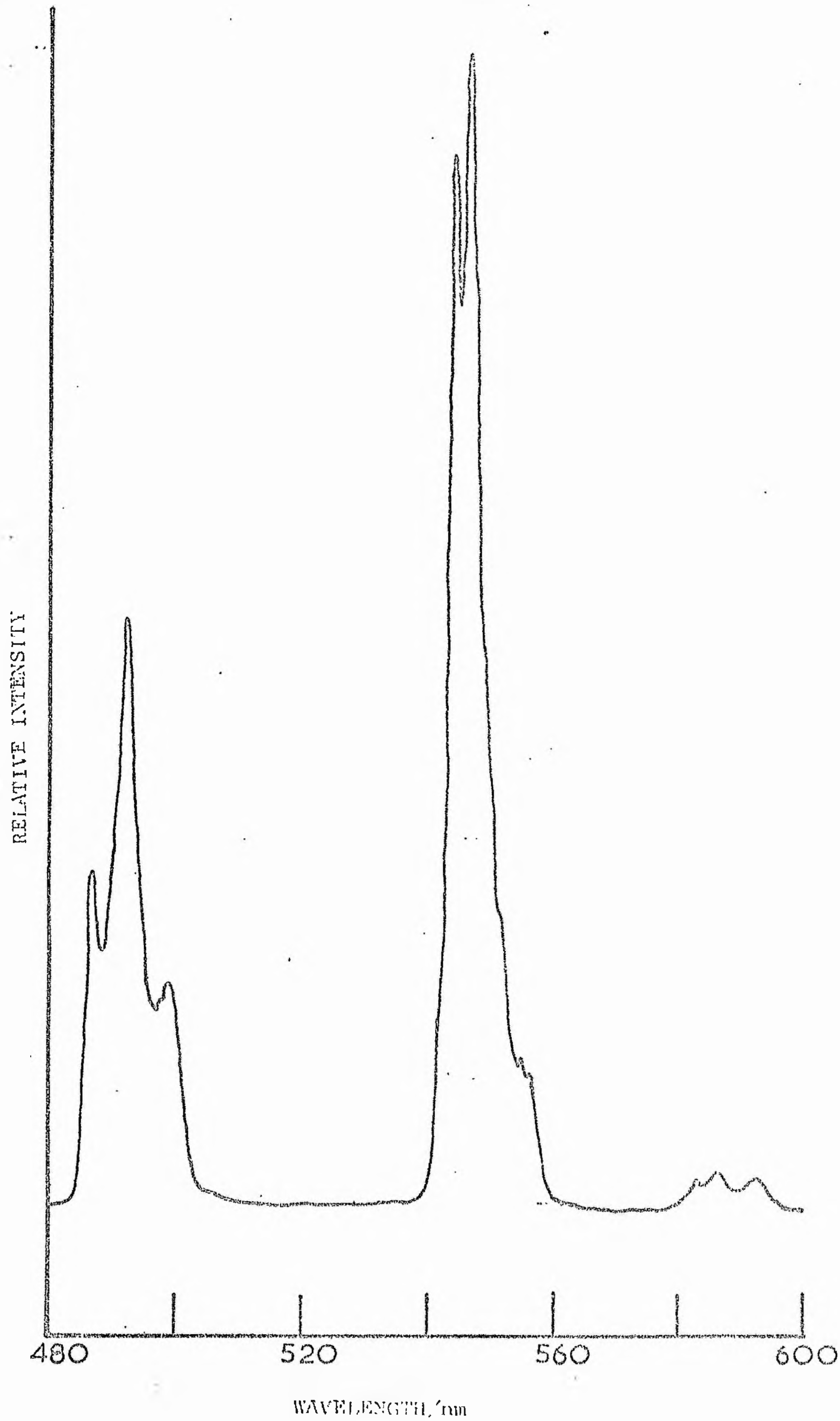

Fig. 4.4 Uncorrected emission spectrum of solid Tb(hfaa)$_4$picH·pic

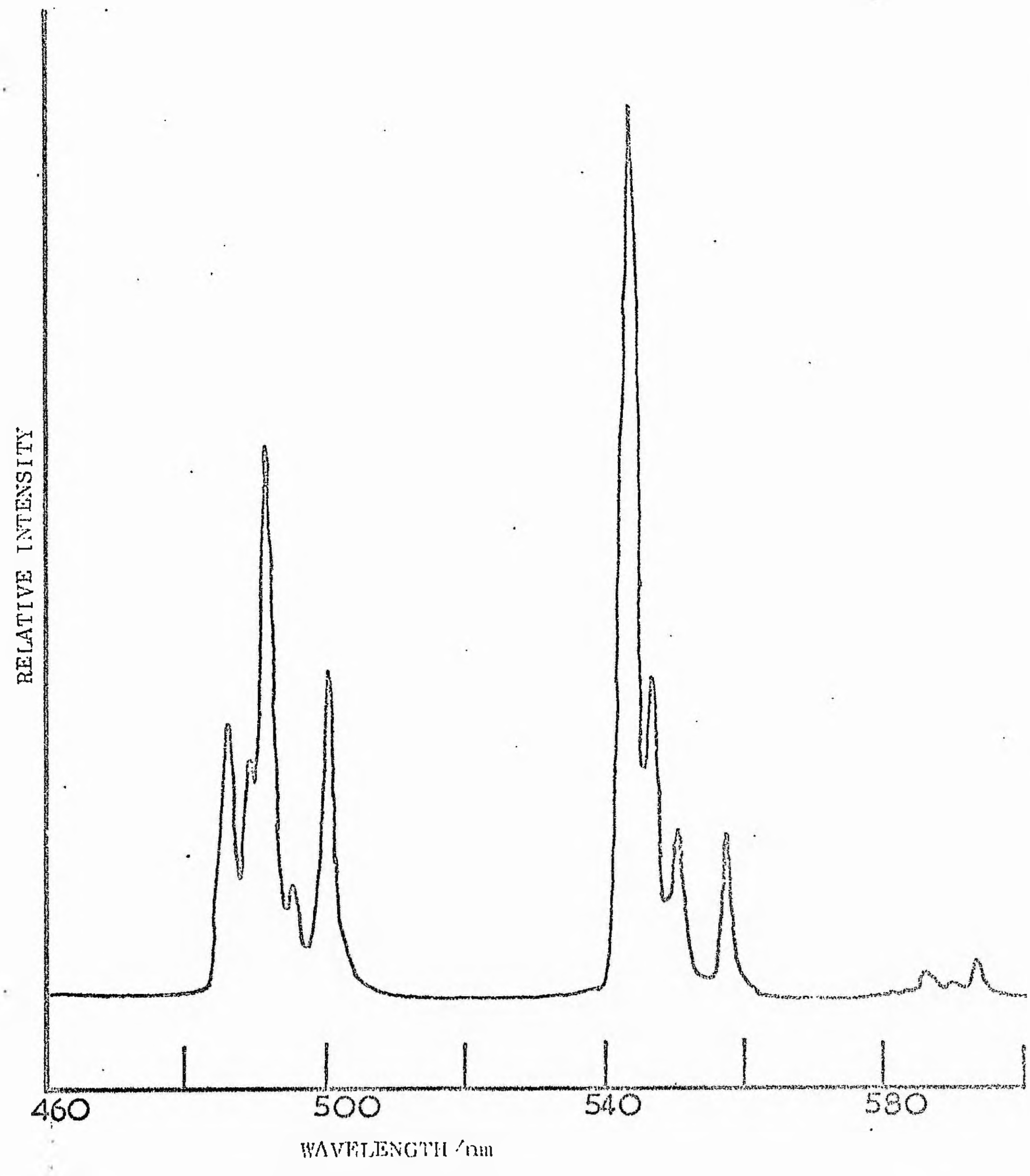

Fig. 4.5 Uncorrected emission spectrum of solid $Tb(hfaa)_4Et_3NH$

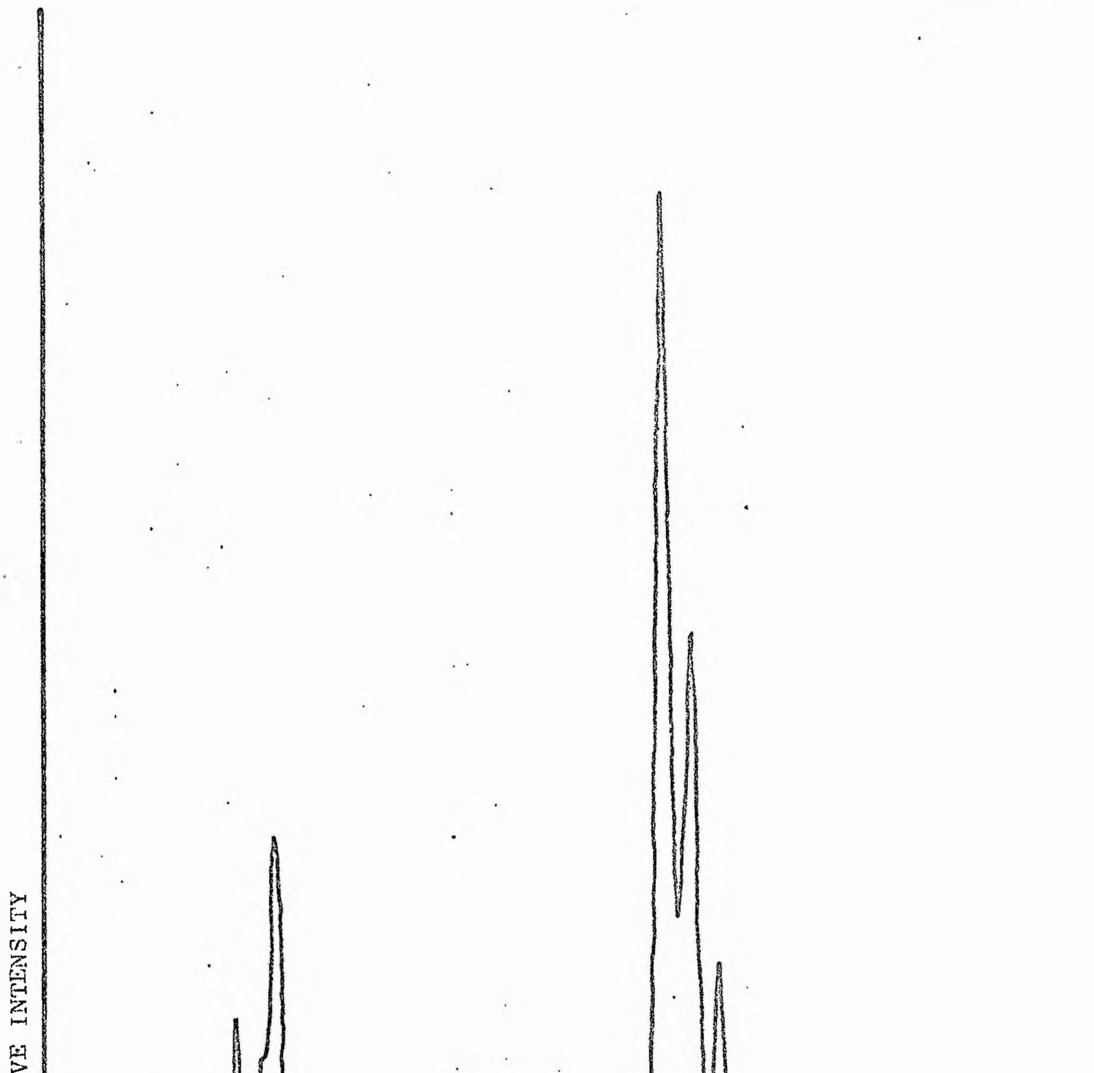

Fig. 4.6 Uncorrected emission spectrum of solid Tb(tfaa)$_4$ pipH

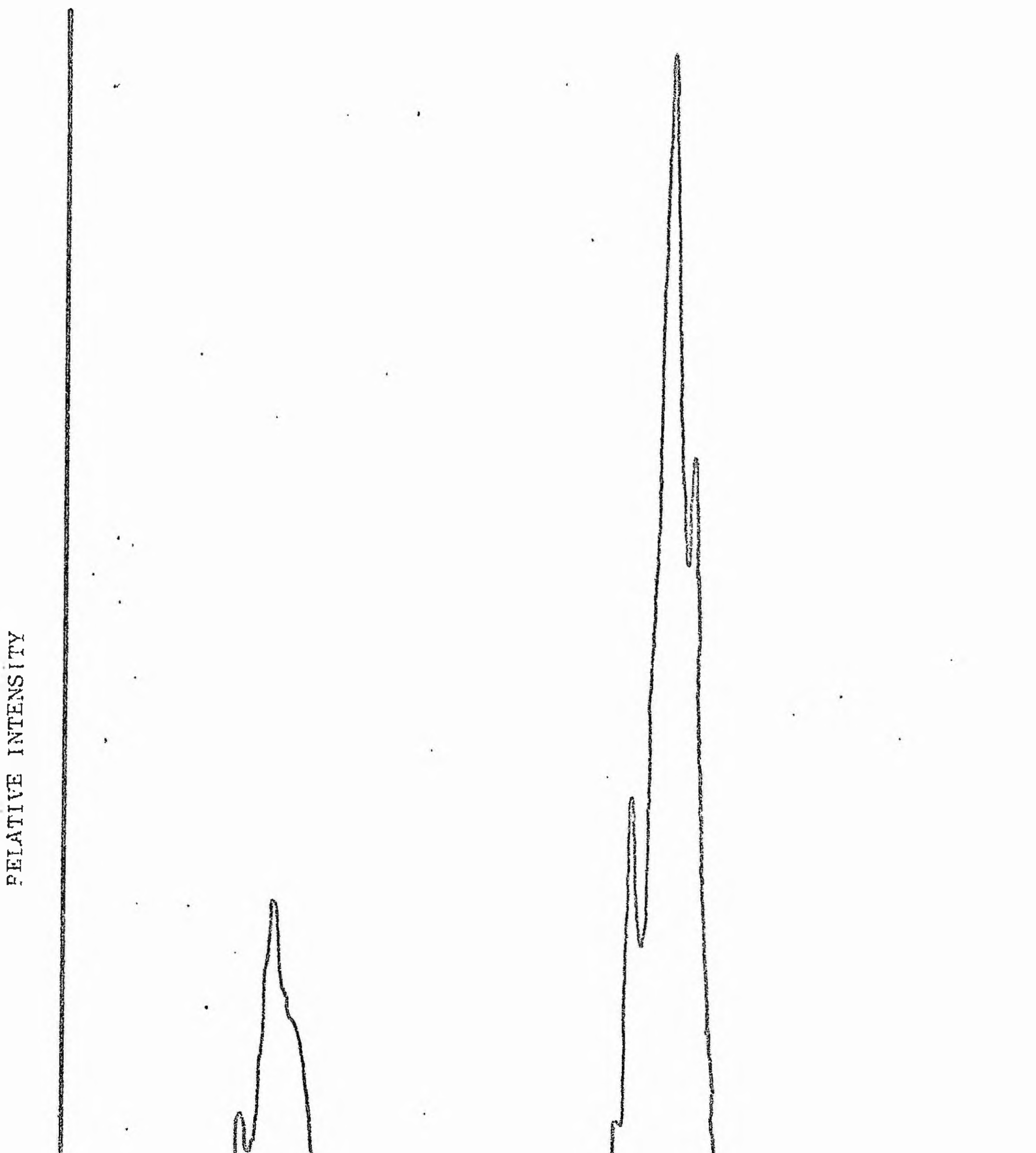

Fig. 4.7 Uncorrected spectrum of solid $Tb(tfaa)_4 \cdot Cs$

A possible explanation for the diversity of the temperature dependence of the lifetimes of the two series of compounds may be due to the different degrees of thermal depopulation of the $^5D_4$ Tb^{3+} level. Similar treatment of the lifetime data shown in table 4.1 to that shown in table 3.1 was performed within the temperature range 263-323K for those compounds giving measurable fluorescence output at these temperatures. Linear plots, within experimental error of log $(\frac{1}{\tau} - \frac{1}{\tau_{77}})$ against 1/T were obtained indicating that thermal depopulation is essentially occurring to a single energy level although slight deviations at higher temperatures suggested that higher levels might also be involved. The values of E and A in table 4.3 were obtained by use of a least squares treatment to obtain the best straight line. In order to obtain the energies

Table 4.3

Spectroscopic parameters for solid terbium chelates

Compound	E^b /cm^{-1}	E spec^c /cm^{-1}	$^5D_4$^{d} /cm^{-1}	10^{-3}A/ s^{-1}
$Tb(hfaa)_3 \cdot 2H_2O$	880	950	20,330	4.6
$Tb(hfaa)_4 \cdot$pipH	1220	1130	20,280	16
$Tb(hfaa)_4 . NH_4$	1770	1460	20,280	3100
$Tb(hfaa)_4 \cdot Ph_4As^f$	1440	1710	20,370	960
$Tb(hfaa)_4 \cdot Me_4N^f$	1050	1000	20,280	250
$Tb(hfaa)_4 \cdot Et_3NH^f$	980	1040	20,240	33
$Tb(hfaa)_4 \cdot Bu^tNH_3$	1150	1310	20,480	12
$Tb(hfaa)_4$picH·pic	1020	1000	20,280	33
$Tb(tfaa)_3 \cdot 2H_2O$	2100	1750	20,330	3200
$Tb(tfaa)_4$	840	910	20,370	5.8
$Tb(tfaa)_4$	1810	1460	20,370	890
$Tb(tfaa)_4$	1940	1940	20,280	680
$Tb(tfaa)_4$	1570	1380	20,410	170
$Tb(tfaa)_4$	1740	1380	20,410	700
$Tb(tfaa)_4$	1880	1380	20,410	830

Table 4.3 continued

b $^5D_4$ - ligand acceptor level energy difference calculated from lifetime data

c $^5D_4$ - ligand triplet energy difference using triplet energies derived from corresponding Gd complexes

d See text

e Pre-exponential term in equation 3.3

f E determined from data at temperatures below 263K

of the ligand levels predicted by the E values obtained from the lifetime data it is necessary to use a value of the $^5D_4$ - $^7F_6$ energy difference. This requires some form of approximation since the Tb^{3+} levels are split by the crystal field to an extent of several hundred cm^{-1}. The centre of gravity of the $^5D_4 \longrightarrow {}^7F_6$ emission lines have therefore been used to obtain the $^5D_4$ energies, ν_{Tb}, in table 4.3. Values of E_{spec}, where $E_{spec} = \nu_T - \nu_{Tb}$ are also shown.

The agreement found between E and E_{spec} (see table 4.3) is within experimental error in both the hfaa and tfaa series and it is concluded that the observed decreases in the $^5D_4$ lifetimes are consistent with a thermal depopulation mechanism involving the triplet states spectroscopically observed in the corresponding gadolinium complexes.

In view of the marked differences in the lifetime at room temperature for the various chelates due to thermal depopulation it is worth considering whether this effect alone may be responsible for the differing quantum efficiencies of the solids. Thus if the assumption is made that the radiative rate constant k_5 (see figure 3.6) is constant within each series of complexes the quantum efficiencies of the $^5D_4$ level, $\emptyset_{^5D_4}$, should be proportional to the lifetimes as shown in equation 4.3. Table 4.4 lists τ_{293} values along

$$\emptyset_{^5D_4} = k_5 \tau_T \qquad 4.3$$

with qualitative visual estimations of the relative fluorescence yields of the complexes at room temperature. In the case where low fluorescence yields precluded direct measurement of τ at 293K the values have been extrapolated from data at lower temperatures.

Table 4.4

Room-temperature lifetimes and relative fluorescence yields

Compound	τ_{293} / μs	Relative fluorescence[a]	Compound	τ_{293} / μs	Relative fluorescence[a]
$Tb(hfaa)_3 \cdot 2H_2O$	553	****	$Tb(tfaa)_3 \cdot 2H_2O$	473	***
$Tb(hfaa)_4 \cdot pipH$	589	*****	$Tb(tfaa)_4 \cdot pipH$	603[b]	*
$Tb(hfaa)_4 \cdot NH_4$	170[b]	***	$Tb(tfaa)_4 \cdot NH_4$	481	****
$Tb(hfaa)_4 \cdot Ph_4As$	106[b]	****	$Tb(tfaa)_4 \cdot Ph_4As$	659	*****
$Tb(hfaa)_4 \cdot Me_4N$	68[b]	*	$Tb(tfaa)_4.Na$	610	***
$Tb(hfaa)_4 \cdot Et_3NH$	296[b]	**	$Tb(tfaa)_4 \cdot K$	474	***
$Tb(hfaa)_4 \cdot Bu^tNH_3$	730	****	$Tb(tfaa)_4 \cdot Cs$	503	*****
$Tb(hfaa)_4 \cdot picH \cdot pic$	293[b]	*****			

a Visual estimate of fluorescence output at 293K when irradiated in 300-400 nm region; ***** very strong, * very weak.

b Derived from least-squares treatment of lifetime data.

It is evidence that no direct correlation between the overall quantum efficiency and the $^5D_4$ lifetime exists. For example in the hfaa series $Tb(hfaa)_4 \cdot Ph_4As$ and $Tb(hfaa)_4 \cdot Me_4N$ have similar lifetimes but quite different overall quantum efficiencies. In the tfaa series $Tb(tfaa)_4 \cdot pipH$ has a very low quantum yield but a lifetime similar to complexes with relatively high quantum efficiencies. It is apparent therefore that although thermal depopulation causes decreases in quantum efficiencies of these compounds between 77 and 293K it is not sufficient to entirely explain the observed ordering of quantum efficiencies at 293K and other loss mechanisms must operate to varying extents.

Significant energy losses at least in some cases may occur before the $^5D_4$ emitting level. Figure 4.8 illustrates some of the possible routes for deactivation of excitation energy in terbium chelates prior to the $^5D_4$ level. The first excited singlet state

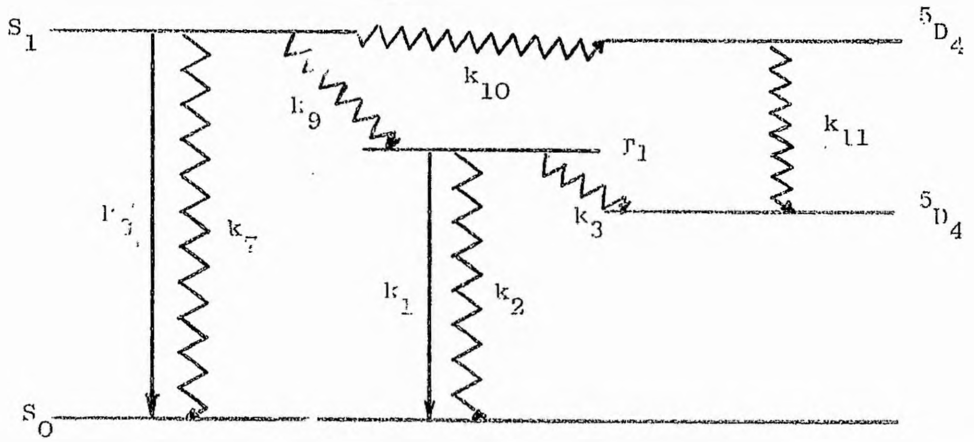

Fig. 4.8 Possible routes for deactivation of excitation energy in Tb^{3+} chelates prior to the $^5D_4$ level

may lose energy (a) by internal conversion, k_7, (b) by fluorescence, k_8, (c) by intersystem crossing to T_1, k_9 and (d) by intersystem crossing to another Tb^{3+} excited state level such as $^5D_3$, k_{10}. No singlet fluorescence was detected for these chelates and intersystem crossing is expected to be a very efficient process. It is therefore improbable that singlet deactivation via k_7 and/or k_8 is a major process. If deactivation of the T_1 level k_1 and/or k_2, which may have a cation dependence, has a comparable or greater rate to k_3, the rate of transfer to the Tb^{3+} $^5D_4$ emitting level then differences in the quantum yields of these solids may be attributed to competitive deactivation of the T_1 state.

The probability of energy transfer between the Tb^{3+} $^5D_3$ and $^5D_4$ levels which are separated by approximately 5,500 cm^{-1} in various metaphosphate glasses has been shown to be dependent on the immediate environment of the Tb^{3+} ions[297]. Hass et al[205] and Dawson et al[288] have obtained similar evidence for environmental dependence of $^5D_1 \rightsquigarrow {}^5D_0$ energy transfer in Eu^{3+} salts and chelates respectively in both hydrolytic and non-hydrolytic solvents. Hass et al[205] found that the $^5D_1 \rightsquigarrow {}^5D_0$ Eu^{3+} transfer probability for $Eu(ClO_4)_3$ and $Eu(NO_3)_3$ in various solvents varied between ca 0.4 to 0.6 which were similar to the results of ca 0.3 to 0.8 obtained by Dawson et al[288] for various europium chelates in methanol, ethanol and acetone. The low quantum yields of the terbium chelates and the uncertainty of direct population of the $^5D_3$ level because of its proximity to the S_1 state prevented accurate determinations of the $^5D_3 \rightsquigarrow {}^5D_4$ transition probabilities in the solvents mentioned above[288]. However determinations on $TbCl_3$ in water and deuterium oxide indicated values of 0.70 and 0.81 respectively[288]. It is apparent therefore that appreciable energy losses may be incurred by transfer to higher excited levels of the Tb^{3+} ions e.g. $^5D_3$ level.

(e) Conclusion

Thermal depopulation of the $^5D_4$ emitting level in various hfaa and tfaa chelates has been shown to explain the diversities in the $^5D_4$ decay times as a function of temperature (see figure 4.1 and table 4.1). This depopulation mechanism does not explain the surprising differences in quantum yields within the two series of compounds and it is reasoned that appreciable energy losses occur prior to excitation energy reaching the $^5D_4$ emitting level. It is apparent from the emission spectra of these solid chelates that various cations change the immediate environment of the chelated Tb^{3+} ions and it is suggested that these changes in environment may be responsible for altering the various rate constants of the energy transfer processes within the molecule. This environmental dependence of quantum efficiency is consistent with the results obtained for europium salts[205] and chelates[288] in solution.

Experimentally excitation spectra are difficult to obtain for luminescenct solids because of reflectance problems. It has been previously shown in chapter 3.3 that the terbium fluorescence of $Tb(aa)_3 \cdot 3H_2O$ and $Tb(dpm)_3$ in ethanol and carbon tetrachloride solutions results from both $n-\pi^*$ and $\pi-\pi^*$ absorptions. It is very probable that the solids behave similarly and no dependence of the quantum yield on excitation wavelength (region 250-400 nm) would be expected.

Dawson et al[288], have assigned the pre-exponential term, A_1 in the Arrhenius equation 3.3 as being the rate of deactivation of the ligand triplet i.e. k_1+k_2(figure 4.8). If this is assumed to be a correct interpretation the values obtained from plots of log $(^1/\tau_T - {}^1/\tau_{77})$ against $^1/T$ (see table 4.1) would indicate that if one assumes the rate k_3 (figure 4.8) to be similar to that obtained for Tb^{3+} complexes in solution[217,298,299] i.e. 10^9 s^{-1} that the k_1+k_2 rate would have little effect in the overall quantum yields of the chelates as they are all at least two orders of magnitude lower than 10^9 s^{-1} (see table 4.3). On the other hand the possibility remains that the rate of transfer from the triplet to the $^5D_4$ Tb^{3+} level, k_3, may be considerably lower in the solid state than in solution and that competition between k_3 and k_1+k_2 does play a major role in determining the overall quantum efficiency of the chelates. The relatively low values of A (see table 4.3) derived from solid terbium complexes, suggest that if in fact they are comparable with the triplet deactivation rates then in at least some of the gadolinium complexes ligand phosphorescence should be detectable at room temperature. The room temperature emission spectra of the solid gadolinium complexes were determined by use of the high resolution spectrofluorimeter and in all cases ligand triplet phosphorescence was observed. Two examples of these spectra are given in figures 4.9 and 4.10. An interesting feature of all these spectra is the terbium and europium emissions which are due to impurities in the original Gd_2O_3 starting material at less than the 0.1% level. The intensities of the Eu^{3+} and Tb^{3+} emissions are disproportionately high in terms of their relative concentrations suggesting that efficient migration of energy transfer occurs in these lanthanide chelate crystals. The fact that the intensity of ligand phosphorescence could not be directly related to the A values reported in table 4.3 may be explained by the differences in the efficiency of this intermolecular energy transfer from chelate to chelate which would influence the triplet deactivation value.

It is apparent therefore before more positive conclusions can be formulated about energy losses in these solids, it is necessary to determine either absolute or relative quantum yields and to obtain, at least, approximate values for the various rate constants for the energy transfer processes within the solid chelates.

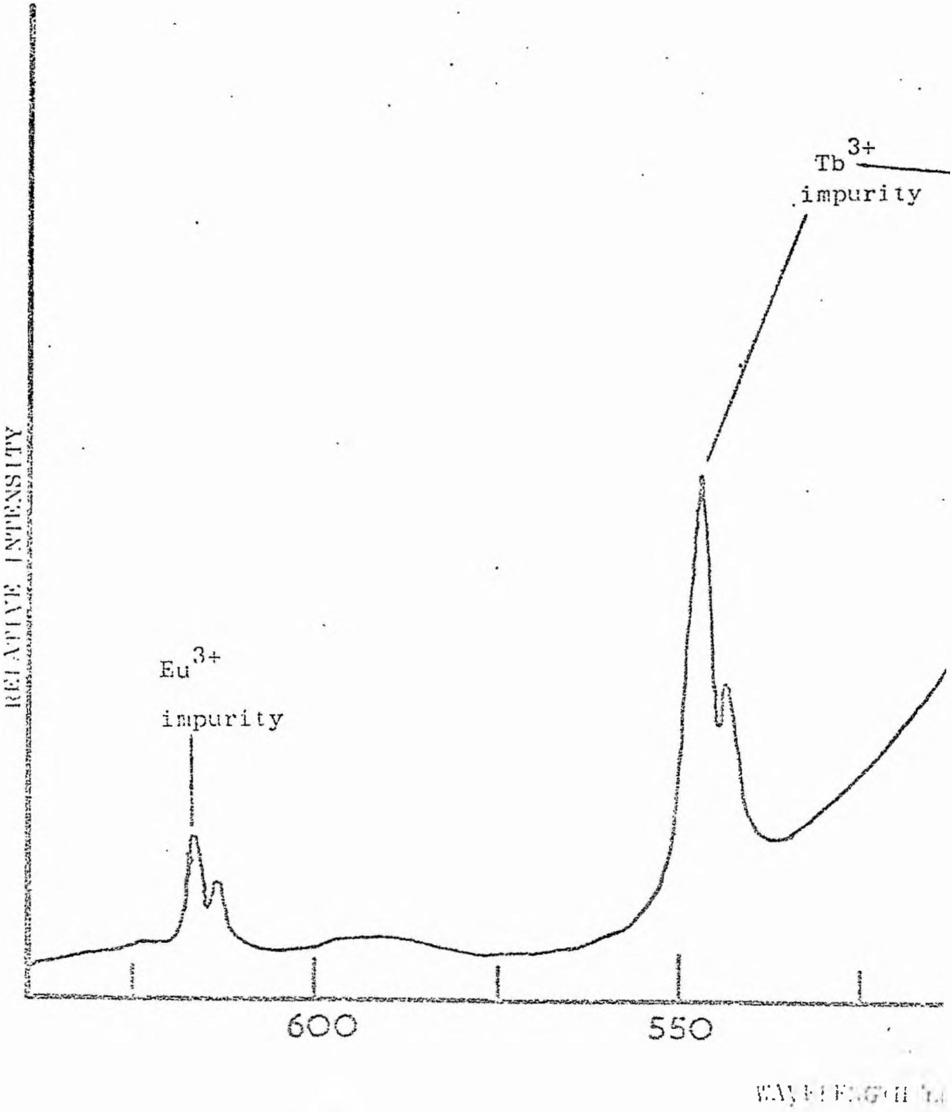

Fig. 4.9 Uncorrected emission spectrum of se

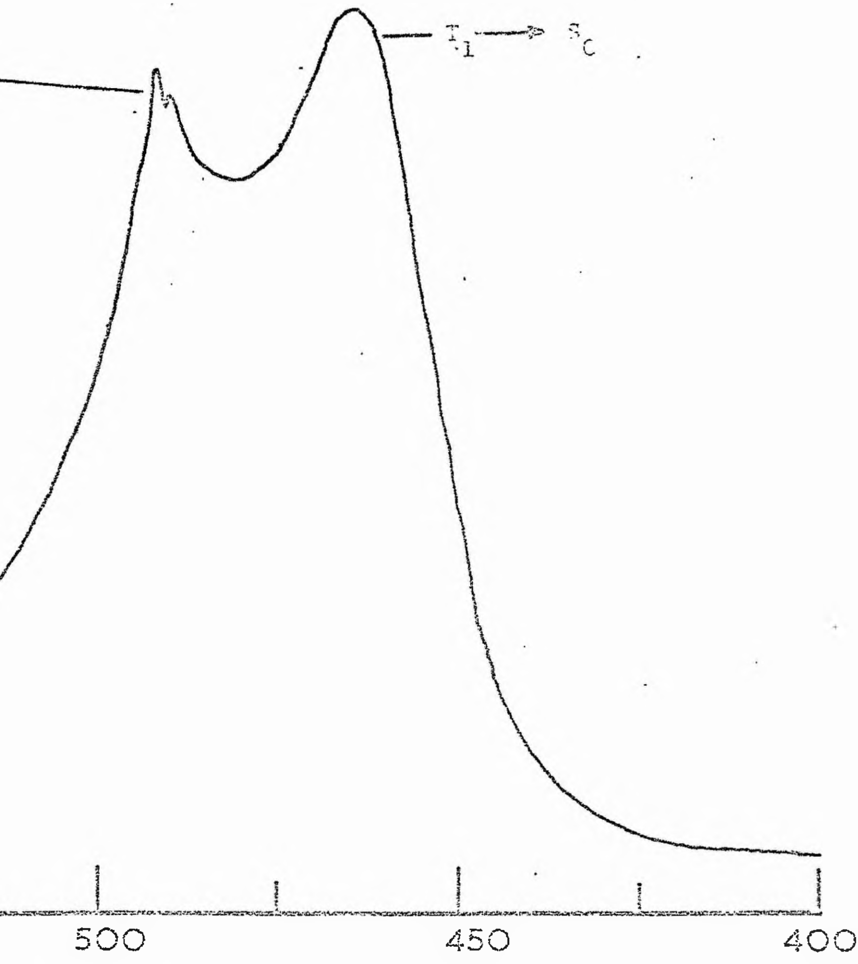

[illegible]$)_4$Bu^{t}NH$_3$

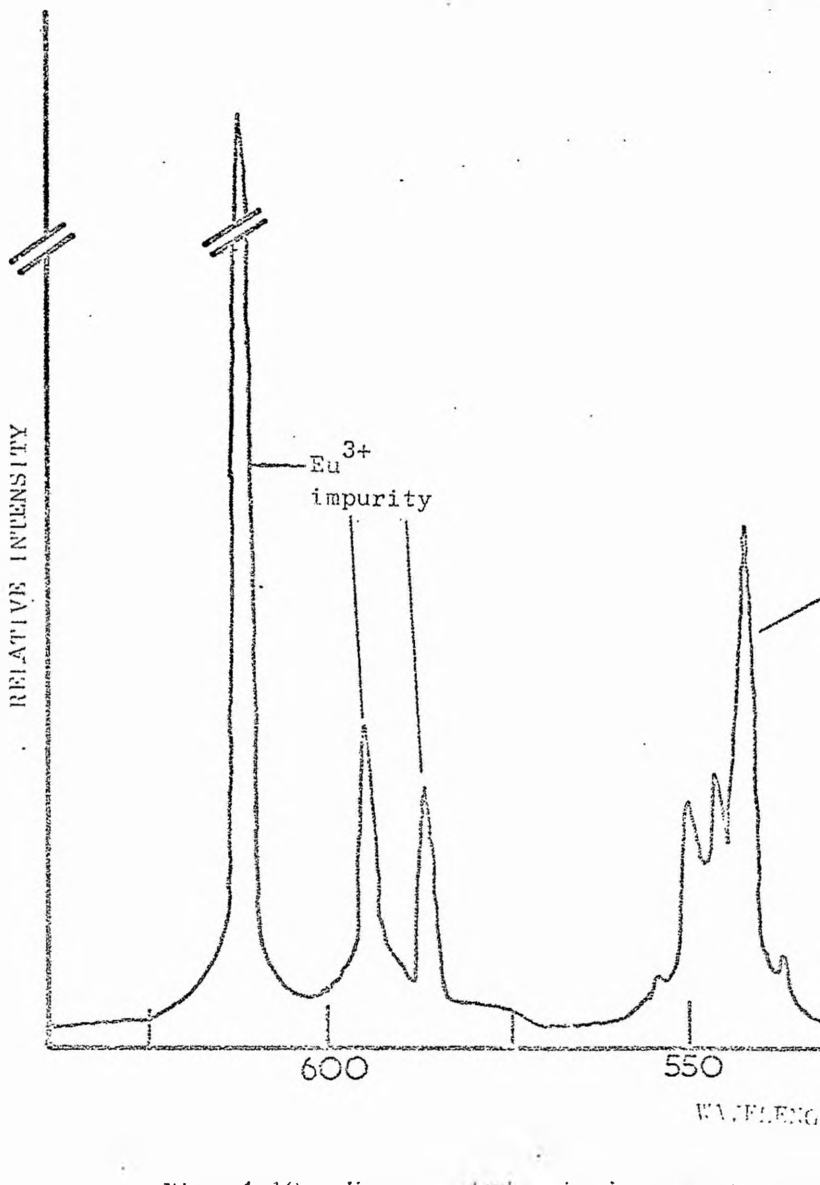

Fig. 4.10 Uncorrected emission spectrum

nm

of solid Gd(hfaa)$_4$

CHAPTER 5

RELATIVE QUANTUM YIELD DETERMINATIONS OF RELATED EUROPIUM AND TERBIUM CHELATES IN THE SOLID STATE AND IN SOLUTION

1. INTRODUCTION

Filipescu et al[300] have investigated the effect of solvent and temperature on the quantum yields of some tris europium β-diketoenolates. They observed that the higher fluorescence intensities were obtained in the more polar solvents. Two types of solvent-chelate interaction which may affect the fluorescence intensity are collisions and complex formation. The collisional deactivation depends on temperature, steric effects and the nature of the solvent. The result is a degradation of energy from the excited chelate states by conversion to vibrational and/or transitional energy. The complex formation may involve the replacement of ligand groups in the case of high polarity solvents. Two effects were suggested by Filipescu et al[300] (a) an increase in energy transfer from the ligand to the ion and/or an increase in the intra 4f radiative transition probability as a result of the increased Stark field introduced by the complexing solvents, (b) a "cloud" formation around the ion by the more polar solvent molecules, resulting in a decreased collisional quenching efficiency. The observed decrease in fluorescence intensity with increasing temperature within a particular solvent was explained by both the tendency to dissociate the solvent-chelate complex with subsequent removal of the shielding effects and an increase in the number of solvent-chelate collisions. Winston et al[194] have obtained relative quantum yields for a thenoyltrifluoroacetonate europium chelate in acetone, toluene, and ethanol but their results can not be quantitatively compared to those obtained by Filipescu et al[300] because the exact stoichiometry of the chelate was not established.

Fluorescence quantum efficiencies of several β-diketoenolates of Tb^{3+} and Eu^{3+} in various solvents at 300K have been reported by Bhaumik et al[301]. The values reported show a significant solvent dependence but are consistent with the results of Filipescu et al[300]. For example, they found that absolute quantum yields for $Eu(hfaa)_3 \cdot 2H_2O$ in EPA, Ø = 0.35, in 3/1 ethanol/methanol, Ø = 0.38, in acetone Ø = 0.36 and in dimethylformamide, Ø = 0.44 (5×10^{-3}M quinine sulphate in 1N H_2SO_4 having an absolute quantum yield = 0.51 was used as a reference). Charles et al[294], investigated the differences in quantum yield for some tetrakis europium chelates derived from Hbtfa having different cations in the solid state and in acetonitrile solution. They observed a considerable cation dependence of the quantum yields in the solid state but when the corresponding chelates were dissolved in acetonitrile, with a few notable exceptions, the yields showed little cation dependence. They explained the significant cation dependence in the case of the solids as being due to a perturbation caused by the cations on the resonance levels of the Eu^{3+} ion which was partially if not completely removed in solution. Significant variations in the quantum yields of several chelates of the type $[R\text{-}CO\text{-}CH\text{-}CO\text{-}CF_3)_4Eu]^-[\text{piperidinium}]^+$, where R is an aromatic group have been observed in the solid state and in solution[226]. The larger deviations observed in the solid state have also been attributed to greater variations in local symmetry of the chelated Eu^{3+} ion in the solid state. The significant variations in the quantum yields in solution indicate that the R group affects the nature of the ligand-Eu^{3+} bond through inductive and resonance interactions which result in differences in intramolecular energy transfer efficiencies within the chelates[226].

Absolute quantum yields of several chelates of europium and terbium in solution have been reported by Dawson _et al_[288]. The yields have been determined in the case of the europium chelates by (a) excitation in the ligand absorption bands and (b) by selective excitation to individual upper levels of the Eu^{3+} ion. Selective ion absorption to a higher level than $^5D_4$ in Tb^{3+} chelates was obscured by ligand absorption and comparisons of the $\phi_{^5D_4}$ and $\phi_{^5D_3}$ were restricted to $TbCl_3$ in water and deuterium oxide. Yields obtained by upper-ion-level excitation were all found to be lower than when the emitting level was excited directly. As an example the quantum yields obtained by selective excitation to the $^5D_0$, $^5D_1$, $^5D_2$, and $^5L_7$ levels of the Eu^{3+} ion of $Eu(aa)_3 \cdot H_2O$ in methanol were found to be 0.18, 0.10, 0.06 and 0.01 respectively. These values were all considerably higher than the value of <0.002 obtained for the quantum yield of the chelate when pumped in the absorption band of the ligands[288]. Dawson _et al_[288] found that the quantum yield of lanthanide fluorescence was independent of the exciting wavelength when the excitation was absorbed by the chelated ligands. A similar observation was reported by Riedel _et al_[196] who found that the quantum efficiency of a _tetrakis_ europium α-naphthoyltrifluoroacetonate chelate did not vary with wavelength over the range 260-390 nm. This is consistent with the results reported in section 3.3e for some terbium chelates.

Investigations of the radiative and nonradiative transitions in the Eu^{3+} ion in phosphate glasses[209] and in various protonated and deuterated solvents[205] have included the measurement of absolute quantum yields. The probability of populating the $^5D_0$ Eu^{3+} ion level by excitation to higher Eu^{3+} levels has been calculated from determinations of the quantum yields of the $^5D_0$ level[205,209]. The values obtained for the various transition probabilities were found to be very dependent on local environment of the Eu^{3+} ion. For example, the probability of the $^5D_1 \rightsquigarrow {}^5D_0$ transition was found to be 0.57, 0.46, 0.86 and 0.91 for $Eu(ClO_3)_3$ and $Eu(NO_3)_3$ in water and the Eu^{3+} ion in phosphate and silicate glasses respectively[209]. Quantum yields have also been measured for europium and terbium chlorides in dimethylformamide solution containing various organic sensitisers[180].

2. QUANTUM YIELD DETERMINATION IN SOLUTION

(a) Emission Spectra

The emission spectra of six anionic europium tetrakis hfaa chelates with different cations were determined in ethanol and acetonitrile solution (10^{-2} M) at 293K using the high resolution spectrofluorimeter. The emission profiles for the various chelates were very similar within a particular solvent but differed somewhat between the two solvents. The corrected emission profiles for $Eu(hfaa)_4$picH·pic in ethanol and acetonitrile are illustrated in figures 5.1 and 5.2 respectively. The profiles are characteristic of all europium emission spectra in having a main peak corresponding to the $^5D_0 \rightarrow {}^7F_2$ transition at ca 615 nm which accounts for more than 95% of the observed europium emission. The less intense peaks at ca 579 nm and ca 593 nm correspond to the $^5D_0 \rightarrow {}^7F_0$ and $^5D_0 \rightarrow {}^7F_1$ transitions respectively; other $^5D_0 \rightarrow {}^7F_j$ transitions were too weak to be observed.

Solution emission spectra are generally much broader and less structured than the corresponding emission spectra in the solid state (see figure 5.3) this being largely due to additional perturbations by the solvent fields on the 4f-shell. The determination of the

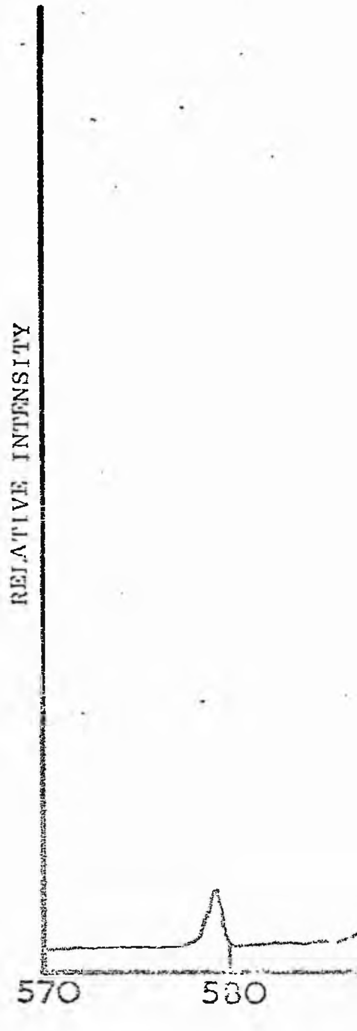

Fig. 5.1 Corrected em

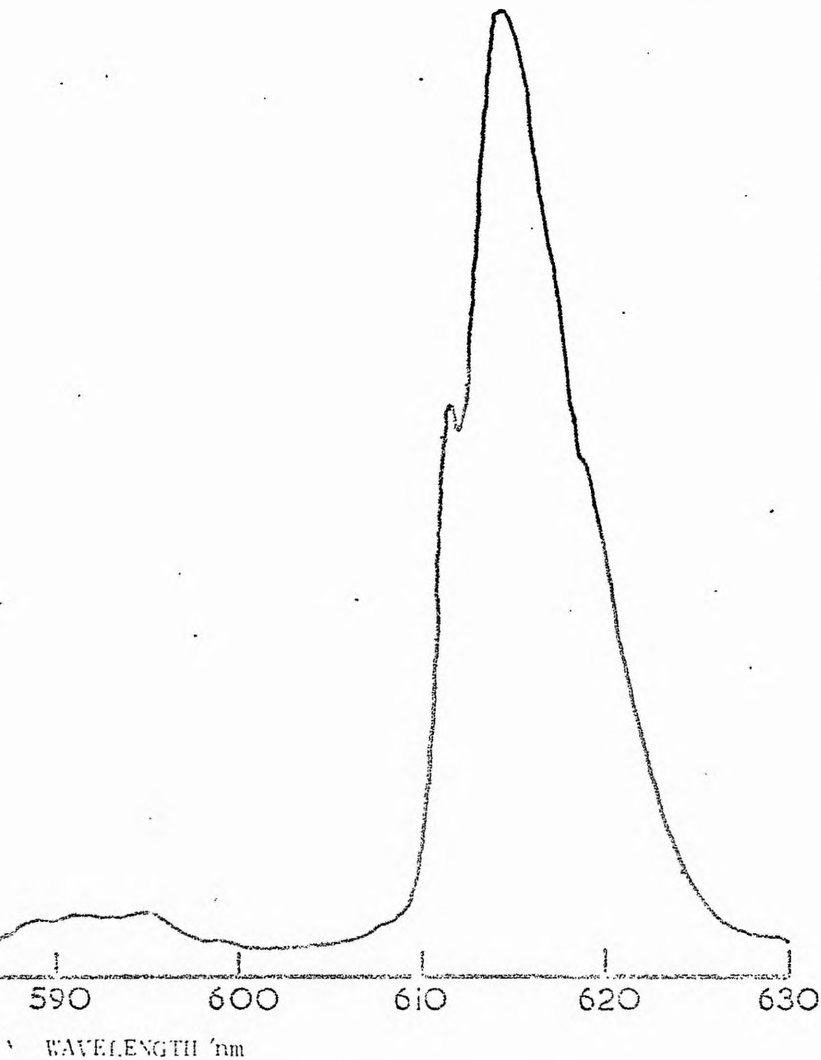

ission spectrum of 10^{-2} M Eu(hfaa)$_4$·picH·pic in EtOH

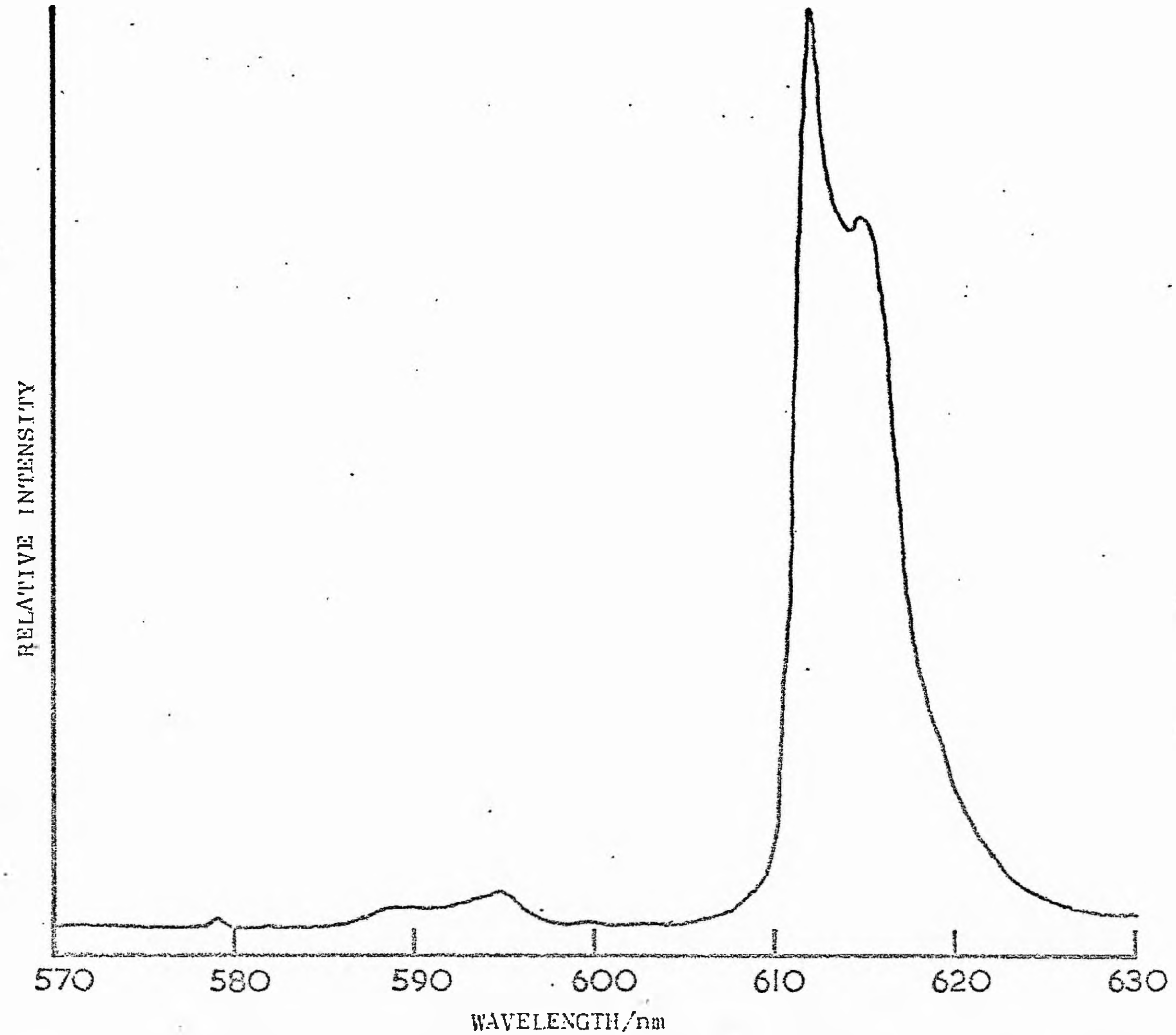

Fig. 5.2 Corrected emission spectrum of 10^{-2} M $Eu(hfaa)_4 \cdot picH.pic$ in MeCN

solution emission spectra of the terbium chelates mentioned in section 3 was precluded because of their very low quantum yields in ethanol and acetonitrile at 293K.

(b) Lifetimes and Quantum Yields

The lifetimes, τ_{293}, of the $^5D_0 \longrightarrow {}^7F_2$ Eu^{3+} ion transition for various europium chelates in both acetonitrile and ethanol were determined at 293K by measuring the emission intensity as a function of time at a wavelength of ca 615 nm. The lifetimes show a slight cation dependence in a particular solvent but differ considerably for the same chelate in ethanol and acetonitrile. The lifetimes measured in ethanol are all significantly lower than the corresponding lifetimes in acetonitrile.

Relative quantum yields were determined from the various chelates from the areas under their corrected emission spectra obtained by exciting the π,π^* ligand absorption band using the high resolution spectrofluorimeter by the method discussed in chapter 2. The normalised quantum yields, ϕ_N, together with τ_{293} are presented in table 5.1 and 5.2 for the chelates in acetonitrile and ethanol respectively. Table 5.3 presents the normalised relative quantum yields for the europium chelates in both acetonitrile and ethanol which were obtained by comparing the areas under the corrected emission spectra of $Eu(hfaa)_4 \cdot Ph_4As$ under identical conditions in both solvents. The correction for refractive index, , (see Chapter 2) was performed using η_{EtOH} = 1.3611 and η_{MeCN} = 1.3442. The quantum yields of the particular chelates are all greater in acetonitrile than in ethanol as can be inferred from the ϕ_{EtOH}/ϕ_{MeCN} values shown in table 5.3.

Table 5.1

Quantum yield and lifetime data for some europium chelates in MeCN

Compound	$\tau_{293}/\mu s$	ϕ_N (a)	$\phi_N \cdot \frac{\tau_{Et_3NH}}{\tau_{cation}}$ (b)
$Eu(hfaa)_4 \cdot Ph_4As$	617	1.0	0.96
$Eu(hfaa)_4 \cdot Me_4N$	568	0.96	1.00
$Eu(hfaa)_4 \cdot$picHpic	618	0.96	0.92
$Eu(hfaa)_4 \cdot Et_3NH$	671	0.94	0.83
$Eu(hfaa)_4 \cdot 2NH_2pyrH$	654	0.84	0.76
$Eu(hfaa)_4 \cdot$quinH	604	0.81	0.80

(a) Relative quantum yield normalised to unity for highest value

(b) Function normalised to unity

Table 5.2

Quantum yield and lifetime data for some europium chelates in EtOH

Compound	$\tau_{293}/\mu s$	ϕ_N (a)	$\phi_N \cdot \frac{\tau_{Ph_4As}}{\tau_{cation}}$ (b)
$Eu(hfaa)_4 \cdot Ph_4As$	505	1.0	1.0
$Eu(hfaa)_4(Me)_4N$	473	0.94	1.0
$Eu(hfaa)_4 \cdot$picHpic	475	0.83	0.88
$Eu(hfaa)_4 \cdot Et_3NH$	491	0.81	0.83
$Eu(hfaa)_4 \cdot$quinH	444	0.75	0.85
$Eu(hfaa)_4 \cdot 2NH_2pyr$	472	0.73	0.78

(a) Relative quantum yield normalised to unity for highest value

(b) Function normalised to unity

Table 5.3

Quantum yield and lifetime data for some Eu^{3+} chelates in EtOH and MeCN

Compound	ϕ_{MeCN} (a)	ϕ_{EtOH} (b)	τ_{EtOH}/τ_{MeCN}	ϕ_{EtOH}/ϕ_{MeCN}	$\frac{\phi_{EtOH}}{\phi_{MeCN}} \cdot \frac{\tau_{MeCN}}{\tau_{EtOH}}$
$Eu(hfaa)_4 \cdot Et_3NH$	0.94	0.57	0.73	0.61	0.84
$Eu(hfaa)_4 \cdot Ph_4As$	1.00	0.70	0.82	0.70	0.85
$Eu(hfaa)_4 \cdot quinH$	0.81	0.53	0.74	0.65	0.88
$Eu(hfaa)_4 \cdot (Me)_4N$	0.96	0.66	0.83	0.69	0.83
$Eu(hfaa)_4 \cdot 2NH_2pyrH$	0.84	0.51	0.72	0.61	0.85
$Eu(hfaa)_4 \cdot picH.pic$	0.96	0.58	0.77	0.61	0.79

(a) Relative quantum yield

(b) Relative quantum yield normalised to ϕ_{MeCN}

(c) Discussion

Both the lifetime of the $^5D_0 \rightarrow {}^7F_j$ Eu^{3+} ion emission and the quantum yield obtained by excitation of the ligands bands of each chelate are considerably lower in ethanol than in acetonitrile. This difference might be attributed to the better coordinating ability of the ethanol solvent which in turn could lead to more efficient quenching of the excitation energy. Charles *et al*[294] have found that, with a series of acetonitrile solutions containing *tetrakis* europium btfa chelates with different cations, the quinolinium and pyridinium cations enhance dissociation into the *tris* btfa chelate causing a decrease in overall quantum efficiency of the solution which is due to the lower quantum yield of the *tris* chelate. A similar mechanism may be responsible for the lower quantum yields observed for $Eu(hfaa)_4 \cdot quinH$ and $Eu(hfaa)_4 \cdot 2NH_2pyrH$ in both ethanol and acetonitrile (see table 5.1 and 5.2). The possible dissocation scheme is given in equations 5.1 and 5.2. The

$$[Eu(hfaa)_4]^-(QH)^+ \rightleftharpoons [Eu(hfaa)_4]^- + (QH)^+ \qquad 5.1$$

$$[Eu(hfaa)_4]^- + (QH)^+ \rightleftharpoons Eu(hfaa)_3 + (QH)^+(hfaa)^- \qquad 5.2$$

higher quantum yields in acetonitrile may also be explained by equations 5.1 and 5.2 in that any tris chelate formed will be solvated to a much greater extent in ethanol than acetonitrile permitting quenching of the excitation energy by, for example, the -OH vibrational modes of the coordinated ethanol molecules.

If it is assumed that the $^5D_0 \longrightarrow {}^7F_j$ radiative deactivation rate is similar for each chelate within a particular solvent then correction of $\emptyset_N$ for change in lifetime due to radiationless deactivation of the $^5D_0$ level may be accomplished by multiplying $\emptyset_N$ by (τ_{293} of the chelate with the highest lifetime/τ_{293} of the particular chelate). This has been done for these particular chelates in acetonitrile and ethanol and the normalised values obtained are reported in tables 5.1 and 5.2 respectively. It is apparent from the values in the last column of tables 5.1 and 5.2 that the differences between quantum yields within a particular solvent cannot be solely attributed to changes in the deactivation rate of the $^5D_0$ level although this is not unimportant. When the relative quantum yields are corrected for change in the deactivation rate of the $^5D_0$ Eu^{3+} ion level the particular ordering of the chelates with respect to quantum yield are within experimental error identical suggesting that changing the solvent environment of the chelate only changes the deactivation rate of the $^5D_0$ level. This is further substantiated by the comparisons made between lifetimes and quantum efficiencies of the respective chelates in ethanol and acetonitrile. The values obtained for the various comparisons are reported in table 5.3. The last function in table 5.3 compares the quantum yield of each particular chelate in ethanol and acetonitrile after making allowances for changes in the $^5D_0 \rightarrow {^7F_j}$ Eu^{3+} ion lifetimes. The values are all found to be identical within experimental error giving further evidence that the energy transfer processes prior to the $^5D_0$ Eu^{3+} ion level are solvent independent.

The slight cation dependence which is observed in ethanol and to a lesser extent in acetonitrile, may be due to differing degrees of dissociation within the solvents; however, the ordering of the quantum yields for the various chelates in both solvents is experimentally indistinguishable. This does suggest that at the concentrations employed i.e. 10^{-2}M that dissociation is not a major factor in the quantum efficiency ordering although it may be important at lower concentrations. The highest quantum yields are obtained with the $(Ph_4As)^+$ and $(Me_4N)^+$ cations. In these cations the positive charge is largely localised on the As and N atoms respectively and if ion pairing occurs in solutions then these cations would be expected to perturb the chelate anion to a lesser extent than any of the other cations studied because of the steric shielding of the positive charge. Therefore, another possible interpretation of the relatively small variation in quantum yields between these chelates is that some ion pairing may occur even in solvents with as high a dielectric constant as acetonitrile and that the perturbation of the cation may affect one or more of the rate constants in the $[Eu(hfaa)_4]^-$ anion.

3. QUANTUM YIELD DETERMINATIONS IN THE SOLID STATE

(a) Emission Spectra

The corrected emission spectra of some solid *tetrakis* terbium and europium hfaa chelates were determined at 293K and 77K using the high resolution spectrofluorimeter. The Eu^{3+} ion emission profiles in the crystalline complexes were much narrower than the corresponding solution spectra and the room temperature profiles had less fine structure (the notable exception being $Eu(hfaa)_4 \cdot Ph_4As$) than the emission spectra of the same chelates determined at 77K. In contrast all the solid terbium chelate emission spectra at room temperature retained much of the fine structure observable at 77K. In the terbium emission spectra it was apparent that the spectral profiles were dependent on the nature of the cation, the reasons for which have been discussed in section 4.2c. Examples of emission spectra of some solid europium chelates are illustrated in figures 2.4a and 5.3 and some terbium chelates in figures 5.4 and 5.5.

The presence of considerable fine structure in the Tb^{3+} ions $^5D_4 \rightarrow {}^7F_j$ emissions at 293K compared to the more or less structureless Eu^{3+} ion $^5D_0 \rightarrow {}^7F_2$ emission may be attributed to the greater theoretical number of transitions possible in the Tb^{3+} ion. The $^5D_4$ Tb^{3+} emitting level may split into a maximum of 9 levels in low symmetry whereas the Eu^{3+} $^5D_0$ level cannot be split. In addition the possible number of split levels from the lower energy states of the ^7F multiplet of the Tb^{3+} ion (ground state $^7F_6$) is much greater than the inverted ^7F multiplet of the Eu^{3+} level with a $^7F_0$ ground state.

(b) Lifetimes and Quantum Yields

A greater cation dependence was observed for the lifetimes of the $^5D_0 \rightarrow {}^7F_2$ Eu^{3+} ion emissions of the solid chelates than those of the corresponding chelates in acetonitrile and ethanol; similarly the quantum yields for the solid europium chelates showed a very marked cation dependence. In the case of the terbium chelates no comparisons could be made between the $^5D_4 \rightarrow {}^7F_4$ Tb^{3+} ion lifetimes

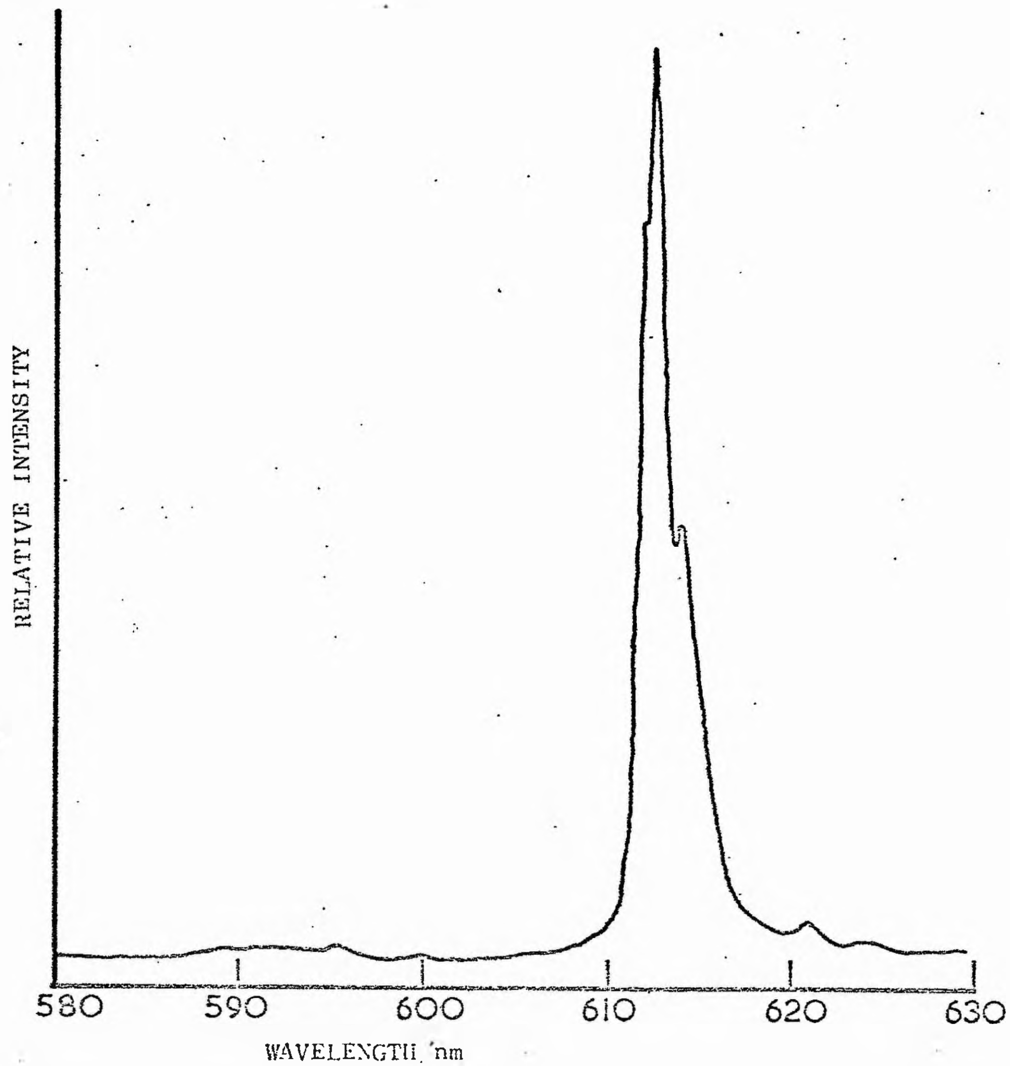

Figure 5.3 Corrected emission spectrum of solid $Eu(hfaa)_4 \cdot Ph_3As$ at 293K

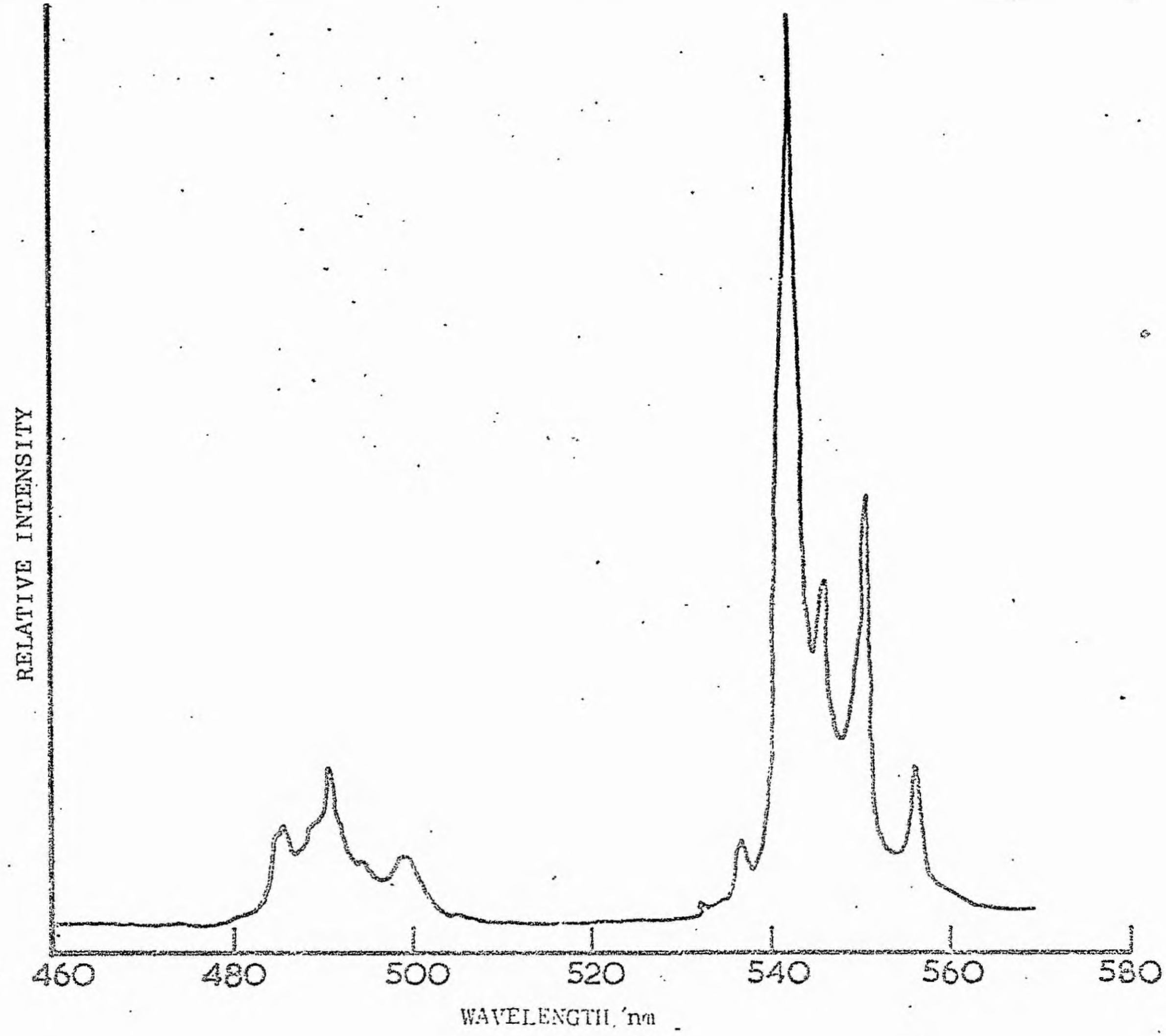

Fig. 5.4 Corrected emission spectrum of $Tb(hfaa)_4 \cdot Et_3NH$ determined at 293K in the solid state

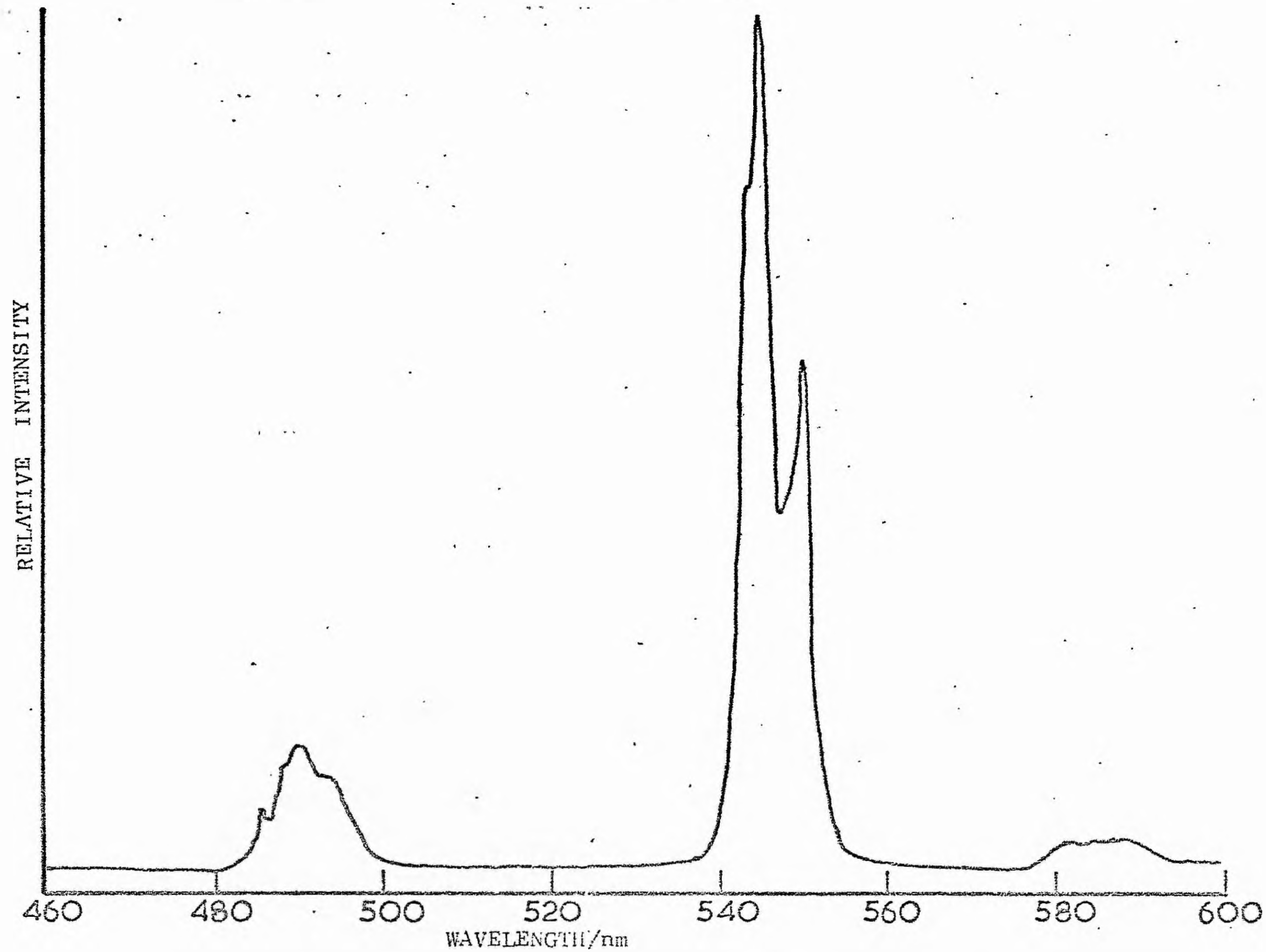

Fig. 5.5 Corrected emission spectrum of $Tb(hfaa)_4 \cdot Ph_4As$ determined at 293K in the solid state

and overall quantum yields in the solid state to that in solution at 293K because of the very low quantum yields in solution. However, in the case of the solid terbium chelates a significant cation dependence of lifetime and quantum yield was observed between the particular complexes. The relevant data for the crystalline europium and terbium chelates are given in tables 5.4 and 5.5 respectively. The lifetime of the $^5D_0 \longrightarrow {^7F_2}$ Eu^{3+} ion emission in the solid chelates, with the exception of $Eu(hfaa)_4 \cdot Ph_4As$, are all considerably

Table 5.4

Lifetime and quantum yield data for some solid europium chelates

Compound	τ_{293}/µs	$\varnothing_N$ (a)	$\varnothing \frac{\tau_{MeCN}}{\tau_{cation}}$ (b)
$Eu(hfaa)_4 \cdot Ph_4As$	368	0.89	1.00
$Eu(hfaa)_4 \cdot$ picHpic	703	1.00	0.59
$Eu(hfaa)_4 \cdot (Me)_4N$	1678	0.63	0.16
$Eu(hfaa)_4 \cdot$ quinH	1088	0.42	0.16
$Eu(hfaa)_4 \cdot 2NH_2$pyrH	1083	0.37	0.14
$Eu(hfaa)_4Et_3NH$	1313	0.25	0.08

(a) Relative quantum yield normalised to unity for highest value and corrected for reflectance of the samples

(b) Function normalised to unity

Table 5.5

Lifetime and quantum yield data for some solid europium chelates

Compound	τ_{293} µs	τ_{77} µs	$\varnothing_V^{(a)}$	$\varnothing_N^{(b)}$	$\varnothing_N \frac{\tau_{77}}{\tau_{293}}$ (c)	$\varnothing_N \frac{\tau_{77Me4N}}{\tau_{293}}$ (c)
$Tb(hfaa)_4 \cdot Ph_4As$	113	626	0.29	0.32	1.00	1.00
$Tb(hfaa)_4 \cdot 2H_2O$	525	849	0.83	1.00	0.92	0.68
$Tb(hfaa)_4 \cdot$ pipH	582	991	1.00	0.93	0.90	0.56
$Tb(hfaa)_4 \cdot$ picH·pic	344	843	0.51	0.40	0.57	0.42
$Tb(hfaa)_4 \cdot (Me)_4N$	109	1347	0.05	0.06	0.43	0.20
$Tb(hfaa)_4 \cdot Et_3NH$	109	1305	0.07	0.06	0.42	0.20
$Tb(hfaa)_4Bu^tNH_3$	633	1066	0.23	0.17	0.16	0.09

(a) Relative quantum yield without correction for reflectance normalised to unity for highest value

(b) Relative quantum yield corrected for reflectance normalised to unity for highest value

(c) Function normalised to unity

higher than the values for the corresponding chelates in both acetonitrile and ethanol solution. This may be attributed to the decrease in the nonradiative deactivation rate of the $^5D_0$ Eu^{3+} ion level in the solid state compared to that in solution, where further quenching processes are possible. The quantum yields for the various solid europium chelates vary over a much wider range than the corresponding chelates in solution (cf tables 5.1, 5.2 and 5.4). The solid terbium chelates (table 5.5) show greater variations in $^5D_4 \rightarrow {}^7F_4$ Tb^{3+} ion lifetime and overall quantum yield when the cation is varied. The values, $\emptyset_V$ (table 5.5) are the relative quantum yields obtained without corrected for the differences in the reflection coefficients of the particular chelates. These values are in good agreement with the visual quantum yield estimates reported in chapter 4 for the same chelates. With the exception of $Tb(hfaa)_3 \cdot 2H_2O$ the correction made for the reflectance does not alter the ordering of $\emptyset_V$ and $\emptyset_N$ for the particular chelates.

(c) Discussion

There is significant cation dependence of the lifetime of the resonance level and the overall quantum efficiency of solid terbium and europium chelates at 293K. If a correction is made for the thermal depopulation of the $^5D_4$ Tb^{3+} ion level in the solid terbium chelates (see section 4.2d) at 293K the quantum yield is still dependent on the nature of the cation (table 5.5). This correction was made on the assumption that there is no significant thermal depopulation of the $^5D_4$ level at 77K i.e. the $^5D_4 \rightarrow {}^7F_j$ lifetime can be represented as $1/[k_5+k_6]$ (see figure 3.6).

Variation in $\emptyset_N$ for a series of Eu^{3+} tetrakis btfa chelates has been previously reported[294] and it was suggested that changes in local environment of the bonded Eu^{3+} ion caused by the cation were responsible for the observed differences. It was argued that similarities of the same chelates in acetonitrile solution could be explained by removal of the perturbation of the cation due to ionic dissociation into $[Eu(btfa)_4]^-$ and the cation which are sufficiently separated in solution to prevent any significant anion-cation interaction.

Assuming the radiative deactication rate of the resonance levels of the Tb^{3+} and Eu^{3+} ions to be identical within their respective series an allowance for the differences in the nonradiative deactivation of the emitting levels similar to that performed for the europium chelates solutions (see section 5.2c) can be made to their observed quantum yields. The values modified for differences in nonradiative deactivation are reported in the final column in tables 5.4 and 5.5 for the europium and terbium chelates respectively. It is apparent from these values that the changes in deactivation rate of the resonance levels do not completely explain the differences in quantum yields of these chelates in the crystalline state, suggesting that the cations may be responsible for changing the rate constants of the energy transfer processes within the chelates. It may be inferred from the larger variations in the case of the solid terbium quantum yields that the cation has a more important role in determining the fate of the excitation energy. This would be possible if one or more of the transfer rates within the terbium chelates differed significantly from the corresponding rate in the europium chelates. It is unlikely that any of the deactivation rates involving the chelate ligands alone could have a significant lanthanide ion dependence but it is very probable that the triplet-lanthanide transfer rate has a marked lanthanide dependence in the solid state. Rate constants for this transfer have been determined for europium and terbium complexes in solution and the rate for the europium complexes found to be an order of magnitude higher than for the terbium complexes[217,298,299]. In section 4.2e the competition between the rate of transfer to the Tb^{3+} ion $^5D_4$ emitting level from the ligand triplet, k_3, (see figure 3.6) and the rate of transfer to the ground state from the ligand triplet, k_1+k_2 (see figure 3.6) was suggested as a possible reason for the variation in the quantum efficiencies of the solid terbium chelates. The further evidence obtained from lifetime data at 77K and qualitative determinations of Ø have given increased support to this suggestion and the implication that the $T \rightsquigarrow {}^5D_4$ transition rate may be less in the solid state than in solution. The lesser variation, with the exception of $Eu(hfaa)_4 \cdot Ph_4As$ in the case of the crystalline europium chelates could be explained by an increased $k_3/(k_1+k_2)$ ratio.

(d) Conclusion

The solvent dependence of the quantum yields of the europium chelates in ethanol and acetonitrile can be explained within experimental error as being due to differing rates of nonradiative deactivation of the $^5D_0$ level by the solvent environment. In solution there is a relatively small cation dependence on quantum yield which may be caused by dissociation and/or ion-pair formation. The former may only be important at lower concentrations since the ordering of the chelates with respect to quantum yield was the same in both solutions.

The results obtained in the solid state for the quantum yield variations cannot be explained simply by variations in the nonradiative deactivation rate of the lanthanide resonance levels but are probably due to perturbations of other transfer processes within the chelates by the cation. This appears to be more important in the case of the solid terbium chelates and it is suggested that differences in the k_3 rate constant (see figure 3.6), which has been shown to vary by an order of magnitude in solution, for terbium and europium chelates may be responsible because of the competitive k_1+k_2 deactivation rate of the triplet. In addition it was suggested that these rates may be slower in the solid state than in solution.

In the solid state and in solution the chelates with the highest quantum yields are all associated with the $(Ph_4As)^+$ cation. It therefore seems likely that the highest quantum yields for tetrakis lanthanide chelates will be obtained when large bulky cations having their positive centre well shielded from the anion are employed. It is unlikely that cation absorption plays any significant role in the ordering of quantum efficiencies because of the relatively weak absorptions of the cations compared to the chelated ligands at the exciting wavelength[294].

CHAPTER 6

9-COORDINATION IN SOME LANTHANIDE β-DIKETOENOLATES IN THE SOLID STATE AND IN SOLUTION

1. INTRODUCTION

The ready solvation of lanthanide tris β-diketoenolates indicates that the 6-coordinate Ln^{3+} ion is coordinatively unsaturated and prefers a coordination number of seven or greater. Mono-, di- and trihydrated lanthanide acetylacetonates, $Ln(aa)_3nH_2O$, have been characterised[89]. Attempts to prepare anhydrous lanthanide β-diketoenolates by removal of the coordinated water from the corresponding hydrated chelate have usually been unsuccessful[89] except with bulky β-diketoenolates such as the dipivaloylmethanato anion[75]. The possibility of coordinative unsaturation of the lanthanide ions in tetrakis compounds has received little attention although large numbers of tetrakis chelates have been reported and characterised.

9-Coordination has been reported for very few lanthanide chelates and most of the examples referred to in the literature involve monodentate ligands. The most common stereochemistry of 9-coordinate complexes is the symmetrical tricapped trigonal prism which may have D_{3h} symmetry[302]. This coordination polyhedron is characteristic of the complex ions $[Ln(H_2O)_9]^{3+}$ which occurs, for example, in the crystalline ethyl sulphates, $Ln(C_2H_5SO_4)_3 \cdot 9H_2O$[303] and the crystalline bromates, $Ln(BrO_3)_3 \cdot 9H_2O$, (Ln = Nd)[304] and also the $[Ln(OH)_9]^{6-}$ ions (Ln = La, Pr, Nd, Sm, Gd and Dy) in the crystalline trihydroxides[305]. Other compounds, the crystal lattices of which are based upon symmetrical tricapped trigonal prismatic units are $LnCl_3$ (Ln = La-Gd)[306,307], $LnBr_3$ (Ln = La, Ce, Pr)[307], $NaLnF_4$ (Ln = La-Tm, Y)[308], HoD_3[309], LnF_3 (Ln = La-Eu, Ho, Tm)[310,311], $NdCl_3 \cdot 9H_2O$[304] and LnOX (X = Cl, Br, I)[312,313]. Nine coordination is also found in the salts M^1 $[Ln(EDTA)(H_2O)_3] \cdot 5H_2O$ ($M^1 = K^+$, Ln = La,Nd,Gd; $M^1 = Na^+$, Ln = La,Nd,Tb,Gd,Er; $M^1 = NH_4$, Ln = Nd,Gd)[314]. The lanthanum and terbium containing salts have been examined in detail and in each instance the coordination polyhedron is defined by the four oxygen atoms and the two nitrogen atoms from the $EDTA^{4-}$ ion and the three oxygen atoms from the coordinated water molecules. As a consequence of the large size of each Ln^{3+} ion, the $EDTA^{4-}$ ion is constrained to a single hemisphere with the water molecules in the second hemisphere. The resulting geometry departs substantially from the trigonal prismatic and is quasi D_2 dodecahedral, with the donor sites from the $EDTA^{4-}$ ion and one of the water molecules defining seven of the sites and the other two being roughly established by the remaining two water molecules.

There is evidence that lanthanide <u>tetrakis</u> chelates interact significantly with strong donor molecules such as amides and sulphoxides. For example, the emission spectrum of the $[Eu(aa)_4]^-$, $[Eu(btfa)_4]^-$, $[Eu(ba)_4]^-$ and $[Eu(dbm)_4]^-$ anions in ethanol are grossly altered on addition of dimethylformamide, suggestive of complex formation[221]. $Eu(ba)_4 \cdot pipH$ when recrystallised from an ethanol solution containing DMF is isolated as $Eu(ba)_4 \cdot pipH \cdot DMF$[221]. Nine coordination involving lanthanide β-diketoenolates has also been suggested by Lempicki <u>et al</u>[315] who proposed the existence of the species $[Eu(btfa)_4 \cdot MeCN]^-$ in acetonitrile solution at 77K. Workman <u>et al</u>[92] have also reported spectroscopic and analytical evidence for 9-coordination in the adducts of $Eu(ba)_4 \cdot pipH$ and $Eu(btfa)_4 \cdot pipH$ in the solid state.

2. 9-COORDINATION IN THE SOLID STATE

(a) Analytical Evidence

During the synthesis of several tetrakis hfaa chelates with different cations for the investigations of thermal depopulation of the $^5D_4$ Tb^{3+} level (chapter 4) it was noted from the analysis of the γ-picolinium cation chelate that it had been isolated containing an extra molecule of γ-picoline. Analogous results were obtained when the preparation of the corresponding gadolinium and europium chelates was attempted (see table 2.1). Elemental analyses of all the other chelates prepared were found to correspond to the characteristic tetrakis chelate stoichiometry $Tb(hfaa)_4$·cation. Similar syntheses were therefore attempted for the Eu^{3+}, Tb^{3+} and Gd^{3+} ions using pyridine as base because of its similarity in molecular shape to γ-picoline. It was concluded from the analyses that the products isolated in the case of the Tb^{3+} and Gd^{3+} ions corresponded to a chelate of the type $Ln(hfaa)_4$·pyrH·pyr, and for the Eu^{3+} ion to a chelate of the type $Ln(hfaa)_4$·pyrH. However, recrystallisation of the $Eu(hfaa)_4$pyrH chelate from pyridine afforded a compound which was characterised as containing a further molecule of pyridine. The extra molecules may (a) be occluded in the crystal lattice or (b) form a Ln^{3+}-ligand bond producing a 9-coordinate Ln^{3+} ion.

Vacuum sublimation and/or melting of these chelates containing the extra molecule of base indicated that the pyridine molecule was more loosely bound than the γ-picoline molecule since only in the case of the pyridinium adducts did vacuum treatment produce a compound corresponding to $Ln(hfaa)_4$·cation. Analysis of the γ-picolinium chelates after vacuum sublimation suggested that only a small fraction of the extra γ-picoline molecules had been removed indicating that the ligands are probably held by weak Van der Waal forces rather than occupying convenient holes in the crystal lattice. Further evidence for this is reported below in section (b).

(b) Spectroscopic Evidence

Workman et al[92] investigated the α and β forms of $Eu(dpm)_4 \cdot pipH$ reported by Bauer et al[74] and found them not to be stereoisomers of the same chelate but to correspond to the chelates, $Eu(dbm)_4 \cdot pipH$ and $Eu(dbm)_4 \cdot pipH \cdot H_2O$ respectively. Similar results were obtained for $Eu(ba)_4 \cdot pipH$. Analyses also showed that the crystals isolated from dimethylformamide solutions containing the chelates had one molecule of DMF per molecule of complex.

The theoretical elemental analyses of tetrakis compounds and hydrated tetrakis compounds are within the experimental error of the microanalyser i.e. ± 0.3%. Direct analytical evidence for the presence of a single water molecule is therefore impossible. However, changes in the environment of the Ln^{3+} ion affect the emission spectrum which is therefore a sensitive probe of the molecular geometry. The $^5D_0 \longrightarrow {}^7F_0$ Eu^{3+} ion transition at ca 597 nm is ideal for such investigations because in all symmetries a single peak in this region is predicted since the excited $^5D_0$ level and the ground state $^7F_0$ level cannot be split by the Stark field of the ligands. Any 'splitting' observed in this transition may therefore be attributed to the presence of another fluorescent species.

High resolution spectra of the region containing the $^5D_0 \longrightarrow {}^7F_0$ Eu^{3+} transition were obtained for all the europium tetrakis chelates investigated in Chapter 5. Examination of the spectra of the compounds $Eu(hfaa)_4Bu^tNH_3$ and $Eu(hfaa)_4Ph_4As$ after recrystallisation and satisfactory microanalyses (table 2.1) showed the presence of two sharp peaks in the region 579-580 nm. All the other samples examined had a single peak attributable to the $^5D_0 \longrightarrow {}^7F_0$ transition in this region. Vacuum sublimation and/or vacuum melting of the tertiary butylammonium and the tetraphenylarsonium salts resulted in compounds with only one sharp $^5D_0 \rightarrow {}^7F_0$ emission band near 579 nm.

Careful recrystallisation of crude $Eu(hfaa)_4Bu^4NH_3$ from chloroform afforded a chelate having an emission spectrum containing a single $^5D_0 \rightarrow {}^7F_0$ Eu^{3+} ion peak at 579.4 nm indicating the presence of only one europium fluorescent species. However after vacuum sublimation of the chelate the $^5D_0 \rightarrow {}^7F_0$ Eu^{3+} ion transition occurred at 579.8 nm while the total emission profile had altered suggesting that the Eu^{3+} ion had undergone a change in environment during sublimation. As the $^5D_0 \rightarrow {}^7F_0$ Eu^{3+} transition in both instances is a single peak which indicates chemical purity with respect to Eu^{3+} ion fluorescence it is suggested that the former chelate corresponds to $Eu(hfaa)_4Bu^tNH_3 \cdot H_2O$ and the latter $Eu(hfaa)_4 \cdot Bu^tNH_3$. This inference was corroborated by the infrared spectrum of the chelates. The proposed $Eu(hfaa)_4 \cdot Bu^tNH_3 \cdot H_2O$ showed the characteristic O-H stretching modes as a broad band at <u>ca</u> 3740 cm^{-1} which was absent in the ir spectrum of the other chelate. Corrected emission spectra of the two chelates are given in figures 6.1 and 6.2 respectively.

(c) Discussion

Both the analytical and spectroscopic information obtained for these europium *tetrakis* hfaa chelates support the presence of a coordinatively unsaturated Ln^{3+} ion in these complexes. Vacuum sublimation and/or melting suggests that the neutral ligands are held by weak forces which are dependent on the nature of the ligands. The apparently stronger γ-picoline - Ln^{3+} bond with respect to the pyridine - Ln^{3+} bond in their respective chelates may be explained by the increased basic character of the nitrogen atom in γ-picoline

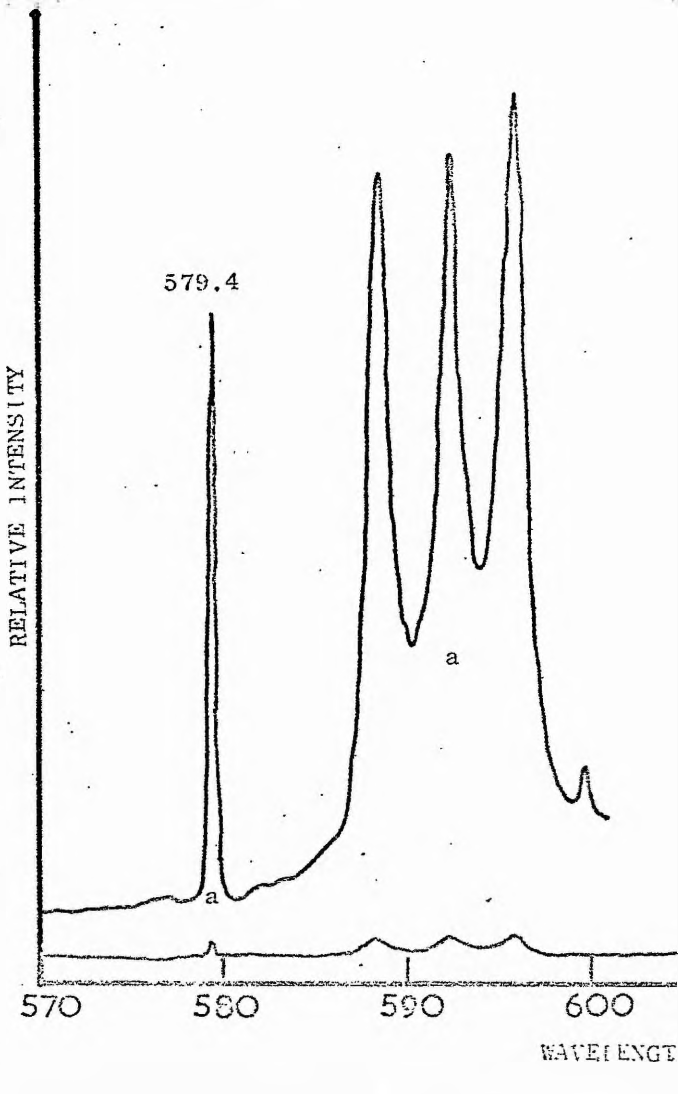

Fig 6.1 Corrected emission spectrum of so.

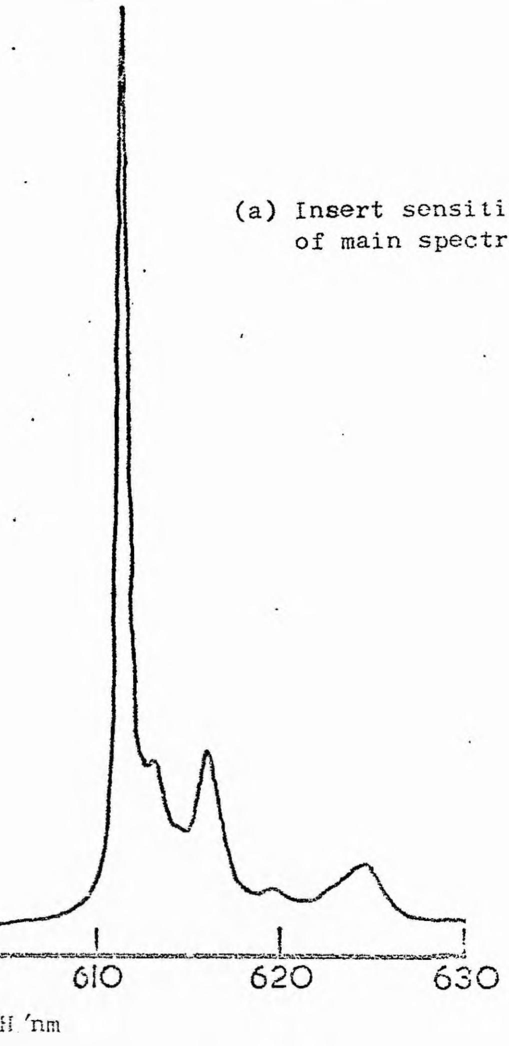

id $Eu(hfaa)_4Bu^tNH_3 \cdot H_2O$ at 293K

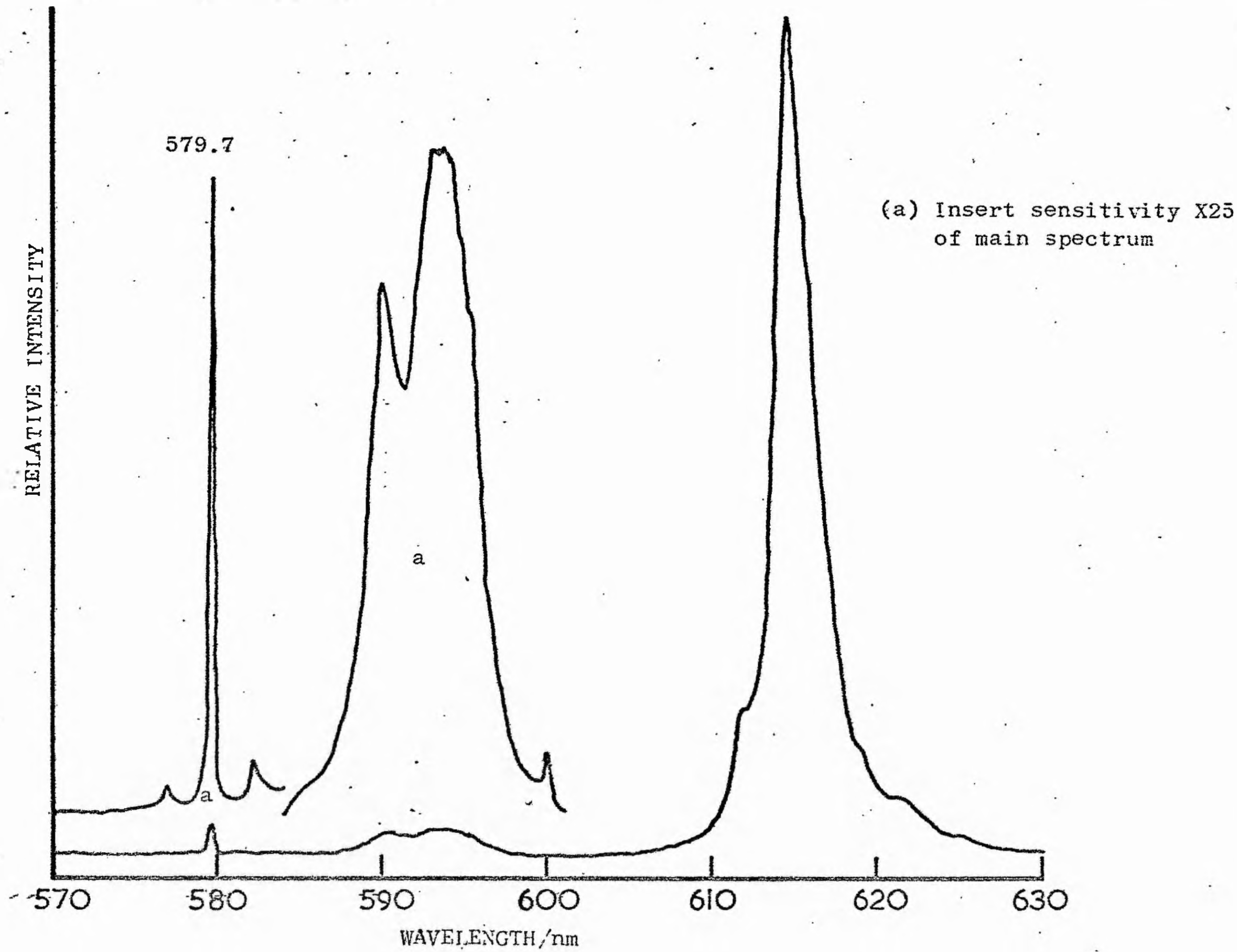

Fig. 6.2 Corrected emission spectrum of solid $Eu(hfaa)_4Bu^tNH_3$ at 293K

due to the electron donating ability of the methyl group. Isolation of the $Eu(hfaa)_4 \cdot Bu^tNH_3 \cdot H_2O$ and $Eu(hfaa)_4 \cdot Bu^tNH_3$ chelates having different emission profiles emphasises the necessity of careful chemical identification of the species from which interpretations of spectra are to be made. The question as to whether the water, γ-picoline and pyridine molecules are in the coordination sphere of the Ln^{3+} ion or in the crystal lattice can only be resolved unambiguously by X-ray crystallographic methods. The fact that, of the bases investigated, only γ-picoline and pyridine formed compounds containing an extra molecule of base might suggest that their molecular shapes have suitable dimensions to fill the holes in the crystal lattice. However, the unsuccessful attempt to remove completely the γ-picoline by vacuum sublimation and the significant effect of the extra water molecule on the emission spectrum of the hydrated $Eu(hfaa)_4Bu^tNH_3$ (see figures 6.1 and 6.2) provides substantial, if not conclusive, evidence for 9-coordination in these lanthanide β-diketoenolates.

The possibility of 9-coordination in lanthanide β-diketoenolates in solution may be investigated by nmr spectroscopy using the theory of lanthanide shift reagents discussed in section 1.le. The following section describes a nmr spectroscopic investigation of $Eu(hfaa)_4 \cdot Ph_4As$ in CD_3CN and $CDCl_3$ containing γ-picoline. This chelate was selected because of its relatively high solubility in both the polar CD_3CN and the relatively nonpolar $CDCl_3$.

3. 9-COORDINATION IN SOLUTION

(a) Nmr Evidence

The induced shifts in nmr spectra of organic molecules caused by lanthanide shift reagents depends on the nature and extent of the adduct formation equilibria occurring in solution. The observed shift, δ, of any resonance is related to the absolute shift by equation 6.1 where x = concentration of complexed organic molecules,

$$\delta = x\Delta/B \qquad 6.1$$

B = total concentration of organic molecules and Δ = absolute shift. Thus, if one assumes that only monoadduct formation takes place i.e. that illustrated in equation 6.2 then by substitution the association

$$Eu(hfaa)_4 \cdot Ph_4As + ligand \rightleftharpoons Eu(hfaa)_4 \cdot Ph_4As \cdot ligand \qquad 6.2$$

equilbrium constant, $K(lm^{-1})$, may be represented by equation 6.3 where

$$1/K = (\Delta - \delta)(A/\delta - B/\Delta) \qquad 6.3$$

A and B are the molar concentrations of the lanthanide complex and the added organic ligand, respectively.

The observed shift for the protons of γ-picoline in CD_3CN and $CDCl_3$ containing $Eu(hfaa)_4 \cdot Ph_4As$ (0.02-0.03M) were obtained as a function of the volume of γ-picoline added using the method described in section 2.6. In both solutions significant Eu^{3+} ion - γ-picoline interaction was indicated by the spectral shift of the γ-picoline protons which decreased with increasing γ-picoline concentration. Plots of $1/\delta$ against volume of γ-picoline added are illustrated in figures 6.3 and 6.4 respectively for the CD_3CN and $CDCl_3$ solutions containing the lanthanide shift reagent. Tables 6.1 and 6.2 present the data from which the values of K for the reaction in CD_3CN and $CDCl_3$ illustrated in equation 6.2 are determined using a procedure similar to that of Mackie and Shepherd[122]. Using the data in tables 6.1 and 6.2 Δ was varied in equation 6.3 until the most consistent set of K values for the various values of B (in terms of % standard deviation) was obtained. In both cases

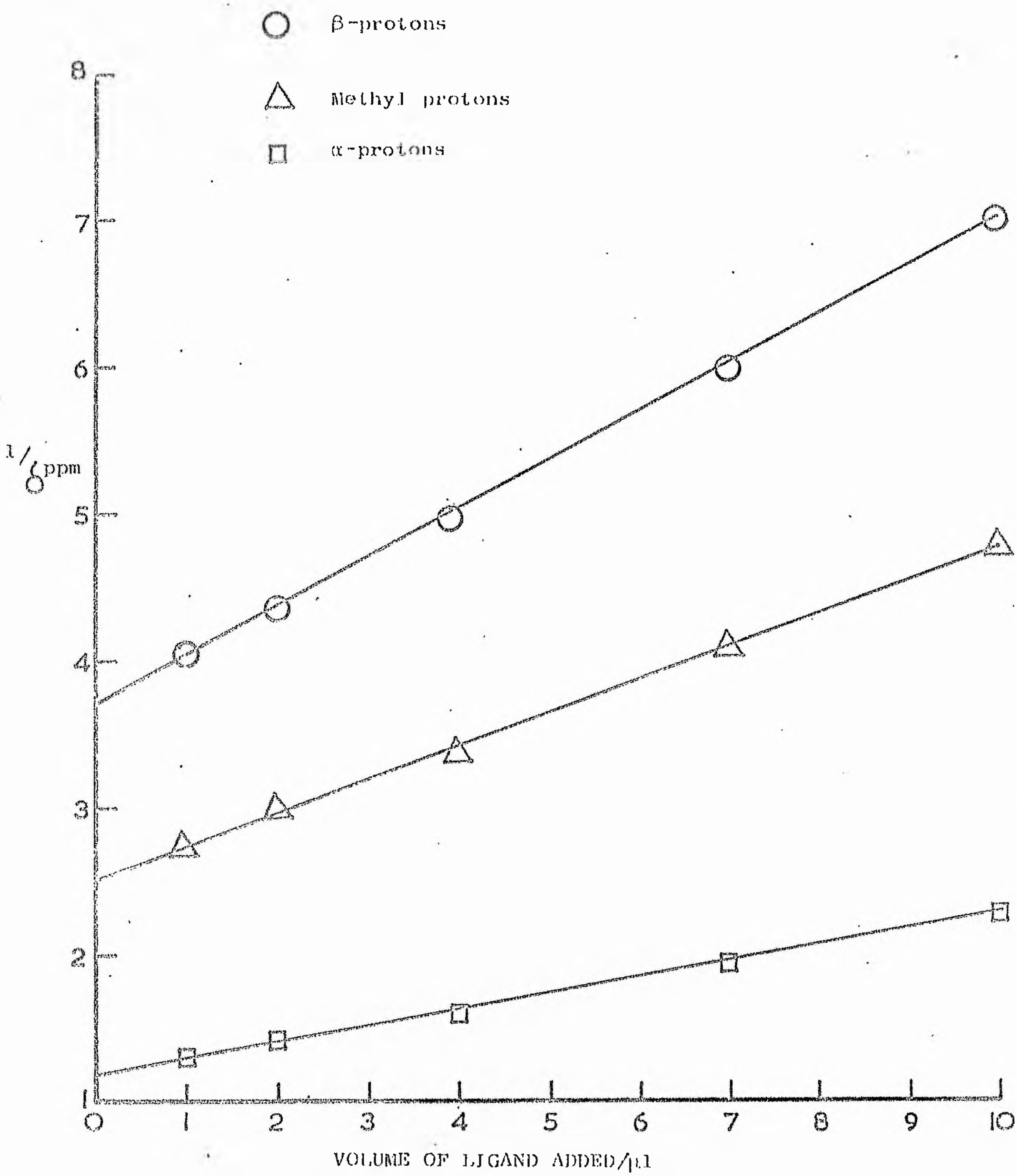

Fig. 6.3 Plot of 1/δ v. volume of ligand added to a solution of CD_3CN containing $Eu(hfaa)_4 \cdot Ph_4As$

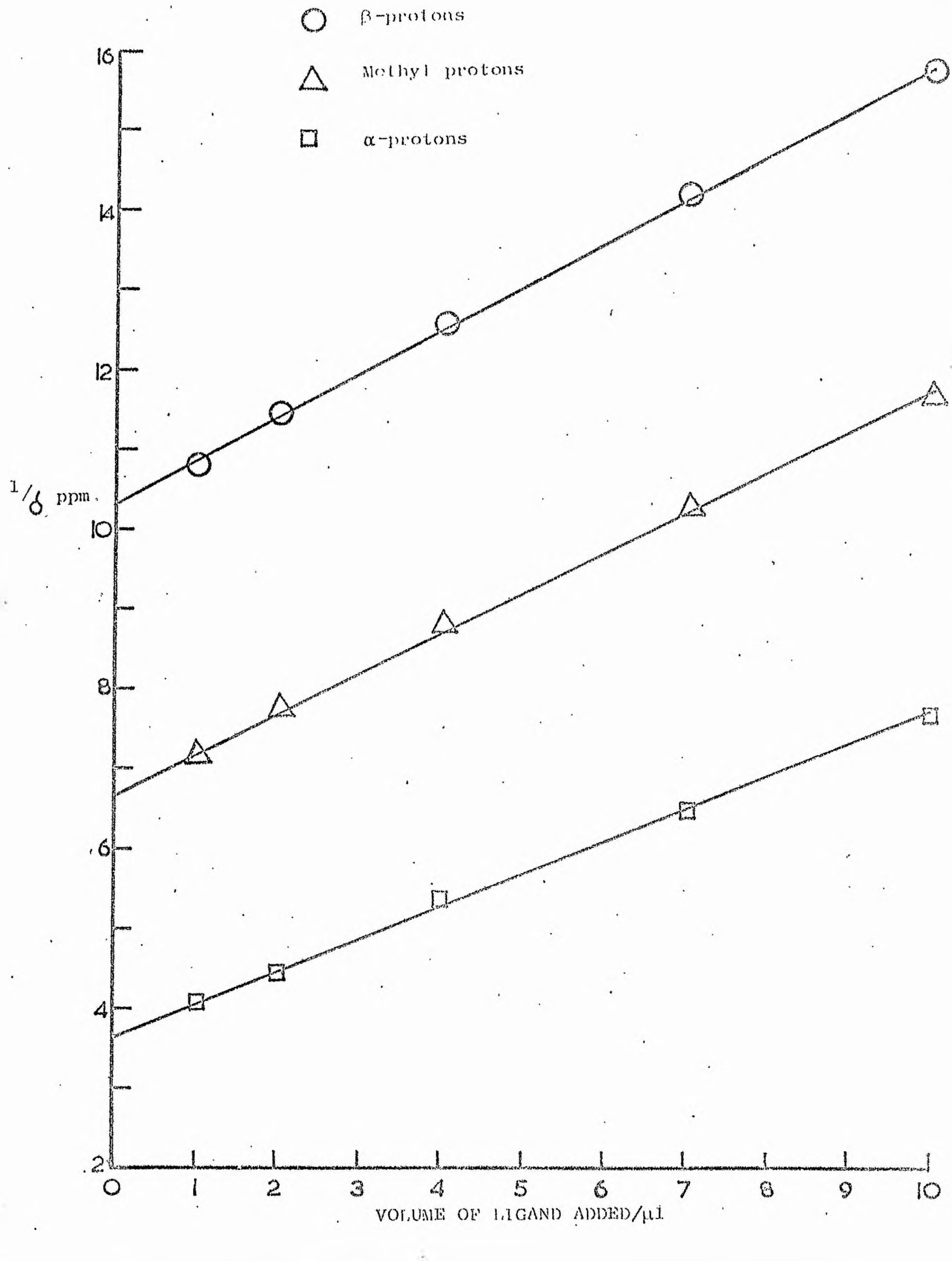

Fig. 6.4 Plot of 1/δ v. volume of ligand added to a solution of $CDCl_3$ containing $Eu(hfaa)_4 \cdot Ph_4As$

Table 6.1

Data of observed shift for γ-picoline protons in CD_3CN containing $Eu(hfaa)_4 \cdot Ph_4As$

$Eu(hfaa)_4 \cdot Ph_4As$ conc/ml^{-1}	Ligand conc/ml^{-1}	CH_3 /ppm	β-H /ppm	α-H /ppm
0.02601	0.01975	0.365	0.247	0.770
0.02596	0.03942	0.332	0.229	0.709
0.02586	0.07853	0.296	0.204	0.620
0.02572	0.13664	0.245	0.167	0.518
0.02557	0.19409	0.209	0.141	0.434

Table 6.2

Data of observed shift for γ-picoline protons in $CDCl_3$ containing $Eu(hfaa)_4 \cdot Ph_4As$

$Eu(hfaa)_4 \cdot Ph_4As$ conc/ml^{-1}	Ligand conc/ml^{-1}	CH_3 /ppm	β-H /ppm	α-H /ppm
0.02551	0.04681	0.138	0.092	0.239
0.02540	0.07012	0.128	0.087	0.220
0.02530	0.11633	0.114	0.078	0.180
0.02523	0.17341	0.097	0.070	0.153
0.02600	0.22990	0.085	0.063	0.127

examined the % standard deviation of K converged satisfactorily to a value of less than 5%. The K values and the absolute shifts determined by this method are given in table 6.3. The observed convergence and the agreement between K values derived from different protons of γ-picoline in CD_3CN containing $Eu(hfaa)_4 \cdot Ph_4As$ provides strong evidence that in the concentration ranges examined monoadduct formation is the predominant equilibrium. The marked deviation in

Table 6.3

K values calculated from the various spectral shift of the γ-picoline protons

Solvent	K/lm^{-1}			Absolute shift/ppm		
	$-CH_3$	β-H	α-H	$-CH_3$	β-H	α-H
CD_3CN	5.38	5.66	5.73	3.22	2.14	6.56
$CDCl_3$	3.99	2.96	7.23	1.64	1.47	1.93

the K value derived from the α-protons compared to the K values calculated from the methyl and β-protons of γ-picoline in $CDCl_3$ is due to the difficulty of assigning the nmr peaks of the α-protons because of their overlap with the $(Ph_4As)^+$ proton peaks of the lanthanide shift reagent. The most accurate value of K for the equilibrium illustrated in 6.2 in $CDCl_3$ will therefore be the value of 3.99 derived from the methyl protons of γ-picoline since they have a relatively large shift with no interference from the lanthanide shift reagent protons.

Evidence of ion-pairing between the $[Eu(hfaa)_4]^-$ anion and the $(Ph_4As)^+$ cation in $CDCl_3$ was obtained by interpretation of the concentration dependence on the position of the peaks corresponding to the $(Ph_4As)^+$ protons. At a chelate concentration of ca $2.5 \times 10^{-2}M$ two peaks were attributed to the $(Ph_4As)^+$ protons at 9.25 and 8.82 ppm downfield from the TMS lock signal. As the chelate concentration was increased both peaks shifted further downfield indicating that the protons of the cation were experiencing an increased induce shift caused by a decrease in the anion-cation interaction distance. This is consistent with ion-pair formation. The absence of an observed concentration dependent of the peak attributed to the $(Ph_4As)^+$ cation in CD_3CN (in the region 7.7-7.9 ppm) suggests that appreciable ion-pair formation does not occur at the concentrations studied.

(b) Discussion

Monoadduct formation of the type shown in equation 6.2 has been demonstrated in CD_3CN and $CDCl_3$ solutions containing the lanthanide shift reagent $Eu(hfaa)_4 \cdot Ph_4As$ using nmr spectroscopy. Calculations based on equilibria other than monoadduct formation equilibria have shown that they would give rise to considerably different types of $1/\delta$ against B plots from those derived for monoadduct formation[122]. The values of K determined by the method outlined above are not absolute values of the equilibrium constant, since additions of ligands alter the dielectric constant of the solvent and activities rather than concentrations, should therefore be used in equation 6.3. At the concentrations used in the investigations these effects are unlikely to cause serious deviations, however. The lower value of K at $CDCl_3$ may be attributed to the observed ion-pairing of the $[Eu(hfaa)_4]^-$ anion and $(Ph_4As)^+$ cation which would restrict the approach of the γ-picoline molecule to the chelated anion hindering bond formation between the Eu^{3+} ion and the ligand. Both values of K for the reaction discussed above are considerably lower than the value of 140 reported by Mackie _et al_[122] for γ-picoline in $CDCl_3$ solution containing $Eu(dpm)_3$. The decreased steric environment of the Eu^{3+} ion and the absence of ion-pairing in the _tris_ chelate may be attributed to the differences in the K values obtained for γ-picoline in $CDCl_3$ solution containing $Eu(hfaa)_4 \cdot Ph_4As$ and $Eu(dpm)_3$. Similarly the lower values of Δ obtained for the protons of γ-picoline in $CDCl_3$ using $Eu(hfaa)_4 \cdot Ph_4As$ compared to that obtained using $Eu(dpm)_3$ in the same solvent[122] may result from poorer

Eu^{3+} - ligand interaction, caused by the steric restrictions in the case of $Eu(hfaa)_4 \cdot Ph_4As$.

(c) Conclusion

Evidence based on analytical and spectroscopic data are consistent, for at least some lanthanide tetrakis β-diketoenolates, in that the coordination number of the Ln^{3+} ion can be increased from 8 to 9 in both the solid state and in solution. It is apparent that the basic strength and possibly the shape of the molecules employed to increase the coordination number of the Ln^{3+} ion in the crystalline state and in solution is important. The fact that γ-picoline and pyridine which have basic strengths comparable or less than the other bases employed in the synthesis coupled with the inferences obtained from vacuum sublimation suggest that a contribution from both factors may be necessary to obtain 9-coordination in the solid state. In solution the steric restriction caused by ion-pairing has been used to explain the differences in the K values obtained in CD_3CN and $CDCl_3$. Steric factors have been attributed to the relatively low K value of 2,4,6-trimethylpyridine in $CDCl_3$ solution containing $Eu(dpm)_3$[122].

The ready inclusion of water in some of the lanthanide tetrakis β-diketoenolates and the effect of its presence on the emission spectrum of the chelates emphasises the importance of rigorous chemical characterisation. There seems little doubt, therefore, that some tetrakis compounds reported previously in the literature have been hydrated.

CHAPTER 7

INTERMOLECULAR ENERGY TRANSFER IN SOME MIXED LANTHANIDE β-DIKETOENOLATES IN THE SOLID STATE AND IN SOLUTION

1. INTRODUCTION

Many of the investigations of intermolecular energy transfer involving lanthanide compounds have been reviewed by Anikina *et al*[218]. Triplet-triplet transfer has been reported for various lanthanide chelates in solutions containing ketones as sensitisers[175,176]. This transfer mechanism involves migration of the excited triplet energy of the ketone to the triplet level of the lanthanide chelate. Subsequent intramolecular transfer to the resonance levels of the Ln^{3+} ion results in ion-fluorescence. Triplet-lanthanide ion transfer has been reported by Filipescu *et al*[180-183] who employed various ketones to directly sensitise Tb^{3+} and Eu^{3+} ion-fluorescence. Rates of triplet-lanthanide ion transfer have been determined for $SmCl_3 \cdot 6H_2O$, $TbCl_3 \cdot 6H_2O$, $DyCl_3 \cdot 6H_2O$, $ErCl_3 \cdot 6H_2O$ and $EuCl_3$ in methanol from studies of the photoelimination reaction of p-methoxyvalerophenone (0.01 M)[315]. The transfer rates were found to be some two orders of magnitude slower than the average rate of diffusion. The low values were attributed to efficient solvation of the bare ions in the protic solvent preventing close approach of the ketone triplets to the Ln^{3+} ions and the orbital overlap necessary for effective exchange interaction.

Investigations of lanthanide-lanthanide energy transfer have been restricted mainly to inorganic glasses activated by lanthanide ions because of the poor quenching ability of the host medium. Van Uitert and co-workers have published a series of papers[186,187,316-319] on the interaction between lanthanide activators. In one of their papers[316] they presented data on the sensitising effect of terbium on the luminescence of europium. The experiments were performed with tungstates having composition $M_{0.5}Tb_{0.5-x}Eu_xWO_4$ and $M_{0.5}Y_{0.5-x}Eu_xWO_4$, where M = Na, K, Rb, or Cs and $x = 10^{-4}$, 10^{-3}, 10^{-2}, 10^{-1} or 0.5. It was shown that the intensity of the luminescence of europium in some tungstates was increased by the presence of the terbium in proportion to the terbium concentration. Up to 90% of the energy absorbed by the Tb^{3+} ions was transferred to the Eu^{3+} ions. When terbium was replaced by yttrium the intensity of the europium fluorescence diminished. It was also established that the relative intensity of the terbium and europium decreased with increasing radius of the alkali metal ions in the crystal lattice. In other studies[317,318] the authors investigated the mechanism of energy transfer from terbium to samarium in the $Na_{0.5}Y_{0.5(x+y)}Tb_ySm_xWO_4$ system, from europium to neodymium in $Na_{0.5}(Y,Eu,Nd)_{0.5}WO_4$ and $(Y,Eu,Nd)_2O_3$ and from dysprosium to terbium in $Na_{0.5}(Y,Tb,Dy)_{0.5}WO_4$. The quenching of the luminescence by samarium was suggested to be mainly a dipole-quadrupole interaction whereas energy transfer from europium to neodymium was regarded mainly as a dipole-dipole interaction.

Ghallagher et al[320] examined two stage energy transfer in solution and showed that only in the presence of terbium ions is energy transferred from 4,4'-di-m-hydroxybenzophenone (DMB) to europium. The authors concluded that the terbium ions constitute an intermediate link in energy transfer from DMB to europium causing fluorescence which is characteristic of the Eu^{3+} ion. It was also noted that other Ln^{3+} ions (Ln = Pr, Nd, Ho, Er, Tm) quench the luminescence of a mixture of DMB and terbium. It was suggested that the quenching involves an exchange-resonance mechanism.

Karpick et al[189] have studied the effects of temperature and concentration on the energy transfer process between erbium and holmium in yttrium aluminium garnet (YAG). They studied the energy transfer process between Er^{3+} and Ho^{3+} in YAG by measuring the spectral distribution and the decay patterns of the infrared fluorescence of three samples: YAG, Er (2%), Ho (0.2%); YAG, Er (50%), Ho (2%) and YAG, Er(50%), Tm (6.7%), Ho (6.7%) over the wide temperature range of 77-700K.

Kononenkov et al[321] have observed sensitised Eu^{3+} and Sm^{3+} ion fluorescence in β-diketoenolates containing terbium. Both the europium and samarium chelates are incapable of fluorescence in the absence of terbium. They proposed the energy transfer schemes represented by equations 7.1 and 7.2 for the $Tb^{3+} \rightsquigarrow Eu^{3+}$ and $Tb^{3+} \rightsquigarrow Sm^{3+}$ processes respectively.

$$Tb(^5D_4) \longrightarrow Tb(^7F_4), \qquad Eu(^5D_0) \longleftarrow Eu(^7F_1) \qquad 7.1$$

$$Tb(^5D_4) \longrightarrow Tb(^7F_4), \qquad Sm(^4G_{5/2}) \longleftarrow Sm(^6H_{5/2}) \qquad 7.2$$

2. INTERMOLECULAR ENERGY TRANSFER IN SOLUTION

(a) General Introduction

Intermolecular energy transfer between lanthanide chelate molecules in solution may occur by one or more of the following processes,

(a) Triplet-triplet transfer involving only the ligands,

$$T^*_{Ln} + S_{Ln'} \longrightarrow T^*_{Ln'} + S_{Ln} \qquad 7.3$$

(b) Ligand triplet-lanthanide ion transfer,

$$T^{*}_{Ln} + Ln' \longrightarrow S_{Ln} + Ln'^{*} \qquad 7.4$$

(c) Lanthanide-lanthanide ion transfer,

$$Ln^{*} + Ln' \longrightarrow Ln + Ln'^{*} \qquad 7.5$$

The singlet level of these chelates is unlikely to have any involvement in intermolecular energy transfer mechanisms because of the fast intersystem crossing rate constants. The transfer processes mentioned above will be in competition with the possible intramolecular transfer processes in the chelates (see figure 1.1) and are likely to be diffusion controlled. To investigate the relative importance of intermolecular energy transfer in solution four systems involving the hydrated lanthanide tris acetylacetonates, $Ln(aa)_3.3H_2O$, (Ln = Tb, Gd, Eu, Sm, Nd) in ethanol have been studied. The lanthanide acetylacetonates were selected for investigation because of their relatively high solubility in ethanol and for the negligible thermal depopulation of the $^5D_4$ Tb^{3+} ion level in $Tb(aa)_3 \cdot 3H_2O$ due to the large $^5D_4$-ligand triplet energy separation ($\sim$ 5000 cm^{-1}). The terbium complex fluoresces strongly in ethanol at room temperature, $\emptyset = 0.19$[288], whereas the europium complex gives only a relatively weak fluorescence, < 0.002[288]. The Gd^{3+}, Nd^{3+} and Sm^{3+} tris acetylacetonates do not give measureable fluorescence. All measurements were made on freshly prepared solutions due to the quite rapid decomposition of these chelates in ethanol (see chapter 3).

(b) Triplet-Triplet and Triplet-Lanthanide ion Transfer

In a solution of a single fluorescence lanthanide chelate triplet-triplet transfer should not alter the quantum efficiency since the triplet energy is being redistributed but not lost. With two different lanthanide chelates in solution triplet-triplet transfer could alter the quantum efficiencies if one chelate is a more efficient "trap" than the other. Relative fluorescence yields of the Tb^{3+} ion in various solutions having a total chelate concentration of 10^{-2} M, $(Tb_xGd_{1-x})(aa)_3 \cdot 3H_2O$ have been determined to investigate the importance of triplet-triplet energy transfer. Since the Gd^{3+} ion has no excited state levels below approximately 33,000 cm^{-1} (see figure 1.2) which is considerably above the lowest triplet level of the acetylacetonato ligand (ca 25,000 cm^{-1}), the possibility of intermolecular transfer involving the Gd^{3+} ion may be neglected. Two intermolecular transfer processes that may occur in this system are (a) transfer between the ligand triplet states and (b) transfer from a ligand triplet directly to an excited level of the Tb^{3+} ion. Processes (a) and (b) are illustrated in figure 7.1. The rate

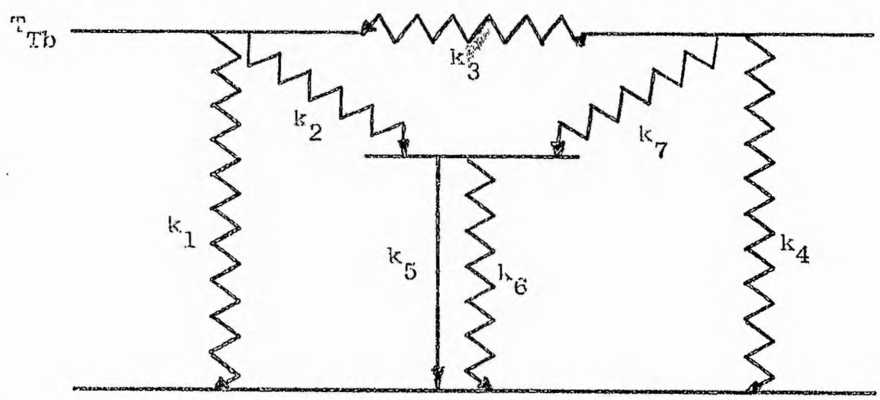

Fig. 7.1 Illustration of triplet-triplet and triplet-Ln^{3+} ion intermolecular energy transfer

of intramolecular deactivation of the terbium chelate triplet level, T_{Tb}, (i.e. k_1+k_2) is likely to exceed that of T_{Gd}, (i.e. k_4) since k_1 and k_4 are expected to be similar in magnitude. Using a method similar to Kananskaya et al[217] and employing isoprene as quencher the value of $k_2 = 6.7 \times 10^8$ s^{-1} for $Tb(aa)_3 \cdot 3H_2O$ in ethanol has been obtained[299]. If triplet-triplet transfer was a significant process in this case this should be reflected in an increase in Tb^{3+}

fluorescence relative to its mole fraction in the mixed solution since a net transfer from T_{Gd} to T_{Tb} would result. Within experimental error the relative fluorescence, F_{293}, of the Tb^{3+} ion was found to be proportional to its mole fraction (table 7.1). The lifetime of

Table 7.1

Relative fluorescence and τ_{293} data of various ethanol solutions (0.1M) containing $(Tb_xGd_{1-x})(aa)_3 \cdot 3H_2O$

Tb^{3+} ion conc/x	F_{293} [a]	$\tau_{293}/\mu s$
1.00	1.00 ± 0.02	734 ± 20
0.80	0.80 ± 0.02	720 ± 20
0.70	0.71 ± 0.02	716 ± 20
0.60	0.61 ± 0.02	734 ± 20
0.50	0.49 ± 0.02	715 ± 20
0.40	0.40 ± 0.02	724 ± 20
0.30	0.31 ± 0.02	730 ± 20
0.20	0.21 ± 0.02	737 ± 20

(a) Normalised to unity for 100% Tb^{3+} solution

the $^5D_4$ Tb^{3+} level was constant within experimental error over the Tb^{3+} concentration range investigated. Identical results, within experimental error were obtained employing degassed solutions, indicating that any effects due to oxygen quenching may be neglected.

Assuming that the intermolecular transfer rate (i.e. k_3) is independent of the nature of the metal ion, the relative fluorescence intensity, F_{293}, of a solution of total molarity M and containing mole fraction x of Tb^{3+} ion may be expressed as equation 7.6 (see appendix for derivation) if only triplet-triplet transfer occurs i.e. k_7 is not important.

$$F_{293} = \frac{1+c}{1+c/x} \qquad F_{293} = 1 \text{ when } x = 1 \qquad 7.6$$

$$\text{where } c = \frac{k_4(k_1+k_2+k_3M)}{k_3M(k_1+k_2-k_4)} \qquad 7.7$$

If $k_1=k_4$ then

$$c = \frac{k_1(k_1+k_2+k_3M)}{k_2k_3M} \qquad 7.8$$

Dawson et al[288] have reported an overall quantum yield, $\emptyset = 0.19$ for terbium tris acetylacetonate at 296K in ethanol ($2 \times 10^5 - 3 \times 10^{-2}$M) and a quantum yield $\emptyset_{^5D_4} = 0.33$ for the $^5D_4$ Tb^{3+} ion level. From figure 7.1 in the absence of Gd^{3+} the overall quantum yield, $\emptyset_{293}$, may be expressed as equation 7.9. Substitution of the values of Dawson et al[288] for $\emptyset_{293}$ and $\emptyset_{^5D_4}$ and the

$$\emptyset_{293} = \frac{k_2}{k_1+k_2}\emptyset_{^5D_4} \qquad 7.9$$

$$\text{where } \emptyset_{^5D_4} = \frac{k_5}{k_5+k_6} \qquad 7.10$$

$k_2 = 6.7 \times 10^8\ s^{-1}$, obtained from the quenching experiment referred to above[299], in equation 7.9 results in a value of $k_1 = 4.9 \times 10^8\ s^{-1}$. Taking the bimolecular diffusion rate constant i.e. k_3 as 5.4×10^{-9} ($lm^{-1}s^{-1}$)[139] and assuming triplet-triplet transfer occurs on every collision then by substitution into equation 7.8 when M = 0.01 M a value c = 16.4 is obtained. Using this value for c when x = 0.5 a value of $F_{293} = 0.515$ is obtained from equation 7.6. This is within experimental error of the measurements. It may be concluded that these results exclude efficient long range transfer but cannot preclude the possibility of triplet-triplet transfer in solution at the concentration studied. They do suggest that if it does occur it is difficult to detect experimentally by this method. Similar treatment using a triplet-lanthanide ion energy transfer model indicates that such transfer is possible but cannot be definitely established from the present data in 10^{-2}M solution.

(c) Lanthanide ion-Lanthanide ion Transfer

The results of relative quantum efficiency of the $^5D_4 \rightarrow {}^7F_4$ Tb^{3+} ion emission obtained for mixed solutions of $(Tb_xLn_{1-x})(aa)_3 \cdot 3H_2O$ where Ln = Eu, Sm and Nd at various concentrations (0.01, 0.005, 0.0025, and 0.00125 M) in ethanol at 293K are reported in tables 7.2, 7.3 and 7.4 respectively. Figures 7.2, 7.3 and 7.4 respectively illustrate the marked decrease in Tb^{3+} ion fluorescence below the value expected in terms of its mole fraction for the series of Eu^{3+}, Sm^{3+} and Nd^{3+}

Table 7.2

F_{293} and τ_{293} data for the Tb^{3+} ion in an ethanol solution containing

$Tb_x/Eu_{1-x}(aa)_3 \cdot 3H_2O$

Mole fraction Tb^{3+} ion/x	1.25×10^{-3}M		2.5×10^{-3}M		5×10^{-3}M		10^{-2} M	
	F_{293} a	$\tau/\tau_{1.0}$ x	F_{293} a	$\tau/\tau_{1.0}$ x	F_{293} a	$\tau/\tau_{1.0}$ x	F_{293} a	$\tau/\tau_{1.0}$ x
1.00	1.00	1.00	1.00	1.00	1.00	1.00	1.00	1.00
0.80	0.75	0.77	0.69	0.69	0.61	0.60	0.54	0.60
0.70	0.63	0.62	0.58	0.55	0.49	0.47	0.41	0.48
0.60	0.54	0.52	0.48	0.46	0.39	0.40	0.29	0.39
0.50	0.44	0.43	0.38	0.36	0.30	0.31	0.23	0.33
0.40	0.33	0.32	0.29	0.28	0.23	0.24	0.16	0.27
0.30	0.24	0.24	0.21	0.21	0.15	0.18	0.11	0.22
0.20	0.16	0.15	0.13	0.13	0.10	0.11	0.07	0.15

(a) Normalised to unity for 100% $Tb(aa)_3 \cdot 3H_2O$ ethanol solution i.e. x = 1

Table 7.3

F_{293} and τ_{293} data for the Tb^{3+} ion in an ethanol solution containing

$Tb_x/Sm_{1-x}(aa)_3 \cdot 3H_2O$

1.00	1.00	1.00	1.00	1.00	1.00	1.00	1.00	1.00
0.80	0.70	0.69	0.61	0.65	0.55	0.59	0.45	0.52
0.70	0.59	0.55	0.49	0.52	0.42	0.46	0.34	0.41
0.60	0.48	0.48	0.38	0.40	0.32	0.35	0.23	0.31
0.50	0.39	0.40	0.29	0.35	0.23	0.28	0.18	0.28

Table continued overleaf

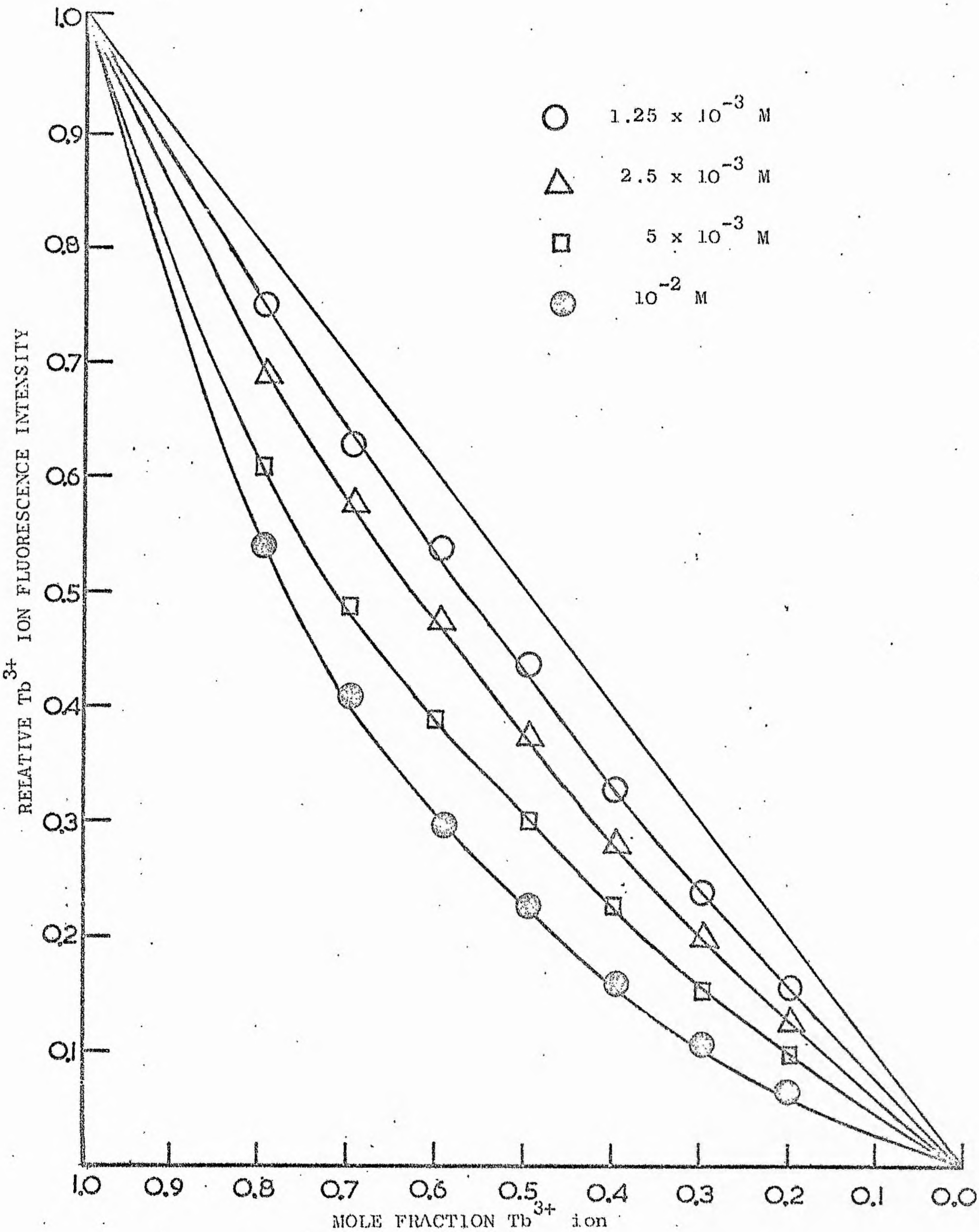

Fig. 7.2 Tb^{3+} fluorescence as a function of mole fraction in an ethanol solution containing $Tb/eu(aa)_3 \cdot 3H_2O$ at 293K

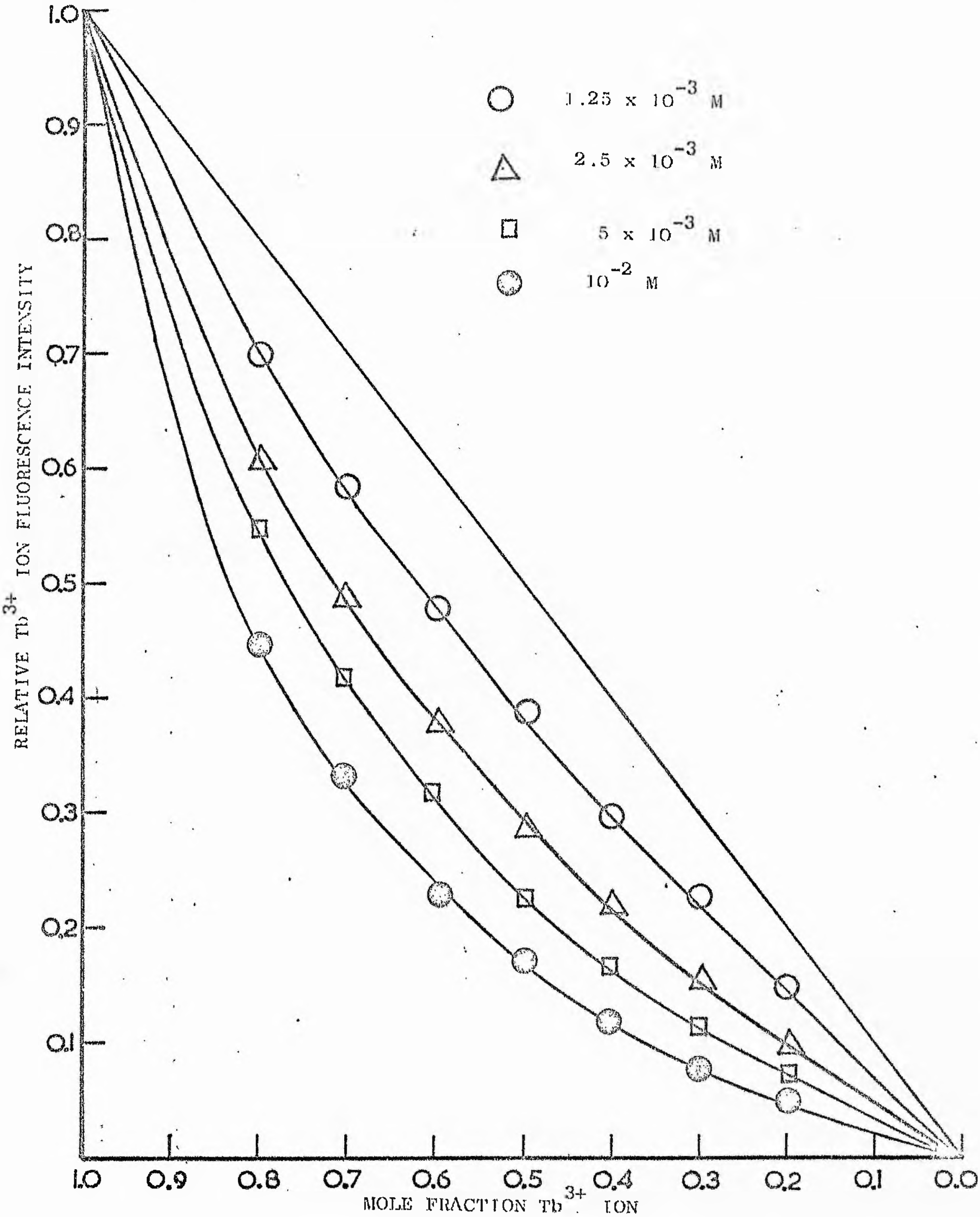

Fig. 7.3 Tb^{3+} fluorescence as a function of mole fraction in an ethanol solution containing $Tb/Sm(aa)_3 \cdot 3H_2O$ at 293K

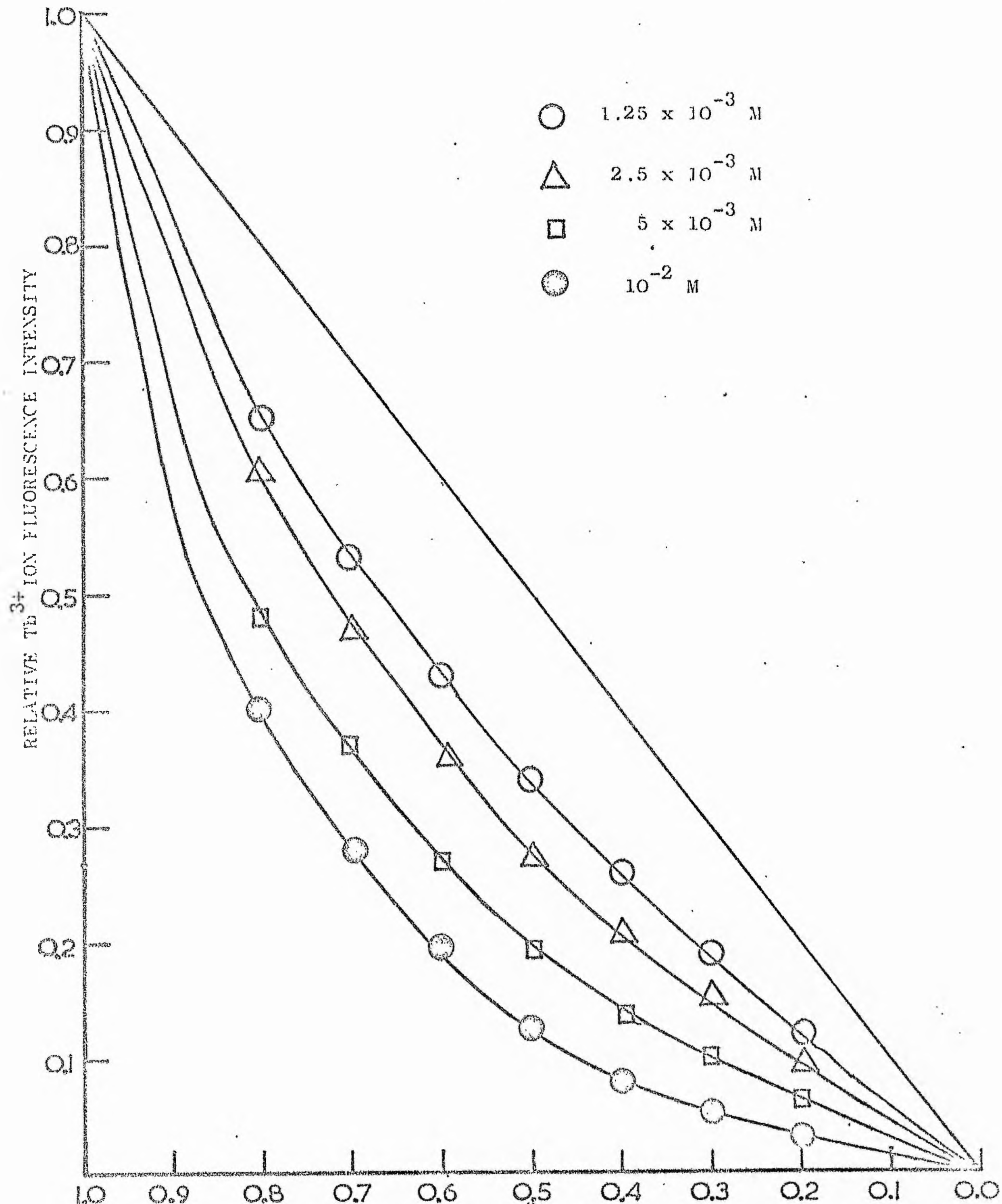

Fig. 7.4 Tb^{3+} fluorescence as a function of mole fraction in an ethanol solution containing $Tb/Nd(aa)_3 \cdot 3H_2O$ at 293K

Table 7.3 (cont.)

Mole fraction Tb^{3+} ion/x	1.25×10^{-3}M		2.5×10^{-3}M		5×10^{-3}M		10^{-2}M	
	F_{293}^{a}	$\frac{\tau}{\tau_{1.0}} \cdot x$	F_{293}^{a}	$\frac{\tau}{\tau_{1.0}} \cdot x$	F_{293}^{a}	$\frac{\tau}{\tau_{1.0}} \cdot x$	F_{293}^{a}	$\frac{\tau}{\tau_{1.0}} \cdot x$
0.40	0.30	0.31	0.23	0.30	0.17	0.25	0.12	0.24
0.30	0.23	0.23	0.16	0.19	0.12	0.17	0.08	0.21
0.20	0.15	0.15	0.10	0.12	0.08	0.11	0.06	0.13

(a) Normalised to unity for 100% $Tb(aa)_3 \cdot 3H_2O$ in ethanol solution i.e. x = 1

Table 7.4

F_{293} and τ_{293} data for Tb^{3+} ion in an ethanol solution containing

$Tb_x/Nd_{1-x}(aa)_3 \cdot 3H_2O$

1.00	1.00	1.00	1.00	1.00	1.00	1.00	1.00	1.00
0.80	0.65	0.67	0.61	0.61	0.48	0.58	0.40	0.53
0.70	0.53	0.54	0.47	0.50	0.37	0.47	0.28	0.46
0.60	0.43	0.44	0.36	0.39	0.27	0.36	0.20	0.40
0.50	0.34	0.34	0.27	0.28	0.19	0.30	0.13	0.38
0.40	0.26	0.27	0.21	0.24	0.13	0.24	0.08	0.33
0.30	0.19	0.20	0.16	0.17	0.10	0.18	0.05	0.28
0.20	0.12	0.13	0.10	0.11	0.06	0.13	0.03	0.21

(a) Normalised to unity for 100% $Tb(aa)_3 \cdot 3H_2O$ ethanol solution i.e. x = 1

containing solutions having various total chelate concentrations. Eu^{3+}, Sm^{3+} and Nd^{3+} all have excited levels at lower energies than the Tb^{3+} $^5D_4$ emitting level which are potential energy acceptors. The decrease in relative Tb^{3+} ion fluorescent is most marked in the case of Nd^{3+} with Sm^{3+} being a more efficient quencher than Eu^{3+}. On the basis of the previous results obtained for the $Tb_x/Gd_{1-x}(aa)_3 \cdot 3H_2O$ solutions the possibility of triplet-triplet and/or triplet-lanthanide ion transfer may be neglected as a possible cause of this behaviour. The possibility of lanthanide-lanthanide transfer may therefore be investigated. Figure 7.5 represents a possible mechanism for such energy transfer. The relative

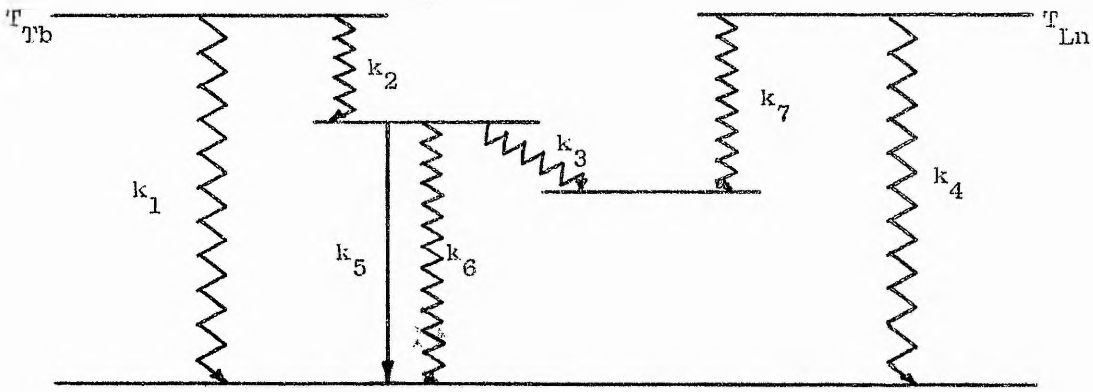

Fig. 7.5 Illustration of possible lanthanide-lanthanide transfer mechanism

fluorescence of these solutions can be expressed in the form of equation 7.6 where c in this case has the value given below (see

$$c = -\left(\frac{k_5+k_6}{k_3 M} + 1\right) \qquad 7.11$$

appendix for derivation). The various values of F_{293} obtained for each mixed lanthanide system with change in concentrations were computed to obtain the best value of c using equation 7.6. The best value of c was then used to calculate the theoretical value of F_{293} and in all cases there was good agreement with the experimental values. From the τ_{293} values obtained for the 100% Tb^{3+} ion solutions a mean value of 724 μs was calculated i.e. $k_5+k_6 = 1.38 \times 10^{-3}$ s^{-1}. Using this value of k_5+k_6 and the value obtained for c for the respective concentrations, a value for k_3 can be obtained by substitution into equation 7.11. Table 7.5 contains the various values of c and the calculated values of k_3 for the various mixed lanthanide systems at the particular total concentration. The values of k_3 for the various systems are all in reasonably good agreement for the measurements made at different concentrations

Table 7.5

Values of c and k_3 for the various lanthanide systems

lanthanide system	c value				$10^{-5}k_3/lm^{-1}s^{-1}$			
	1.25 x 10^{-3}M	2.5 x 10^{-3}M	5 x 10^{-3}M	10^{-2}M	1.25 x 10^{-3}M	2.5 x 10^{-3}M	5 x 10^{-3}M	10^{-2}M
Tb/Eu	-4.122	-2.501	-1.716	-1.409	3.54	3.45	3.86	3.38
Tb/Sm	-2.704	-1.700	-1.445	-1.268	6.84	7.89	6.19	5.15
Tb/Nd	-2.004	-1.631	-1.318	-1.194	11.00	8.74	8.69	7.12

but all are considerably lower than the value of 5.4 x 10^9 $lm^{-1}s^{-1}$ for the diffusion controlled rate constant. This indicates that lanthanide-lanthanide transfer does not take place on every collision but has a probability of ca 6.6 x 10^{-5}, 1.2 x 10^{-4} and 1.6 x 10^{-4} for the Tb/Eu, Tb/Sm and Tb/Nd systems respectively.

(d) Discussion

Energy transfer via triplet-triplet and lanthanide-triplet mechanisms has been shown to be extremely small in the concentration ranges studied. The main mechanism responsible for the quenching of the Tb^{3+} ion in $Tb(aa)_3 \cdot 3H_2O$ in ethanol containing various amounts of Eu, Sm and Nd acetylacetonates is lanthanide-lanthanide transfer. It is apparent from the quenching rate constants for the various mixed systems that energy transfer is inefficient. Investigations by Wagner et al[315] have resulted in the determination of rate constants for the quenching of a ketone by various lanthanide ions in methanol. The values obtained were all considerably lower than the diffusion controlled rate constant. They attributed this marked decrease as being due to steric shielding of the lanthanide quenching levels caused by extensive solvation of the Ln^{3+} ions preventing the necessary orbital overlap for exchange interaction.

The even greater difference between the diffusion controlled rate constant and the quenching rate constants for the chelate systems may be explained by more efficient steric shielding of the Ln^{3+} ions. The observed quenching ability of the lanthanide ions investigated i.e. Nd > Sm > Eu may be explained in terms of ΔE the energy between the $^5D_4$ Tb^{3+} level and acceptor level of the quenching Ln^{3+} ions. If ΔE is small more efficient deactivation would be expected as a consequence of less energy having to be lost to the immediate environment. Transfer from the $^5D_4$ Tb^{3+} level to the Eu^{3+} manifold probably goes via the $^5D_1$ Eu^{3+} level because although enhancement of Eu^{3+} fluorescence is observed in solutions containing Tb^{3+} it is not sufficient to explain a $Tb_{^5D_4} \rightsquigarrow Eu_{^5D_0}$ transition. Dawson et al[288] have obtained a value of ca 0.5 for the $^5D_1 \rightsquigarrow {}^5D_0$ Eu^{3+} ion transition in $Eu(aa)_3 \cdot 3H_2O$ in methanol indicating that about 50% of the energy is dissipated non-radiatively in the transition.

If the model illustrated in figure 7.5 for lanthanide-lanthanide energy transfer is correct a decrease in the lifetime of the $^5D_4$ Tb^{3+} level with decrease in Tb^{3+} ion concentration would be expected when the total lanthanide concentration is kept constant. The functions $\tau x/\tau_{1.0}$ reported in tables 7.2, 7.3 and 7.4 give the relative fluorescence intensities predicted from the lifetime data for the various solutions within their respective total lanthanide concentrations. In all three systems the values predicted from lifetime data for F_{293} are in very good agreement with the observed value of F_{293} for the solutions having 1.25×10^{-3}M and 2.5×10^{-3}M total lanthanide concentration indicating that the experimental data are consistent with the model suggested in figure 7.5. However in the 5×10^{-3}M and 10^{-2}M solutions the Tb^{3+} $^5D_4$ lifetimes do not decrease sufficiently to explain the reduction in Tb^{3+} fluorescence - this is particularly marked in the case of neodymium. This apparently anomalous behaviour in the lifetime data may be explained if the experimentally determined τ are not that of a single species but of two or more species occurring in the higher concentration solutions. The slight deviation from exponentiality in these lifetimes are within experimental error. In addition since τ remained constant in 10^{-2}M Tb/Gd(aa)$_3$·3H$_2$O solutions this type of explanation implies that the nature of the metal ions present significantly influence the associative or dissociative equilibria which may occur in mixed solutions.

3. INTERMOLECULAR ENERGY TRANSFER IN THE SOLID STATE

(a) General Introduction

The emission spectra of the gadolinium chelates reported in chapter 4 all showed disproportionately high emission peaks characteristic of Tb^{3+} and Eu^{3+} ion fluorescence. These ions were present as impurities in the original Gd_2O_3 starting material at less than the 0.1% level. Neutron activation analysis indicated that the chelates only contained a few ppm of the Eu^{3+} and Tb^{3+} impurities. It was suggested therefore that very efficient energy migration within the chelates was responsible for the enhancement of the lanthanide fluorescence. To investigate this enhancement in the solid state two series of mixed crystalline solids were prepared, $Eu_x/Gd_{1-x}(hfaa)_4Bu^tNH_3.H_2O$ and $Eu_x/Gd_{1-x}(tfaa)_4 \cdot Ph_4As$ (x = mole fraction of Eu^{3+}) and the relative quantum yields determined. In both cases a higher Eu^{3+} fluorescence was observed than that expected in terms of the mole fraction of Eu^{3+} present (tables 7.6 and 7.7 respectively. Figure 7.6 illustrates this enhancement. It is apparent from the tables and the figure that enhancement is more

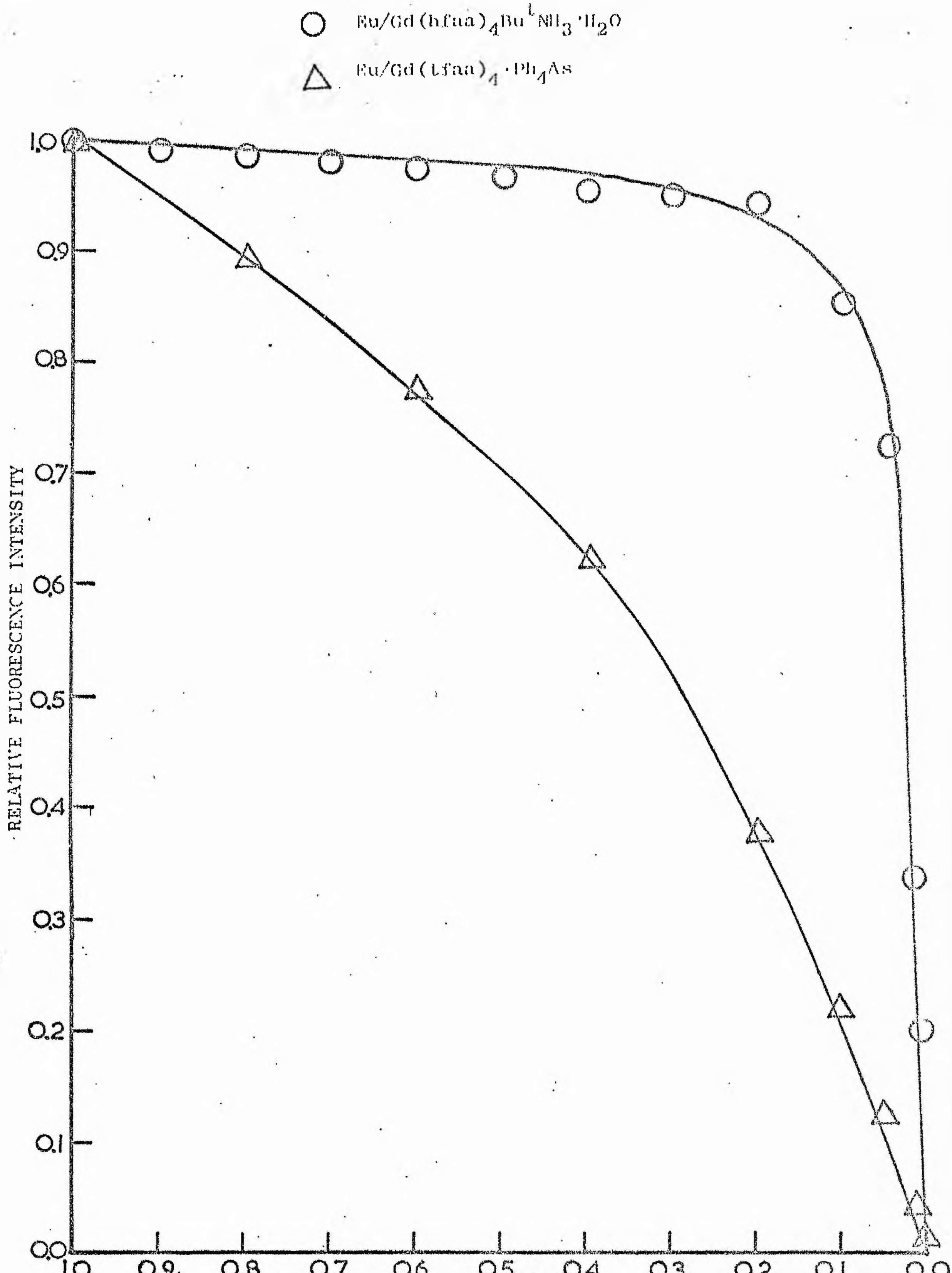

Fig. 7.6 Illustration of enhancement of Eu^{3+} fluorescence on solid $Eu/Gd(hfaa)_4Bu^tNH_3 \cdot H_2O$ and $Eu/Tb(tfaa)_4 \cdot Ph_4As$

Table 7.6

Relative fluorescence and lifetime data on Eu/Gd(hfaa)$_4$·Bu^{t}NH$_3$·H$_2$O

Mole fraction Eu^{3+}	F_{293}^{a}	$\tau_{293}/\mu s$
1.00	1.00	526 ± 20
0.90	0.99	528 ± 20
0.80	0.98	540 ± 20
0.70	0.98	539 ± 20
0.60	0.97	542 ± 20
0.50	0.96	550 ± 20
0.40	0.95	550 ± 20
0.30	0.95	536 ± 20
0.20	0.94	538 ± 20
0.10	0.85	548 ± 20
0.05	0.72	540 ± 20
0.01	0.34	537 ± 20
0.005	0.20	532 ± 20

(a) Normalised to unity for 100% Eu^{3+}

Table 7.7

Relative fluorescence and lifetime data on Eu/Gd(tfaa)$_4$·Ph$_4$As

Mole fraction Eu^{3+}	F_{293}^{a}	$\tau_{293}/\mu s$
1.00	1.00	894 ± 20
0.80	0.90	893 ± 20
0.60	0.77	890 ± 20
0.40	0.63	892 ± 20
0.20	0.37	897 ± 20
0.10	0.23	889 ± 20
0.05	0.13	889 ± 20
0.01	0.04	890 ± 20
0.005	0.02	894 ± 20

(a) Normalised to unity for 100% Eu^{3+}

marked in the case of the hfaa mixed chelate. Lifetime measurements of the $^5D_0 \rightarrow {}^7F_2$ Eu^{3+} transition for both mixed chelate systems were constant within experimental error.

The various energy transfer processes referred to in equations 7.3, 7.4 and 7.5 are all possible in the case of solid mixtures. Lanthanide-lanthanide transfer however is precluded from the systems mentioned above because the first excited state of Gd^{3+} ion lies well above the S_1 state of the chelated ligands excluding the Gd^{3+} level from any involvement in energy transfer. Singlet-singlet and/or triplet-triplet transfer may therefore be responsible for the disproportionately high Eu^{3+} fluorescence. The involvement of the triplet level in energy transfer may be shown by investigating the $^5D_4 \rightarrow {}^7F_4$ lifetime in a series of Tb^{3+} chelates similar to those mentioned above.

(b) Triplet-Triplet Transfer

A thermal depopulation mechanism of the $^5D_4$ Tb^{3+} ion level in the chelates studied in chapter 4 was shown to be responsible for the observed temperature dependence of the lifetime of the $^5D_4 \rightarrow {}^7F_j$ transition. If the triplet is involved in intermolecular energy transfer and thermal depopulation of the $^5D_4$ Tb^{3+} level occurs, it may be possible to observe a $^5D_4 \rightarrow {}^7F_j$ lifetime dependence on the concentration of Gd^{3+} ion present in the mixed chelate. The concentration dependence of the lifetime would result since further deactivation routes are possible by transfer of terbium ligand triplet energy to the gadolinium triplet with subsequent energy loss via $T_{Gd} \rightsquigarrow S_0$. The probability of such a loss mechanism would increase as the Gd^{3+} ion concentration increased. Figure 7.7 shows the possible triplet-triplet deactivation of the $^5D_4$ Tb^{3+} level involving thermal depopulation. k_1 and k_4 are the overall triplet

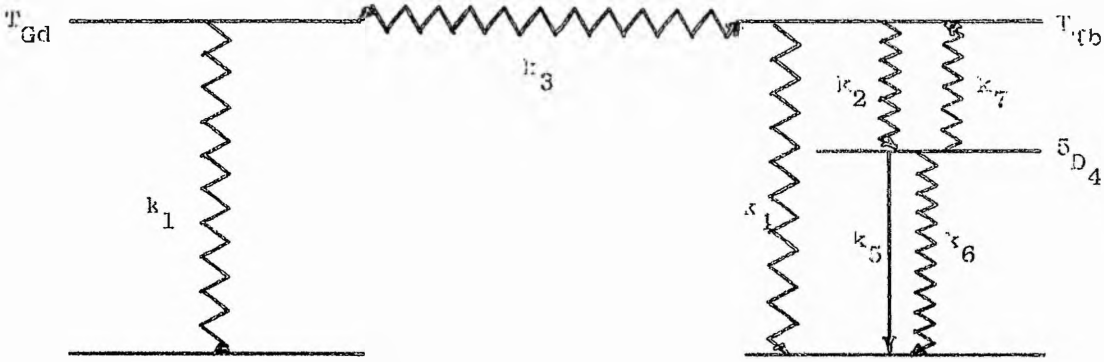

Fig. 7.7 Illustration of the triplet-triplet deactivation of the $^5D_4$ Tb^{3+} level

deactivation rate constants for gadolinium triplet, T_{Gd}, and the terbium triplet, T_{Tb}, respectively in the mixed chelate, k_7 is the temperature dependent thermal depopulation rate constant.

Two mixed chelate systems $Tb_xGd_{1-x}(hfaa)_4Bu^tNH_3 \cdot H_2O$ and $Tb_xGd_{(1-x)}(tfaa)_4 \cdot Ph_4As$ were prepared to investigation the possibility of triplet involvement in energy transfer. These chelate systems were selected since thermal depopulation of $^5D_4$ Tb^{3+} level was observed in the pure terbium chelates (see chapter 4). Lifetime and relative quantum efficiencies for the various mixtures within the series were determined at 293K and are reported in tables 7.8 and 7.9 respectively. The relative quantum efficiency values of the various samples within mixed chelate systems were all higher than would be excepted on the basis of the mole fraction of Tb^{3+} present (figures 7.8 and 7.9). In both cases the lifetime of the $^5D_4 \rightarrow {}^7F_j$ Tb^{3+} level decreased as the gadolinium concentration increased (figure 7.10). The functions in the last column of tables 7.8 and 7.9 makes an allowance to the quantum yield for energy losses caused by the Gd^{3+} from thermal depopulation of the $^5D_4$ Tb^{3+} level. It is apparent even when the quantum yields are corrected for energy losses

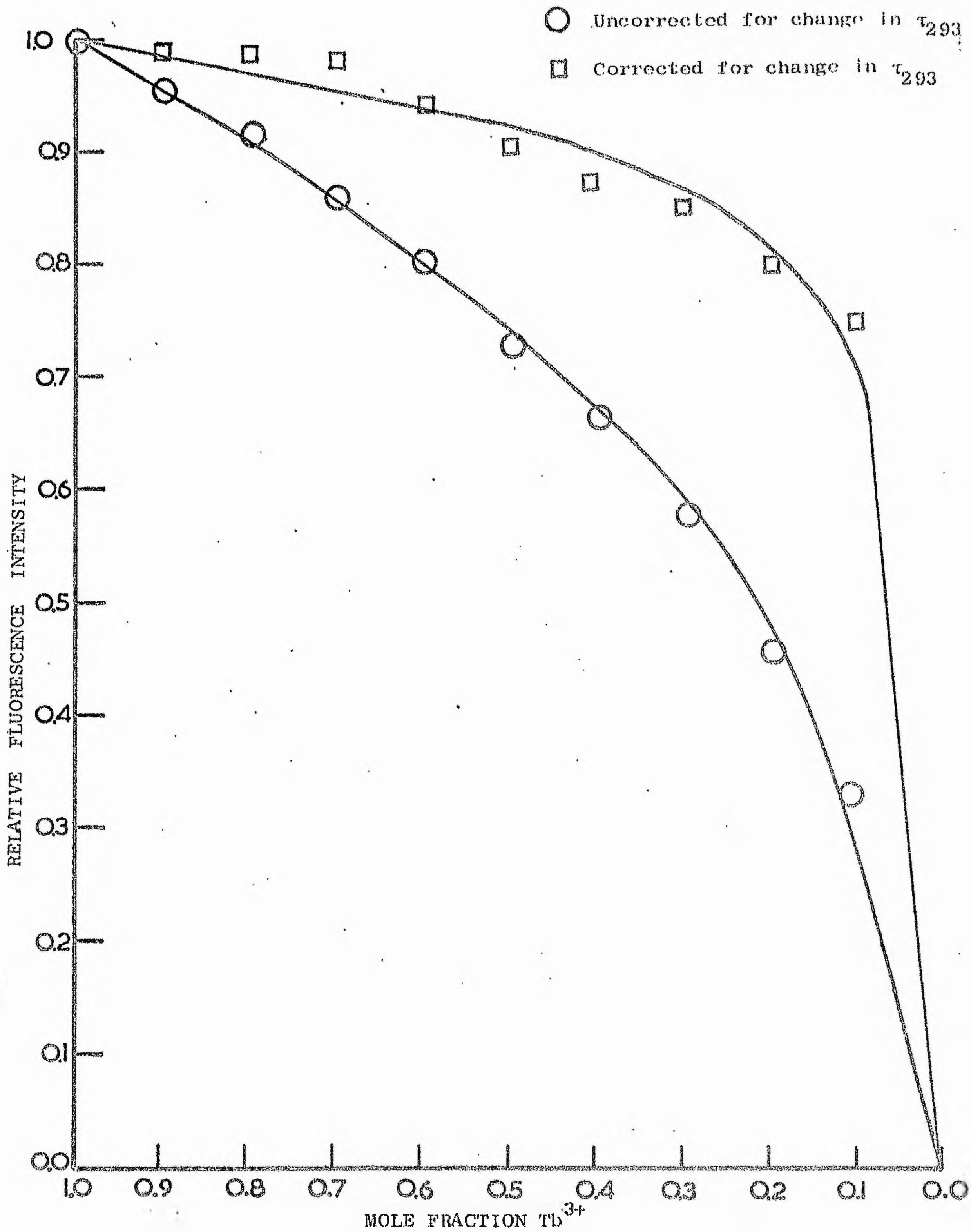

Fig. 7.8 Illustration of Tb^{3+} emission enhancement in solid $Tb/Gd(hfaa)_4 \cdot Bu^tNH_3 \cdot H_2O$ at 293K

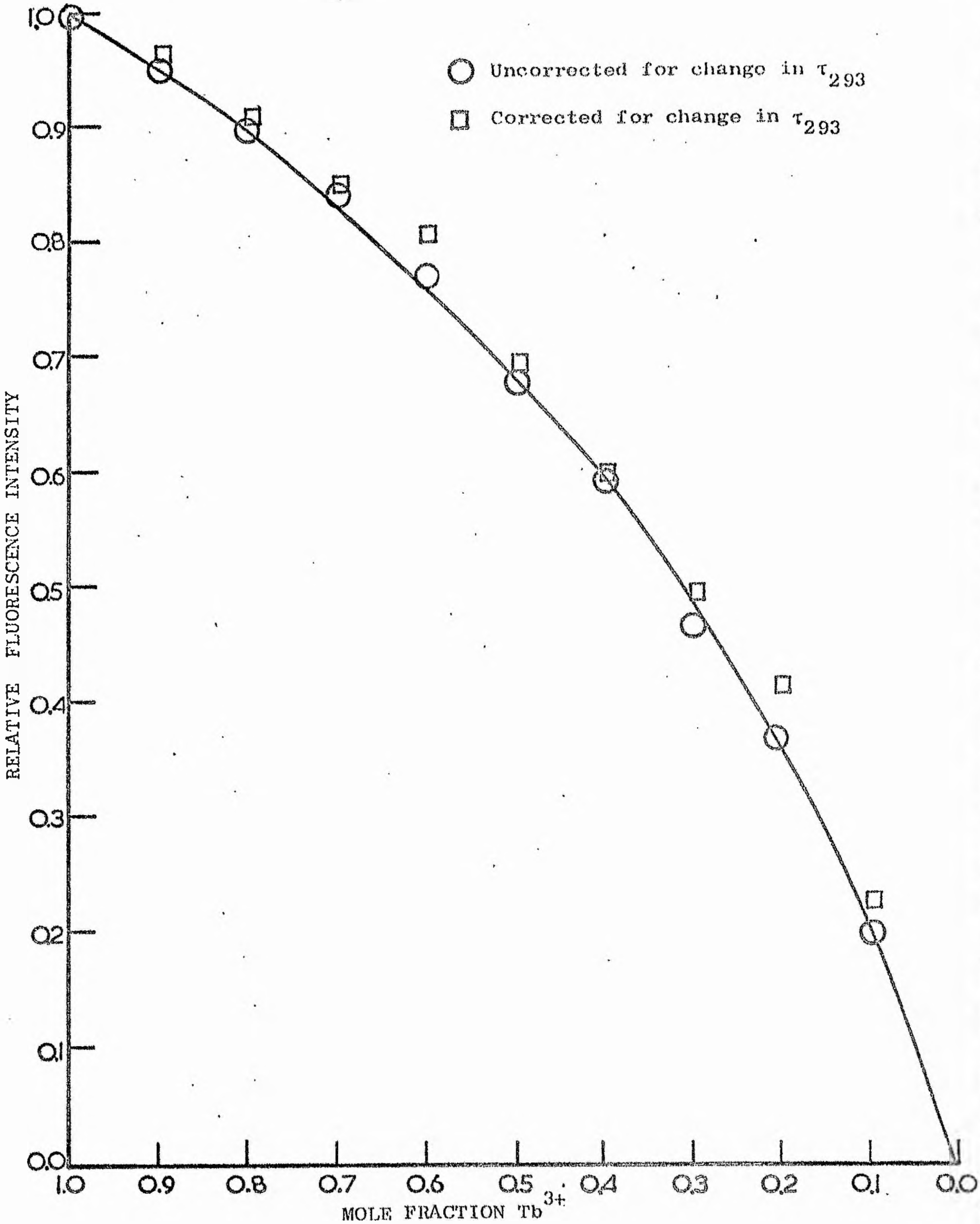

Fig. 7.9 Illustration of Tb^{3+} emission enhancement in solid $Tb/Gd(tfaa)_4 \cdot Ph_4As$ at 293K

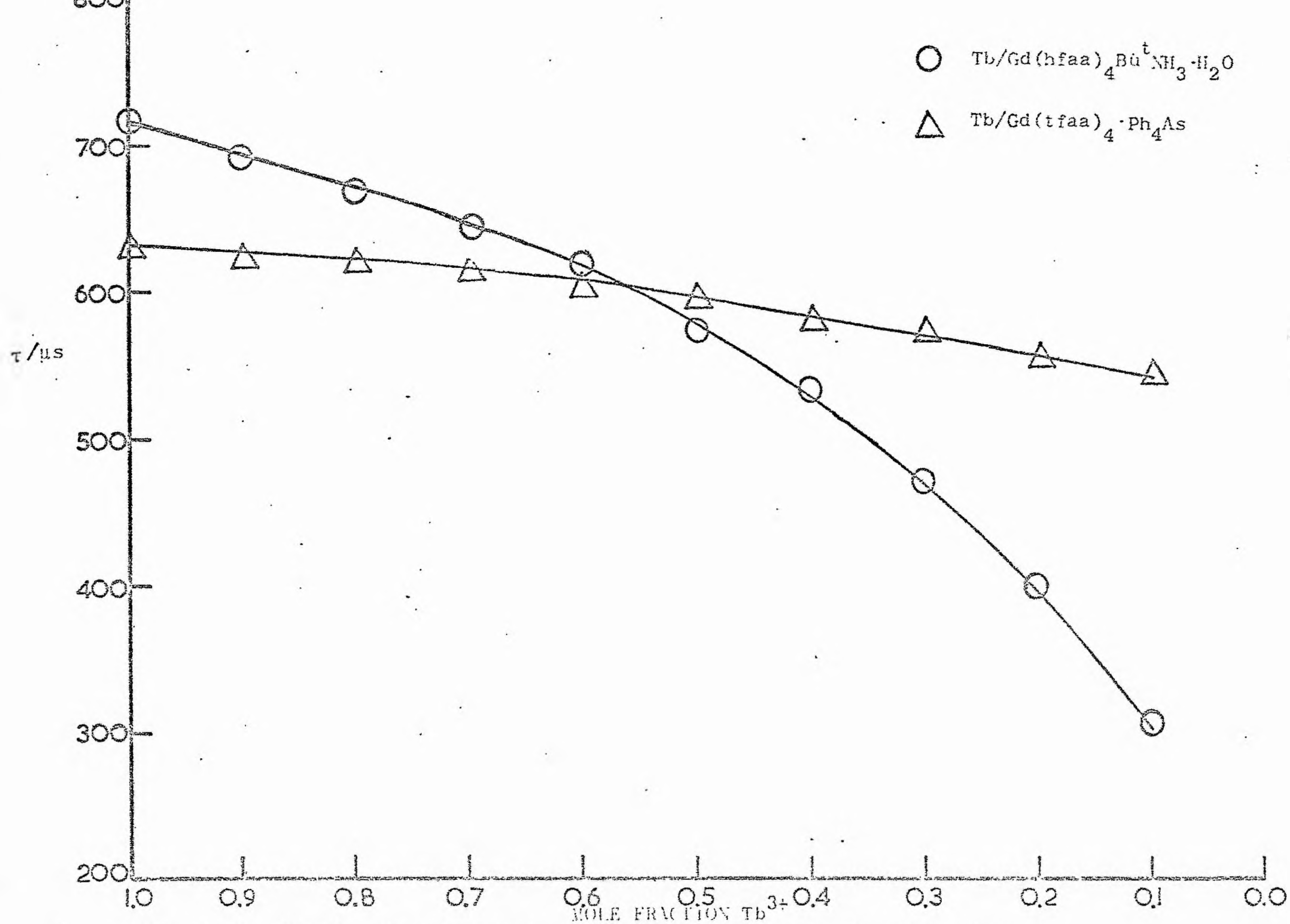

Fig. 7.10 Lifetime dependence of mixed Tb/Gd chelates in the solid state

Table 7.8

Relative fluorescence and lifetime data on $Tb_x/Gd_{1-x}(hfaa)_4Bu^tNH_3 \cdot H_2O$

Mole fraction Tb^{3+}	$\emptyset_{293}^{a}$	$\tau_{293}/\mu s$	$\frac{\tau_{1.0}}{\tau} \cdot \emptyset_{293}$
1.00	1.00	715	1.00
0.90	0.96	690	0.99
0.80	0.92	665	0.99
0.70	0.86	630	0.98
0.60	0.80	608	0.94
0.50	0.72	574	0.90
0.40	0.66	541	0.87
0.30	0.57	477	0.85
0.20	0.45	404	0.80
0.10	0.33	316	0.75

(a) Normalised to unity for 100% Tb^{3+}

Table 7.9

Relative fluorescence and lifetime data on $Tb_x/Gd_{1-x}(tfaa)_4 \cdot Ph_4As$

Mole fraction Tb^{3+}	$\emptyset_{293}^{a}$	$\tau_{293}/\mu s$	$\frac{\tau_{1.0}}{\tau} \cdot \emptyset_{293}$
1.00	1.00	628	1.00
0.90	0.95	622	0.96
0.80	0.90	620	0.91
0.70	0.84	618	0.85
0.60	0.78	602	0.81
0.50	0.68	596	0.67
0.40	0.59	580	0.60
0.30	0.46	576	0.50
0.20	0.37	552	0.42
0.10	0.20	542	0.23

(a) Normalised to unity for 100% Tb^{3+}

due to the presence of Gd^{3+} that there is significant differences in transfer efficiency between the two systems (see figures 7.8 and 7.9). This may be due to considerable differences in one or more of the rate constants k_1, k_2, k_3 and k_4. The Gd^{3+} dependence of $^5D_4 \longrightarrow {}^7F_j$ Tb^{3+} lifetime provides strong evidence for the involvement of the triplet level in the intermolecular energy transfer in these mixed chelate systems and suggests that k_3 is at least comparable if not greater than k_2. If the assumption is made that the singlet level of the chelates is not involved in energy transfer then the fluorescent intensity of these mixed chelates using a similar model to figure 7.1 may be given as equation 7.6 where c is represented by expression 7.12 (see appendix for derivation).

$$c = \frac{k_4(k_1+k_2+k_3)}{k_3(k_1+k_2-k_4)} \qquad 7.12$$

assuming $k_1 = k_4$

$$c = \frac{k_1(k_1+k_2+k_3)}{k_2k_3} \qquad 7.13$$

This differs from the solution triplet-triplet transfer equations (7.7 and 7.8) in that k_3 replaces k_3M. The best value of c was obtained by computing the F_{293} and $\tau_{1.0}F_{293}/\tau$ data reported in tables 7.8 and 7.9. The results predicted from the best c values were in good agreement with the experimentally observed values.
The $Tb_x/Gd_{1-x}(aa)_4K{\cdot}MeOH$ system was also investigated since the thermal depopulation of the $^5D_4$ Tb^{3+} in the acetylacetonate system should be negligible. An enhancement of fluorescence was observed while the Tb^{3+} lifetime remained constant within experimental error (table 7.10, figure 7.11). Table 7.11 presents the values of c obtained for the various mixed chelate systems in the solid state.

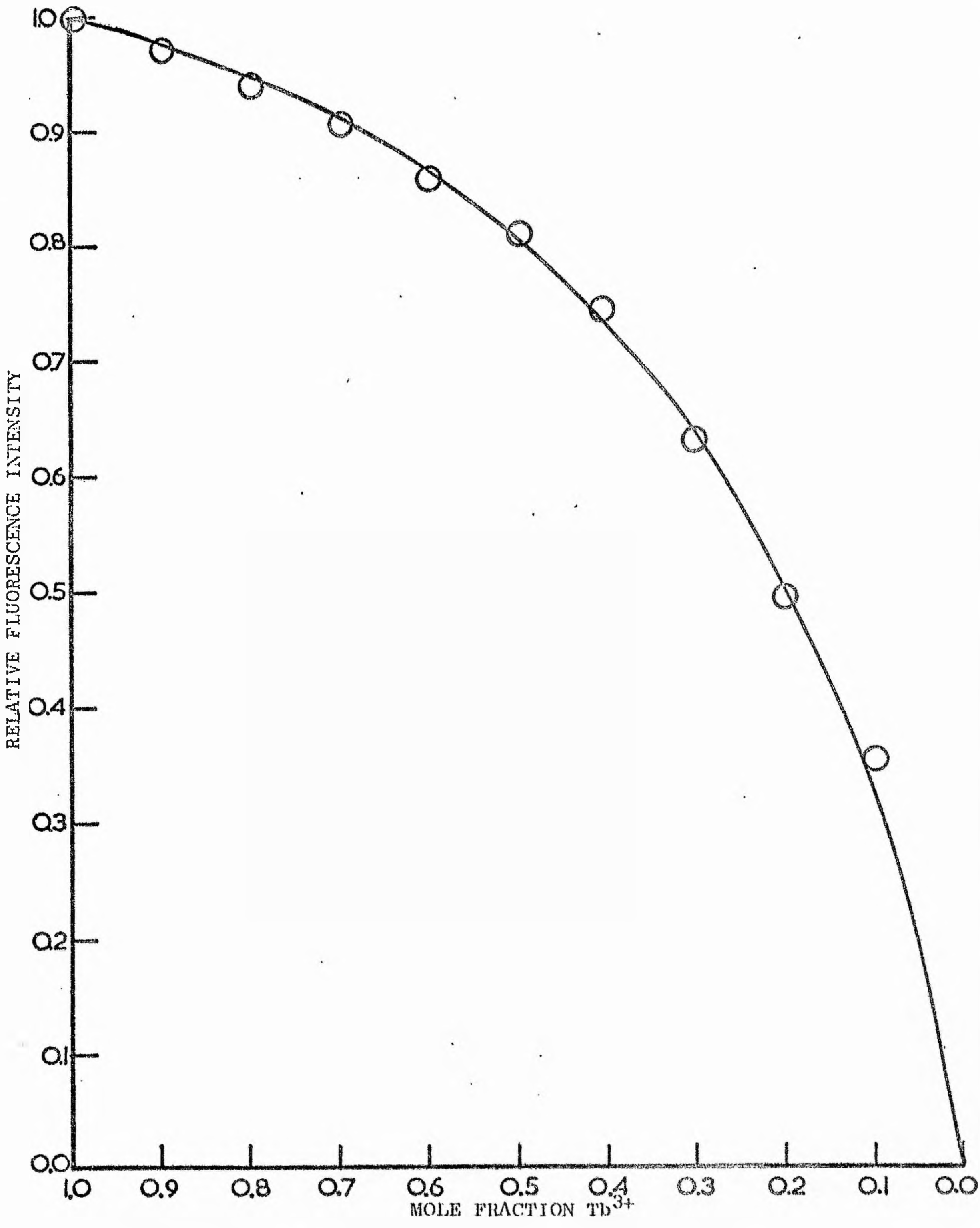

Fig. 7.11 Illustration of Tb^{3+} emission enhancement in solid $Tb/Gd(aa)_3 \cdot K \cdot MeOH$ at 293K

Table 7.10

F_{293} and τ_{293} data on solid Tb/Gd(aa)$_4$K·MeOH

Mole fraction Tb^{3+}	F_{293} [a]	τ_{293}
1.00	1.00	1007 ± 20
0.90	0.96	1006 ± 20
0.80	0.93	1010 ± 20
0.70	0.88	1014 ± 20
0.60	0.85	1002 ± 20
0.50	0.81	990 ± 20
0.40	0.77	1020 ± 20
0.30	0.68	998 ± 20
0.20	0.60	1010 ± 20
0.10	0.45	1000 ± 20

(a) Normalised to unity for 100% Tb^{3+} chelate

Table 7.11

Calculated values for the various mixed Ln^{3+} systems

Mixed chelate system	calculated c value	% standard deviation
Eu/Gd(hfaa)$_4$Bu^{t}NH$_3$·H$_2$O	0.019	± 0.010
Eu/Gd(tfaa)$_4$·Ph$_4$As	0.610	± 0.010
Tb/Gd(hfaa)$_4$Bu^{t}NH$_3$·H$_2$O	0.490	± 0.013
Tb/Gd(hfaa)$_4$Bu^{t}NH$_3$·H$_2$O [a]	0.055	± 0.015
Tb/Gd(tfaa)$_4$·Ph$_4$As	0.662	± 0.012
Tb/Gd(aa)$_4$·K·MeOH	0.199	± 0.003

(a) Corrected for change in lifetime due to the presence of Gd^{3+}

(c) Lanthanide-Lanthanide Transfer

The possibility of lanthanide-lanthanide transfer in the solid state was investigated using Tb$_{0.5}$/Eu$_{0.5}$(hfaa)$_4$·Bu^{t}NH$_3$·H$_2$O and Tb$_{0.5}$/Eu$_{0.5}$(tfaa)$_4$·Ph$_4$As mixed chelates. In these systems both triplet-triplet and lanthanide-lanthanide transfer are possible. The $^5D_1$ and $^5D_0$ Eu^{3+} ion levels are of lower energy than the $^5D_4$ Tb^{3+} level and are therefore potential energy acceptors. Figure 7.11 illustrates the two energy transfer processes. The deactivation routes of the Tb^{3+} and Eu^{3+} resonance levels are omitted.

Quantum yields relative to their respective 100% Ln^{3+} ion

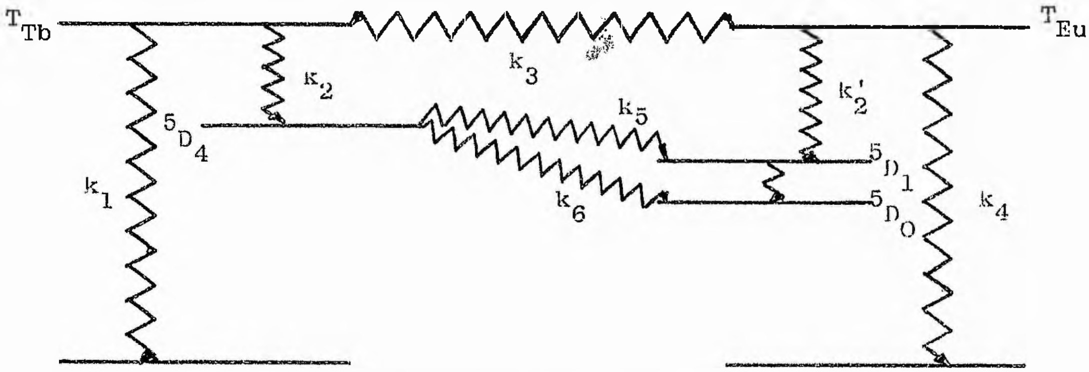

Fig. 7.11   Illustration of both lanthanide-lanthanide and triplet-triplet transfer in mixed chelates

chelates were determined at 293K from the Tb^{3+} and Eu^{3+} emissions in the mixed complexes (table 7.12). In the case of the tfaa mixed chelate the Tb^{3+} emission intensity is ca 22% less than that

Table 7.12

$Tb/Eu(hfaa)_4Bu^tNH_3 \cdot H_2O$				$Tb/Eu(tfaa)_4 \cdot Ph_4As$			
Mole fraction Tb/Eu	F_{293} [a]	F_{293} [b]	τ_{77} [c] /µs	Mole fraction Tb/Eu	F_{293} [a]	F_{293} [b]	τ_{77} [c] /µs
1.0/0.0	1.00	-	1035	1.00/0.0	1.00	-	1164
0.5/0.5	0.08	1.03	854	0.5/0.5	0.39	0.61	1116
0.0/1.0	-	1.00	-	0.0/1.0	-	1.00	-

(a) Tb^{3+} emission normalised to unity for 100% Tb^{3+}

(b) Eu^{3+} emission normalised to unity for 100% Eu^{3+}

(c) Tb^{3+} lifetime

expected for the Tb^{3+} present, while the Eu^{3+} emission intensity is ca 22% greater than that expected for the Eu^{3+} present, suggesting that all the energy lost by the Tb^{3+} has migrated to the Eu^{3+}. However, in the case of hfaa mixed chelate the Tb^{3+} emission intensity is depleted by 84% while the Eu^{3+} emission is enhanced by 106% relative to that expected for the respective Ln^{3+} concentrations. This indicated that at least some of the energy lost from the Tb^{3+} is transferred to the Eu^{3+} by a more efficient route than is possible intramolecularly in the 100% Eu^{3+} complex. Lifetimes of the Tb^{3+} emission in the mixed chelates were determined at 77K where thermal depopulation can be regarded as negligible (table 7.12). It can be concluded from the τ_{77} results in the case of tfaa chelate that ca 4% of the energy reaching the $^5D_4$ level is dissipated by a mechanism which is absent in the 100% Tb chelate. The energy loss in the case of hfaa is more significant, ca 17.5%. It is suggested therefore that this energy loss is caused by lanthanide-lanthanide transfer as triplet-triplet energy transfer would not affect the Tb^{3+} lifetime when thermal depopulation is negligible. Preliminary investigations of Tb/Gd/Eu mixed β-diketoenolates support the existence of lanthanide-lanthanide transfer since the lifetime at 77K of the $^5D_4$ Tb^{3+} level of the mixed chelate approaches that of the 100% Tb chelate as the Gd^{3+} concentration is increased i.e. the Tb^{3+}- Eu^{3+} internuclear distance is increased reducing the probability of Ln-Ln transfer. The relatively poor lanthanide-lanthanide transfer in the case of the tfaa mixed chelate may explain why the energy lost by the Tb^{3+} is, within experimental error, equivalent to that gained by the Eu^{3+}, i.e. all the energy transferred from the Tb^{3+} to the Eu^{3+} in the mixed chelate occurs via the Eu^{3+} triplet. This is certainly not the case for the hfaa mixed chelate and the 17.5% lanthanide-lanthanide transfer observed at 77K may be attributed to the fact that the energy enhancement of the Eu^{3+} is greater than the energy lost by the Tb^{3+} when the values are calculated relative to the 100% Ln^{3+} chelates. The results obtained for the two Tb/Eu mixed chelates are consistent with the $T_{Eu} \rightsquigarrow {}^5D_{1,0}$ rate constant, k_2', being greater than $T_{Tb} \rightsquigarrow {}^5D_4$ rate constant, k_2, since in both cases when considering only triplet-triplet energy transfer there is an enhancement of Eu^{3+} fluorescence.

(d) Discussion

Triplet-triplet and lanthanide-lanthanide energy transfer has been shown to occur in the solid state. The marked differences in the relative quantum yields as a function of Ln^{3+} concentrations indicate that the various rate constants responsible for intra and intermolecular transfer may alter depending on the nature of the β-diketoenolate ligand and/or cation. The lifetime dependence of the ${}^5D_4$ Tb^{3+} level on Gd^{3+} concentration in the mixed Tb/Gd chelates gives further evidence for the involvement of the ligand triplet in energy transfer and suggests that the triplet-triplet transfer rate, k_3, is comparable, at least, with the triplet-Tb^{3+} ion energy transfer process. The significant decrease in ${}^5D_4$ Tb^{3+} lifetime in the case of the Tb/Gd hfaa mixed chelate further suggests that the $T_{Gd} \rightsquigarrow S_0$ rate, k_1, must be comparable or less than k_3. If $k_1 \gg k_3$ then enhancement of Tb^{3+} fluorescence would be expected to be extremely small since the $T_{Tb} \leftrightsquigarrow T_{Gd}$ transition would have a low probability. Investigations using Tb/Eu mixed chelates provide evidence for both triplet-triplet and lanthanide-lanthanide transfer occurring in the solid state. When lanthanide-lanthanide transfer is negligible it was found that the increase in Eu^{3+}

emission could be attributed to the transfer of energy from the Tb^{3+} chelate resulting in a decrease of Tb^{3+} emission. The $^5D_4$ Tb^{3+} lifetime at 293K in the case of the tfaa mixed chelate was experimentally indistinguishable from the value obtained for the 100% Tb^{3+} chelate i.e. 650 μs indicating little, if any, energy is lost via the T_{Eu} level by thermal depopulation of the $^5D_4$ level. It may therefore be assumed that the 22% Eu^{3+} emission enhancement is a direct result of k_2' being greater than k_2. Further, the relative quantum efficiency values of the $Tb_{0.5}/Eu_{0.5}$ tfaa mixed chelate reported in table 7.12 suggest that the k_2'/k_2 ratio is ca 1.6. Assuming the ca 18% lanthanide-lanthanide transfer observed at 77K in the Tb/Eu hfaa mixed chelate is operational at 293K and energy losses from the $^5D_4$ level to the T_{Eu} level is unimportant, then the k_2'/k_2 ratio can be shown to be ca 4.9 since 66% of the Tb^{3+} triplet energy has been transferred to the Eu^{3+} ion in the mixed chelate. Since $k_2' > k_2$ this suggests that energy transfer from the triplet level of the mixed chelate to the Eu^{3+} resonance level occurs via the $T_{Eu} \rightsquigarrow {}^5D_2$ Eu^{3+} transition. The $^5D_2$ Eu^{3+} level lies approximately 1000 cm^{-1} above the $^5D_4$ Tb^{3+} level therefore a more efficient transfer rate from the ligand triplet would be expected because of the smaller T_{Eu} — $^5D_2$ Eu^{3+} energy separation compared to the T_{Tb} — $^5D_4$ energy separation. If, in the case of the hfaa mixed chelate, Tb $\rightsquigarrow$ Eu lanthanide-lanthanide transfer occurs exclusively to the $^5D_1$ Eu^{3+} level then the overall $T_{Eu} \rightsquigarrow {}^5D_1$ transition probability may be assumed to be 0.45 since the ca 18% lanthanide-lanthanide transfer is responsible for a 40% Eu^{3+} enhancement relative to the 100% Eu chelate.

The involvement of the ligand singlet levels in energy transfer has not been considered for the mixed chelated systems investigated. However, since the experimental data obtained for the mixed chelates are in good agreement with the models proposed in figures 7.1 and 7.7 (i.e. equation 7.6 can be used satisfactorily to obtain a value of c using the F_{293} data) this suggests little involvement of the singlet levels in intermolecular transfer. This is in contrast to results obtained for the Eu/Gd$(btfa)_4$pipH system where F_{293} results do not fit the relationship given in equation 7.6[322].

(e) Conclusion

In contrast to the mixed chelate solutions triplet-triplet transfer has been shown to be a significant process in the solid state. Relative quantum efficiency data in solution and in the solid state have supported the transfer mechanisms proposed. $Tb(^5D_4) \rightsquigarrow Eu(^5D_1)$ lanthanide-lanthanide transfer has been suggested as the major inter-lanthanide process occurring in the Tb/Eu mixed chelates in solution and in the solid state. Lanthanide-lanthanide transfer rate constants derived for the various mixed chelate solutions are all considerably lower than the diffusion controlled rate constant and it is concluded that intermolecular energy transfer in solution is relatively inefficient at the concentrations investigated.

Results obtained from investigations of the mixed solid chelates indicates that the various intra- and intermolecular transfer rate constants may be dependent on the nature of the ligand and/or cation. The $T_{Eu} \rightsquigarrow {}^5D_j$ rate constant has been shown to be greater in magnitude than the $T_{Tb} \rightsquigarrow {}^5D_4$ rate constant in the two Tb/Eu mixed chelate systems investigated. These differences in rate constants are consistent with the results obtained from quantum yield investigations in the solid state where it was suggested that differences in the k_2 rate constants could explain the more marked variation in Ø for the Tb chelates (see chapter 5). The good agreement of F_{293} data with equation 7.6 suggests that investigations of mixed chelate systems in the solid state could provide absolute values for the various rate constants expressed in equation 7.13.

Further evidence for 9-coordination in the solid state has been obtained during the preparation of Tb/Gd aa mixed chelates which were characterised as containing one molecule of methanol when recrystallised from that solvent.

APPENDIX I

DERIVATION OF RATE OF THERMAL DEPOPULATION, k(T), FROM $^5D_4$ LEVEL OF Tb^{3+} IN TERMS OF OTHER RATE CONSTANTS (see page 76)

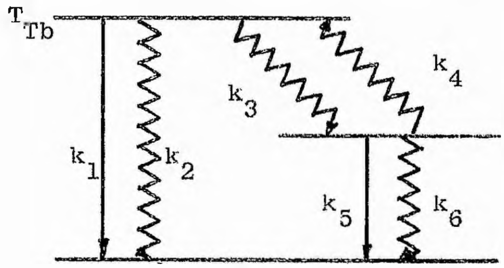

Probability of $T \longrightarrow {}^5D_4 = \dfrac{k_3}{k_1+k_2+k_3} = Pa$ (i)

Probability of ${}^5D_4 \longrightarrow T = \dfrac{k_4}{k_4+k_5+k_6} = Pb$ (ii)

Probability of ${}^5D_4 \longrightarrow {}^7F$(radiative) $= \dfrac{k_5}{k_4+k_5+k_6} = Pc$ (iii)

The probability of $^5D_4$ exicted level giving rise to Tb^{3+} fluorescence, P^*, is then given by the infinite series

$$P^* = Pc + PaPbPc + Pa^2Pb^2Pc + \ldots\ldots\ldots\ldots Pa^nPb^nPc + \ldots\ldots\ldots$$

$$= Pc\,(1 + PaPb + Pa^2Pb^2 + \ldots\ldots\ldots\ldots Pa^nPb^n + \ldots\ldots\ldots\ldots)$$

$$= \frac{Pc}{1-PaPb} \qquad \text{(iv)}$$

By substitution from (i), (ii) and (iii), P^* may be expressed in terms of the rate constants k_1 to k_6. P^* is equivalent to the quantum efficiency of the $^5D_4$ Tb^{3+} level, $\phi_{^5D_4}$.

Thus

$$\phi_{^5D_4} = \frac{k_5(k_1+k_2+k_3)}{(k_1+k_2)(k_4+k_5+k_6) + k_3(k_5+k_6)} \qquad \text{(v)}$$

The quantum efficiency of the Tb^{3+} $^5D_4$ level may also be expressed as:-

$$\phi_{^5D_4} = \frac{k_5}{k_5+k_6+k(T)} \qquad \text{(vi)}$$

where k(T) is the rate constant for loss from the $^5D_4$ to the ground state by a route involving $T \rightsquigarrow S_0$ i.e. by thermal depopulation and subsequent loss directly from the triplet to the ground state.

From (v) and (vi),

$$k(T) = \frac{k_4(k_1+k_2)}{(k_1+k_2+k_3)}$$

APPENDIX II

INTERMOLECULAR ENERGY TRANSFER

Model 1 Intermolecular ligand triplet-triplet transfer between analogous chelates of Tb^{3+} and Gd^{3+} in solution (see page 134)

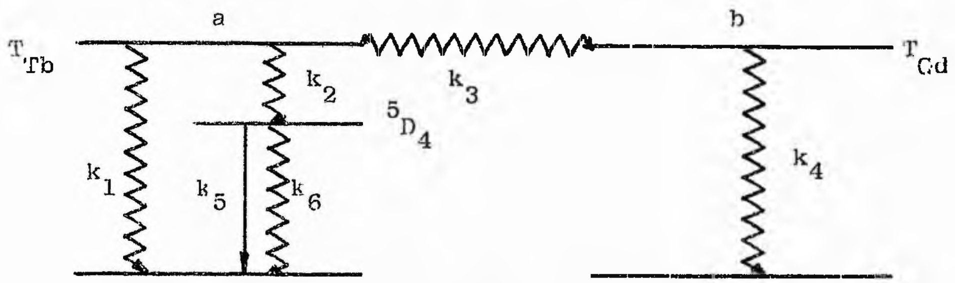

k_1 = Total radiative and non-radiative deactivation rate of ligand triplet state directly to ground state in Tb^{3+} chelate

k_2 = Tb^{3+} ligand triplet to Tb^{3+} $^5D_4$ intramolecular transfer rate constant

k_3 = Bimolecular rate constant for triplet-triplet intermolecular transfer - this is assumed to be independent of the nature of the metal ion

k_4 = Analogous to rate constant k_1 but referring to Gd^{3+} chelate

k_5 = Tb^{3+} $^5D_4 \longrightarrow {}^7F_j$ radiative rate constant

k_6 = Tb^{3+} $^5D_4 \rightsquigarrow {}^7F_j$ non-radiative rate constant

a = Population of excited ligand triplet states in Tb^{3+} chelates

b = Population of excited ligand triplet states in Gd^{3+} chelates

x = $[Tb^{3+}$ chelate$]$

y = $[Gd^{3+}$ chelate$]$

I = Intensity of incident light

$$-\frac{da}{dt} = (k_1+k_2)a + k_3(ay-bx) - xI \qquad \text{(i)}$$

$$-\frac{db}{dt} = k_4b + k_3(bx-ay) - yI \qquad \text{(ii)}$$

Under steady state conditions:-

$$(k_1+k_2+k_3y)a = k_3bx + xI \qquad \text{(iii)}$$

$$(k_4+k_3x)b = k_3ay + yI \qquad \text{(iv)}$$

$$a = \frac{xI(k_3y + k_3x + k_4)}{(k_1+k_2)(k_3x + k_4) + k_3k_4y} \qquad \text{(v)}$$

If the total concentration (x+y) is constant and equal to M, the mole fraction of Tb^{3+} chelate, m = x/M. By substitution:-

$$a = \frac{IMm(k_3M + k_4)}{(k_1+k_2)(k_3Mm+k_4) + k_3k_4M(1-m)} \qquad \text{(vi)}$$

In the case of the pure Tb^{3+} solution, m = 1 and

$$a_{m=1} = a' = \frac{IM}{k_1 + k_2} \qquad \text{(vii)}$$

The Tb^{3+} fluorescence is directly proportional to a since the rate of emission from the $^5D_4$ level = $ak_2[k_5/(k_5+k_6)]$ = constant a. Therefore the Tb^{3+} fluorescence, R, in any solution of total concentration M, relative to unit fluorescence of the pure Tb^{3+} solution is given by:-

$$R = a/a' \qquad \text{(viii)}$$

$$R = \frac{m(k_1+k_2)(k_3M+k_4)}{(k_1+k_2)(k_3Mm+k_4) + k_3k_4M(1-m)} \qquad \text{(ix)}$$

If $k_1=k_4$ then

$$R = \frac{m(k_1+k_2)(k_1+k_3M)}{(k_1+k_2)(k_1+k_3Mm) + k_1k_3M(1-m)} \qquad \text{(x)}$$

By manipulation of (x)

$$R = \frac{1+c}{1+c/m} \qquad \text{(xi)}$$

where $$c = \frac{k_1(k_1+k_2+k_3M)}{k_2k_3M}$$

Model 2 Intermolecular ligand triplet-triplet transfer between analogous Ln^{3+} and Gd^{3+} chelates in the solid state ($Ln^{3+} = Tb^{3+}$ or Eu^{3+}) (see page 146) Compound stoichiometry:- (Ln_m,Gd_{1-m}) chelate

The solid state model may be derived similarly to Model 1 except that k_3 = unimolecular rate constant for triplet-triplet transfer. In the solid state

$$R = \frac{1+c}{1+c/m} \qquad (i)$$

$$\text{where } c = \frac{k_1(k_1+k_2+k_3)}{k_2k_3} \qquad (ii)$$

Model 3 Intermolecular energy transfer between the Tb^{3+} $^5D_4$-level and Ln^{3+} acceptor levels of lanthanide chelates in solution ($Ln^{3+} = Eu^{3+}, Sm^{3+}, Nd^{3+}$) (see page 138)

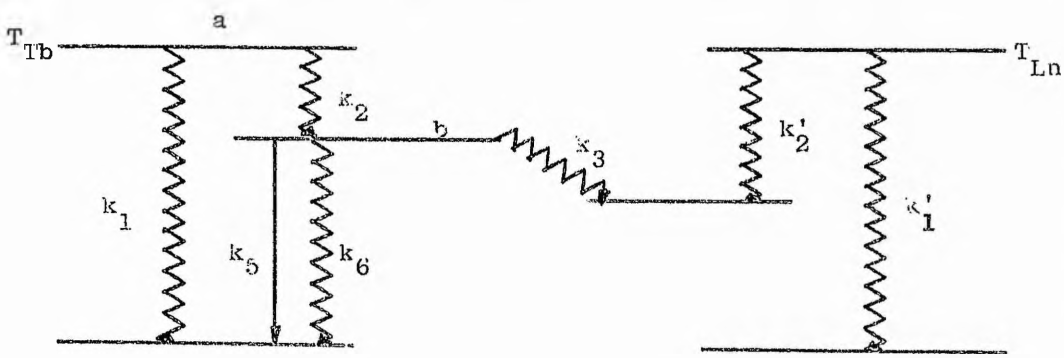

k_1, k_2, k_5 and k_6 are identical to those rate constants given on page 156.

k_1' and k_2' are analogous to k_1 and k_2.

k_3 = Bimolecular rate constant for transfer from the Tb^{3+} $^5D_4$ level to Ln^{3+} acceptor level

a = Tb^{3+} chelate triplet population

b = Tb^{3+} ion $^5D_4$ population

It is assumed that all energy absorbed by ligands reaches the triplet level and that all ligands have identical absorbance.

For solutions of total concentration M and mole fraction m of Tb^{3+} chelate

$$-\frac{da}{dt} = (k_1+k_2)a - IMm \qquad \text{(i)}$$

$$-\frac{db}{dt} = (k_5+k_6)b + k_3b(1-m)M - k_2a \qquad \text{(ii)}$$

Under steady state conditions

$$b = \frac{k_2a}{k_5+k_6+k_3(1-m)M} \quad \text{where} \quad a = \frac{IMm}{(k_1+k_2)} \qquad \text{(iii)}$$

If m = 1 i.e. pure Tb^{3+} solution

$$b_{m=1} = b' = \frac{k_2[IM/(k_1+k_2)]}{(k_5+k_6)} \qquad \text{(iv)}$$

The relative Tb^{3+} fluorescence, R, as previously defined may be written

$$R = b/b' = \frac{m(k_5+k_6)}{k_5+k_6+k_3(1-m)M} \qquad \text{(v)}$$

By manipulation of (v)

$$R = \frac{1+c}{1+c/m} \qquad \text{(vi)}$$

$$\text{where } c = -\left(\frac{(k_5+k_6)}{k_3M} + 1\right) \qquad \text{(vii)}$$

APPENDIX III

PROGRAM SPECTRUM

```
C           PROGRAM SPECTRUM
C           ----------------
C
C
C       THIS PROGRAM CORRECTS SPECTRA FOR CHANGING PHOTOMULTIPLIER
C       SENSITIVITY, AND WILL PLOT THE CORRECTED SPECTRUM VERSUS
C       WAVELENGTH AND/OR WAVENUMBER.  THE INTEGRATED AREA (ON A WAVE-
C       NUMBER SCALE) MAY ALSO BE CALCULATED.  SPECTRUM ALSO ALLOWS:
C       A.  AVERAGING OF SEVERAL SPECTRA TO REDUCE NOISE.
C       B.  SUBTRACTION OF BLANKS TO CORRECT FOR CHANGING BASELINE.
C       C.  PLOTTING OF INSETS TO SHOW MAGNIFIED (OR 1/2 SIZE)
C           SECTIONS OF THE SPECTRUM.
C       D.  STORING OF SPECTRA ON MAGNETIC TAPE.
C
C
C   CONTROL CARDS.
C   --------------
C
C     REQUEST 44PS, BACKGROUND, PLOTTER, PAPER TAPE AND MAG. TAPE
C     'SA0221'  W  ON WHITE CARD.
C       //YOURJOBA   JOB .   A. N. OTHER.    CHEM..
C       //SYS002  ACCESS  XYPTR,PTAPE=
C       //SYSRDR  ACCESS CLOPT(PLOTTER)
C       //SYS007  ACCESS TAPE,2400='SA0221'
C       /*
C       // EXEC XYTRYSPC
C       ( DATA CARDS HERE )
C       /*
C       /&
C     IF NONE OF THE SPECTRA ARE TO BE RECORDED ON MAG. TAPE. THEN
C     REPLACE 4TH CONTROL CARD WITH     //SYS007  ACCESS ION        AND
C     OMIT REQUEST FOR MAG. TAPE ON WHITE CARD.
C     (THE FIRST 2 LETTERS OF JOBNAME SHOULD BE YOUR SIGN ON INITIALS)
C     (IF MORE THAN 1 JOB IS INPUT AT ONE TIME, USE DIFFERENT JOBNAMES.
C      EG.   YOURJOBA, YOURJOBB )
```

```
C
C
C     DATA INPUT.  CARDS.
C     -----------
C
C     1.  NRUN,NTAPE
C           NRUN    FORMAT I2   COLS 1-2.    NO. OF SPECTRA TO BE INPUT.
C           NTAPE   FORMAT I2   COLS 11-12.  NO. OF PAPER TAPES TO BE
C                                            INPUT.
C     2.  NVAL(J)       THESE ARE THE 4 CHARACTER CODES OF THE PAPER TAPES
C                       THAT ARE TO BE USED.  FORMAT FOR EACH IS (A4).
C                       USE COLS 1 TO (NTAPE*4).
C                       ( EACH TAPE SHOULD HAVE A DIFFERENT 4 CHARACTER CODE)
C                       ( CR  IS  MULT PCH 8589 )
C                       ( LF  IS  MULT PCH 8289 )
C                       ( OTHER CHARACTERS ARE AS ON CARD PUNCH. )
C     3.  TITLE.        ( FORMAT 20A4 )
C     4.  A,B,N1,N2,N3,N4,FYL,NPL,LSIGN,NINST,NKODE,AB
C           A   FORMAT F5.0  COLS 1-5.   NM/" FOR WAVELENGTH PLOT.
C                                        A = 0  FOR NO PLOT.
C           B   FORMAT F5.0  COLS 6-10. CM-1/" FOR WAVENUMBER PLOT.
C                                        B = 0  FOR NO PLOT.
C           N1  FORMAT I1    COL 15.     = 1 FOR STORAGE ON MAG. TAPE.
C                                        = 0 FOR NO STORAGE.
C           N2  FORMAT I2    COLS 19-20.  NO. OF SPECTRA TO BE AVERAGED.
C                                        N2 = 0 OR 1  FOR NO AVERAGING.
C           N3  FORMAT I2    COLS 29-30.  NO. OF BLANKS.
C           N4  FORMAT I2    COLS 39-40.  NO. OF INSETS TO BE PLOTTED.
C           FYL FORMAT F4.1  COLS 47-50.  Y-AXIS LENGTH=5.0*FYL".
C                                         Y-AXIS=5.0"  IF FYL=0.0
C           NPL FORMAT I1    COL  60.=0 FOR INCR. WAVELENGTH PLOT.
C                                   =1 FOR DECR. WAVELENGTH PLOT.
C           LSIGN  FORMAT I1  COL65. =1 IF SPEC RECD. RUNNING -VE.
C           NINST  FORMAT I1  COL 70.    =0  FOR MONOSPEX 1000.
C                                        =1  FOR P-E HITACHI.
C           NKODE  FORMAT I3  COLS 73-75.       IF IT IS REQUIRED TO
C                       OVERWRITE A SPECTRUM ALREADY ON MAG. TAPE,
C                       NKODE IS THE CODE OF THE SPECTRUM THAT IS TO
```

```
C                       BE OVERWRITTEN.
C           AP   FORMAT F1.0   COL 80.    =1  FOR AREA CALCULATIONS.
C   5-(4+N4)  N2 AND N3 FOR INSETS. COLS 19-20 AND 29-30 RESPECTIVELY.
C
C
C   DATA INPUT.  TAPE.
C   ------------
C
C   1.    BEGIN EACH PAPER TAPE WITH A 4 CHARACTER CODE (MUST BE THE SAME
C         AS ON 2ND. DATA CARD).  DO NOT FOLLOW WITH  CR LF
C   2.    CODE NUMBER OF SPECTRUM (I3), START OF SPECTRUM (I3) IN NM.,
C         END OF SPECTRUM (I3) IN NM.,,FILTER NO. (I1) .  CR  LF
C         ( MONOSPEX  FILTER NO. =0 FOR NO FILTER, =1 FOR YELLOW FILTER.
C         P-E HITACHI  =0 FOR EMISSION.  =1 FOR EXCITATION. )
C   3.    DIGITALISED SPECTRUM TERMINATED BY  * CR LF
C   4.    REPEAT 3 FOR EACH OF THE AVERAGING AND BLANK SPECTRA.
C   5.      FOR INSETS.  START (I3), END (I3), FILTER NO. (I1), CR LF
C           FOLLOWED BY THE DIGITALISED INSET, TERMINATED  * CR LF.
C           REPEAT 5 FOR EACH INSET.
C   6.    START SECOND SPECTRUM AT 2.
C
C  LABEL ALL TAPES WITH THE JOBNAME AND WITH YOUR NAME.
C  IF MORE THAN 1 TAPE PER JOB, THEN LABEL THE TAPES IN THE ORDER THAT
C  THEY ARE TO BE INPUT (EG.  YOURJOBA(1), YOURJOBA(2) ETC)
C
C
C
      COMMON V(8000),ITIT(20),NFILI(10),FINI(10),START,FIN,WINC,KODE
      COMMON N,N2,N3,N4,NFILB,FACTOR,VI(8000),STARTI(10),WINCI(10)
      COMMON FAINI(10),NI(11),M,MM
      DIMENSION NVAL(20)
      CALL CLOUNS
      NT=0
      READ(5,10)NRUN,NTAPE
   10 FORMAT(I2,8X,I2)
      IF(NRUN.EQ.0)NRUN=99
      IF(NTAPE.EQ.0)NTAPE=1
      READ(5,10)(NVAL(J),J=1,NTAPE)
```

```
101 FORMAT(20A4)
    NVALI=NVAL(1)
    NEXT=2
    DO 999 MMM=1,NRUN
    CALL LOAD('XYTRYAAA')
    IF(MMM.EQ.1)CALL CLFTVL(2,NVALI)
604 IJK=0
    NSS=1
    READ(5,20)ITIT
 20 FORMAT(20A4)
    READ(5,30)A,B,N1,N2,N3,N4,FYL,NPL,LSIGN,NINST,NKODE,AP
 30 FORMAT(2F5.0,4X,I1,3X,I2,8X,I2,8X,I2,6X,F4.1,9X,I1,4X,I1,4X,I1,2X,
   2I3,4X,F1.0)
    ASIGN=1.0
    IF(LSIGN.EQ.1)ASIGN=-1.0
    NAVE=N2
    NBLA=N3
    GG=1.0
    IF(NPL.GT.0)GG=-1.0
    IF(FYL.LT.0.000001) FYL=1.0
    IF(FYL.GT.2.0) FYL=2.0
    NINST=NINST*10
  1 CALL XYREAD(10,NSW,&2,&1,&600)
    READ(5,41)KODE,START,FIN,NFIL
 41 FORMAT(I3,2F3.0,I1)
    NFILA=NFIL
    NFIL=NFIL+NINST
    NFILB=NFIL
    N=0
 40 N=N+1
400 CALL XYREAD(11,NSW,&995,&50,&400)
    READ(5,42)NC,V(N),NR
 42 FORMAT(I2,1X,F6.0,1X,I1)
    NR=NR+1
    G=(10**NR)
    V(N)=V(N)*G/10000.0
    V(N)=V(N)*ASIGN
    GO TO 40
```

Program Spectrum (continued)

```
    2 IF(NEXT.GT.NTAPE)GO TO 997
      NVALI=NVAL(NEXT)
      NEXT=NEXT+1
      CALL CLFTVL(2,NVALI)
      GO TO 1
  600 IF(N2.EQ.0)N2=1
      N2S=N2+N3
  701 IF(N4.EQ.0)GO TO 601
      DO 602 J=1,N4
      READ(5,31)N2,N3
      IF(N2.EQ.0)N2=1
  602 N2S=N2+N3+N2S
  601 N2SK=N2S
      CALL XYSKIP(N2SK,&603)
      GO TO 604
  603 N2S=N2S-N2SK
      N2SK=N2S
      IF(NEXT.GT.NTAPE)GO TO 997
      NVALI=NVAL(NEXT)
      NEXT=NEXT+1
      CALL CLFTVL(2,NVALI)
      CALL XYSKIP(N2SK,&603)
      GO TO 604
  700 IF(N2.EQ.0)N2=1
      N2S=N2+N3
      N4=N4-JJ
      GO TO 701
   50 N=N-1
      G=(N-NSS)
      WINC=(START-FIN)/G
      N2=N2-1
      IF(N2.LT.1)GO TO 54
      MN=N2
      GN=1.0
   58 DO 12 JA=1,MN
      NN=0
      DO 13 J=1,N
      IF(NN.EQ.1)GO TO 55
   11 CALL XYREAD(11,NSW,&401,&55,&11)
      READ(5,42)NC,VA,NR
      NR=NR+1
      G=(10**NR)
      VA=VA*G/10000.0
      VA=VA*ASIGN
      VAA=VA
      V(J)=V(J)+VA*GN
      GO TO 13
  401 IF(J.NE.1)GO TO 995
      IF(NEXT.GT.NTAPE)GO TO 997
      NVALI=NVAL(NEXT)
      NEXT=NEXT+1
      CALL CLFTVL(2,NVALI)
      GO TO 11
   55 V(J)=V(J)+VAA*GN
      NN=1
   13 CONTINUE
      N2SK=1
      IF(NN.EQ.0)CALL XYSKIP(N2SK,&995)
   12 CONTINUE
      G=(N2+1)
      GM=N3
      IF(N3.EQ.0)GM=1.0
      DO 14 J=1,N
   14 V(J)=V(J)*GM/G
   54 IF(N3.EQ.0)GO TO 57
      MN=N3
      GN=-1.0
      N2=N3-1
      N3=0
      GO TO 58
   57 CONTINUE
      VWEE=V(NSS)
      NST=NSS+1
      DO 60 J=NST,N
   60 IF(V(J).LT.VWEE) VWEE=V(J)
      MM=0
```

Program Spectrum (continued)

```
      VBIG=0.0
      DO 70 J=NSS,N
      V(J)=V(J)-VWEE
      L=J-NSS
      X=START-L*WINC
      IF(NFILA.EQ.9) GO TO 70
      CALL CORECT(X,V(J),NFIL)
   70 IF(V(J).GT.VBIG)VBIG=V(J)
      IF(IJK.EQ.1) GO TO 94
      FACTOR=100.0/VBIG
      DO 90 J=1,N
   90 V(J)=V(J)*FACTOR
C
C
      IF(N4.EQ.0)GO TO 91
      NP=N
      NI(1)=1
      N=0
      STARTP=START
      FINP=FIN
      WINCP=WINC
      IJK=1
      DO 92 J=1,NP
   92 VI(J)=V(J)
      DO 93 JJ=1,N4
      READ(5,31)N2,N3
   31 FORMAT(18X,I2,8X,I2)
    6 CALL XYREAD(7,NSW,35,86,8700)
      READ(5,43)START,FIN,NFIL
   43 FORMAT(2F3.0,I1)
      NFILA=NFIL
      NFIL=NFIL+NINST
      NFILI(JJ)=NFIL
      GO TO 40
    5 IF(NEXT.GT.NTAPE)GO TO 997
      NVALI=NVAL(NEXT)
      NEXT=NEXT+1
      CALL CLFTVL(2,NVALI)
      GO TO 6
   94 STARTI(JJ)=START
      WINCI(JJ)=WINC
      FINI(JJ)=FIN
      JJJ=JJ+1
      NI(JJJ)=N+1
      NSS=NI(JJJ)
      N2=IFIX((STARTP-START+WINCP)/WINCP)
      N3=IFIX((STARTP-FIN+WINCP)/WINCP)
      IF(N2.LT.N3) GO TO 99
      IV=N2
      N2=N3
      N3=IV
   99 CONTINUE
      VMAX=VI(N2)
      VMIN=VI(N2)
      DO 95 J=N2,N3
      IF(VMAX.LT.VI(J))VMAX=VI(J)
   95 IF(VMIN.GT.VI(J))VMIN=VI(J)
      FAIN=(95.0-VMIN)/(VMAX-VMIN)
      NFAIN=FAIN
      IF(NFAIN.LT.5)GO TO 96
      NFAIN=(NFAIN/5)*5
   96 FAIN=NFAIN
      IF(NFAIN.EQ.0)FAIN=0.5
      WRITE(6,61)JJ,FAIN
   61 FORMAT(1H ,2X,'THE FACTOR FOR INSET NO. ',I2,'  IS ',F7.1)
      NNN=NI(JJJ)-1
      FAINI(JJ)=FAIN
      FAIN=FAIN*(VMAX-VMIN)/VBIG
      NIJ=NI(JJ)
      DO 98 J=NIJ,NNN
   98 V(J)=(V(J)*FAIN)+5.0
   93 CONTINUE
      NSS=N
      IF(NP.GT.N)NSS=NP
      DO 97 J=1,NSS
      VA=V(J)
```

```
      V(J)=VI(J)
   97 VI(J)=VA
      WINC=WINCP
      START=STARTP
      FIN=FINP
      N=NP
   91 M=MMM
      CALL LOAD('XYTRYBBB')
      CALL XYPLOT(A,B,FYL,GC)
      IF(AP.LT.0.000001) GO TO 530
      CALL XYAREA
  530 CONTINUE
      IF(NI.EQ.0) GO TO 409
      CALL LOAD('XYTRYCCC')
      N2=NAVE
      N3=NPLA
      CALL XYTAPW(NT,NKODE,NI)
C                       INFORMATION PRINT-OUT. ________________________
  409 WRITE(6,410)KODE,ITIT
  410 FORMAT(1H1,'  SPECTRUM NUMBER ',I3,'.      ',20A4)
      WINK=1.0/WINC
      WRITE(6,411)START,FIN,WINC,WINK
  411 FORMAT(1H0,' SPECTRUM FROM ',F4.0,' NM. TO ',F4.0,' NM.. ',2X,
     2'THE WAVELENGTH INCREMENT WAS ',F8.5,' NM. OR ',F9.5,' POINTS PER
     3 NM..')
      NFILA=NFILP/10
      NFIL=NFILP-(10*NFILA)
      WRITE(6,412)N2,N3,NFIL,NFILA,FACTOR
  412 FORMAT(1H0,' AVERAGE OF ',I2,' RUNS, WITH ',I2,' BLANKS, WITH FILT
     2ER NUMBER ',I1,' ON INSTRUMENT NUMBER ',I1,'.  THE NORMALISING FAC
     3TOR WAS ',F10.5)
      WRITE(6,413)N4
  413 FORMAT(1H0,I2,' INSETS WERE INCLUDED.')
      IF(N4.EQ.0) GO TO 419
      WRITE(6,414)
  414 FORMAT(1H0,'INSET NO.    START     FINISH    INCREMENT    FACTOR
     2 INSTRUMENT NO.    FILTER NO.')
      DO 415 J=1,N4
```

```
      NFILA=NFILI(J)/10
      NFIL=NFILI(J)-10*NFILA
  415 WRITE(6,416)J,STARTI(J),FINI(J),WINCI(J),FAINI(J),NFILA,NFIL
  416 FORMAT(1H ,3X,I2,8X,F4.0,5X,F4.0,6X,F7.5,6X,F7.1,10X,I1,15X,I1)
  419 CONTINUE
      IF(A.LT.0.000001) GO TO 440
      WRITE(6,430)
  430 FORMAT(1H0,'THE WAVELENGTH SPECTRUM HAS BEEN PLOTTED.')
      WRITE(6,431)A
  431 FORMAT(1H ,'THE SCALE IS ',F4.0,' NM. PER INCH.')
  440 IF(B.LT.0.000001) GO TO 460
      WRITE(6,450)
  450 FORMAT(1H0,'THE WAVENUMBER SPECTRUM HAS BEEN PLOTTED.')
      WRITE(6,451)B
  451 FORMAT(1H ,'THE SCALE IS ',F4.0,' CM-1 PER INCH.')
  460 CONTINUE
      IF(N1.EQ.0) GO TO 459
      WRITE(6,452)
  452 FORMAT(1H0,' THE SPECTRUM HAS BEEN STORED ON MAGNETIC TAPE.')
      IF(NKODE.EQ.0)GO TO 459
      WRITE(6,490)NKODE
  490 FORMAT(1H0,' THE SPECTRUM CODED ',I3,' ON MAGNETIC TAPE HAS BEEN O
     2VERWRITTEN.')
  459 CONTINUE
  999 CONTINUE
      GO TO 998
  995 WRITE(6,461)
  461 FORMAT(1H0,' THE END OF A PAPER TAPE WAS REACHED WITHOUT ANY TERMI
     1NATION OF THE DATA SET.')
  997 CONTINUE
      CALL LOAD('XYTRYOOO')
  998 IF(NT.NE.1)GO TO 996
      CALL XYJCLC(7,2,0)
  996 CONTINUE
      STOP
      END
```

Program Spectrum (continued)

```
      SUBROUTINE CORECT(W,Y,NF)
      DIMENSION C(74)
      COMMON VXCCS(16091),M,MM
      IF (MM.NE.0) GO TO 1
      IF(NF.GT.9) GO TO 4
      IF (NF-1)2,3,3
    2 C(1)=0.365
      C(2)=0.365
      C(3)=0.365
      C(4)=0.365
      C(5)=0.372
      C(6)=0.401
      C(7)=0.444
      C(8)=0.460
      C(9)=0.478
      C(10)=0.501
      C(11)=0.537
      C(12)=0.594
      C(13)=0.658
      C(14)=0.760
      C(15)=0.881
      C(16)=1.000
      C(17)=1.196
      C(18)=1.527
      C(19)=1.761
      C(20)=2.334
      C(21)=4.201
      C(22)=7.473
      C(23)=12.156
      C(24)=18.807
      C(25)=28.156
      C(26)=42.663
      C(27)=69.239
      C(28)=0.0
      C(29)=0.0
      WMIN=420.0
      WMAX=660.0
      WRITE(6,60)
   60 FORMAT(1H ,'  SPECTRUM FROM MONOSPEX 1000.    NO FILTER.')
      GO TO 10
    3 C(1)=0.0
      C(2)=0.0
      C(3)=0.0
      C(4)=39.531
      C(5)=6.974
      C(6)=1.984
      C(7)=0.731
      C(8)=0.519
      C(9)=0.469
      C(10)=0.482
      C(11)=0.511
      C(12)=0.565
      C(13)=0.677
      C(14)=0.721
      C(15)=0.839
      C(16)=1.000
      C(17)=1.121
      C(18)=1.450
      C(19)=1.419
      C(20)=2.012
      C(21)=3.258
      C(22)=5.523
      C(23)=9.051
      C(24)=13.543
      C(25)=19.940
      C(26)=32.204
      C(27)=49.190
      C(28)=73.657
      C(29)=117.308
      WRITE(6,61)
   61 FORMAT(1H ,'  SPECTRUM FROM MONOSPEX 1000.    YELLOW FILTER.')
   10 WR=400.0
      WS=10.0
      WMIN=430.0
      WMAX=680.0
      GO TO 1
```

Program Spectrum (continued)

```
    4 IF(NF-11)20,21,21
   20 C(1)=0.71
      C(2)=2.46
      C(3)=0.96
      C(4)=0.26
      C(5)=0.32
      C(6)=0.41
      C(7)=0.52
      C(8)=0.59
      C(9)=0.71
      C(10)=0.88
      C(11)=1.00
      C(12)=1.11
      C(13)=1.24
      C(14)=1.44
      C(15)=1.57
      C(16)=1.78
      C(17)=2.00
      C(18)=2.24
      C(19)=2.54
      C(20)=2.80
      C(21)=3.15
      C(22)=3.55
      C(23)=4.08
      C(24)=4.92
      C(25)=5.76
      C(26)=7.10
      C(27)=8.99
      C(28)=12.11
      C(29)=13.56
      C(30)=16.59
      C(31)=24.12
      C(32)=46.68
      C(33)=93.59
      C(34)=144.38
      C(35)=272.04
      C(36)=407.69
      C(37)=593.30
      C(38)=906.04
      C(39)=1512.20
      C(40)=2283.85
      C(41)=4518.67
      C(42)=8342.22
      C(43)=13409.03
      C(44)=24609.44
      C(45)=42605.15
      C(46)=45112.66
      WB=300.0
      WS=10.0
      WMIN=300.0
      WMAX=750.0
      WRITE(6,62)
   62 FORMAT(1H ,'  EMISSION SPECTRUM FROM P-E HITACHI.')
      GO TO 1
   21 C(1)=5.000
      C(2)=4.000
      C(3)=3.333
      C(4)=2.000
      C(5)=1.820
      C(6)=1.430
      C(7)=1.180
      C(8)=0.950
      C(9)=0.710
      C(10)=0.590
      C(11)=0.500
      C(12)=0.420
      C(13)=0.351
      C(14)=0.294
      C(15)=0.250
      C(16)=0.213
      C(17)=0.182
      C(18)=0.156
      C(19)=0.134
      C(20)=0.112
      C(21)=0.096
      C(22)=0.081
```

Program Spectrum (continued)

```
C(23)=C.C69
C(24)=0.061
C(25)=C.C53
C(26)=C.C47
C(27)=0.042
C(28)=0.038
C(29)=C.C35
C(30)=C.033
C(31)=0.031
C(32)=C.C29
C(33)=C.C27
C(34)=0.026
C(35)=C.C27
C(36)=C.C27
C(37)=0.026
C(38)=0.027
C(39)=C.C29
C(40)=0.027
C(41)=0.029
C(42)=C.C26
C(43)=0.C26
C(44)=0.023
C(45)=C.C21
C(46)=C.C18
C(47)=0.016
C(48)=0.012
C(49)=C.C14
C(50)=0.017
C(51)=0.015
C(52)=C.C17
C(53)=C.C14
C(54)=0.016
C(55)=C.C16
C(56)=0.C16
C(57)=0.016
C(58)=0.015
C(59)=C.C16
C(60)=0.015
```

```
      C(61)=C.C15
      C(62)=0.015
      C(63)=0.015
      C(64)=C.C16
      C(65)=C.C15
      C(66)=0.015
      C(67)=C.C15
      C(68)=C.C15
      C(69)=0.015
      C(70)=0.016
      C(71)=C.C17
      C(72)=0.018
      C(73)=0.019
      C(74)=C.C2C
      WB=235.C
      WS=5.0
      WMIN=235.C
      WMAX=6CC.C
      WRITE(6,63)
   63 FORMAT(1H ,'  EXCITATICN SPECTRUM FROM P-E HITACHI.')
    1 CONTINUE
      MM=MM+1
      IF(W.GT.WMAX)GC TC 700
      IF(W.LT.WMIN)GC TC 7C1
      K=(1.0+((W-WB)/WS))
      A=W-WB+WS-K*WS
      COR=C(K)+A*(C(K+1)-C(K))/WS
      Y=Y*COR
      RETURN
  7CO WRITE(6,600)W,WMAX
  6CC FORMAT(1H ,' THE WAVELENGTH ',F8.4,' IS CREATER THAN THE MAXIMUM A
     2LLOWED = ',F5.1)
      Y=0.0
      RETURN
  7O1 WRITE(6,6C1)W,WMIN
  6O1 FORMAT(1H ,' THE WAVELENGTH ',F8.4,' IS LESS THAN THE MINIMUM ALLC
     2WED = ',F5.1)
      Y=C.C
```

```
      RETURN
      END
```

```
      SUBROUTINE XYREAD(N,NSW,*,*,*)
C         TAPE READING SUBROUTINE , XYREAD,C.R.S.DEAN,W.C.COVELL
      INTEGER CARD(80),LF/ZCA404040/,CR/Z0D404040/,AST/Z5C404040/,
     1F9/ZF9404040/,MM/0/,M/1/,IB/0/
      LOGICAL*1 LCARD(320),RCARD(80)
      EQUIVALENCE (LCARD(1),CARD(1))
      NSW=0
    1 CALL CLEADT(2,LEN,CARD,IND,LF)
      MM=MM+1
C
C         IF END OF TAPE (IND=0) RETURN 1
C
      IF(IND.EQ.0) RETURN 1
      NN=N+2
      IF(LEN.NE.NN)GO TO 2
      CALL VALID(CARD,N,IVAL)
      IF(IVAL.EQ.1)GO TO 3
      IF=NN
      JSUM=1
      DO 11 J=1,N
      RCARD(J)=LCARD(JSUM)
   11 JSUM=JSUM+4
      CALL COREIO(RCARD,N)
C
C         NO ERRORS DETECTED , NORMAL RETURN
C
      RETURN
C
C         CHECK CARD FOR ERRORS OR TERMINATION
C
    2 IF(CARD(1).EQ.F9)GO TO 5
      DO 12 J=1,LEN
      IF(CARD(J).NE.AST)GO TO 12
      IF(CARD(J+1).EQ.CR)GO TO 5
   12 CONTINUE
    3 WRITE(6,60)MM,M
   60 FORMAT(1H1,' DATA MISTAKE AT CALL NO. ',I5,' IN DATA SET NO. ',
     2I3,'.',/)
```

```
      JJ=4*LEN
      WRITE(6,61) LEN,NN,(LCARD(J),J=1,JJ,4)
   61 FORMAT(1H ,'FOUND ',I2,'  SET ',I2,4X,100A1/)
      IF(NN.NE.IP)GO TO 6
      WRITE(6,62)
   62 FORMAT(1H ,' THE PREVIOUS LINE OF DATA HAS BEEN SUBSTITUTED.')
      NSW=1
      CALL COREIO(RCARD,N)
      RETURN
C
C        END OF RUN , RESET COUNTERS. RETURN 2
C
    5 N=N+1
      NN=0
      IP=0
      RETURN 2
C
C         UNRECOVERABLE MISTAKE.     RETURN 3.
C
    6 WRITE(6,63)
   63 FORMAT(1H ,' MISTAKE CANNOT BE RECOVERED.')
      RETURN 3
C
C      XYSKIP READS FROM TAPE UNTIL N END OF DATA SETS HAVE BEEN READ.
C
      ENTRY XYSKIP(N,*)
      DO 70 JJ=1,N
      DO 7 J=1,10000
      CALL CLEADT(2,LEN,CARD,IND,LF)
C
C         IF END OF TAPE (IND=0) RETURN 1
C
      IF(IND.EQ.0)GO TO 50
      IF(CARD(1).EQ.F9) GO TO 19
      DO 20 J=1,LEN
      IF(CARD(J).NE.AST) GO TO 20
      IF(CARD(J+1).EQ.CR) GO TO 19
   20 CONTINUE
```

Program Spectrum (continued)

```
  7 CONTINUE
 19 M=M+1
 70 CONTINUE
    MM=0
    IP=0
    RETURN
 50 N=JJ-1
    RETURN 1
    END
```

```
      SUBROUTINE XYPLOT(A,B,FYL,GC)
      COMMON V(8000),ITIT(20),NFILI(10),FINI(10),START,FIN,WINC,KODE
      COMMON N,N2,N3,N4,NFILE,FACTOR,VI(8000),STARTI(10),WINCI(10)
      COMMON FAINI(10),AI(11),M,MM
      YMIN=0.0
      YMAX=100.0
      YL=5.0*FYL
      YD=10.0
C
      IF(A.LT.0.000001) GO TO 300
C                                     WAVELENGTH PLOT STARTS. ____________
      NST=(START/A)
      NFI=(FIN/A)
      IF(FIN.GT.START)GO TO 201
  200 IMAX=NST
      IMIN=NFI
      G=NST
      G=(START/A)-G
      IF(G.GT.0.05)IMAX=IMAX+1
      GO TO 202
  201 IMAX=NFI
      IMIN=NST
      G=NFI
      G=(FIN/A)-G
      IF(G.GT.0.05)IMAX=IMAX+1
  202 XL=IMAX-IMIN
      INI=IMAX
      INF=IMIN
      IF(GC.GT.0.0) GO TO 206
      NST=IMIN
      IMIN=IMAX
      IMAX=NST
  206 XMAX=IMAX*A
      XMIN=IMIN*A
      ZA=XMIN+A*GG
      ZF=XMIN-2.0*A*GG
      XD=GG
      IF(A.GT.10.0) XD=A*0.1*GG
```

Program Spectrum (continued)

```
      IX=A
C
      CALL PLOT(1,XMIN,XMAX,XL,XD,YMIN,YMAX,YL,YD)
      CALL PLOT(99)
C
      DO 210 I=IWE,IEI
      IIX=I*IX
      XX=IIX
      G=-2.5/FYL
      CALL PLOT(90,XX,0.0)
      CALL PLOT(90,XX,G)
      CALL PLOT(99)
      XX=XX-0.1312*A*CG
      G=-5.0/FYL
      CALL PLOT(91,XX,G)
      WRITE(3,205)IIX
  205 FORMAT(I3,100X)
      CALL CHAR(0.1,10)
  210 CALL PLOT(99)
C
      G=-10.0/FYL
      CALL PLOT(91,ZA,G)
      WRITE(3,220)
  220 FORMAT(15HWAVELENGTH (NM),100X)
      CALL CHAR(0.1,10)
      CALL PLOT(99)
C
      DO 240 K=10,110,10
      IY=K-10
      YY=IY
      CALL PLOT(91,ZB,YY)
      WRITE(3,230)IY
  230 FORMAT(18X,I3,100X)
  240 CALL CHAR(0.1,10)
      CALL PLOT(99)
      ZB=XMIN-0.6*A*CG
      CALL PLOT(91,ZB,35.0)
      WRITE(3,231)
  231 FORMAT(19HRELATIVE INTENSITY.,100X)
      CALL CHAR(0.1,1)
      CALL PLOT(99)
C
      G=100.0+7.5/FYL
      CALL PLOT(91,ZA,G)
      WRITE(3,250)KODE
  250 FORMAT(16HSPECTRUM NUMBER ,I3,100X)
      CALL CHAR(0.1,10)
      CALL PLOT(99)
      G=100.0+12.5/FYL
      CALL PLOT(91,XMIN,G)
      WRITE(3,251)ITIT
  251 FORMAT(20A4,100X)
      CALL CHAR(0.1,10)
      CALL PLOT(99)
C
      DO 260 J=1,N
      U=J
      W=START-(U-1.0)*WINC
  260 CALL PLOT(90,W,V(J))
      CALL PLOT(99)
      IF(N4.EQ.0)GO TO 261
      DO 262 JJ=1,N4
      JJJ=JJ+1
      NSS=NI(JJJ)-1
      NST=NI(JJ)
      DO 263 J=NST,NSS
      U=J-NI(JJ)
      W=STARTI(JJ)-U*WINCI(JJ)
  263 CALL PLOT(90,W,VI(J))
      CALL PLOT(99)
      U=(NSS-NST)
      U=U/2.0
      ZD=STARTI(JJ)-U*WINCI(JJ)-0.4*A*CG
      G=100.0+2.5/FYL
      CALL PLOT(91,ZD,G)
      WRITE(3,264)FAINT(JJ)
```

```
  264 FORMAT(1HX.F7.1,100X)
      CALL CHAR(C.1,10)
  262 CALL PLOT(99)
  261 CALL PLOT(7)
C                          WAVELENGTH PLOT FINISHES. ___________________
  300 IF(B.LT.0.000001) GO TO 400
C                                WAVENUMBER PLOT STARTS. ______________
      XST=(10.0**7.0)/START
      XFI=(10.0**7.0)/FIN
      NST=(XST/B)
      NFI=(XFI/B)
      IF(XFI.GT.XST) GO TO 301
      IMIN=NFI
      IMAX=NST
      G=NST
      G=(XST/B)-G
      IF(G.GT.0.05)IMAX=IMAX+1
      GO TO 302
  301 IMIN=NST
      IMAX=NFI
      G=NFI
      G=(XFI/B)-G
      IF(G.GT.0.05)IMAX=IMAX+1
  302 XL=IMAX-IMIN
      IBI=IMAX
      IWE=IMIN
      IF(GG.LT.0.0) GO TO 306
      NST=IMIN
      IMIN=IMAX
      IMAX=NST
  306 XMAX=IMAX*B
      XMIN=IMIN*B
      ZA=XMIN-B*CC
      ZB=XMIN+2.0*B*GG
      XD=-B*0.1*GG
      IX= B
C
      CALL PLOT(1,XMIN,XMAX,XL,XD,YMIN,YMAX,YL,YD)
```

Program Spectrum (continued)

```
      CALL PLOT(99)
      DO 320 I=IWE,IPI
      XX=(I*IX)
      G=-2.5/FYL
      CALL PLOT(90,XX,0.0)
      CALL PLOT(90,XX,G)
      CALL PLOT(99)
      XY=XX+0.2087*P*GG
      G=-5.0/FYL
      CALL PLOT(91,XY,G)
      XX=XX/1000.0
      WRITE(3,310)XX
  310 FORMAT(F5.2,100X)
      CALL CHAR(0.1,10)
  320 CALL PLOT(99)
C
      G=-10.0/FYL
      CALL PLOT(91,ZA,G)
      WRITE(3,330)
  330 FORMAT(24HWAVENUMBER (CM-1 X 10-3),100X)
      CALL CHAR(0.1,10)
      CALL PLOT(99)
C
      DO 350 K=10,110,10
      IY=K-10
      YY=IY
      CALL PLOT(91,ZB,YY)
      WRITE(3,340)IY
  340 FORMAT(18X,I3,100X)
  350 CALL CHAR(0.1,10)
      CALL PLOT(99)
      ZB=XMIN+0.6*P*GG
      CALL PLOT(91,ZB,35.0)
      WRITE(3,231)
      CALL CHAR(0.1,1)
      CALL PLOT(99)
C
      G=100.0+7.5/FYL
      CALL PLOT(91,ZA,G)
      WRITE(3,360)KODE
  360 FORMAT(16HSPECTRUM NUMBER ,I3,100X)
      CALL CHAR(0.1,10)
      CALL PLOT(99)
      G=100.0+12.5/FYL
      CALL PLOT(91,XMIN,G)
      WRITE(3,251)ITIT
      CALL CHAR(0.1,10)
      CALL PLOT(99)
C
      DO 370 J=1,N
      U=J
      W=START-(U-1.0)*WINC
      WN=(10.0**7.0)/W
  370 CALL PLOT(90,WN,V(J))
      CALL PLOT(99)
      IF(N4.EQ.0)GO TO 371
      DO 372 JJ=1,N4
      JJJ=JJ+1
      NSS=NI(JJJ)-1
      NST=NI(JJ)
      DO 373 J=NST,NSS
      U=J-NI(JJ)
      W=STARTI(JJ)-U*WINCI(JJ)
      WN=(10.0**7.0)/W
  373 CALL PLOT(90,WN,VI(J))
      CALL PLOT(99)
      U=(NSS-NST)
      U=U/2.0
      ZD=STARTI(JJ)-U*WINCI(JJ)
      ZD=(10.0**7.0)/ZD
      ZD=ZD+0.4*P*GG
      G=100.0+2.5/FYL
      CALL PLOT(91,ZD,G)
      WRITE(3,375)FAINI(JJ)
  375 FORMAT(1HX,F7.1,100X)
      CALL CHAR(0.1,10)
```

```
  372 CALL PLOT(99)
  371 CALL PLOT(7)
C                                      WAVENUMBER PLOT FINISHED.
  400 CONTINUE
      RETURN
      END
```

Program Spectrum (continued)

```
      SUBROUTINE XYAREA
      COMMON V(8000),ITIT(20),NFILI(10),FINI(10),START,FIN,WINC,KODE
      COMMON N,N2,N3,N4,NFILB,FACTOR,VI(8000),STARTI(10),WINCI(10)
      COMMON FAINI(10),NI(11),M,MM
      DIMENSION XAREA(6),NAREA(6),NW(6),NV(6)
      WRITE(6,484)KODE,ITIT
  484 FORMAT(1H1,'SPECTRUM NUMBER ',I3,5X,20A4,//)
      WRITE(6,485)
  485 FORMAT(1H ,' A   INTEN  AREA',5('        A   INTEN  AREA'))
      MM=0
      AREA=0.0
      K=0
      W=START
      DO 520 J=1,N
      K=K+1
      U=J
      IF (J.EQ.1) GO TO 490
      W2=W
      W=START-(U-1.0)*WINC
      W1=(10.0**7.0)*((1.0/W2)-(1.0/W))
      W1=ABS(W1)
      AREA=AREA+((W1*0.5*(V(J)+V(J-1)))/FACTOR)
      XAREA(K)=AREA/10.0
      NAREA(K)=IFIX(XAREA(K))
      IF(XAREA(K).GT.999.9) MM=1
      GO TO 500
  490 NAREA(1)=0.0
      XAREA(1)=0.0
  500 NW(K)=W*10.0
      NV(K)=V(J)*100.0
      IF(K.LT.6) GO TO 520
      IF(MM.EQ.0) GO TO 511
      WRITE(6,510)(NW(K),NV(K),NAREA(K),K=1,6)
  510 FORMAT(1H ,I4,1X,I5,1X,I5,5(6X,I4,1X,I5,1X,I5))
      K=0
      GO TO 520
  511 WRITE(6,512)(NW(K),NV(K),XAREA(K),K=1,6)
  512 FORMAT(1H ,I4,1X,I5,1X,F5.1,5(6X,I4,1X,I5,1X,F5.1))
```

Program Spectrum (continued)

```
      K=0
  520 CONTINUE
      RETURN
      END
```

```
      SUBROUTINE XYJCLO(N,M,L)
      CALL JCLOSE(N,M,L)
      RETURN
      END
```

```
      SUBROUTINE XYTAPW(NT,NKODE,NI)
      COMMON V(8000),ITIT(20),NFILI(10),FINI(10),START,FIN,WINC,KODE
      COMMON N,N2,N3,N4,NFILB,FACTOR,VI(8000),STARTI(10),WINCI(10)
      COMMON FAINI(10),NI(11),M,MM
      DIMENSION P(1000),IP(1000)
      DIMENSION NCAR(1000)
      EQUIVALENCE (P(1),IP(1))
      IF(NT.EQ.1) GO TO 51
      NT=1
      CALL JOPEN(7,0,0)
   77 CALL JPNTR(7,1000,&78,&22)
      GO TO 77
   78 CALL JREAD(7,NCAR,4000,&76,&22)
      CALL JCLOSE(7,0,0)
      CALL JOPEN(7,0,1)
      GO TO 151
   51 CALL JPNTR(7,-1,&76,&22)
      CALL JCLOSE(7,0,2)
      CALL JOPEN(7,0,0)
      GO TO 78
  151 NBINS=0
      IF(N4.EQ.0)GO TO 70
      NBRUN=N4+1
      NBINS=(NI(NBRUN)/1000)+1
   70 NBRUN=(N/1000)+1
      NBLOC=NBRUN+NBINS
      NC=NCAR(1)
      DO 75 J=1,NC
      JJ=J+1
      IF(KODE.EQ.NCAR(JJ))GO TO 74
   75 CONTINUE
      IF(NKODE.EQ.0)GO TO 73
      DO 72 J=1,NC
      JJ=J+1
      IF(NKODE.EQ.NCAR(JJ))GO TO 71
   72 CONTINUE
      WRITE(6,64)NKODE
   64 FORMAT(1H ,' THE CODE ',I3,' HAS NOT PREVIOUSLY BEEN USED.  CONSUL
```

Program Spectrum (continued)

```
  2I SPECLIST.')
   NKODE=0
   GO TO 73
74 IF(NKODE.EQ.KODE) GO TO 71
   WRITE(6,62)KODE
62 FORMAT(1H ,' THE CODE ',I3,' HAS ALREADY BEEN USED - CONSULT SPECL
  2IST AND TRY ANOTHER CODE.')
   NI=0
   RETURN
71 CALL JCLOSE(7,1,2)
   CALL JOPEN(7,1,0)
83 CALL JREAD(7,B,4000,&76,&2)
   IF(IB(1).EQ.NKODE)GO TO 81
   NO=IB(92)
   CALL JPNTR(7,NO,&76,&22)
   GO TO 83
81 NO=IB(92)
   IF(NBLOC.GT.NO)GO TO 84
   NOAR(JJ)=KODE
   CALL JCLOSE(7,0,0)
   CALL JOPEN(7,0,1)
   CALL JPNTR(7,-1,&95,&22)
   GO TO 85
73 CALL JPNTR(7,-2,&86,&22)
86 NOAR(1)=NOAR(1)+1
   J=NOAR(1)+1
   NOAR(J)=KODE
85 IB(1)=KODE
   DO 10 J=1,20
   JJ=J+1
10 IB(JJ)=ITIT(J)
   IB(22)=N
   B(23)=START
   B(24)=FIN
   B(25)=WINC
   IB(26)=NFIL3
   IB(27)=N2
   IB(28)=N3
```

Program Spectrum (continued)

```
      P(29)=FACTOR
      IB(30)=N4
      DO 11 J=1,11
      JJ=30+J
   11 IB(JJ)=NI(J)
      DO 12 J=1,10
      JJ=41+J
   12 P(JJ)=STARTI(J)
      DO 13 J=1,10
      JJ=51+J
   13 B(JJ)=FINI(J)
      DO 14 J=1,10
      JJ=61+J
   14 P(JJ)=WINCI(J)
      DO 15 J=1,10
      JJ=71+J
   15 P(JJ)=FAINI(J)
      DO 16 J=1,10
      JJ=81+J
   16 IB(JJ)=NFILI(J)
      IB(92)=NBLOC
      IB(93)=NBRUN
      IB(94)=NBINS
      CALL JWRITE(7,B,4000,830,831)
      DO 40 JJ=1,NBRUN
      DO 41 J=1,1000
      JJJ=(JJ-1)*1000+J
   41 B(J)=V(JJJ)
   40 CALL JWRITE(7,B,4000,830,831)
      IF(NBINS.EQ.0)GO TO 87
      DO 42 JJ=1,NBINS
      DO 43 J=1,1000
      JJJ=(JJ-1)*1000+J
   43 B(J)=VI(JJJ)
   42 CALL JWRITE(7,B,4000,830,831)
   87 CONTINUE
      IF(NKOOF.EQ.0)GO TO 90
      CALL JCLOSE(7,0,2)
```

```
      CALL JOPEN(7,0,0)
  101 CALL JCNTR(7,1000,&100,&22)
      GO TO 101
  100 CALL JCLOSE(7,0,0)
      CALL JOPEN(7,0,1)
      GO TO 110
   90 CALL JWEOF(7,&30,&31)
  110 CALL JWRITE(7,NCAR,4000,&30,&31)
      RETURN
   30 WRITE(6,68)
   68 FORMAT(1H ,' EOF ENCOUNTERED.')
      GO TO 201
   31 WRITE(6,69)
   69 FORMAT(1H ,' ERROR IN CALLING SEQUENCE - 3.')
      GO TO 201
   84 WRITE(6,160)NKODE,KODE
  160 FORMAT(1H0,' THE RECORDED SPECTRUM ',I3,' DOES NOT HAVE SUFFICIENT
     2 BLOCKS TO STORE THE INPUT SPECTRUM ',I3,'.')
      GO TO 200
    2 WRITE(6,166)
  166 FORMAT(1H ,' ERROR IN CALLING SEQUENCE - 2')
      GO TO 200
   76 WRITE(6,161)
  161 FORMAT(1H0,' END OF FILE ENCOUNTERED.')
  200 CALL JCLOSE(7,1,0)
      N1=0
      NT=0
      RETURN
   22 WRITE(6,60)
   60 FORMAT(1H ,' ERROR IN CALLING SEQUENCE - 1')
  201 CALL JCLOSE(7,1,2)
      N1=0
      NT=0
      RETURN
      END
```

Program Spectrum (continued)

```
/*
//  EXEC PL360
 GLOBAL PROCEDURE VALID(R14) ; BEGIN STM (R14,R12,B13(12)) ; BEGIN
   GLOBAL DATA VALIDAT BASE R10 ; ARRAY 128 CHARACTER TTABLE
      = (32("¬")," ",10("¬"),"¬ ¬¬",10(" "),70("¬"))  ;
   BYTE CHAR ;
   DUMMY BASE R2 ; ARRAY 320 BYTE CARD ;
   R2 := B1 ; R3 := B1(4) := R3 - 1 SHLA 2 ; R4 := B1(8) ;
   R5 - R5 => R4 ;
         FOR R1 :=  0  STEP 4 UNTIL R3 DO
   BEGIN R5 := @CARD + R1 ; CLI("0",R5) ; IF >= THEN
           BEGIN CLI("9",B5) ; IF <= THEN GOTO OK ; END ;
         CLI(" ",B5) ; IF = THEN GOTO OK ;
         CLI("+",B5) ; IF = THEN GOTO OK ;
         CLI("-",B5) ; IF = THEN GOTO OK ;
         CLI("*",B5) ; IF = THEN GOTO OK ;
       GOTO  INVALID ;
    OK : END ;
     GOTO SKIP ;
   INVALID : R5 := 1 => R4 ;
  SKIP :
            LM(R14,R12,B13(12)) ; END ; END .
/*
// EXEC PLNKEDT(KEEP,SYS006,REPLACE)
 PHASE XYTRYSPC,ROOT
 INCLUDE XYTRYSPC,L
 PHASE XYTRYAAA,*
 INCLUDE XYREAD,L
 INCLUDE CORECT,L
 INCLUDE VALID,L
 INCLUDE VALIDAT,L
 PHASE XYTRYBBB,XYTRYAAA
 INCLUDE XYPLOT,L
 INCLUDE XYATTA,L
 PHASE XYTRYCCC,XYTRYBBB
 INCLUDE XYTAPE,L
 INCLUDE XYJCLD,L
/*
/&
```

APPENDIX IV

PROGRAM LIFETIME

```
C                PROGRAM  LIFETIME.
C
C             THIS PROGRAM EVALUATES THE EXCITED STATE LIFETIMES USING
C      PAPER TAPE INPUT AND CARD INPUT.
C
C
C        CONTROL CARDS.    CONTROL CARDS.     CONTROL CARDS.
C
C         //LIFETIME  JOB ,     A. N. OTHER.    CHEM..
C         //SYS002  ACCESS XYPTR,PTAPE=
C         /*
C         // EXEC XYLIFETA
C         ( DATA CARDS HERE. )
C         /*
C         /&
C
C
C   CARDS.     CARDS.     CARDS.     CARDS.     CARDS.     CARDS.
C
C (1)   NO, OF RUNS - I3 -(MAXIMUM 999)
C         ( IF THIS IS LEFT BLANK, NO. OF RUNS SET AT 999 )
C         COLUMN 10.     FIRST CARD.
C         BLANK -    NEED 3 TITLE CARDS PER RUN.
C         0     -    AS FOR BLANK.
C         1     -    NEED 3 CARDS FOR RUN 1, BUT 2 THEREAFTER.
C         2     -    NEED 3 CARDS FOR RUN 1, BUT 1 THEREAFTER.
C         3     -    NEED 3 CARDS FOR RUN 1, BUT NONE THEREAFTER.
C         COLUMNS 17-20.       FIRST CARD
C         FOUR CHARACTER CODE IDENTICAL TO CODE ON PAPER TAPE.
C         ( FOR CR   MULT PCH   &589 )
C         ( FOR LF   MULT PCH   &289 )
C         ( OTHER SYMBOLS (0123456789*+- AND SP) ARE AS ON CARD PUNCH.
C         COLUMN 30.   FIRST CARD.     NCOR ( FORMAT I1 )
C              NCOR = 0 FOR NO BASE-LINE CORRECTIONS.
C              NCOR = 1 FOR BASE-LINE CORRECTIONS.
```

```
C        COLUMN 40.   FIRST CARD.    NRAT ( FORMAT I1 )
C              NRAT = 0 FOR PRINT-OUT OF RATE CONSTANT AND LN(RATE CONSTANT).
C              NRAT = 1 FOR NO PRINT-OUT.
C (2)-(4)     TITLE CARDS FOR RUN 1.
C ( IF NCOR = 1; FIRST CORRECTION GOES HERE.  FORMAT F7.4 (VOLTS)).
C CORRECTIONS FOR RUNS 2 - NRUN GO AFTER THE TITLE CARDS FOR THAT RUN ( IF
C  PRESENT -- IE IF COLUMN 10 OF DATA CARD 1 CONTAINS CHARACTER .LT. 3 )
C (5) ONWARDS.     CARDS FOR TITLES DEPENDING ON COL. 10 OF CARD 1.
C
C
C   TAPE.     TAPE.     TAPE.     TAPE.     TAPE.     TAPE.
C
C          AT START OF TAPE MANUALLY PUNCH FOUR CHACACTER CODE ( THIS
C          MUST BE IDENTICAL WITH THE CODE ON DATA CARD 1 ) ( THIS CODE
C          MUST NOT BE FOLLOWED BY  CR  LF ).
C
C (1)     MANUALLY PUNCH - AVERAGING CYCLES, TEMPERATURE KELVIN,
C         SWEEP TIME, DELAY BEFORE SWEEP, CR, LF
C          E.G. 064077010020 CR LF
C    '64 SWEEPS AT 77K SWEEP TIME 1.0 MS  DELAY 2 MS.
C (2)     AUTO RUN PUNCH AT A RATE OF 50 READINGS PER SWEEP TIME -
C      MORE THAN 50 READINGS MAY BE TAKEN.
C (3)     TERMINATE EACH RUN BY MANUALLY PUNCHING  99 +00000 0 CR LF
C         OR BY PUNCHING  * CR LF  ( * = MANUAL PUNCH F4 = TIME )
C
C         CONTINUE AS (1),(2),(3) FOR EACH RUN.
C
C
C
      DIMENSION  V(120),X(120),ITIT(60)
      DIMENSION TAU(999),NTEM(999),DEL(999),SCAN(999)
      READ(5,50)NDATA,NCR,NVAL,NCOR,NRAT
   50 FORMAT(I3,6X,I1,6X,A4,9X,I1,9X,I1)
      CALL CLPTVL(2,NVAL)
      NDR=3
      IF(NDATA.EQ.0)NDATA=999
      DO 10 M=1,NDATA
```

```
30  CALL XYREAD(12,NSW,&610,&30,&19)
    READ(5,70)NAV,NTEMP,ST,DELAY
70  FORMAT(2I3,2F3.1)
    N=0
 1  N=N+1
    CALL XYREAD(11,NSW,&610,&2,&19)
    READ(5,71)NC,V(N),NR
71  FORMAT(I2,1X,F6.0,1X,I1)
    NR=NR+1
    G=(10**NR)
    QX=V(N)*G/10000000.0
    V(N)=QX
    GO TO 1
19  CALL XYSKIP(1,&610)
    GO TO 10
72  READ(5,75)VCOR
75  FORMAT(F7.4)
    WRITE(6,76)VCOR
76  FORMAT(1H0,' THE BASE-LINE CORRECTION WAS ',F7.4,' VOLTS.')
77  CONTINUE
    DO 74 N=7,37
    QX=V(N)-VCOR
    V(N)=ABS(QX)
74  IF(V(N).EQ.0.0)V(N)=0.00000001
    GO TO 73
 2  WRITE(6,60)M
60  FORMAT(1H1,2X,'RUN NO. ',I3,17X,'FLUORESCENT LIFETIME RESULTS.')
    IF(NDR.EQ.0) GO TO 103
    DO 15 JJ=1,NDR
    JL=JJ*20
    JK=JL-19
15  READ(5,51)(ITIT(J),J=JK,JL)
51  FORMAT(20A4)
    NDR=3-NCR
103 WRITE(6,61) ITIT
61  FORMAT(1H ,3(1X,20A4,/))
    WRITE(6,62)NAV,ST
```

```
62 FORMAT(1H0,5X,I3,' AVERAGES OVER A TOTAL SWEEP TIME OF ',F4.1,' MI
  1LLISECONDS.')
   WRITE(6,63)NTEMP,DELAY
63 FORMAT(1H0,5X,'THE SAMPLE TEMPERATURE WAS ',I3,' DEGREES KELVIN AN
  1D A DELAY OF ',F4.1,' MILLISECONDS WAS OPERATED.')
   IF(KCOR.GT.0) GO TO 72
   VCOR=0.0
   GO TO 77
73 CONTINUE
   SUMX=0.0
   SUMY=0.0
   SUMXY=0.0
   SUMXX=0.0
   DO 11 N=7,37
   Y=ALOG10(V(N))
   X(N)=(N-7)*ST*0.02
   SUMX=SUMX+X(N)
   SUMY=SUMY+Y
   SUMXY=SUMXY+X(N)*Y
11 SUMXX=SUMXX+X(N)*X(N)
   G=31.0
   DENOM=SUMX*SUMX-G*SUMXX
   SLOPE=(SUMX*SUMY-G*SUMXY)/DENOM
   B=(SUMX*SUMXY-SUMY*SUMXX)/DENOM
   RATE=0.30103/ABS(SLOPE)
   XRATE=RATE*1.44268
   WRITE(6,64)RATE
64 FORMAT(1H0,30X,' CALCULATED HALF-LIFETIME = ',F10.4,' MILLISECONDS
  1.')
   WRITE(6,65) XRATE
65 FORMAT(1H0,30X,' EXPONENTIAL LIFETIME = ',F10.4,' MILLISECONDS.')
   IF(KRAT.GT.0) GO TO 79
   RRATE=1000.0/XRATE
   RLNR=ALOG(RRATE)
   RECT=NTEMP
   RECT=1.0/RECT
   WRITE(6,73)RRATE,RLNR,RECT
```

```
 78 FORMAT(1H0,' RATE CONSTANT = ',E12.5,' SEC.-1.   LN(RATE CONSTANT)
   1 = ',E12.5,5X,'1.0/T = ',E12.5)
 79 CONTINUE
    WRITE(6,66)SLOPE
 66 FORMAT(1H0,30X,'THE VALUE OF A IN Y=AX+B IS ',F10.4)
    WRITE(6,67)B
 67 FORMAT(1H0,30X,'THE VALUE OF B IN Y=AX+B IS ',F10.4)
    WRITE(6,68)
 68 FORMAT(1H0,20X,'THE INPUT DATA WAS',//6X,'TIME',12X,' OBSERVED VAL
   1UE',10X,'CALCULATED VALUE',16X,'DIFFERENCE',14X,'PERCENT DEVN.')
    PSUM=0.0
    DO12 N=7,37
    C=SLOPE*X(N)+B
    C=10.0**C
    DIV=V(N)-C
    PDEV=100.0*DIV/C
    PSUM=PSUM+ABS(PDEV)
 12 WRITE(6,69)X(N),V(N),C,DIV,PDEV
 69 FORMAT(1H ,F9.5,16X,F9.6,16X,F9.6,16X,F9.6,16X,F10.5)
    PSUM=PSUM/G
    WRITE(6,80)PSUM
 80 FORMAT(1H0,25X,' THE AVERAGE PERCENTAGE DEVIATION FROM TRUE EXPONE
   1NTIAL BEHAVIOUR = ',F5.2)
    TAU(M)=XRATE
    NTEM(M)=NTEMP
    DEL(M)=DELAY
    SCAN(M)=ST
    MMX=M
 10 CONTINUE
610 WRITE(6,600)
600 FORMAT(1H1,' RUN NO.  EXP.LIFE   TEMP   SCAN   DELAY',/)
    DO 650 M=1,MMX
    WRITE(6,601)M,TAU(M),NTEM(M),SCAN(M),DEL(M)
601 FORMAT(1H ,2X,I3,3X,F10.4,3X,I3,3X,F4.1,4X,F4.1)
650 CONTINUE
    STOP
    END
```

```
C          TAPE READING SUBROUTINE , XYREAD, C.R.S.DEAN, W.D.COVELL
      BLOCK DATA
      COMMON /XYDATA/ CARD,MM,M,IB,LEN,AST,CR,LF,RCARD
      INTEGER CARD(80),LF/Z0A404040/,CR/Z0D404040/,AST/Z5C404040/,
     1MM/0/,M/1/,IB/0/
      LOGICAL*1 RCARD(80)
      END
      SUBROUTINE XYREAD(N,NSW,*,*,*)
      COMMON /XYDATA/ CARD,MM,M,IB,LEN,AST,CR,LF,RCARD
      INTEGER CARD(80),F9/ZF9404040/,AST,CR
      LOGICAL*1 LCARD(320),RCARD(80)
      EQUIVALENCE (LCARD(1),CARD(1))
      NSW=0
    1 CALL CLPADT(2,LEN,CARD,IND,LF)
      MM=MM+1
C
C          IF END OF TAPE (IND=0) RETURN 1
C
      IF(IND.EQ.0) RETURN 1
      NN=N+2
      IF(LEN.NE.NN)GO TO 2
      CALL VALID(CARD,N,IVAL)
      IF(IVAL.EQ.1)GO TO 3
      IB=NN
      JSUM=1
      DO 11 J=1,N
      RCARD(J)=LCARD(JSUM)
   11 JSUM=JSUM+4
      CALL CORRIO(RCARD,N)
C
C          NO ERRORS DETECTED , NORMAL RETURN
C
      RETURN
C
C          CHECK CARD FOR ERRORS OR TERMINATION
C
    2 IF(CARD(1).EQ.F9)GO TO 5
```

Program Lifetime (continued)

```
      DO 12 J=1,LEN
      IF(CARD(J).NE.AST)GO TO 12
      IF(CARD(J+1).EQ.CR)GO TO 5
   12 CONTINUE
    3 WRITE(6,60)MM,M
   60 FORMAT(1H1,' DATA MISTAKE AT CALL NO. ',I5,' IN DATA SET NO. ',
     2I3,'.',/)
      JJ=4*LEN
      WRITE(6,61) LEN,NN,(LCARD(J),J=1,JJ,4)
   61 FORMAT(1H ,'FOUND ',I2,'  SET ',I2,4X,100A1/)
      IF(NN.NE.IB) GO TO 6
      WRITE(6,62)
   62 FORMAT(1H ,' THE PREVIOUS LINE OF DATA HAS BEEN SUBSTITUTED.')
      NSW=1
      CALL COREIO(RCARD,N)
      RETURN
C
C         END OF RUN , RESET COUNTERS. RETURN 2
C
    5 M=M+1
      MM=0
      IB=0
      RETURN 2
C
C          UNRECOVERABLE MISTAKE.    RETURN 3.
C
    6 WRITE(6,63)
   63 FORMAT(1H ,' MISTAKE CANNOT BE RECOVERED.')
      RETURN 3
C
C       XYSKIP READS FROM TAPE UNTIL N END OF DATA SETS HAVE BEEN READ.
C
      ENTRY XYSKIP(N,*)
      DO 70 JJ=1,N
   91 DO 7 J=1,10000
      CALL CLEADT(2,LEN,CARD,IND,LF)
```

```
C
C          IF END OF TAPE (IND=0) RETURN 1
C
       IF(IND.EQ.0)GO TO 90
       IF(CARD(1).EQ.F9)  GO  TO  19
       DO 20  J=1,LEN
       IF(CARD(J).NE.AST)  GO  TO  20
       IF(CARD(J+1).EQ.CB)  GO  TO  19
  20   CONTINUE
   7   CONTINUE
       GO  TO  91
  19   M=M+1
  70   CONTINUE
       MM=0
       IB=0
       RETURN
  90   MM=0
       N=N-JJ+1
       RETURN  1
       END
/*
//  EXEC PL360
 GLOBAL PROCEDURE VALID(R14) ; BEGIN STM (R14,R12,B13(12)) ; BEGIN
   GLOBAL DATA VALIDAT BASE R10 ; ARRAY 128 CHARACTER TTABLE
      = (32("¬")," ",10("¬"),"¬ ¬¬",10(" "),70("¬"))   ;
   BYTE CHAR ;
   DUMMY BASE R2 ; ARRAY 320 BYTE CARD ;
   R2 := B1 ; R3 := B1(4) := B3 - 1 SHLA 2 ; R4 := B1(8) ;
   R5 - R5 => B4 ;
        FOR R1 :=  0  STEP 4 UNTIL R3 DO
   BEGIN R5 :=  @CARD + R1 ; CLI("0",B5) ; IF >= THEN
         BEGIN CLI("9",B5) ; IF <= THEN GOTO OK ; END ;
       CLI(" ",B5)  ; IF = THEN GOTO OK ;
       CLI("+",B5)  ; IF = THEN GOTO OK ;
       CLI("-",B5)  ; IF = THEN GOTO OK ;
       CLI("*",B5)  ; IF = THEN GOTO OK ;
     GOTO  INVALID ;
    OK : END ;
     GOTO SKIP ;
```

```
 INVALID : B5 := 1 => B4 ;
 SKIP :
          LM(B14,B12,B13(12)) ; END ; END .
/*
// EXEC LNKEDT(KEEP,REPLACE)
/*
/&
```

REFERENCES

1. D.N. Trifonov, The Rare Earth Elements (Pergamon Press, 1963)
2. N.E. Topp, Topics in Inorganic and General Chemistry, Vol. 4, 1965
3. F.A. Cotton and G. Wilkinson, Advanced Inorganic Chemistry (Interscience, 1973).
4. W.M. Latimer, Oxidation Potentials (Prentice-Hall, 1952)
5. G. Blasse, Nato Advanced Study Institute - Analysis and application of rare earth materials, 1972
6. J.E. Mathers, Nato Advanced Study Institute - Analysis and application of rare earth materials, 1972
7. P.N. Yocom, Nato Advanced Study Institute - Analysis and application of rare earth materials, 1972
8. A.E. Martell and R.C. Plumb, J. Phys. Chem., 1952, 56, 993
9. S.P. Sinha, Complexes of the Rare Earths (Pergamon Press, 1966)
10. R.C. Vickery, J. Mol. Spectroscopy, 1958, 2, 308
11. J. Bjerrum, G. Schwarzenbach and L.G. Sillen, Stability Constants (The Chem. Soc., London, 1957)
12. F.A. Hart and F.P. Laming, Proc. Chem. Soc., 1963, 107
13. S.P. Sinha, Spectrochim. Acta, 1964, 20, 879
14. F.A. Hart and F.P. Laming, J. Inorg. Nuclear Chem., 1964, 26, 579
15. F.A. Hart and F.P. Laming, J. Inorg. Nuclear Chem., 1965, 27, 1605
16. F.A. Hart and F.P. Laming, J. Inorg. Nuclear Chem., 1965, 27, 1825
17. K.K. Rohatgi and S.K. Sen Gupta, J. Inorg. Nuclear Chem., 1970, 32, 2247
18. F.A. Hart, J.E. Newbery and D. Shaw, J. Inorg. Nuclear Chem., 1970, 32, 3585

19. V.E. Plyushchev and L.P. Shklover, Russ. J. Inorg. Chem., 1964, 9, 183

20. L.P. Shklover and V.E. Plyushchev, Russ. J. Inorg. Chem., 1964, 9, 186

21. V.V. Sorebrennikov, E.I. Ivanova and L.A. Alekseenko, Russ. J. Inorg. Chem., 1959, 4, 619

22. N.K. Dutt and H.G. Mukherjee, J. Indian Chem. Soc., 1953, 30, 272

23. N.K. Dutt and N. Goswami, J. Indian Chem. Soc., 1953, 30, 275

24. S.P. Sinha, Z. Naturforsch, 1965, 20a, 552

25. R.J. Foster, Coordination Chem. Rev., 1973, 10, 195

26. R.J. Foster and D.G. Hendricker, Inorg. Chim. Acta, 1972, 6, 371

27. R.J. Foster, R.L. Bodner and D.G. Hendricker, J. Inorg. Nuclear Chem., 1972, 34, 3795

28. D.G. Hendricker and R.J. Foster, J. Inorg. Nuclear Chem., 1972, 34, 1949

29. T. Moeller and H.E. Kremers, J. Phys. Chem., 1944, 48, 395

30. F. Ephraim and R. Block, Chem. Ber., 1926, 59, 2692

31. A.I. Popov and W.W. Wendlandt, J. Amer. Chem. Soc., 1965, 77, 857

32. W.W. Wendlandt, Science, 1955, 122, 197

33. L.J. Charpentier and T. Moeller, J. Inorg. Nuclear Chem., 1970, 32, 3575

34. T. Moeller, D.F. Martin, L.C. Thompson, R. Ferrus, G.R. Feistel and W.J. Randall, Chem. Rev., 1965, 65, 1

35. A. Sonesson, Acta Chem. Scand., 1958, 12, 165

36. A. Sonesson, Acta Chem. Scand., 1958, 12, 1937

37. A. Sonesson, Acta Chem. Scand., 1960, 14, 1495

38. P.B. Sarkar, Bull Soc. Chim. France, 1926, 4, 1390

39. W.R. Stagg and J.E. Powell, Inorg. Chem., 1964, 3, 242

40. J.E. Powell, R.S. Kolat and G.S. Paul, Inorg. Chem., 1964, 3, 518

41. M. Bobtelsky and A.H.I. Ben-Basset, Bull. Soc. Chim. France, 1958, 1138

42. S.P. Sinha, C.K. Jørgensen and R. Pappalardo, Z. Naturforsch., 1964, 19a, 434

43. S.P. Sinha, Z. Naturforsch., 1965, 20a, 319

44. D.C. Bradley and M.M. Faktor, Chem. and Ind., 1958, 1332

45. S.N. Misra, T.N. Mirsa, R.N. Kapoor and R.C. Mehrotra, Chem. and Ind., 1963, 120

46. S. Sankhla, S.N. Misra and R.N. Kapoor, Chem. and Ind., 1965, 382

47. K.V. Tserkasevich and N.S. Poluktov, Ukrain. khim. Zhur., 1964, 30, 146; Chem. Abs., 60:12877

48. R.M. Izatt, W.C. Fernelius, C.G. Haas and B.P. Block, J. Phys. Chem., 1955, 59, 170

49. I. Grenthe and W.C. Fernelius, J. Am. Chem. Soc., 1960, 82, 6258

50. G.W. Pope, J.F. Steinbach and W.F. Wagner, J. Inorg. Nuclear Chem., 1961, 20, 304

51. N.K. Dutt and P. Bandyopadhyay, J. Inorg. Nuclear Chem., 1964, 26, 729

52. J. Prášilova, J. Inorg. Nuclear Chem., 1964, 26, 661

53. G. Urbain, Bull. Soc. Chim. France, 1896, 15, 347

54. A. Sonesson, Acta Chem. Scand., 1959, 13, 998

55. A. Sonesson, Acta Chem. Scand., 1959, 13, 1437

56. N.K. Davidenko, Russ. J. Inorg. Chem., 1962, 7, 1412

57. M. Cefola, A.S. Tompa, A.V. Celiano and P.S. Gentile, Inorg. Chem., 1962, 1, 290

58. N.K. Davidenko, Russ. J. Inorg. Chem., 1959, 4, 1135

59. K.L. Malyarov and F.P. Sudakov, Russ. J. Inorg. Chem., 1961, 6, 800

60. J.L. Bear, G.R. Choppin and J.V. Quagliano, J. Inorg. Nuclear Chem., 1962, 24, 1601

61. J.L. Bear, G.R. Choppin and J.V. Quagliano, J. Inorg. Nuclear Chem., 1963, 25, 513

62. C.K. Jørgensen, Mol. Phys., 1962, 5, 271

63. J.P. Surls and G.R. Choppin, J. Inorg. Nuclear Chem., 1957, 4, 62

64. G. Wilkinson and J.M. Birmingham, J. Amer. Chem. Soc., 1954, 76, 6210

65. J.M. Birmingham and G. Wilkinson, J. Amer. Chem. Soc., 1956, 78, 42

66. J.P. Fackler, Progr. Inorg. Chem., 1966, 7, 361

67. J. Lewis, R.F. Long and C. Oldham, J. Chem. Soc. (A), 1965, 6740

68. D. Gibson, J. Lewis and C. Oldham, J. Chem. Soc. (A), 1966, 1453

69. J. Lewis and C. Oldham, J. Chem. Soc. (A), 1966, 1456

70. D. Gibson, Coordination Chem. Rev., 1969, 4, 225

71. N.K. Dutt and S. Sur, J. Inorg. Nuclear Chem., 1971, 33, 115

72. S.J. Lyle and A.D. Witts, Inorg. Chim. Acta, 1971, 5, 481

73. L.R. Melby, N.J. Rose, E. Abramson and J.C. Caris, J. Amer. Chem. Soc., 1964, 86, 5117

74. H. Bauer, J. Blanc and D.L. Ross, J. Amer. Chem. Soc., 1964, 86, 5125

75. R.E. Sievers and K.J. Eisentraut, J. Amer. Chem. Soc., 1965, 87, 5254

76. T. Moeller, Lanthanides and Actinides, ed. K.W. Bagnall (Butterworths, 1972)

77. D.C. Bradley, J.S. Ghotra and F.A. Hart, J.C.S. Chem. Comm., 1972, 349

78. R.V. Parish, Coordination Chem. Rev., 1966, 1, 439

79. P. Singh, A. Clearfield and I. Bernal, J. Coordination Chem., 1971, 1, 29

80. T.A. Beineke and J. Delgaudio, Inorg. Chem., 1968, 7, 715

81. M. Ul-Haque, F.A. Hart and C.N. Caughlan, J.C.S. Chem. Comm., 1970, 1240

82. A.R. Al-Karaghouli and J.S. Wood, J.C.S. Chem. Comm., 1970, 135

83. J.G. Bergmann and F.A. Cotton, Inorg. Chem., 1966, 5, 1208

84. J. Drummond and J.S. Wood, J. Chem. Soc. (A), 1970, 226

85. D.G. Hendricker and R.L. Bodner, Inorg. Nuclear Chem. Letters, 1970, 6, 187

86. R.L. Bodner and D.G. Hendricker, Inorg. Nuclear Chem. Letters, 1970, 6, 421

87. A. Clearfield, P. Singh and I. Bernal, J.C.S. Chem. Comm., 1970, 389

88. D.G. Hendricker and R.L. Bodner, Inorg. Chem., 1970, 9, 273

89. M.F. Richardson, W.F. Wagner and D.E. Sands, Inorg. Chem., 1968, 7, 2495

90. R.E. Creamer and K. Seff, J.C.S. Chem. Comm., 1972, 400

91. J. Reuben, J. Amer. Chem. Soc., 1973, 95, 3534

92. M.O. Workman and J.H. Burns, Inorg. Chem., 1969, 8, 1542

93. B.G. Wyborne, Spectroscopic Properties of Rare Earths (Interscience, 1965)

94. D. Sutton, Electronic Spectra of Transition Metal Complexes (McGraw-Hill, 1968)

95. A. Heller, J. Mol. Spectroscopy, 1968, 28, 208

96. E.I. Onstott and C.J. Brown, Analyt. Chem., 1958, 30, 172

97. J.L. Kropp and M.W. Windsor, J. Chem. Phys., 1965, 42, 1599

98. F. Varsany and G. Dieke, J. Chem. Phys., 1959, 31, 1066

99. G. Dieke and L. Hall, J. Chem. Phys., 1957, 27, 465

100. J.L. Kropp and M.W. Windsor, J. Chem. Phys., 1963, 39, 2769

101. J.K. Kropp and W.R. Dawson, J. Opt. Soc. Amer., 1965, 55, 822

102. R. Borkowski, H. Forest and D. Grafstein, J. Chem. Phys., 1965, 42, 2974

103. J.L. Kropp and W.R. Dawson, J. Chem. Phys., 1966, 45, 2419

104. J.J. Freeman, G.A. Crosby and K.E. Lawson, J. Mol. Spectroscopy, 1964, 13, 399

105. S.I. Weissman, J. Chem. Phys., 1942, 10, 214

106. M.L. Bhaumik and M.A. El-Sayed, J. Chem. Phys., 1965, 42, 787

107. M.L. Bhaumik and M.A. El-Sayed, Appl. Opt. Supplement, 1965, 2, 214

108. M.L. Bhaumik and L.J. Nugent, J. Chem. Phys., 1965, 43, 1680

109. G.A. Crosby, R.E. Whan and R.M. Alire, J. Chem. Phys., 1961, 34, 743

110. G.A. Crosby, R.E. Whan and J.J. Freeman, J. Phys. Chem., 1962, 66, 2493

111. L.I. Katzin and M.L. Barnett, J. Phys. Chem., 1964, 68, 3779

112. R.E. Whan and G.A. Crosby, J. Mol. Spectroscopy, 1962, 8, 315

113. C.C. Hinckly, J. Amer. Chem. Soc., 1969, 91, 5160

114. F.A. Hart, J.E. Newbery and D. Shaw, Nature, 1967, 216, 261

115. P.J. McCarthy, Spectroscopy and Structure of Metal Chelate Compounds, ed. K. Nakamoto and P.J. McCarthy (Wiley, 1968, p. 346)

116. H.M. McConnell and R.E. Robertson, J. Chem. Phys., 1958, 29, 1361

117. B. Bleany, J. Mgn. Resonance, submitted for publication

118. D.R. Eaton, J. Amer. Chem. Soc., 1965, 87, 3097

119. E.R. Birnbaum and T. Moeller, J. Amer. Chem. Soc., 1969, 91, 7274

120. B.C. Mayo, J.C.S. Chem. Soc. Rev., 1973, 2, 49

121. L. Ernst and A. Mannschreck, Tetrahedron Letters, 1971, 3023

122. R.K. Mackie and T.M. Shepherd, Org. Magnetic Resonance, 1972, 4, 557

123. R.P. Wayne, Photochemistry (Butterworths, 1970)

124. P.A. Leermakers, Techniques of Organic Chemistry, Vol. 8, (Interscience, 1969)

125. W.A. Noyes, G. Porter, and V.G. Jolly, Chem. Rev., 1956, 56 49

126. I.B. Berlman, Handbook of Fluorescence Spectra of Aromatic Molecules (Academic Press, 1965)

127. A.N. Terenin, Acta Physicochim, 1943, 18, 210

128. G.N. Lewis and M. Kasha, J. Amer. Chem. Soc., 1944, 66, 2100

129. G.N. Lewis and M. Kasha, J. Amer. Chem. Soc., 1945, 67, 994

130. G. Herzberg, Atomic Spectra and Atomic Structure (Dover, 1944)

131. A.C. Day, Chem. Soc. Ann. Rev., 1967, 64B, 161

132. S.K. Lower and M.A. El-Sayed, Chem. Rev., 1966, 66, 199

133. P. Suppan, Chem. Brit., 1968, 4, 538

134. N.J. Turro, J. Chem. Educ., 1969, 46, 2

135. J.S. Swenton, J. Chem. Educ., 1969, 46, 7

136. A. Jablonski, Nature, 1933, 131, 839

137. A. Jablonski, Z. Physik, 1935, 94, 38

138. D.M. Hercules, Fluorescence and Phosphorescence Analysis (Wiley, 1966)

139. C.A. Parker, Photoluminescence of Solutions (Elsevier, 1968)

140. R.S. Becker, Theory and Interpretation of Fluorescence and Phosphorescence (Interscience, 1969)

141. M. Kasha, Discuss. Faraday Soc., 1950, 9, 14

142. M. Beer and H.C. Longuet-Higgins, J. Chem. Phys., 1955, 23, 1390

143. G. Viswanath and M. Kasha, J. Chem. Phys., 1956, 24, 574

144. G. Binsch, E. Heilbronner, R. Jankow and S. Schmidt, Chem. Phys. Letters, 1967, 1, 135

145. C.E. Easterly, L.G. Christophorau, R.P. Blaunstein and J.G. Carter, Chem. Phys. Letters, 1970, 6, 579

146. C.E. Easterly, L.G. Christophorau and J.G. Carter, J.C.S. Faraday II, 1973, 69, 471

147. W.R. Dawson and J.L. Kropp, J.Phys. Chem., 1969, 73, 1752

148. G.I. Kobyshev and A.N. Terenin, Proc. Int. Conference on Luminescence (Akademiai Kiado Budapest, 1968, p. 520)

149. V.V. Zelenskii, V.P. Kolobkov and A.A. Saganenko, Opt. Spektrosk (Suppl. 1, Luminescence), 1963, p. 28

150. Yu.V. Morozov, Biofizika, 1963, 8, 165

151. L.S. Forster and D. Dadley, J. Phys. Chem., 1962, 66, 838

152. H. Labhart, Helv. Chim. Acta, 1964, 47, 2279

153. A.R. Horrocks, T. Medinger and F. Wilkinson, International Luminescence Symposium (Thiemig, Munich, W. Germany) 1966, p. 16

154. H. Islikawa and A.W. Noyes, J. Chem. Phys., 1962, 37, 583

155. E.C. Lim and J.D. Laposa, J. Chem. Phys., 1964, 41, 3527

156. T. Medinger and F. Wilkinson, Trans. Faraday Soc., 1965, 61, 620

157. V.L. Ermolaev and E.B. Sveshnikova, Opt. Spectroscopy, 1964, 16, 320

158. J.D. Laposa, E.C. Lim and R.E. Kellogg, J. Chem. Phys., 1965, 42, 3025

159. J.B. Birks and T.A. King, Phys. Letters, 1965, 18, 128

160. A. Sklar, J. Chem. Phys., 1937, 5, 699

161. S.P. McGlynn, T. Azumi and M. Kinoshita, Molecular Spectroscopy of the Triplet State (Prentice-Hall, 1969)

162. R.S. Mulliken, J. Chem. Phys., 1939, 7, 20

163. R.S. Mulliken, J. Chem. Phys., 1955, 23, 1997

164. J.R. Platt, J. Chem. Phys., 1950, 18, 1168

165. J.R. Platt, J. Opt. Soc. Amer., 1953, 43, 252

166. A.N. Terenin and V.L. Ermolaev, Trans. Faraday Soc., 1956, 52, 1042

167. V.L. Ermolaev, Opt. Spectroscopy, 1959, 6, 417

168. H.L.J. Bäckström and K. Sandros, Acta Chem. Scand., 1958, 12, 823

169. G. Porter and G. Wilkinson, Proc. Roy. Soc., 1961, A264, 1

170. B. Smaller, E.C. Avery and J.R. Remko, J. Chem. Phys., 1968, 43, 922

171. V.L. Ermolaev and E.B. Sveshnikova, Izvest. Akad. Nauk SSSR, Ser. Fiz., 1962, 26, 29

172. R.G. Bennett, R.P. Schwenker and R.E. Kellogg, J. Chem. Phys., 1964, 41, 3042

173. N. Mataga, H. Obashi and T. Okada, J. Chem. Phys., 1969, 73, 370

174. J.B. Birks, Photophysics of Aromatic Molecules (Wiley-Interscience, 1970)

175. M.A. El-Sayed and M.L. Bhaumik, J. Chem. Phys., 1963, 39, 2391

176. M.L. Bhaumik and M.A. El-Sayed, J. Phys. Chem., 1965, 69, 275

177. E. Matovich and C.K. Suzuki, J. Chem. Phys., 1963, 39, 1442

178. R.E. Ballard and J.W. Edwards, Spectrochim. Acta, 1965, 21, 1353

179. A. Heller and E. Wasserman, J. Chem. Phys., 1965, 42, 949

180. N. Filipescu and G.W. Mushrush, J. Phys. Chem., 1968, 72, 3516

181. N. Filipescu and G.W. Mushrush, J. Phys. Chem., 1968, 72, 3522

182. F.L. Minn, G.W. Mushrush and N. Filipescu, J. Chem. Soc. (A), 1971, 63

183. G.W. Mushrush, F.L. Minn and N. Filipescu, J. Chem. Soc. (B), 1971, 427

184. B.M. Antipenko and V.L. Ermolaev, Opt. Spectroscopy, 1970, 28, 504

185. J.L. Sommerdijk, J. Luminescence, 1971, 4, 441

186. J.L. Sommerdijk, W.L. Wanmaker and J.G. Verriet, J. Luminescence, 1971, 4, 404

187. L.G. Van Uitert, E.F. Dearborn and W.H. Grodkiewicz, J. Chem. Phys., 1968, 49, 4400

188. L.G. Van Uitert, J. Luminescence, 1971, 4, 1

189. J.T. Karpick and B. Di Bartolo, J. Luminescence, 1971, 4, 309

190. E.J. Schimitschek and E.G.W. Schwarz, Nature, 1962, 196, 832

191. A. Lempicki and H. Samelson, Proc. Sym. Opt. Masers, 1963, 347

192. E.J. Schimitschek, Appl. Phys. Letters, 1963, 3, 117

193. A. Lempicki and H. Samelson, Phys. Letters, 1963, 4, 133

194. H. Winston, O.J. Marsh, C.K. Suzuki and C.L. Telk, J. Chem. Phys., 1963, 39, 267

195. S. Bjorklund, G. Kellermeyer, C.R. Hurt, N. McAvory and N. Filipescu, Appl. Phys. Letters, 1967, 10, 160

196. E.P. Riedel and R.G. Charles, J. Chem. Phys., 1966, 45, 1908

197. A. Lempicki, H. Samelson and C. Brecker, J. Chem. Phys., 1964, 41, 1214

198. M.L. Bhaumik, P.C. Fletcher, L.J. Nugent, S.M. Lee, S. Higa, C.L. Telk and M. Weinberg, J. Chem. Phys., 1964, 68, 1490

199. H. Samelson, A. Lempicki, V.A. Brophy and C. Brecker, J. Chem. Phys., 1964, 40, 2547

200. T.M. Shepherd, J. Inorg. Nuclear Chem., 1967, 29, 2551

201. H. Samelson, C. Brecker and A. Lempicki, J. Mol. Spectroscopy, 1966, 19, 349

202. R.G. Charles and E.P. Riedel, J. Inorg. Nuclear Chem., 1966, 28, 527

203. W.J. McCarthy and J.D. Winefordner, Analyt. Chem., 1966, 38, 848

204. Y. Hass and G. Stein, J. Phys. Chem., 1972, 76, 1093

205. Y. Hass and G. Stein, J. Phys. Chem., 1971, 75, 3668

206. Y. Hass, G. Stein and M. Tomkiewicz, J. Phys. Chem., 1970, 74, 2558

207. Y. Hass and G. Stein, Chem. Phys. Letters, 1969, 3, 313

208. R. Reisfield, R.A. Velapoldi, L. Boehm and M. Ish-Shalom, J. Phys. Chem., 1971, 75, 3980

209. R. Reisfield, R.A. Velapoldi and L. Boehm, J. Phys. Chem., 1972, 76, 1293

210. V.L. Ermolaev and E.B. Sveshnikvo, Opt. Spectroscopy, 1970, 28, 98

211. V.L. Ermolaev, N.A. Kazanskaya, A.A. Petrov and Yu. I. Kheruze, Opt. Spectroscopy, 1970, 28, 113

212. N.S. Poluektov and S.A. Gava, Opt. Spectroscopy, 1971, 31, 45

213. V.I. Kosyakov, B.V. Makashkin, A.I. Ponyaev and E.P. Smirnova, Opt. Spectroscopy, 1972, 32, 229

214. M.I. Gaiduk, Opt. Spectroscopy, 1971, 31, 48

215. N.A. Kazanskaya and E.B. Sveshnikova, Opt. Spectroscopy, 1970, 28, 376

216. R.L. DeKock and W. Weltner, J. Phys. Chem., 1971, 75, 514

217. N.A. Kazanskaya, V.L. Ermolaev, A.A. Moshinskaya, A.A. Petrov and Yu. I. Kheruze, Opt. Spectroscopy, 1970, 28, 619

218. L.I. Anikina and A.V. Karyakin, Russ. Chem. Rev., 1970, 39, 673

219. E. Nakazawa and S. Shionoya, J. Phys. Soc. Japan, 1970, 28, 1260

220. H. Samelson and A. Lempicki, J. Chem. Phys., 1963, 39, 110

221. C. Brecker, H. Samelson and A. Lempicki, J. Chem. Phys., 1965, 42, 1081

222. L.J. Nugent, M.L. Bhaumik, S. George and S.M. Lee, J. Chem. Phys., 1964, 41, 1305

223. T. Moeller and W.F. Ulrich, J. Inorg. Nucl. Chem., 1956, 2, 164

224. N. Filipescu, W.F. Sager and F.A. Serafin, J. Phys. Chem., 1964, 68, 3324

225. W.F. Sager, N. Filipescu and F.A. Serafin, J. Phys. Chem., 1965, 69, 1092

226. R.G. Charles and E.P. Riedel, J. Inorg. Nuclear Chem., 1967, 29, 715

227. J.G. Stiles, C.N. McCarthy and L.L. Quill, J. Amer. Chem. Soc., 1948, 70, 3142

228. Y. Matsuda, S. Makishima and S. Shionoya, Bull. Chem. Soc. Japan, 1969, 42, 356

229. C.Y. Liang, E.J. Schimitschek and J.A. Trias, J. Inorg. Nuclear Chem., 1970, 32, 811

230. R. Belcher, J. Majer, R. Perry and W.I. Stephen, J. Inorg. Nuclear Chem., 1969, 31, 471

231. N. Filipescu, Appl. Spectroscopy, 1968, 22, 513

232. J. Selbin, N. Ahamad and N. Bhaccu, Inorg. Chem., 1971, 10, 1383

233. J.P. Fackler, J. Chem. Soc., 1962, 1957

234. R.B. Charles, Org. Synth., 39, 61

235. A. Spassow, Org. Synth., 21, 46

236. J.D. Winefordner and P.A. St. John, Anal. Chem., 1963, 35, 2211

237. R. Argauer and C.E. White, Fluorescence Analysis (Dekker, 1970)

238. J.F. Ireland, Ph.D. Thesis, St. Andrews, 1972

239. R. Lippert, W. Nägele, I. Seibold-Blankenstein, W. Staiger and W. Voss, Z. Anal. Chem., 1959, 170, 1

240. W.H. Meluish, J. Phys. Chem., 1960, 64, 762

241. C.A. Parker and W.T. Rees, Analyst, 1960, 85, 587

242. C.R.S. Dean, unpublished work

243. F.R. Lipsett, J. Opt. Soc. Amer., 1962, 49, 673

244. C.A. Parker, Anal. Chem., 1962, 34, 502

245. G.K. Turner, Science, 1964, 146, 183

246. G.M. Edelman, Rev. Sci. Instr., 1965, 39, 809

247. H.V. Drushel, A.L. Sommers and R.C. Cox, Anal. Chem., 1963, 35, 2166

248. P. Byron and J.B. Hudson, Talanta, 1968, 15, 714

249. W.R. Ware, in Creation and Detection of the Excited State (Dekker, 1971)

250. E. Gaviola, Z. Physik, 1926, 35, 748

251. E. Gaviola, Ann. Physik, 1926, 81, 681

252. S.S. Brody, Rev. Sci. Instr., 1957, 31, 1021

253. L. Huntley, T. Coburn, E. Garwin and L. Stryer, Rev. Sci. Instr., 1967, 38, 488

254. H.T. Witt, Nobel Symposium, 1967

255. F.P. Schäfer and K. Röllig, Z. Phys. Chem., 1964, NF40, 198

256. M. Ch. Studer, U.P. Wild and Hs. H. Günthard, J. Phys., 1970, 3, 847

257. T.D. Brown and T.M. Shepherd, J.C.S. Dalton, 1972, 1616

258. T.D. Brown and T.M. Shepherd, J.C.S. Dalton, 1973, 335

259. P.P. Sorokin, J.R. Lankard, V.L. Moruzzi and E.C. Hammond, J. Chem. Phys., 1968, 48, 4726

260. J.G. Calvert and J.N. Pitts, Photochemistry (Wiley, 1966)

261. B.R. Henry and M. Rasha, Ann. Rev. Phys. Chem., 1968, 19, 161

262. S.J. Strickler and R.A. Berg, J.Chem. Phys., 1962, 37, 814

263. F.E. Lytle and D.M. Hercules, J. Amer. Chem. Soc., 1969, 91, 253

264. J.N. Demas and G.A. Crosby, J. Phys. Chem., 1971, 75, 991

265. S.I. Vavilov, Z. Phys., 1924, 22, 266

266. G. Weber and F.W.J. Teale,Trans. Faraday Soc., 1957, 53, 646

267. W.R. Dawson and M.W. Windsor, J. Phys. Chem., 1968, 72, 3251

268. F.R. Lipsett, Progr. Dielectrics, 1967, 7, 217

269. N.J. Nygaard, Brit. J. Appl. Phys., 1964, 15, 597

270. N. Kristianpoller, J. Opt. Soc. Amer., 1964, 54, 1285

271. R. Allison, J. Burns and A.J. Tuzzolino, J. Opt. Soc. Amer., 1964, 54, 747

272. J.J. Hermans and S. Levinson, J. Opt. Soc. Amer., 1951, 41, 460

273. R.H. Müller and H.J. Stolten, Anal. Chem., 1953, 25, 1103

274. A.P. Brady, H. Huff and J.W. McBain, J. Phys. Chem., 1951, 55, 305

275. S.B. Kulkarni,Nature, 1953, 171, 219

276. A.V. Hill, Proc. Roy. Soc., 1930, 127A, 9

277. W.I. Higuchi, M.A. Schwartz, E.G. Rippre, and T. Higuchi, J. Phys. Chem., 1959, 63, 996

278. J.E. Sicre, J.T. Dubois, K.J. Eisentraut and R.E. Sievers, J. Amer. Chem. Soc., 1969, 91, 3476

279. J.K.M. Sanders, S.W. Hanson and D.H. Williams, J. Amer. Chem. Soc., 1972, 94, 5325

280. M.K. Archer, D.S. Fell and R.W. Jotham, Inorg. Nuclear Chem. Letters, 1971, 7, 1135

281. C.W. Harris, R.E. Sievers and K.J. Eisentraut, U.S. Patent Pending

282. J.P.R. de Villiers and J.C.A. Boeyens, Acta Cryst., 1971, B27, 2335

283. C.S. Erasmus and J.C.A. Boeyens, Acta Cryst., 1970, B26, 1843

284. C.S. Erasmus and J.C.A. Boeyens, J. Cryst. Mol. Struct., 1971, 1, 83

285. W. De W. Horrocks, J.P. Sipe and J.R. Luber, J. Amer. Chem. Soc., 1971, 93, 5258

286. V.A. Mode and G.S. Smith, J. Inorg. Nuclear Chem., 1969, 31, 1857

287. J.S. Ghotra, F.A. Hart, G.P. Moss and M.L. Staniforth, Chem. Comm., 1973, 113

288. W.R. Dawson, J.L. Kropp and M.W. Windsor, J. Chem. Phys., 1966, 45, 2410

289. M.J. Bennet, F.A. Cotton, P. Legzdins and S.J. Lippard, Inorg. Chem., 1968, 7, 1770

290. E.C. Lingafelter, Coordination Chem. Rev., 1966, 1, 151

291. F.A. Cotton and J.J. Wise, Inorg. Chem., 1966, 6, 1200

292. D.W. Thompson and A.L. Allred, J. Phys. Chem., 1971, 75, 433

293. C.R. Hurt and N. McAvoy, J. Inorg. Nuclear Chem., 1966, 28, 1753

294. R.J. Charles and E.P. Riedel, J. Inorg. Nuclear Chem., 1966, 28, 3005

295. Y. Hass and G. Stein, J. Phys. Chem., 1971, 75, 3677

296. E.L. Fink, Appl. Optics, 1968, 7, 29

297. S. Kuboniwa and T. Hoshina, J. Phys. Soc. Japan, 1972, 32, 1059

298. V.L. Ermolaev, N.A. Kazanskaya, A.V. Moshinskaya and Yu.I. Kheruze, Opt. Spectroscopy, 1972, 32, 41

299. T.D. Brown, T.M. Shepherd and D.C. Tipney, unpublished work

300. N. Filipescu and N. McAvoy, J. Inorg. Nuclear Chem., 1966, 28, 253

301. M.L. Bhaumik and C.L. Telk, J. Opt. Soc. Amer., 1964, 54, 1211

302. E.L. Muetterties and C.M. Wright, Quart. Rev. (London), 1967, 21, 109

303. D.R. Fitzwater and R.E. Rundle, Z. Krist., 1959, 112, 362

304. L. Helmholz, J. Amer. Chem. Soc., 1939, 61, 1544

305. K. Schubert and A. Seitz, Z. anorg. u. allegem. Chem., 1947, 254, 116

306. D.H. Templeton and G.F. Carter, J. Phys. Chem., 1954, 58, 940

307. W.H. Zachariasen, Acta Cryst., 1948, 1, 265

308. J.H. Burns, Inorg. Chem., 1965, 4, 881

309. D. Mansmann and W.D. Wallace, J. Phys. (France), 1964, 25, 454

310. A. Zalkin and D.H. Templeton, J. Amer. Chem. Soc., 1953, 75, 2453

311. A. Zalkin, D.H. Templeton and T.E. Hopkins, Inorg. Chem., 1966, 5, 1466

312. W.H. Zachariasen, Acta Cryst., 1956, 9, 1015

313. I. Mayer, S. Zolotov and F. Kassierer, Inorg. Chem., 1965, 4, 1637

314. J.L. Hoard, B. Lee and M.D. Lind, J. Amer. Chem. Soc., 1965, 87, 1612

315. P.J. Wagner and H.N. Schott, J. Phys. Chem., 1968, 72, 3702

316. L.G. Van Uitert and R.R. Soden, J. Chem. Phys., 1962, 36, 1289

317. L.G. Van Uitert, E.P. Dearborm and J.J. Rubin, J. Chem. Phys., 1966, 45, 1578

318. L.G. Van Uitert, E.P. Dearborn and J.J. Rubin, J. Chem. Phys., 1967, 46, 420

319. L.G. Van Uitert, R.R. Soden and R.C. Linares, J. Chem. Phys., 1962, 36, 1793

320. P.K. Gallagher, A. Heller and E. Wasserman, J. Chem. Phys., 1964, 41, 3921

321. L.I. Kononenko, V.N. Drobyazko and N.S. Poluektov, Opt. Spectroscopy, 1972, 32, 165

322. J.S. Curran and T.M. Shepherd, J.C.S. Faraday II, 1973, 69, 126